EXPERIMENTAL INVESTIGATION AND MODELING OF CONCRETE STRUCTURES EXPOSED TO MOLTEN SULFUR

BY

HASSAN A. ALKHALIFAH

A Dissertation Presented to the

DEANSHIP OF GRADUATE STUDIES

KING FAHD UNIVERSITY OF PETROLEUM & MINERALS

DHAHRAN, SAUDI ARABIA

In Partial Fulfillment of the
Requirements for the Degree of

DOCTOR OF PHILOSOPHY

In

CIVIL ENGINEERING

12/2018

KING FAHD UNIVERSITY OF PETROLEUM & MINERALS

DHAHRAN- 31261, SAUDI ARABIA

DEANSHIP OF GRADUATE STUDIES

This thesis, written by **HASSAN A. ALKHALIFAH** under the direction of his thesis advisor and approved by his thesis committee, has been presented and accepted by the Dean of Graduate Studies, in partial fulfillment of the requirements for the degree of **DOCTOR OF PHILOSOPHY IN CIVIL ENGINEERING.**

Dr. Ali Husain Al- Gadhib
(Advisor)

Dr. Salah Uthman Al-Dulaijan
Department Chairman

Dr. Muhammad Kalimur Rahman
(Co-Advisor)

Dr. Salam A. Zummo
Dean of Graduate Studies

Dr. Ahmad Saad Al-Gahtani
(Member)

21/2/19
Date

Dr. Shamsad Ahmad
(Member)

Dr. Salah Uthman Al-Dulaijan
(Member)

I dedicate this work to my family. This work wouldn't have happened without their great support

ACKNOWLEDGMENTS

First, I would like to thank my advisor Dr. Ali Al-Gadhib for his great help and support throughout my doctoral study. I also would like to thank my co-advisor Dr. Muhammad Kalimur Rahman for his substantial contribution and involvement in the research and for the valuable insights he provided me, his encouragement and support helped me overcome many challenges in this research. I also would like to thank all my committee members, Dr. Salah Al-Dulaijan, Dr. Ahmed Al-Qahtani and Dr. Ahmad Shamsad for their guidance and advice.

I would like to express my appreciation to the Civil and Environmental Engineering Department, to KFUPM and to Saudi Aramco for all support and permissions to fulfil my doctoral study. Special thanks to my mentor Dr. Ammar Mohammed and to Dr. Emad Abu Aisheh for their contribution in this research.

I would like to express my gratitude to the staff at KFUPM RI, namely, M. Barry, M. Ibrahim and F. Al-Yusif and to Dr.Tawfik Saleh from the Chemistry Department at KFUPM for their great support. Material supplied by local vendors “Redachem United, Fosroc Saudi Arabia and Saudi-pultrusion is acknowledged.

Last but not the least, I would like to thank my family for supporting me spiritually throughout my doctoral study.

TABLE OF CONTENTS

LIST OF TABLES

LIST OF FIGURES

LIST OF ABBREVIATIONS

OPC	Ordinary Portland Cement
SRPC	Sulphates Resistant Portland
CAC	Calcium Aluminate Cement
UHPC	Ultra-High-Performance Co
FA	Fly ash
AAC	Alkali Activated Concrete
SCMs	Supplementary cementitious
SEM	Scanning electron microscop
SF	Silica fume
XRD	X-ray diffraction

ABSTRACT

Full Name : Hassan A. Alkhalifah

Thesis Title : Experimental Investigation and Modeling of Concrete Structures Exposed to Molten Sulfur

Major Field : Civil Engineering

Date of Degree : 12/2018

A special type of reinforced concrete structure exposed to different forms of sulfate attack is the sulfur storage structure, typically referred to as “Sulfur Pit”. Sulfur Pit is an essential part of oil and gas processing facilities where the sulfur after extraction from the hydrocarbons in Sulfur Recovery Units is stored and maintained in liquid phase at temperatures ranging from 130°C to 160°C. The reinforced concrete sulfur pits are exposed to a very corrosive environment and subject to frequent deterioration in a short span of time, especially the roof slab which is exposed to acidic gases/vapor fumes. This research presents field and laboratory investigation of the deterioration mechanism of special reinforced concrete structures used to store molten sulfur. In addition, it presents laboratory experimental investigation of eight different types of concrete mixes exposed to sulfuric acid at ambient as well as elevated temperature (100^{o}C) temperature. The scope includes evaluation of the physical and mechanical properties (compressive strength, mass loss, permeability, acid penetration and modulus of elasticity) as well as material analysis including SEM, EDX, XRD and FTIR for concrete samples before and after exposure to sulfuric acid. Numerical modeling of the damage was developed and a parametric study was performed to evaluate the role of various parameters in the damage and compared to actual experimental obtained data.

ملخص الرسالة

الاسم الكامل: حسن بن علي بن عبدالله الخليفة

عنوان الرسالة: التحقيق المخبري والنمذجة العددية لتدهور الخرسانة المعرضة للكبريت المصهور

التخصص: الهندسة المدنية

تاريخ الدرجة العلمية: 1440/05/01

تعتبر منشآت تخزين الكبريت المبنية من الخرسانة المسلحة جزء أساسي من مرافق معالجة النفط والغاز حيث يتم تخزين الكبريت بعد استخراجه من الهيدروكربونات في وحدات استرداد الكبريت والحفاظ عليها في المرحلة السائلة في درجات حرارة تتراوح من 130 إلى 160 درجة مئوية. تعتبر منشآت تخزين الكبريت المبنية من الخرسانة المسلحة نوع خاص وفريد من المنشآت المعرضة لأشكال مختلفة من التدهور الذي تسببه الكبريتات. تتعرض الخرسانة المسلحة لبيئة شديدة التآكل وتخضع للتدهور المتكرر في فترة زمنية قصيرة وخصوصا للأجزاء المعرضة للغازات الحمضية والابخرة. يقدم هذا البحث تحقيقات ميدانية ومعملية لآلية التآكل الخاصة بهياكل الخرسانة المسلحة المستخدمة لتخزين الكبريت المنصهر. بالإضافة إلى ذلك، فإنه يقدم تحقيقات تجريبية مختبرية لثمانية أنواع مختلفة من الخلطات الخرسانية المعرضة لحمض الكبريتيك في درجة الحرارة المحيطة وكذلك في درجة الحرارة المرتفعة (100 درجة مئوية). يشمل البحث تقييم الخواص الفيزيائية والميكانيكية (قوة الانضغاط، فقدان الكتلة، النفاذية، اختراق الحمض ومعامل المرونة) بالإضافة إلى تحليل المواد بما في ذلك SEM وEDX وXRD وFTIR لعينات الخرسانة قبل وبعد التعرض لحمض الكبريتيك. تم تطوير النمذجة العددية لمحاكات تدهور الخرسانة وتم إجراء دراسة لتقييم دور العديد من عناصر النمذجة المختلفة في تحديد مدى تدهور الخرسانة ومقارنتها بالبيانات التجريبية الفعلية التي تم الحصول عليها مختبريا.

CHAPTER 1

INTRODUCTION

Concrete is an essential structural material that has long been used for the construction of buildings, bridges, foundations, tanks, pavements, tunnels, dams and other structures. Owing to its physical properties and economical use, concrete has been the backbone of any country's infrastructure. It has also been the backbone of the Oil and Gas facilities infrastructures for building more challenging structures exposed to highly aggressive environment. Concrete is subject to various forms of deterioration mechanisms which affects its ability for the intended use and limit its service life. In general, concrete has a low resistance to chemical attacks. The most common forms of chemical attack on concrete are the corrosion of steel reinforcement due to chloride attack and due to carbonation (carbon dioxide), sulfate attack on the concrete, Alkali-aggregate reactions and acid attacks.

Sulfate attack on concrete has been considered one of the major deterioration mechanisms in concrete structures. Sulphates present in soils, underground water and seawater ingress through the concrete, reacts with its components and form expansive compounds. The reaction leads to an increase in volume of the products resulting in disintegration of the concrete matrix. Traditionally, Sulfate resisting cement (ASTM Type V cement) has been specified by international standards for exposure conditions involving high sulphate.

Although various forms of the attack have been investigated extensively in literature, Neville (2004) referred to the existing debate and understanding of the phenomena. Nevil in his review referred to the various opposing researchers' views of the phenomena and emphasized the need for more field-based research/investigation rather than the laboratory research which in his view has already been addressed extensively.

The main forms of concrete chemical attacks classified as sulfate attack are the internal sulfate attack (ISA) and the external attack (ESA). On the other hand, sulfate attack on concrete due to oxidation of iron sulfide, such as pyrite, in the soil, is another form of chemical attack that involves sulphate but largely referred to as an acid attack because sulfuric acid is formed (Cefis 2014).

In the internal sulfate attack (ISA) the sulfate ions are already present within the material through the mixed cement or aggregate. The external attack on the other hand, sulfate from external source penetrate into the concrete through its porous microstructure. Eventually, sulfate will react with hydrated products of the cement leads to the formation of gypsum and secondary ettringite. The product formed increase in volume and exerts an internal pressure resulting cracking and material degradation Cefis (2014).

Another mechanism of concrete deterioration involving sulfate is the sulfuric acid attack. The sulfuric acid reduces the concrete alkalinity, destroying the passivity protecting steel and causing corrosion. Sulfuric acid exists naturally in groundwater or formed in sewage waste water and chemical waste from industrial sources (Hobbs & Taylor 2000, Fattuhi & Hughes 1988) leads to degradation of concrete. Sulfuric acid damage in concrete is durability issue

that affects the life cycle performance and maintenance cost of vital civil infrastructures (Bassuoni & Nehdi 2007).

A special type of reinforced concrete structure exposed to different forms of sulfate attack is the sulfur storage structure, typically referred to as “Sulfur Pit”. Sulfur Pit is an essential part of oil and gas processing facilities where the sulfur after extraction from the hydrocarbons in Sulfur Recovery Units is stored and maintained in liquid phase at temperatures ranging from130 °C to 160 °C.

Figure 1-1: Deterioration of the roof of a concrete sulfur pit structure

The reinforced concrete sulfur pits are exposed to a very corrosive environment and subject to frequent deterioration in a short span of time. Corrosion of reinforcing steel and sulfate attack are prominent forms of deterioration leading to delamination spalling of concrete cover

in the walls and the roof of the sulfur pit. Heavy deterioration is more prominent in the soffit of the roof slab and the upper part of the walls (vapor zone). The extracted molten sulfur contains some moisture in addition to the ingress of moisture from external sources as well as from the steam coil used to heat the sulfur to maintain the liquid phase. The sulfuric acid and fumes, which are formed when the molten sulfur is combined with moisture, in addition to the residual sulfuric acid and gases which remains after recovery process attack the reinforcing steel causing corrosion.

Investigation of a typical sulfur pit (Figure 1-1) was conducted including, visual inspection, carbonation depth, chloride and sulfate content, compressive strength, corrosion potential. Extensive cracking in the upper part of the walls and the bottom of the roof slab have been noticed along with stains and sign of corrosion. Delamination of the concrete cover and Spalling has been noticed at 60% of the roof soffit. Chloride quantities found were within or lower than threshold (<0.08% by weight of cement). The depth of carbonation measured with a pH color indicating solution (Phenolphthalein) on a sample core, revealed significant carbonation covering almost the full depth of the core.

Although a very high sulfur content was identified through the cores extracted from the submerged part of the walls, a significant increase has been noticed the compressive strength of these cores. From the loading prospective, the reinforced concrete structure is also subjected to extreme stresses due to temperature gradient across the concrete walls and the roof slab. This creates tensile stresses which cause micro and macro cracks and provides pathways for more ingress of sulfur/sulfuric acid, and water from external sources (such as ground water, wash water and steam pipes.

Although sulfuric acid attack has been recognized as a major cause of concrete distress, it remains less understood how the distress develop in reinforced concrete structures exposed to molten sulfur along with moisture and high temperature environment typically encountered in oil and gas facilities.

1.1 Research Significance

Sulfur storage reinforced concrete structures are essential part of oil and gas processing facilities and are subject to frequent deterioration which disturb operations and requires frequent shutdown of the facility to conduct repairs. Moreover, it is a very specialized engineering application that has not been addressed specifically in literature before. Providing an understanding of the problem and developing solution will lead to proper specification and construction of such structures with extended service life to minimize repairs and operation interruptions. This will result in great economic benefit to the Oil/Gas operating facilities.

1.2 Research Objective

The objectives of this research are:

- Analyze and understand the exposure environment and deterioration mechanisms of concrete structures subject to molten sulfur.
- Evaluate the performance of various types of concrete subjected to this environment.
- Develop numerical modeling of the sulfuric acid damage mechanism
- Provide recommendations for building sulfur pit structures for the oil and gas industry

The proposed research will further develop the understanding of the mechanisms of sulfuric acid attack by laboratory and field investigating of concrete exposed to molten sulfur/sulfuric acid at microstructural level.

1.3 Research Methodology

The research will be conducted as follows:

- Literature review of the mechanisms of various forms of sulfate attack and analysis of the exposure environment and various loadings present in sulfur pit structures. Focus of the research will be on sulfuric acid attack which is the prominent form in sulfur pit structures.
- Field investigation of actual sulfur pit structures using visual inspection, nondestructive (NDT) and semi-destructive testing (SDT), which include acoustic impact testing, ground penetrating radar (GPR) testing and ultrasonic Impact echo testing. Laboratory testing on field collected samples (Core and powder samples) include chloride content, sulfate content, depth of carbonation, and concrete compressive strength.
- Experimental program will be established to evaluate the performance of eight different types of concrete exposed to sulfuric acid environment. Laboratory investigation of the physical and mechanical properties and microstructural investigation will be conducted to understand the damage mechanism.
- Numerical modeling of the damage will be developed and a parametric study performed to evaluate the role of various parameters in the damage and compared to actual experimental obtained data. In the multi-physics numerical simulation, both

chemical and physical processes taking place through the concrete body can be simulated. In addition, the resulting distress in the concrete and the subsequent cracking could be determined. The model will be validated by experimental actual data.

1.4 Thesis Outline

Chapter 1 provides and overview of the of the problem and the significance and objectives for conducting this research. Also, it provides general plan for the work to be conducted and the methodology followed.

Chapter 2 provides a literature review to develop understanding of the principles behind the behavior of concrete. It starts by an overview about the material composition of cement and various types of supplementary material used in concrete as well as some special types of concrete. This chapter also provide understanding of the concrete composition and its microstructure. This is followed by discussion of the deterioration mechanism of concrete subjected to sulfate/sulfuric acid and previous attempts by researchers to address the problem. Also, the concept of modeling the deterioration mechanism in order to predict damage and determine service life is discussed.

Chapter 3 provides afield investigation of existing sulfur storage reinforced concrete structures. Laboratory testing on samples obtained from the field is conducted to understand the deterioration mechanism.

Chapter 4 is a description of the experimental program set to evaluate various types of concrete materials subjected to sulfuric acid at different conditions. Detail of the materials

used is discussed in addition on the sulfuric acid exposure set up. This chapter also provide detail of the performance monitoring and testing. Results are presented and discussed in chapter 5.

Chapter 6 provide a description of the numerical modeling for the sulfate/sulfuric acid attack on concrete. Parametric study illustrates the effect of the various model parameters on the damage of concrete. Numerical obtained results are compared with experimental data and discussed.

Chapter 7 provides a concluding remark on the research findings and recommended future work.

CHAPTER 2

LITERATURE REVIEW

2.1 Introduction

Concrete is the most widely used material in construction due to its mechanical and chemical properties as well as to its economical use for many applications. Hydration of cement is the primary mechanism by which fresh and hardened concrete obtain its properties. The physical and chemical composition of cement has direct effect on determining the resulting fresh and hardened concrete properties, and determining its resistant to the exposure environment. Supplementary cement materials such as Silica Fume (SF), Fly Ash (FA), Glass Granulated Blast Furnace Slag (GGBFS) have been widely used as partial replacement to cement due to beneficial physical and chemical properties to concrete. Special formulated cement such as Calcium Aluminate cement and Alkali Activated (Polymer) concrete based on the concept of using alkali activators have been proposed for beneficial application is sulfuric acid exposure.

This chapter provides an overview of the chemical composition of ordinary Portland cement and the formed compounds out of the hydration process in concrete. Other cementitious materials such as GGBFS, FA and SF and their beneficial effect and impact on concrete microstructure is discussed in detail. This chapter also provide detail of some special types of concrete proposed in literature for their resistance to sulfate and sulfuric acid such as Alkali Activated (polymer) concrete and Calcium Aluminate concrete (CAC).

2.2 Composition of Portland Cement

Portland cement is produced by chemical reactions at high temperature of raw material mainly limestone and clay and involving calcium oxide (CaO), silica (SiO_2), alumina (Al_2O_3), and iron oxide (FeO_3) to form what is known as clinker which subsequently is pulverized with a small amount of gypsum. Clinker is composed primarily of Tricalcium silicate (C_3S), Dicalcium silicate (C_2S), Tricalcium aluminate (C_3A), and Tetracalcium aluminoferrite (C4AF). Compounds and their corresponding Abbreviations are given in Table 2-1 and Table 2-2 (Mehta and Monterio 2006). Composition of OPC and SRPC cements is presented in

Table ***2-3***.

Table 2-1: Composition of Portland Cement (Mehta and Monterio 2006).

Chemical Name	Oxide Composition	Abbreviated Formula
Tricalcium silicate	$3CaO.SiO_2$	C_3S
Dicalcium silicate	$2CaO.SiO_2$	C_2S
Tricalcium aluminate	$3CaO.Al_2O_3$	C_3A
Tetracalcium aluminoferrite	$4CaO.Al_2O_3.Fe_2O_3$	C_4AF

Table 2-2: Oxides Composition of Portland cement (Mehta and Monterio 2006).

Oxide	Content %
CaO	60-67
SiO_2	17-25
Al_2O_3	3-8
Fe_2O_3	0.5-6.0
MgO	0.5-4.0
Na2O	0.3-1.2
SO_3	2.0-3.5

Table 2-3: Composition of OPC and SRPC cements

ASTM Type	Description	Compound Composition Range (%)			
		C_3S	C_2S	C_3A	C_4AF
I	Ordinary	50-55	15-20	5-12	6-10
V	Sulphate Resistant	40-50	25-35	0-4	10-15

Alite (C_3S) constitute the largest portion of cement, reacts quickly and has the highest impact on the initial set and early strength development of concrete. Belite (C_2S) is the second largest constituent, hydrates slowly and responsible for the later development of strength. Celite (C_3A) on the other hand, is not directly responsible for strength development, but it has an important role is facilitating the hydration process. brownmillerite (C_4AF), contributes has a slight contribution to strength gain and very important role as flux in the manufacturing. (JUMATE 2011).

The hydration process involving the four mentioned cement compounds can be explained by the following reactions.

Alite reaction	$2C_3S + 6H \rightarrow C_3S_2H_3 + 3CH$
Belite Reaction	$2C_2S + 6H \rightarrow C_3S_2H_3 + CH$
Calcium Ferro aluminate Reaction	$C_3A + 3C\underline{S}H_2 + 26H \rightarrow C_6A\underline{S}_3H_{32}$ in absence of gypsum: $2C_3A + C_6A\underline{S}_3H_{32} + 4H \rightarrow 3C_4A\underline{S}H_{18}$
Calcium Aluminate Reaction	$C_4AF + 3C\underline{S}H_2 + 21H \rightarrow C_6(A,F)\underline{S}_3H_{32} + (A,F)H_3$ in absence of gypsum: $C_4AF + C_6(A,F)\underline{S}_3H_{32} + 7H \rightarrow C_4(A,F)\underline{S}H_{18} + (A,F)H_3$

C=CaO, A=$A_{l2}O_3$, $\underline{S}$ = SO_3, H=H_2O

2.2.1 Calcium Silicate Hydrate (C-S-H)

The calcium silicate hydrate phase (C-S-H) constitutes the largest solids volume of hydrated Portland cement paste (%50-60) and considered the most important phase determining the properties of the paste. Its morphology can be described as poorly crystalline. Due to their colloidal dimensions and a tendency to cluster, C-S-H crystals could only be resolved with the advent of electron microscopy and is largely denoted to as C-S-H gel in literature. Its chemical composition depends on various parameters such as the w/c ratio, hydration age, and temperature. Hence, it widely referenced as C-S-H, a notation that does not imply a fixed chemical composition. On complete hydration, the approximate composition of the material may be assumed as $C_3S_2H_3$; this composition is therefore used for stoichiometric calculations.

2.2.2 Calcium Hydroxide

Calcium hydroxide crystals (also called Portlandite) constitutes 20 to 25 percent of the volume of solids in the hydrated paste. In contrast to the C-S-H, calcium hydroxide is a compound with a definite stoichiometry, $Ca(OH)_2$. It tends to form large crystals with distinctive hexagonal-prism morphology. The morphology usually varies from nondescript to stacks of large plates, and is affected by the available space, temperature of hydration, and impurities present in the system. Compared with C-S-H, the strength-contributing potential of calcium hydroxide is limited as a result of considerably lower surface area.

2.2.3 Calcium Sulphoaluminates Hydrates

Calcium sulphoaluminate hydrates constitute 15 to 20 percent of the solid volume in the hydrated paste and, therefore, play only a minor role in the microstructure-property

relationships. It has already been stated that during the early stages of hydration the sulfate/alumina ionic ratio of the solution phase generally favors the formation of trisulphate hydrate, $C_6A\underline{S}_3H_{32}$, also called ettringite, which forms needle-shaped prismatic crystals. In pastes of ordinary Portland cement, ettringite eventually transforms to the monosulphate hydrate, $C_4A\underline{S}H_{18}$, which forms hexagonal-plate crystals. The presence of the monosulphate hydrate in Portland cement concrete makes the concrete vulnerable to sulfate attack. It should be noted that both ettringite and the monosulphate contain small amounts of iron, which can substitute for the aluminum ions in the crystal structure.

2.3 Supplementary Cementitious Materials (SCMS)

Due to their beneficial impact on the mechanical and durability properties of concrete and driven by the need for sustainability, the use of supplementary cementitious materials (SCMs) has been increasing in the construction industry throughout the world. SCMs such as fly ash, silica fume, ground granulated blast-furnace slag (GGBFS) are waste or by-products of other industries and their use can lead to more sustainability in addition to the economic gain. Their beneficial effect on mechanical and durability properties is due to the pozzolanic reactions nature or due to their effect as a filler (Mehta & Monteiro 2006). Use of SCMs has been adopted and encouraged by most international concrete specifications/standards.

Pozzolana is described as a siliceous or siliceous and aluminous material which by itself possesses little or no cementitious value but will, in finely divided form and in the presence of moisture, chemically react with calcium hydroxide at ordinary temperatures to form compounds possessing cementitious properties (ASTM 618). The reaction leads to formation of more CSH and contribute to enhanced strength and pore structure.

$$C_3S + H \xrightarrow{\text{Fast}} C - S - H + CH$$

$$\text{Pozzolan} + CH + H \xrightarrow{\text{Slow}} C - S - H$$

Pozzolanic redaction is a slow reaction which slows the strength development and associated rates of heat liberation. Moreover, it is lime-consuming which enhance the concrete resistance to acidic environments. The reaction products filling effect of capillary makes the concrete matrix less permeable and therefore improves both the strength and durability of concrete. (Mehta 2006)

The specific benefits of SCMs in durability of concrete subjected to sulfate or sulfuric acid environment can be attributed to the reduction in concrete permeability which slows the diffusion of sulfate ions into the concrete, and to the reduction of calcium hydroxide phases which is subject to quick dissolution in acidic environment. (Osama 2013).

In a research study by (Janina 2013), the pozzolanic reaction effect on durability of concrete subjected to sulphate ion containing solution was investigated in microstructure level. The study described the mechanism by silica contained in FA react with calcium hydroxide to form CSH and confirmed the positive effect on reducing permeability and reduction of calcium hydroxide to form more CSH. (Fang 2017) referred to the same benefit in pozzolanic reaction of GGBFS and FA in reducing Ca(OH)2 and calcium aluminate hydrate in the cement paste to form CSH in addition to the filler effect. He concluded that both would lead to denser matrix and reduce ingress of sulfate ions.

2.3.1 Fly Ash (FA)

Fly ash (FA) is a by-product of coal burning, precipitated from the exhaust gases of coal-burning power generation plants (Neville 1996). It is the most widely used SCM in construction products (Siddique 2004; Vessalas 2009). It consists of four major oxides namely; calcium oxide (CaO), alumina (Al_2O_3), silica (SiO_2), and iron oxide (Fe_2O_3). Silica constitute the largest portion (%40-60), followed by alumina (%20-30). Based on the source of FA, the content of iron is found in wide range. And many researchers have reported associated qualities issues due to this variation. (Kumar & Mehrotra 2007, (Noushini, Babaee & Castel 2015, Sarkar et al. 2005; Vessalas 2009; Woolley & Coombs 1996).

FA particles are spherical in shape and have a size in the range of 1μm and 100 μm which has a positive impact on properties of fresh and hardened concrete (Neville 1996, Malhotra, V. M. 1990; Meyer 2009; Siddique 2004).

The beneficial mechanical and durability benefits depend largely on the percentage replacement of cement. Replacement in excess of %30 could have an adverse effect (Aydın et al. 2007) on both short and long mechanical properties and durability

2.3.2 Silica Fume (SF)

Silica fume (SF) is a by-product from the silicon and ferrosilicon industry. The escaping gaseous SiO oxidizes in the submerged-arc electric furnace, condenses in the form of extremely fine (0.03 and 0.3 μm) and spherical shaped particles of amorphous silica (SiO_2), that is highly reactive and accelerate the calcium hydroxide reaction produced by the hydration of Portland cement (Neville 1996). SF has been widely researched and reported to

improve both mechanical properties and durability of concrete (Massoud, Mohamed & Hassan 2003).

2.3.3 Ground Granulated Blast-Furnace Slag (GGBFS)

Blast furnace slag is a by-product generated during the production of iron, classified as an amorphous material. Unlike FA and SF, it has a self-cementing property (CaO calcium content of %35-40 and does not require calcium hydroxide to form cementitious products such as C-S-H. Its particles are angular and have a size around 45μm (Mehta & Monteiro 2005). GGBFS is, known to improves both mechanical and durability properties of concrete. Its low heat of hydration (Meyer 2009) makes it ideal for mass concrete applications. GGBFS was found to improve concrete resistance to sulfate attack. (Higgins and Crammond 2003)

2.3.4 Calcium Aluminate Cements (CAC)

Calcium Aluminate cement (CAC) was initially developed to resist sulfate attack. Unlike Portland cement, the hydration reaction of CAC, doesn't form calcium hydroxide which is the reason it has a better resistance to sulfate and acidic environments and to elevated temperature exposure (Bassouni and Nehdi 2007). The hydration reaction of CAC forms mainly Alumina gel. (Neville 1996). CAC is the product obtained by pulverizing calcium aluminate cement clinker (hydraulic calcium aluminates). It contains monocalcium aluminate (CA) as the principal cementing compound with $C_{12}A_7$, CA, C_2AS, C_2S, as minor compounds. Al_2O_3 in the range of (%50-80) (ASTM C 219).

Evolution of the hydration reaction and products formed are dependent on both time and temperature, causing a phenomenon that is called "Conversion" where the CAC hydrates and gains strength which drops again after some period of time and temperature rise. Initially at a

temperature of 20ºC it will form CAH_{10}, convert to C_2AH_8 between 21 and 30°C, and finally to C_3AH_6 at higher temperature. Under conditions of elevated temperature C_3AH_6 will form which is the most stable and least soluble.

2.3.5 Alkali Activated (Polymer) Concrete

Polymer concrete is based on aluminosilicate rich material (Such as GGBFS, FA) mixed with a high alkaline solution that is usually composed of an alkali hydroxide and alkali silicate (Borges 2016). The aluminosilicate dissolves in the high pH of the activating solution and undergoes a series of chemical reactions that leads to the formation of solidified material, which hardens and develops mechanical strength comparable to or higher than that of Portland cement-based materials (Borges 2016). The final product of the alkaline activation reaction of aluminosilicates, low-calcium or calcium-free materials produces a matrix composed of a Na_2O-Al_2O_3-SiO_2-H_2O gel (N-A-S-(H)), also described as geopolymer gel. On the other hand, calcium-rich activated materials will also produce a CaO-Al_2O_3-SiO_2-H_2O gel (C-A-S-H), resembling the composition of Portland cement paste (C-S-H gel like structure) (Yep 2005). GGBFS is an example of the calcium rich activated material. (Borges 2016). Activation of two components Aluminosilicate materials to ensure more of calcium availability has been reported advantageous due to acceleration of hardening and setting time and improved mechanical properties (Buchwald 2009). (Zhang 2018) reported that addition of slag leads to more compact microstructure in alkali activated concrete. It has been found that incorporating Additional calcium has a profound beneficial effect on enhancing the strength and microstructure of AAC. (Suwan 2014, Pangdaeng 2014, Mehta 2017).

2.4 Material Characterization of Concrete

Characterization is an essential aspect of materials research that involves the determination of the composition and microstructure of the material. Various techniques have been utilized by researchers in the characterization of cementitious materials, the reactions occurring in the cement hydration process, the hardened concrete microstructure and knowledge of the evolution of the different mechanical and durability properties. Many research studies have examined the microstructure of cementitious materials subjected to sulfuric acid (Shamila, 2016). The main focus of the microstructural analysis in these studies has been on the formation of gypsum and/or ettringite in different areas and crack and micro crack formation and their patterns as it can explain changes of mechanical and structural properties of concrete. Each of these techniques describes different aspects of the material. These techniques and the specific purpose of their use are as follows:

- Scanning Electron Microscopy (SEM) and Energy Dispersive X-ray Spectrometry (EDS) provide magnified images and morphology of the microstructure in addition to quantitative estimation of the elemental composition such as Ca, Si, Al and S.
- X-ray fluorescence (XRF) determines the elemental composition of materials in oxides form. Oxides such as CaO, SiO2, Al2O3, Fe2O3 are examples of very important elements of the cementitious material composition that can be detected by this technique.
- X-ray Diffraction (XRD) determines the compounds crystalline phases such as Portlandite, Calcite, Quarts, gypsum, ettringite, CSH, C_2S and C_3S. Phases that are amorphous in nature are difficult to detect by this technique.
- Fourier-transform infrared spectroscopy (FTIR) describes the material composition based on the type of bonds detected.

Scanning Electron Microscopy (SEM) provides microscale imaging using high-energy beam of electrons in a raster scan pattern. Typical sample of SEM-EDS Output, obtained for OPC

is shown in Figure 2-1. Electron beam is generated by a crystal of Lanthanum hexaboride heated by an electric field. The electrons are accelerated by a tension of 20 KV and suitably collimated toward the sample placed in the vacuum chamber. The interaction between the primary electrons and the atoms of the material investigated generates different particles and in particular secondary electrons and X-ray. Secondary electrons are captured by detector and converted into electrical impulses(signals). These signals are transformed in image on a computer monitor. Photons X are used to perform the Energy Dispersive X-ray Spectrometry (EDS). These rays, emitted as a consequence of excitation of the outer electrons of the material, collide with a crystal generating electric currents. The value of the energy allows a qualitative evaluation of the chemical composition of the investigated material portion.

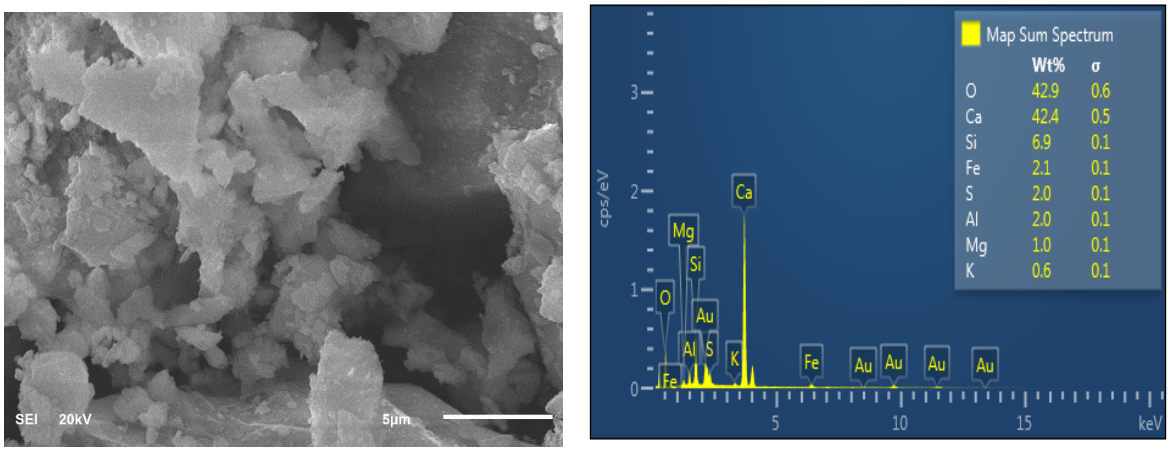

Figure 2-1: Typical sample of SEM-EDS output, obtained for Ordinary Portland Cement (OPC)

X-ray diffraction peaks (XRD) are produced by constructive interference of a monochromatic beam of x-rays scattered at specific angles from each set of lattice planes in a sample and finally, the phases are identified by searching a standard data base (Sharma 2012).

XRF (X-ray Fluorescence). XRF analyzers determine the chemistry of a sample by measuring the fluorescent X-ray emitted from a sample when it is excited by a primary X-ray source.

Fourier-transform infrared spectroscopy (FTIR). The FTIR analysis method uses infrared light to scan test samples and observe chemical properties. FTIR is used to obtain an infrared spectrum of absorption or emission of a solid, liquid or gas. A change in the characteristic pattern of absorption bands clearly indicates a change in the composition of the material or the presence of contamination action, the origin is typically determined by FTIR microanalysis.

2.5 Degradation Mechanism of Concrete Subjected to Sulfate/Sulfuric Acid

Sulfate and sulfuric attack have been discussed extensively in literature and researchers presented different views of the degradation mechanism. Nevil in his paper "The confused world of sulfate attack on concrete" (2004) discussed extensively some of these views and reported that it is not yet a completely understood phenomena. Most of the research conducted was addressing either the sulfate attack or the sulfuric attack on concrete as a separate and different form of attack. One of the best descriptions of the attack was relating the two forms together was provided by Mehta and Monterio (2006) in their book Microstructure of Concrete. They defined the process of sulfate attack as a degradation of concrete resulting from chemical reactions between hydrated Portland cement and sulfate ions from an outside source. The attack can take place in two different forms, the predominant form is determined by concentration and source of sulfate ions (i.e., the associated cation) in the contact water, and composition of the cement paste in concrete. According to the form of attack taking place the damage in concrete will manifest in the form of cracking and expansion (sulfate attack),

or in the form of mass and strength loss (acid attack). In the first, Calcium hydroxide and alumina-bearing phases (C_3A, $C_3AC\underline{S}H_{18}$ and C_4AF) react with sulfate ions in presence of calcium hydroxide converted to form gypsum and subsequently ettringite ($C_3AC\underline{S}H_{32}$) which is 7 times larger in volume than hydrated cement paste.

Cefis (2014) described the mechanism by the sulfates penetration and reaction with CH and CSH to form gypsum which in turn react with aluminates phases to form ettringite. He provided that the kinetic of the reaction depends on the concentration of sulfate, pH of the solution, humidity, temperature and material properties (Cement composition, and in particular aluminate content, pore distribution and diffusivity). Cefis (2014) described the reaction taking place as follow:

$C_4AH_{13}+{}_3C\underline{S}H_2+14H \rightarrow C_6A\underline{S}H_{32}+CH$

$C_4A\underline{S}H_{12}+2C\underline{S}H_2+16H \rightarrow C_6A\underline{S}H_{32}$

$C_3A+3C\underline{S}H_2+26H \rightarrow C_6A\underline{S}H_{32}$

The second form of the attack (acidic attack), manifested by loos of mass and strength is described by gypsum formation as a result of cation-exchange reaction (leaching of Ca^{++} ions as soluble product). It starts with a pH reduction of the system and loss in the stiffness and strength, followed by expansion and cracking, and eventually transformation of the concrete into a mushy or cohesive mass. Both phases of portlandite and CSH in concrete will be attacked. This form of attack was the focus of most of the research conducted on sulfuric attack on concrete. The damage can be characterized by the following reactions, (Salik 2016, Vincke et. al, 2002):

Gypsum Formation $Ca(OH)_2+ H_2SO_4 \rightarrow CaSO_4.2H_2O$

Decalcification $C_3S_2H_3+ H_2SO_4 \rightarrow CaSO_4.2H_2O + C_2S_2H_2$

(Compose 2016) described the sulfuric acid attack by the fact that sulfuric acid diffuses and react with CH to form gypsum which in turn react with calcium aluminates to form ettringite. (Emmanuel 1998) described the sulfuric acid corrosion mechanism for concrete as the result of a combined action of dissolved corrosion caused by hydrogen ion (H^+) and expanded corrosion caused by SO_4^{2-} (sulphate ion). (Men 2018) described the acid effect as $Ca(OH)_2$ (calcium hydroxide) in concrete dissolves in water to form the saturated $Ca(OH)_2$ solution, which produces Ca^{2+} (calcium ion) and OH^- by ionization. Because of the existence of concentration gradient, $Ca^{2+}$and OH^- diffuse into the soaking solution through the corrosion layer from the inner concrete. while H^+(hydrogen ion) and SO_4^{2-} diffuse into the inner concrete. (Dorner 2002) described the acid attack by similar mechanism and added that speed of the corrosion depends on the diffusion rate as well as the reaction rate. Moreover, he reported that phases of concrete will decompose gradually as the pH drop, $Ca(OH)_2$ decompose at a pH of 12.5, Ettringite at pH pf 10.7, CSH at pH of 9, and Aluminate and ferrite hydrates at pH of 4.6, only a silica gel layer remains at pH of 2. The different forms of sulfate/sulfuric acid attack are illustrated in Figure 2-2.

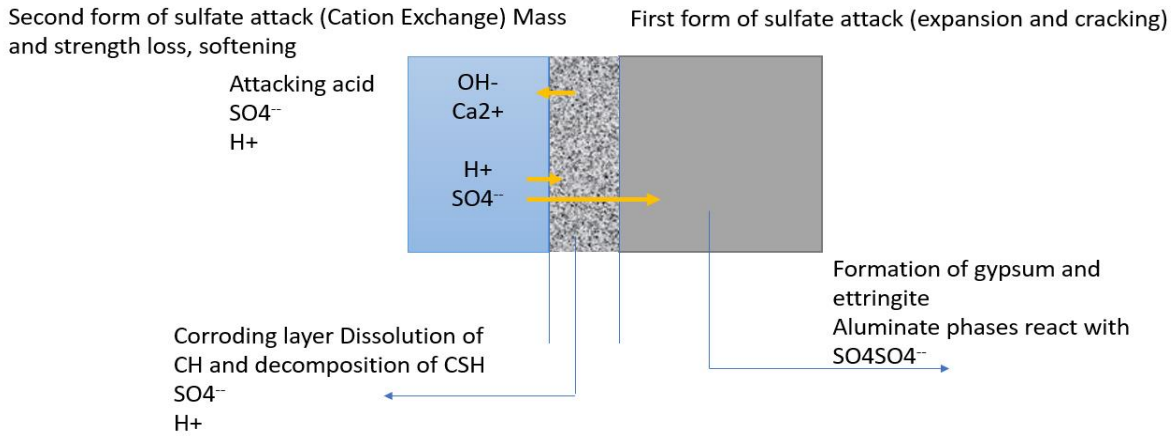

Figure 2-2: Combined Sulfate/sulfuric acid attack

Recent increase in reported attacks by acidic media on concrete structures is due to the growing sources of acidic media resulting from population growth accompanied by increased urban activities and industrialization (Alexander et al. 2013). Acidic environment resulting from the industrial process, natural occurrences and urban activities including agriculture and food production.

Sulfuric acid $H_2(SO_4)$ attack on concrete may be identified by excessive formation of gypsum on (or in) the concrete in contact with the acidic media, gradual disintegration of paste matrix, and consequential loosening of aggregates. Based on the origin of the acid itself, sulfuric acid attacks on concrete can be classified as biogenic/microbial or chemical attack (De Belie et al. 2003; Monteny et al. 2001). The 'biogenic' sulfuric acid attack necessitates the presence of H_2S, moisture, and acidophilic microorganisms to form sulfuric acid (House and Weiss 2014). In contrast, the 'chemical' sulfuric acid attack can originate from acid rain, chemical reaction within the concrete components or simply, accidental spillage of the acid itself. The origin of sulfuric acid can also be labeled as 'external' or 'internal', potentially with different damage manifestations. Alexander and Fourie (2011) described biogenic sulfuric acid attack as moist corroded concrete surface with white slimy corrosion products (sulfate salts of calcium) with corrosion debris and blisters on the surface depending on mixtures designs. Comparatively, in another field study (Tagnit-hamou et al. 2005), petrographic analysis showed direct links between severe deterioration (cracking) of foundations and porches of several houses in Canada after two years of construction and sulfuric acid generated due to usage of pyrrhotite-containing aggregates in concrete. The extent of damage caused by internal attacks are noteworthy and was also reported by other researchers (Rodrigues et al. 2012). Whether or not this softening process is accompanied by expansion, depends on the formation of

excessive amount of gypsum (Torii and Kawamura 1994; Attiogbe and Rizkalla 1988) or 'ettringite' forming away from acidic front (Tagnit-hamou et al. 2005; Monteny et al. 2001). However, given the complex chemistry that makes different cementitious systems unique (e.g. variable amount of portlandite, C-S-H, physical penetrability, and their role in the process).

The corrosion resistance of concrete is dependent on the type and chemical composition of the concrete as well as the pH of the acid under consideration (Dorner H. 2000). Therefore, both the corrosion rate and mechanism of degradation are affected by concentration of the acid along with composition and amount of the hydration products exposed to reaction. Not all the hydration products react with the acids at the same time. Progression of acidic corrosion of concrete is linked to the stability of the components of hydrated cement and reaction products, which depends on the pH level of the attacking media.

2.5.1 Deterioration of Concrete in Sulfur Storage Structure

A special type of reinforced concrete structure exposed to different forms of sulfate attack is the sulfur storage structure, typically referred to as "Sulfur Pit". Sulfur Pit is an essential part of oil and gas processing facilities where the sulfur after extraction from the hydrocarbons in Sulfur Recovery Units is stored and maintained in liquid phase at temperatures ranging from130 °C to 160 °C.

Figure 2-3: Deterioration of the roof of a concrete sulfur pit structure

The reinforced concrete sulfur pits are exposed to a very corrosive environment and subject to frequent deterioration in a short span of time. Corrosion of reinforcing steel and sulfate attack are prominent forms of deterioration. Moreover, the extracted molten sulfur contains some amount of sulfuric acid, in addition to the ingress of moisture from external sources as well as from the steam coil used to heat the sulfur to maintain the liquid phase which react with sulfur at high temperature to form more sulfuric acid. The sulfuric acid gases and fumes have a significant role in accelerating the corrosion process of reinforcing steel (Rahman et. al., 2016). From the loading prospective, the reinforced concrete structure is also subjected to extreme stresses due to temperature gradient across the concrete walls and the roof slab.

2.5.2 Standard Test Methods

There hasn't been any standard test developed specifically to evaluate the performance of concrete in sulfuric acid environment (Girardi & Maggio 2011; Girardi et. al 2010). ASTM C1012 which calculates the expansion of mortar prisms due to sulfate exposure is one such example. The test requires mortar specimens immersed without pH control in %5 Na_2SO_4, and routine measurements of expansion. This test address only the expansive form of the attack without consideration of acid effect. In addition, it only evaluates the expansion of a mortar which doesn't replicate the actual concrete with aggregates. (Girardi & Maggio 2011).

Researchers addressing the sulfuric acid effect on concrete have employed accelerated laboratory testing subjecting concrete specimens to various concentration of sulfuric acid represented by ($\%H_2SO_4$) or its pH. Researchers have conducted observations and testing for various physical and mechanical properties as well as material analysis to investigate the

performance. These include Mass Loss, Visual Appearance, Compressive and tensile strength, corrosion depth and material analysis (SEM, EDX, XRD and FTIR).

Among the studies conducted till date, Fan and Luan 2013; Leemann et al. 2010a; Bassuoni and Nehdi 2007; Ghrici et al. 2007; Gutierrez-Padilla 2007; De Belie et al. 2003; Vincke et al. 2002; Gu et al. 1998) have considered concrete samples while others considered mortar (Chatveera and Lertwattanaruk 2014; Soleimani et al. 2013; Donatello et al. 2013; Makhloufi et al. 2012; Urkel et al. 2007; Okochi et al. 2000; Pavlík 2000; Torii and Kawamura 1994; De Ceukelaire 1992; Chandra 1988)

2.5.3 Code Provisions

The American Concrete Institute specification for concrete based on exposure condition (ACI318, chapter 4) does not include specific category for acid exposure while ACI 201.2R-(2008) provides only very general recommendations.

Canadian standard (CSA 2014), on the other hand, emphasize that both ordinary Portland cement sulfate resistant cements are not resistant to acid or highly corrosive environment. it recommends the use of SCMs, protective coatings, penetrating sealers, or other means for concrete exposed to such environment. The CSA A23.1-14 (CSA 2014) also classifies the sewer pipe (the ‘crown’; most vulnerable part to sulfuric acid attack) as A-XL and limits the requirements for concrete as maximum w/c of 0.4, minimum specified compressive strength of 50 MPa within 56 days, air content of %3-9 based on aggregate size, a certain curing type and a chloride ion penetrability of < 1000 coulombs in 91 days. Thus, both the ACI 201.2R-(2008) and CSA A23.1-14/A23.2-14 (CSA 2014) recommend lower physical penetrability against acid (especially sulfuric acid) attacks.

Similarly, British standards relate the effectiveness of concretes chemical attack resistance to a high degree with their impermeability. The British code specify an Aggressive Chemical Environment for Concrete (ACEC) classification of sites based on the type of ground, water mobility and pH. In section D5.3.2, the code also carefully recommends calcium aluminate cement.

German standard DIN EN 206-1 provide classification (Table 2-4) for the severity of acid attack based on the pH.

Table 2-4: Classification of exposure based on chemical attack per DIN EN 206-1

Property	XA1	XA2	XA3
pH	5.5-6.5	4.5-5.5	4.0-4.5
Severity	Weak	Medium	Strong

2.6 Previous efforts to Improve Resistance of Concrete to Acid attack

For improving the chemical resistance of concrete to sulfuric acid, many researchers have studied the effect of various parameter and properties pf concrete on its resistance to sulfate and sulfuric acid attack. These include the type of cement and the effect of using SCMs, type of aggregate and special types of concrete such alkali activated polymer concrete and calcium aluminate concrete. (Roy et. Al 2001, Shamila 2016, Ehrich et. Monteny et. Al 2001, Vincke et. al, 2002). In this section we discuss the previous attempts of various researcher to evaluate different methods for improving the concrete resistance to sulfuric acid attack.

2.6.1 Effect of Cement type and Content

Many researchers have studied the effect of cement type and content on the performance of mortar and concrete in sulfuric acid environment (Fattuhi and Hughes (1988). Ehrich et. al 1999). The effect of lower C_3A content (Type V) cement on the performance of concrete subjected to sulfuric acid was investigated by Fattuhi and Hughes (1988). The focus of this study was specifically on the acidic form of attack and the main evaluation parameter was on mass stability of the mortar specimens. The results did not reveal any significant improvement compared to that of ordinary Portland cement (Type I) in reducing the mass loss of mortar or concrete specimens. Reduction of the cement content in concrete specimen was found to be beneficial in reducing the deterioration cause by acid.

2.6.2 Effect of Supplementary Cementitious Materials (SCMS)

The effect of SCMs use on the resistance of concrete to sulfuric acid attack is debatable. Some researchers have reported a beneficial effect when SCMs are incorporated in concrete and attributed this to the pozzolanic reaction where portlandite is minimized and more CSH is formed and due to the reduction in concrete permeability (Janina 2013), Durning and Hicks (1991), Mehta (1985). In line with this view Chang (2005), Tamimi (1997) and Girardi et. al (2010), reported similar finding when using SF and FA. Conversely, other researchers reported a negative effect and attribute that to the refinement of capillary pores which allow deeper ingress of the acid ions and higher surface area of reaction. Monteny (2001), Bassuoni and Nahdi (2007)

Several authors reported that the beneficial effect of SCMs in concrete exposed to acid with low concentration, but not when concentrated acids are involved (Attal et al 1992, Santhanam

et al 2003, Glasser et al 2008). Researchers concluded that in general, all the beneficial effects of SCMs in resisting aggressive acidic attack are supposed to be diminished with increase in the severity of chemical attack. Bassuoni and Nahdi (2007), Girardi et al. (2011).

2.6.3 Calcium Aluminate Cement

Calcium Aluminate cement (CAC) was initially developed to resist sulphate attack. Unlike Portland cement, the hydration reaction of CAC, doesn't form calcium hydroxide which is the reason it has a better resistance to sulfate and acidic environments and to elevated temperature exposure (Bassouni and Nehdi 2007). The hydration reaction of CAC forms mainly Alumina gel. (Neville 1996). The final hydration product of CAC is in the form of C_3AH_6 which is the most stable and least soluble which make it ideal for acidic environment.

2.6.4 Change of Aggregate Types

Acid resistant aggregates (quartz) are advantageous in resistance to dissolution but the overall concrete neutralization capacity is reduced. Limestone aggregates on the other hand have more neutralization capacity but subject to higher dissolution ($CaCO_3$). The neutralization capacity provided by the aggregate which dissolves at a slower rate than the paste matrix can result in concrete corrosion rates which are slower than those with acid resistant quartz. (Beddo 2016). Beddo reported that factors such as reaction surface area, grading of aggregates and diffusion can be optimized to increase performance of concrete exposed to acid. Girardi (2011) investigated the effect of aggregate type on concrete resistance to acid and concluded that limestone aggerate demonstrated better performance when compared to natural aggregate.

2.6.5 Variation of Water to Cement Ratio

Because acid specifically attacks cementitious constituents, concretes with a high w/c ratio and a high cementitious volume fraction are more vulnerable to greater mass loss. The effect of reducing the w/c ratio on improving the resistance of concrete to sulfuric acid attack was only significant at lower acid concentrations of %1.0 N. Fattuhi, B. Hughes, (1988). Low permeability was found to have a positive impact on concrete resistance to sulfate attack. Khatri (1997), Young (1998).

2.6.6 Alkali Activated (Polymer) Concrete

Since its early development, alkali activated binders have been widely reported as highly resistant to acid attack (salami et. al 2017). Polymer concrete has shown positive effect in resistance to sulfuric as well as lactic and acetic acids as reported by many researchers (Kaempfer and Berndt, 1998, De Belie et al., 1998, De Belie and Monteny, 1998). Polymer concrete materials improving the resistance of mortar or concrete to sulfuric acid attack in specific (Monteny et. al 2001, Vincke et. al, 2002). In addition to its positive durability improvement effect polymer concrete was encouraged for its environmental effect since it is based on utilization of waste raw materials, such as GGBFS and Fly ash. Few alkali-activated materials have been reported to undergo binder degradation due to acid attack (Pacheco et. al 2014). Shamila (2016) indicated significant better performance of the polymer-based concrete when compared to conventional concrete in terms of mass and compressive strength retained.

Mehta (2017) evaluated sulfuric acid resistance of fly ash based geopolymer concrete with various amount of OPC (0, 10, 20 & %30). Based on Aluminum-silicate bonds, polymer concrete have demonstrated better durability properties in terms of resistance against

aggressive acids and sulfates. The results indicate that the inclusion of OPC improves the compressive strength of fly ash-based polymer concrete significantly.

Ariffin et. al (2013) studied the sulfuric acid resistance of blended ash geopolymer concrete exposed to %2 solution of sulfuric acid for up to 18 months. The study focus was on mechanical properties, mass and changes in chemical composition. Results indicated that geopolymer concrete based demonstrated high resistance to sulfuric acid when compared with ordinary Portland cement. The resistance is attributed to the stronger bonds in aluminosilicate polymer structure.

Some durability aspects of alkali-activated were studied by many researchers. Salami et. al 2017 studies the POFA polymer binder activated by various molarity NaOH subjected to %10 H_2SO_4, HNO_3 and HCl for 9 months. Salami et. Al (2017) found the best performance in term of compressive strength retention in the samples exposure to sulfuric acid as compared to nitric and hydrochloric acids. Bakharev (2005) studied the resistance of fly ash alkali-activated binder subjected to %5 carbonic acid solutions (CH_3COOH) and %5 sulfuric acid (H_2SO_4) for two months. The performance of alkali-activated concrete compared to OPC concrete was found to be superior in resisting deterioration effect of the acid. Similar findings were reported by Thokchom et. Al. (2009) when he investigated the effect of %10 sulfuric acid solution on fly ash-based polymer concrete for 18 weeks. Sreevidya (2012) has also studied acid resistance of fly ash-based alkali-activated mortar for 14 weeks in terms of compressive strength and mass loss. The fly ash-based alkali-activated concrete was reported to be highly resistant against H_2SO_4 and HCL. Similar conclusion was provided out of Ariffin's study for alkali-activated concrete with POFA blended with pulverized fuel ash

exposed to %2 sulfuric acid. The study revealed a better durability performance in comparison to OPC concrete (Ariffinin et. Al. 2013).

Various factors have been reported to influence the mechanical and durability aspects of geopolymer concrete including the quality of the raw materials, their fineness, concentration of the activator and curing conditions. (Huajun et. Al 2013, Rattanasak and Chindaprasirt 2009, Chindaprasirt et. Al. 2009).

2.7 Modeling Deterioration of Concrete

Service life modeling has emerged in the field of infrastructure design to address the challenges associated with decaying structures and to assist engineers in designing structures with specific intended service life. International standards (AASHTO 2013) specification for transportation infrastructure elements, such as bridge decks require minimum 75-year service life. It is not practical to do field testing to monitor and very difficult to anticipate the performance of various/different concrete mix designs (proportions and materials). Therefore, engineers and designers make use of the service life models to support their structural design decisions and satisfy the project demanded service life. Many researchers have investigated the use of numerical modeling to simulate the deterioration of various multi-physics phenomena including chloride ingress, corrosion, and carbonation in addition to the sulfate attack.

Tixier and Mobasher (2003) developed a diffusion-reaction-damage model to simulate the sulfate attack on concrete. The model is based on diffusion of sulfate ions in accordance to Ficks law, coupled with reaction taking place between calcium aluminates (C_3A, C_4AH_{13}, and

C_4ASH_{12}) and sulfate to form gypsum and ettringite. The reaction results in an increase in volume (constitutive response) and subsequently create internal tensile stresses/strains. When these exceed the concrete tensile strength, it cracks and subsequently reduce stiffness. These cracks further increase the diffusion at the crack location (layer). Because of change in diffusivity throughout the depth of concrete, the problem is treated as a moving boundary. Tixier and Mubasher's model has been widely adopted and verified with actual data. Figure 2-4. provide an illustration of the flow of the model progression. model parameters are summarized in Table 2-5.

Table 2-5:Tixier and Mubasher's Model Parameters

Initial Material Properties	Computed material parameters
Geometry of the concrete structure	Mechanical properties
Cement content and composition	Capillary porosity
w/c ratio	C3A and Sulfate content cross the depth
Degree of hydration	Reduced Stiffness
Diffusion, D	Linear Expansion
Sulfate surface concentration	Internal strains
E, F't	
Diffusion of cracked/uncracked (D1/D2)	
Reaction Rate	

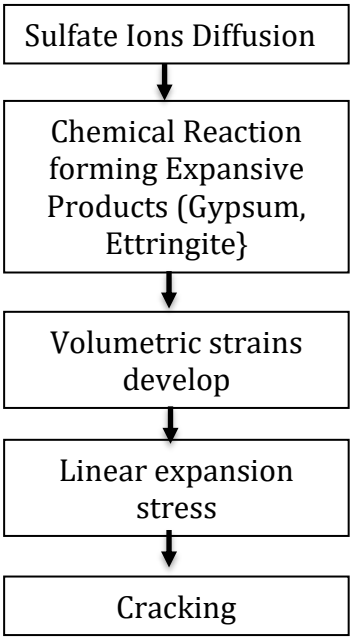

Figure 2-4: Illustration diagram of Tixier and Mubasher model

calcium aluminate phases are represented in the model Pi with i=1-3, and defined as P1=C_4AH_{13}, P2=C_4ASH_{12} calcium aluminate monosulfate hydrate and P3= C_3A. The relative proportions are calculated based on material input data. Volumetric calculations are calculated based on stoichiometry considering the reaction between these phases and sulphate.

$$\frac{\Delta V_P}{V_P} = \frac{(m_V^{C_6A\bar{S}_3H_{32}})^{-1}}{(m_V^{P_i})^{-1} + a(m_V^{C\bar{S}H_2})^{-1}} - 1, \quad \text{with } m_V^k = \frac{d^k}{M^k}$$

where dk, Mk, and mv k are respectively the density, molar mass, and molar volume of a given compound. The reacted and unreacted aluminate phase are denoted as C_{ar} and are calculated as function of time and space. $C_{au}(x,t)$, according to

$$C_{ar}(x,t) = C_a - C_{au}(x,t)$$

Volumetric strain is calculated based on the total reacted Aluminate phases

$$\varepsilon_V^0(x,t) = C_{ar} \sum_P \left(\frac{\Delta V}{V} \right)_P$$

The capillary porosity, ϕ, is calculated from material properties. Capillary porosity plays an important role in accommodating the expansive material. The percentage of this porosity that can be filled is controlled through the input parameter "% of porosity that can be filled with expansive material", the higher this value the more time it will take for the damage to take place. This is incorporated into the model through time delay to the evolution of volumetric strain.

$$\Phi = \max \left(V_c \frac{\frac{w}{c} - 0.39\alpha}{\frac{w}{c} + 0.32}, 0 \right)$$

$$\varepsilon_V^t(x,t) = \varepsilon_V^0(x,t) - f\Phi$$

$$\varepsilon(x,t) = \frac{1}{3} \varepsilon_V^t(x,t)$$

Degradation in stiffness is introduced through a damage function ω applied to the uniaxial strain. In the linear elastic range ω=0, meaning there is no damage. In the non-linear elastic range cracks initiate imposing a damage to the stiffness calculated as function of the crack density ω =16/9*Cd, ε_{th} is threshold strain

$$C_d = 0.16 \times \left(1 - \frac{\varepsilon_{th}}{\varepsilon} \right)^{2.3}$$

$E = E_0 \times (1-\omega)$

In the post peak zone where, maximum stress is reached the damage function is expressed by the relation presented by Nemat-Nasser and Hori (1993).

$$\frac{\sigma}{f_t'} = \sqrt{\frac{\tan(\pi\omega_0/2)}{\tan(\pi\omega/2)}}; \quad \frac{w}{w_0} = \frac{\sigma}{f_t'}\left(\frac{\log(\sec\pi\omega/2)}{\log(\sec\pi\omega_0/2)}\right) - 1$$

Where ω_0 is the accumulated damage at the peak stress. The deformation at peak is w_0 and obtained as $w_0=\varepsilon_p x H$, where H is the gauge length of the specimen and ε_p is the strain at peak. Modulus is calculated as:

$$E = \frac{\sigma}{\varepsilon - \varepsilon_0}, \text{ with } \varepsilon_0 = \varepsilon_p - \frac{f_t'}{E_0}$$

Average expansion throughout the cross section based on average E can be expressed as:

$$\Delta = \sigma_r\left(\frac{1}{E} - \frac{1}{E_0}\right)H$$

Diffusion-reaction based on Fick's law expressed as:

$$\frac{\partial U}{\partial T} = D\frac{\partial^2 U}{\partial X^2} - kU$$

The sulfate concentration (U) is function of both diffusion and reaction. The Numerical solution is obtained using finite difference.

Cefis [11] proposed a diffusion-reaction-damage model in concrete subject to sulfate attack. The model is based on diffusion of sulfate ions and reaction with aluminate phases to form gypsum and ettringite. Volumetric strains develop and lead to damage. Cefis reported various parameters that could affect the reaction and therefore the accuracy of the model. These include the acid effect, concentration of sulfate ions on the surface, temperature and the composition of the concrete (cement content, Aluminates, diffusion, capillary pores).

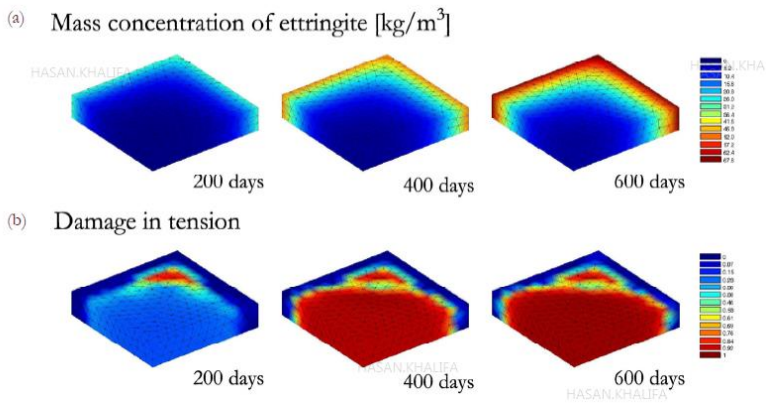

Figure 2-5: 3D Simulation of ettringite formation and mechanical damage Cefis (2014)

Qingke (2015) proposed an extended version of Tixier and Mubasher's model to simulate fly ash concrete. Diffusion-Reaction-damage model. The effect of pozzolanic reaction imposed by fly ash addition was introduced through the chemical reaction model with revised stochiometric calculations for the formation of ettringite and gypsum. Diffusion is based on Fick's law. The model reasonably predicted the linear expansion when compared with field data up to 20 years. However, the perdition after 20 years was much higher.

Yuan et. al (2013) proposed a model to simulate the dissolution of portlandite (CH) and calcium silicate hydrates (C–S–H) based on mass action law. A mechanical damage model based on volumetric expansion due to gypsum formation was considered. As the reaction progress, the porosity of the concrete matrix is decreased and accounted for in the model. The diffusion is based on Nerst-plank equation. Simulation of experimental exposure condition to acid for 90 days at pH of 1did not provide accurate prediction of the damage. Yuan et. al, suggested the need for more accurate prediction of the diffusion of sulfate ions and precipitation of gypsum.

Dorner (2002) introduced a model for the prediction of the corrosion of concrete under acid attack at pH values between 4.0 and 6.5. the model is based on diffusion-reaction and takes in account change in porosity. Reaction considered in the dissolution of the portlandite and CSH phases. Effect of the pH of attacking acid was considered through the rate of the reaction. Liberation of Ca^{2+}, Fe^{3+}, Al^{3+} to the solution was simulated. Diffusion was based on Fick's second law. Beddoe (2016) proposed a modeling following similar approach.

CHAPTER 3

FIELD INVESTIGATION OF SULFUR PIT STRUCTURES

3.1 Introduction

Sulfur pits reinforced concrete structures are subject to aggressive environment involving exposure to sulfur, sulfuric acid, vapor and moisture and elevated operating temperature. The roof slab of the sulfur pit is the primary element, which suffers from major deterioration due to reinforcing steel corrosion. corrosion of reinforcement and spalling of concrete on the underside of the slab have been observed, resulting in severe reduction in load carrying capacity. Figure 3-1 Provides a Schematic sectional view typical sulfur pit structure.

This chapter presents analysis for field investigations of several existing reinforced concrete sulfur pit structures. The scope includes visual inspection and laboratory studies on field concrete samples collected from the structure to investigate the sulfate/sulfuric acid attack on the concrete.

The sulfur pits under assessment have been in service for periods ranging from 4 to 30 years. The sulfur pit is inspected every two years and conventional repair of the deteriorated concrete areas were carried out inside the pit. It is a reinforced concrete structure constructed below grade level consists of retaining wall on the periphery covered with a concrete roof. The layout plan of the sulfur pit longitudinal and transverse sections are shown in Figure 3-2. The overall

length of a typical sulfur pit is about 206.5 feet (63 m) and the width of the sulfur pit is about 48 feet (14.7 m).

The roof slab of the sulfur pit is a flat plate slab supported on column (with capital) in the center and retaining walls at the edges. The clear height of the sulfur pit is 7.5 feet. The reinforced concrete walls and columns are supported on a raft foundation about 18 inches thick. The walls of the sulfur pit are 16-inch-thick and the roof slab is about 15 inches thick. The base slab has reinforcement at the top and bottom. The reinforcement is #7 bars spaced at 10 in c/c both ways. The walls of the pit are also reinforced with 2-layers of reinforcement at the front and the back face. The reinforcement is #8 bars at 8 in c/c in the vertical direction and #7 at 8 in c/c in the horizontal direction both at the front and back face. bars at 6 in c/c at the bottom. The clear cover to the reinforcement on all exposed faces inside the sulfur pit is 3 inches (75 mm). The surfaces exposed to the soil also have 75 mm cover on the reinforcement. At the top surface of the roof slab the reinforcement is at a clear cover of 50 mm.

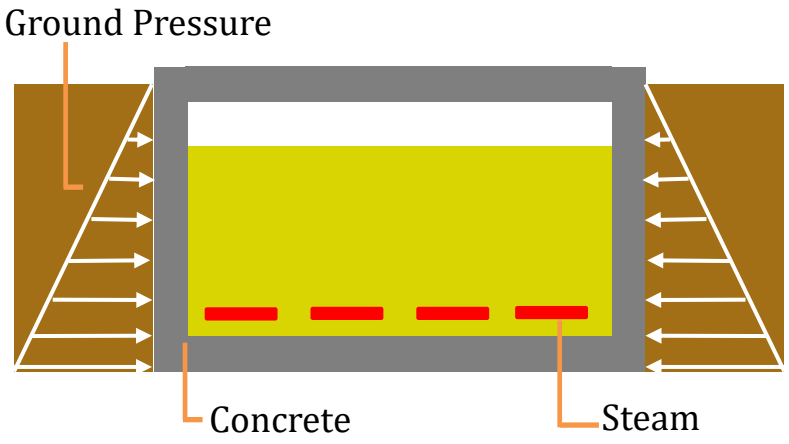

Figure 3-1:. Schematic sectional view typical sulfur pit structure

3.2 Methodology

Field and laboratory studies have been conducted to evaluate the deterioration mechanism. laboratory investigations on the concrete core and powder samples obtained from the walls and slabs of the sulfur pit including visual inspection, compressive strength of concrete, carbonation depth, petrography, chloride and sulfate profile across the depth of concrete elements. Non-destructive testing (NDT) including GPR and impact echo and half-cell corrosion potential. Assessment conducted on sulfur pits SP1, SP2, SP3, SP4 and SP5, SP6 and SP7. Detail of sulfur pits investigated are provided in Figure 3-2.

3-1: Detail of sulfur pits investigated

Sulfur Pit No.	Service Life	Condition	Structural System	Size	Specified Concrete Compressive Strength	Cement Type
SP1	30	Sever	RC Slab (350-400mm) Supported on RC columns and retaining walls (300-400mm) thick.	63x 14x 2.34 m	24.5	SRPC
SP2	30	Sever			24.5	SRPC
SP3	30	Sever			24.5	SRPC
SP4	20	Sever		54.8 x 13.8 x 2.6 m	28	
SP5	30	Sever		63x 14x 2.34 m	24.5	SRPC
SP6	15	Moderate			24.5	SRPC
SP7	4	Moderate			35	SRPC+SF

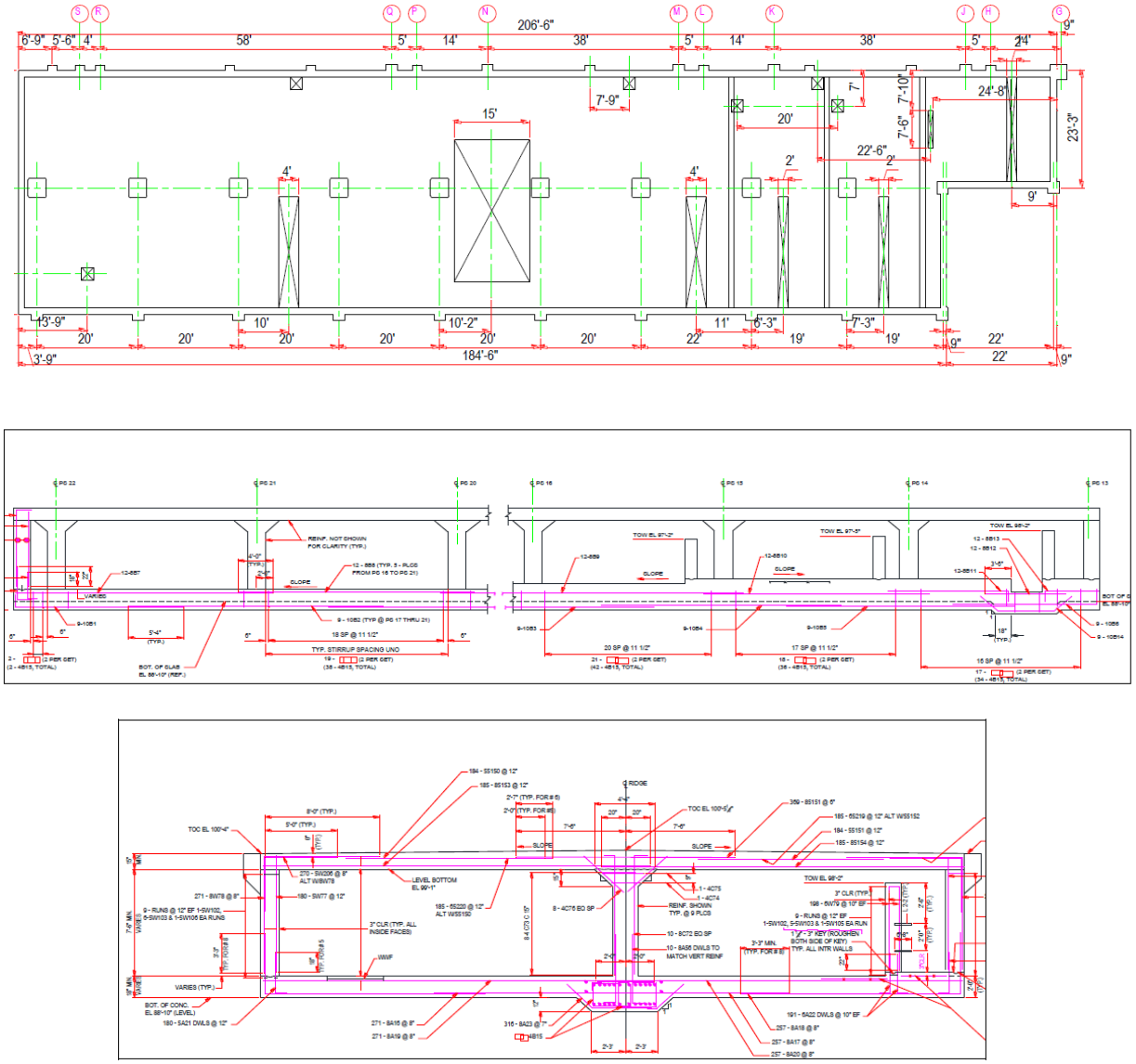

Figure 3-2: Typical Plan view, longitudinal and transverse sections of the SF structure.

3.3 Field Investigation Results and Findings

3.3.1 Visual Inspection and Delamination Survey

A walk-through visual inspection of the roof slab was carried out to record distresses such as delamination and spalling. All the defects observed during the visual inspection were

measured, documented and indicated on the drawings. The visual survey also included photographic evidence of the distresses found in the structural components of the sulfur pit. The delamination survey was conducted by hammer sounding. A hollow sound indicated the presence of delamination. Visual survey for sulfur pits, SP1, SP2, SP3, SP4, SP5, SP6 and SP7 are presented in Figures 3.3-3.9. Mapped cracks and delamination of a typical wall and roof sections are shown in Figures 3.10 and 3.11.

Figure 3-3: SP1 Delamination of the roof slab due to reinforcement corrosion and vertical parallel cracks throughout the walls

Figure 3-4:SP2 Cracking, delamination and bulging at the roof soffit.

Figure 3-5: SP3- Delamination of the roof slab due to reinforcement corrosion

Figure 3-6: SP4 Sever corrosion of the reinforcement specially vapor zone.

Figure 3-7: SP5 Zoom-in view of the bulging of underside of roof slab due to delamination of concrete.

Figure 3-8: SP6 Deterioration on walls of the sulfur pit

Figure 3-9: SP7 Note the horizontal and vertical cracking extending beyond the top layer of reinforcing steel.

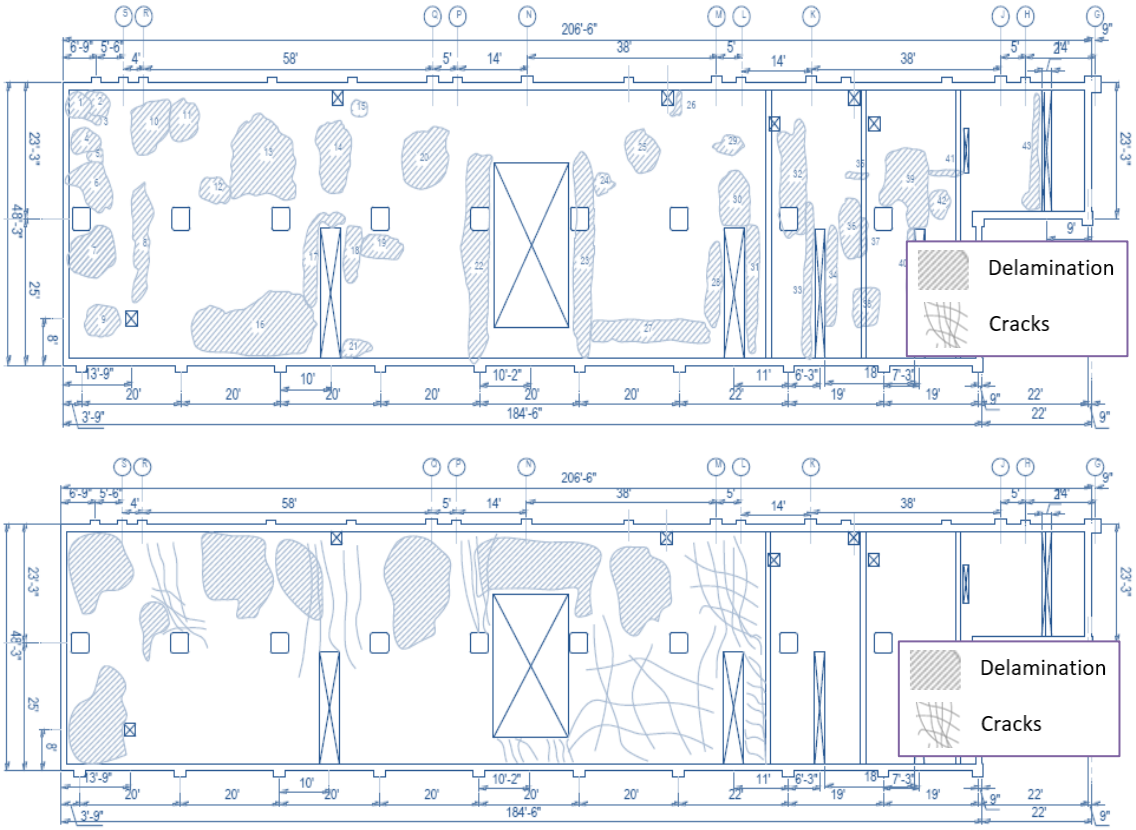

Figure 3-10:sample mapping of cracks and delamination on a) top side of the roof slab and b) the bottom side of the roof slab.

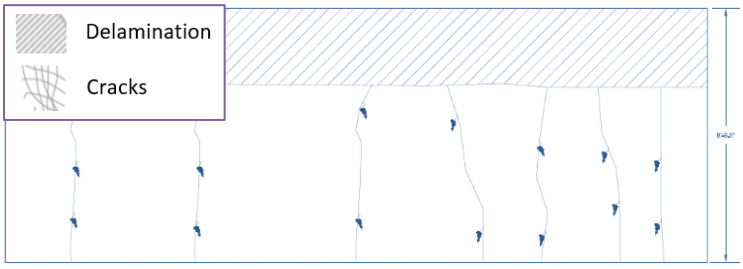

Figure 3-11:sample mapping of cracks and delamination on segment of the wall

3.3.2 Retrieval of Concrete Cores and Powder Samples

Concrete core specimens were obtained from the walls, foundation and roof slab of the sulfur pits for determining the compressive strength and carbonation and petrographic analysis of the hardened concrete in order to determine, cement content utilized in the production of concrete, aggregate gradation and water content. Powder samples by drilling were retrieved for determining the chloride and sulfate profile at selected locations of walls, foundation and roof slab. Before retrieving the cores, steel reinforcement was located using concrete cover meter and core barrel was located in a position to avoid reinforcement in either direction.

Powder samples were collected at each location from various depths. The samples were further crushed to powder passing # 100 sieves. The powder samples were dissolved in acid and hot distilled water and the solution was filtered over a fine filter paper. The filtrate was utilized to determine the acid soluble chloride and sulfate concentration. The chloride concentration was determined by the spectrophotometric method (Vogel 1985) while the sulfate concentration was determined by the method suggested by the American Public Health Association (1985).

3.3.3 Compressive Strength of Concrete

Compressive strength of cored samples was determined according to ASTM C 39. Prior to the testing samples were saw cut on both sides to make the surface smooth capped with the sulfur as illustrated in Figure 3-12. Compressive strength of core samples obtained from the wall, roof slab and foundations are summarized in Figure 3-13: Compressive strength of cores obtained from the walls -3.16.

Figure 3-12: Cored concrete samples after saw cutting and capping.

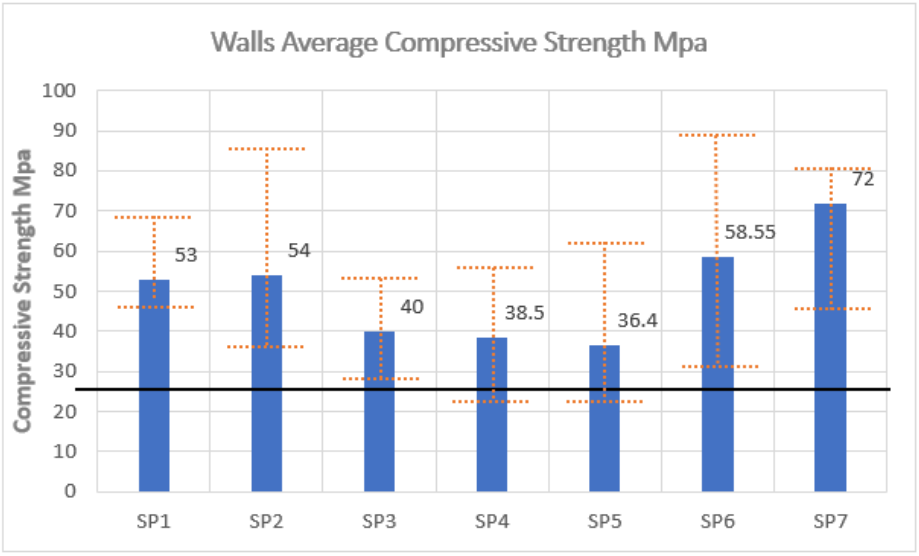

Figure 3-13: Compressive strength of cores obtained from the walls

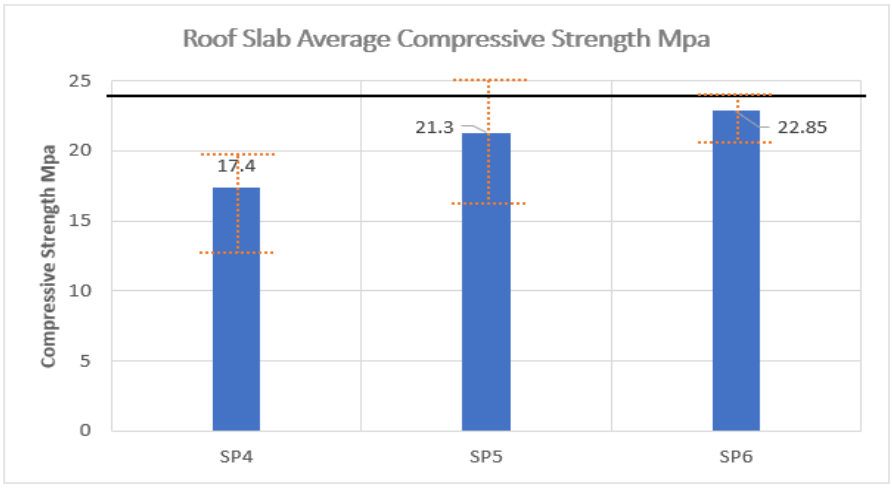

Figure 3-14: Compressive strength of cores obtained from the roof slabs

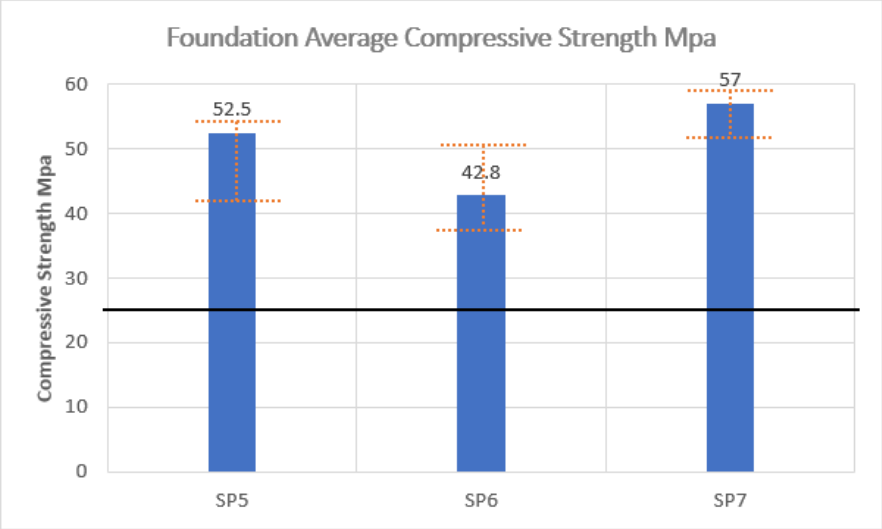

Figure 3-15: Compressive strength of cores obtained from the foundations

3.3.4 Chloride and Sulfate Content in Concrete

Acid soluble chloride content in concrete was measured using the procedure in accordance with ASTM 1152 or BS 1881 Part 6. For this purpose, powder samples were collected from the structural components of the sulfur pit at depths 0-5, 10-15, 25-30, 45-50 and 95-100 mm to obtain chloride content profile at these depths. The powder sample was dissolved in concentrated nitric acid followed by hot distilled water. The contents were boiled to extract bound chlorides, subsequently, the solution was filtered in a flask and the filtrate was made 100 ml. The chloride content was subsequently measured using spectrophotometer. The unit of the values obtained was percent chloride by weight of concrete.

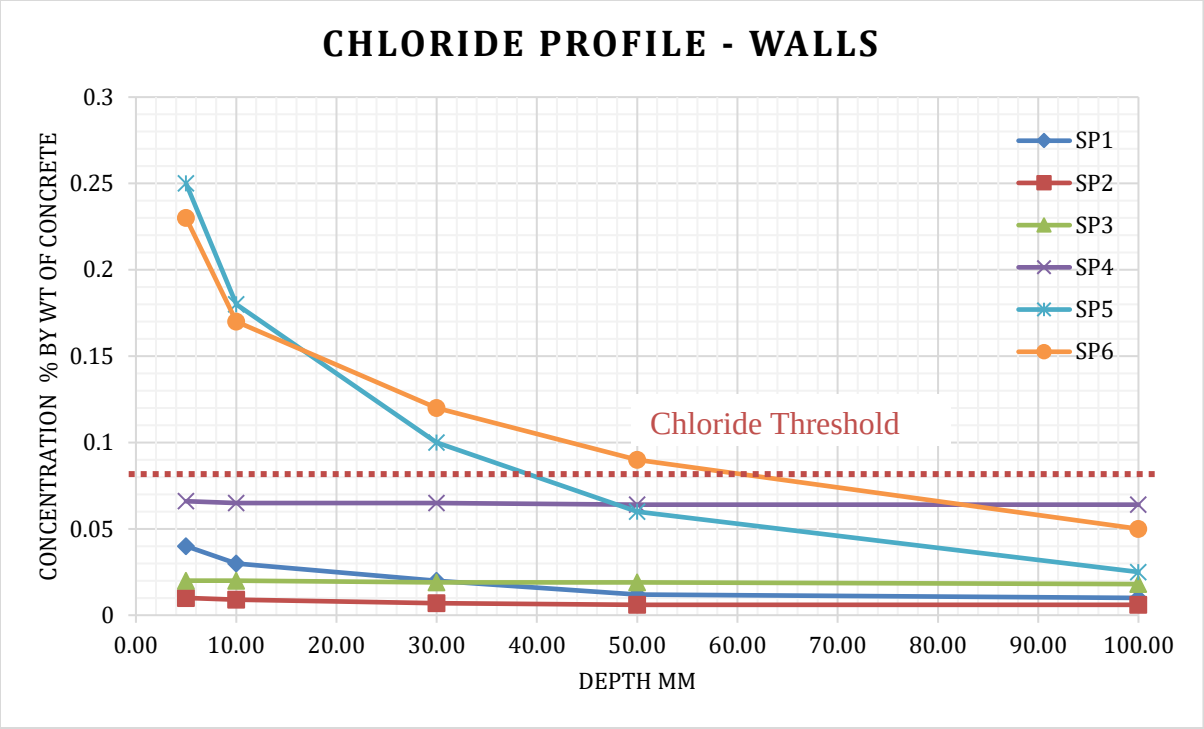

Figure 3-16: Chloride profile for samples obtained from the walls

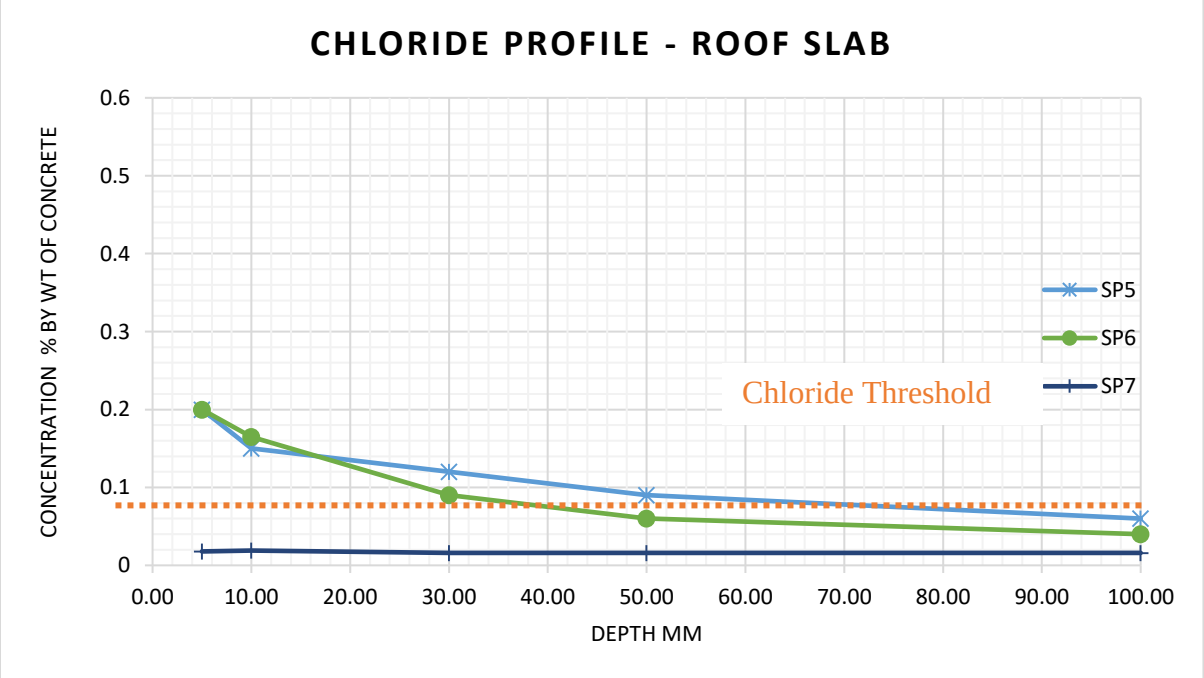

Figure 3-17: Chloride profile for samples obtained from the roof

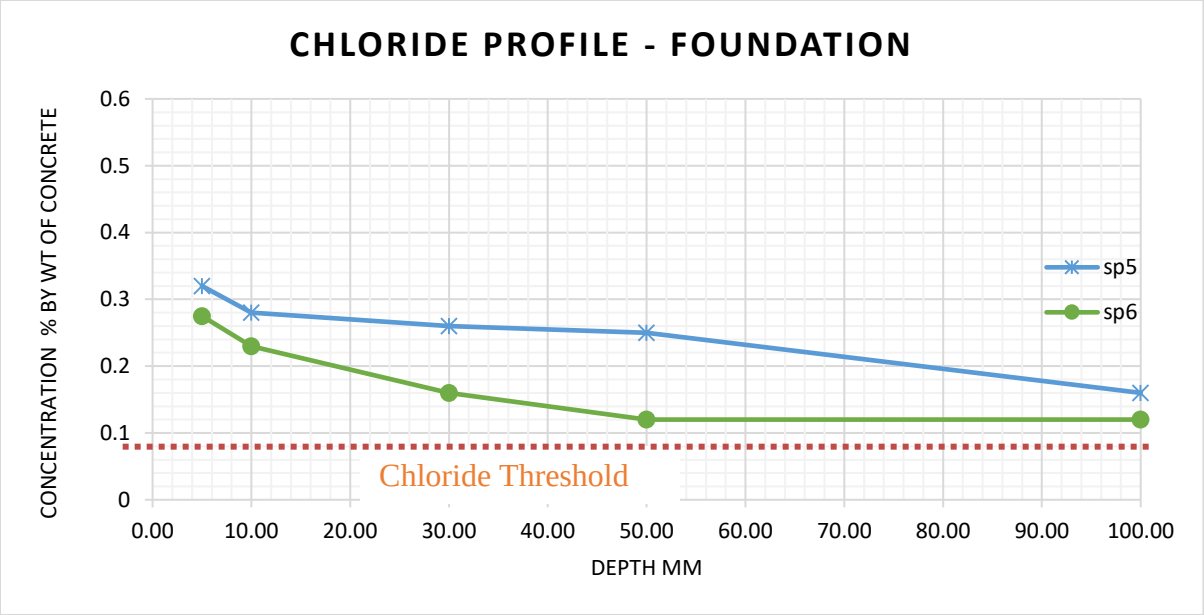

Figure 3-18: Chloride profile for samples obtained from the walls

Chloride profiles were plotted using the chloride contents at various depths to indicate the variation of the chloride concentration in the concrete with depth. The significance of the chloride content in concrete is that passivity of reinforcement in concrete is broken down and corrosion of the reinforcing steel is initiated if chloride exceed threshold value. Thus, chloride content values at the reinforcement level greater than the threshold value indicate whether the steel reinforcement corrosion has initiated. Chloride threshold for corrosion initiation suggested to be in the range of 0.6 kg/m3 Cl^- by weight of cement (%0.08 by weight of concrete). (CEB 1992), (ACI 222.0R 2010). Chloride profiles for samples obtained from the walls, roofs and foundations at different sulfur pits are shown on Figure 3-16-3.18.

Chloride profile for the SP foundations indicates that the all chloride concentration at the rebar level (75 mm from the surface) are higher than the threshold value of %0.08. The chloride concentration at the rebar levels were %0.2 and %0.12 for sulfur pits SP5 and SP6 respectively.

Chloride profile for the SP roof slabs indicates that the all chloride concentration at the rebar level (75 mm from the surface) are less than the threshold value of %0.08. The chloride concentration at the rebar levels were 0.075, 0.05 and %0.016 for sulfur pits SP5, SP6 and SP7 respectively.

Chloride profile for the walls on the other hand indicates that the all chloride concentration at the rebar level (75 mm from the surface) are less than the threshold value of %0.08. The chloride concentration at the rebar levels were 0.075, 0.05 and %0.016 for sulfur pits SP5, SP6 and SP7 respectively.

Similarly, sulfate content of concrete is measured using the filtrate obtained in the same manner and analyzed using spectrophotometer method. In this case the powder is dissolved in hydrochloric acid. A threshold value of %4 sulfate content by weight of cement is used which is equivalent to %0.6 by weight of concrete. Acid soluble sulfate contents were measured at depths 0-5, 10-15, 25-30, 45-50 and 95-100 mm from the surface. Sulfate profile for samples obtained from the walls, roof and foundation at different sulfur pits are shown on Figure 3-19 to Figure 3-21.

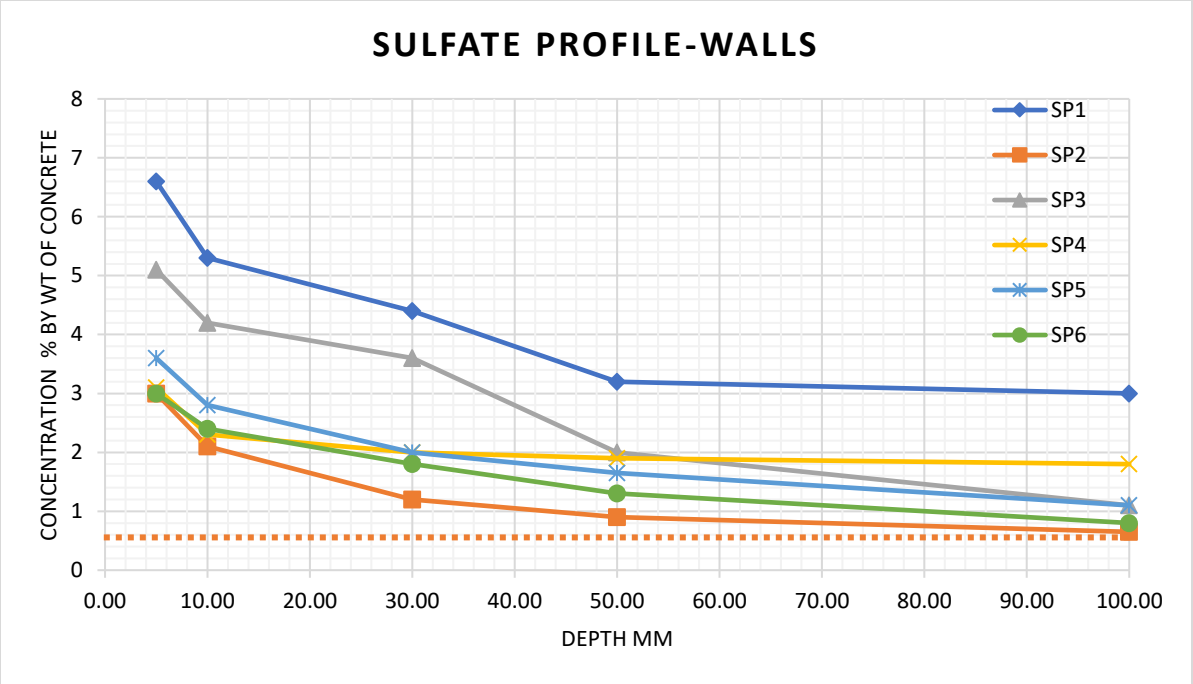

Figure 3-19: Sulfate profile for samples obtained from the walls

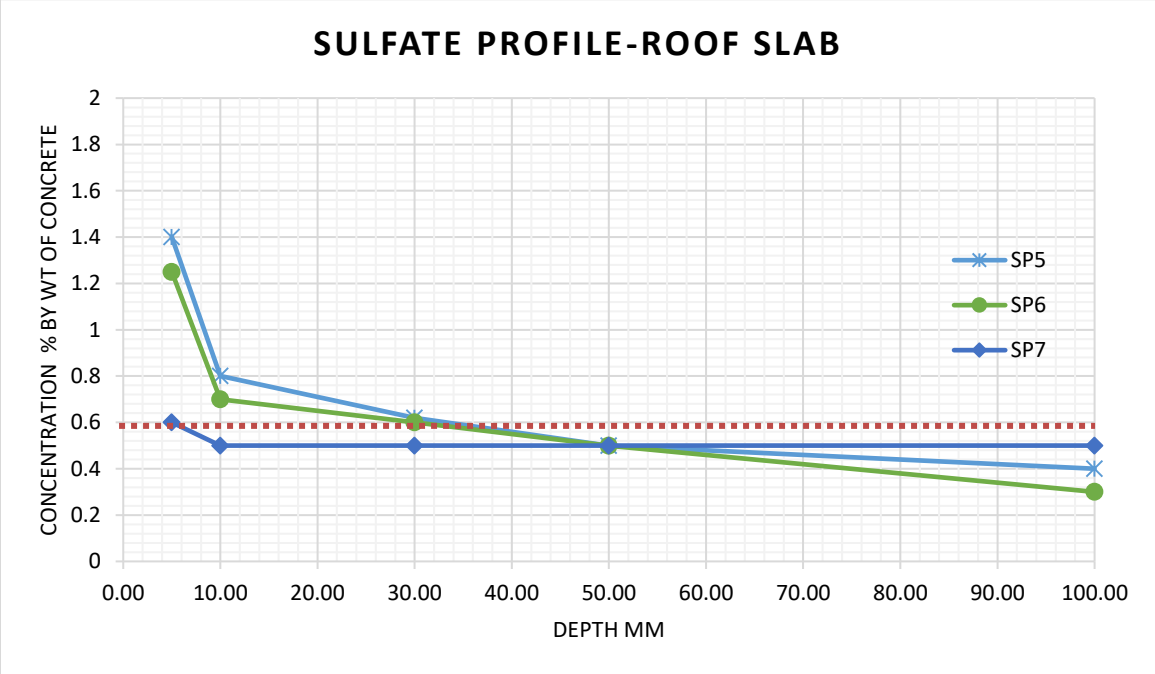

Figure 3-20: Sulfate profile for samples obtained from the roof slab

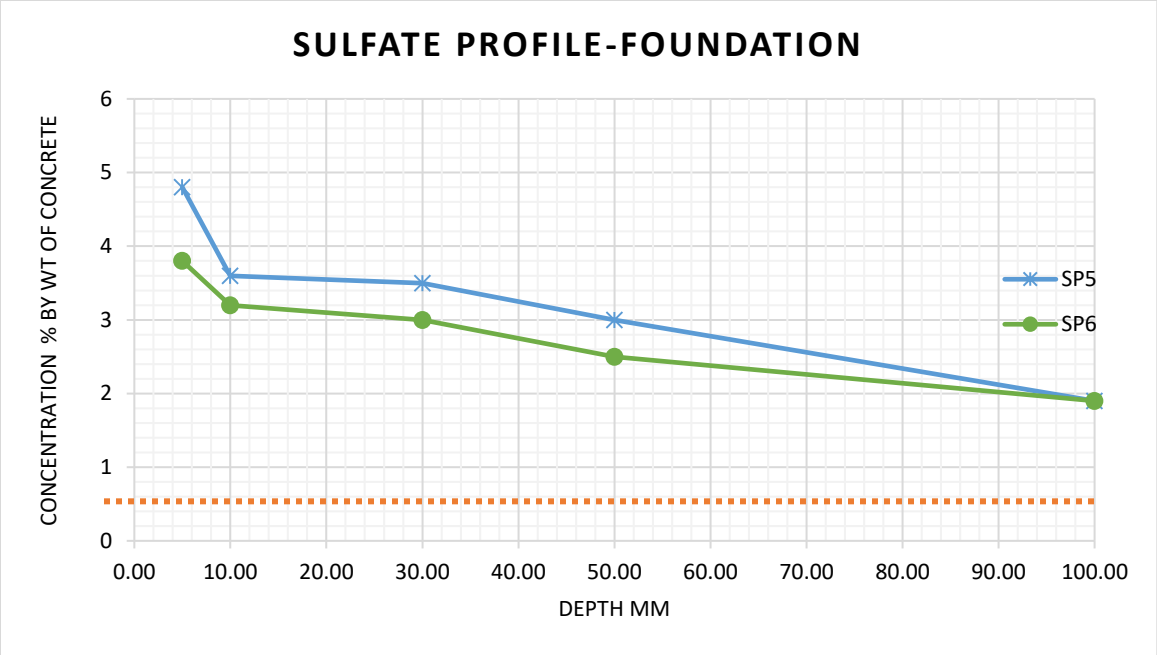

Figure 3-21: Sulfate profile in concrete samples retrieved from foundations

Sulfate concentration reduced as the depth increased from the surface in all the samples collected. A threshold value of acid soluble sulfate concentration of %0.6 by weight of concrete is used in this study. The sulfate concentration was very high on the surface at all collected specimens collected from the walls. The concentration was of the order %6.6, %3.0, %5.1, %3.1, %3.6 and %3.0, respectively, in the walls for SP1to SP6 respectively. This shows that the sulfate concentration on the surface was about 5-10 times the threshold value of %0.6 by weight of concrete. Even though the sulfate concentration reduced with the depth, it remained higher at all levels as compared to the threshold concentration. Similar results were observed for the foundation. This result show that there exists a potential threat of sulfate attack to the cementitious matrix of the concrete.

Sulfate concentration at the bottom surface of the roof slab was found to be %1.4 and %1.25 by weight of concrete for SP5 and SP6 respectively. It is much higher than the threshold

concentration. Concentration at the rebar levels were marginally less than threshold values at %0.45 and %0.4. this is attributed to the fact that slabs are not in direct contact to molten sulfur like the walls and the foundations.

At the surface of the foundation the sulfate concentration was %4.80, %3.8 and %0.6 for SP5 to SP7 respectively. As the sulfate concentration at different depths in the foundation is very high, there exists a strong possibility of sulfate attack occurring to the cementitious matrix of foundations.

3.3.5 Corroded Layer of Concrete (pH Drop)

pH of concrete was measured by spraying phenolphthalein indicator on the freshly cut concrete surface. The area on the surface shows no color change has a pH less than 10.0 while the areas with higher pH exhibit pink color (Figure 3-22). The depth from the surface of the area showing no color change was measured and reported depth in millimeters. The test was done on the surface of freshly cored concrete specimens on the field immediately after retrieving.

Figure 3-22: Phenolphthalein indicator on the freshly cut concrete surface

The depth at which pH dropped below 10.0 was measured on the cores taken from roof slabs. Measurement was taken on the site as soon as the cored sample was retrieved by spraying phenolphthalein. The depths at which pH dropped below 10.0 are provided in Figure 3-23.

pH drop below 10.0 at the rebar level in the core retrieved from the roof slabs at SP3 and SP4. The concrete cover to the reinforcement is about 75 mm (3 inch) in these components.

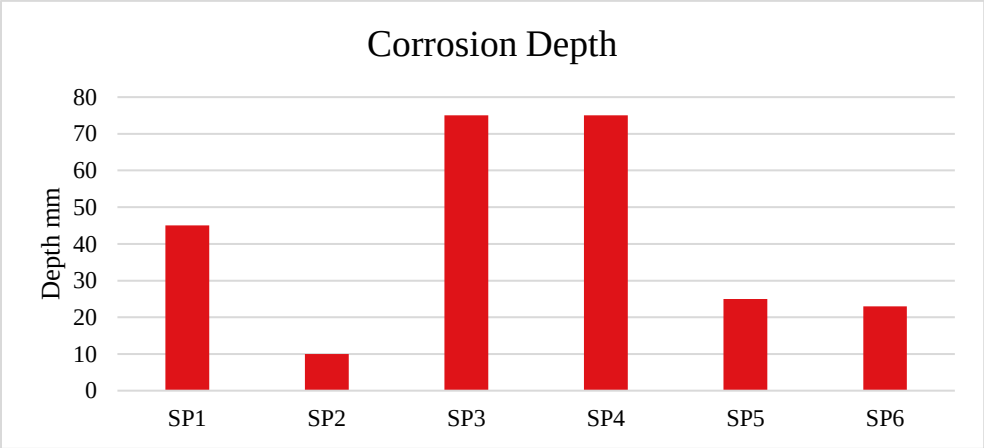

Figure 3-23: Corrosion depth of concrete samples retrieved from roof slab

3.3.6 Ultrasonic Impact ECHO

Ultrasonic impact echo technique is used to detect flaws in the hardened concrete such as, delamination, cracks, honeycombing and voids. The ultrasonic impact echo measurements were carried out on roof slabs at a predetermined grid spacing of 2 feet in both horizontal and vertical directions. Ultrasonic impact echo technique is based on the propagation and reflection of shear waves using 50 kHz transducers. The antenna has dry contact transducers in an array divided into two groups one transmitting the waves and the other receiving them. The average signal recorded by receiving transducers is stored in the hand-held digital touch screen unit as a time domain waveform presented as a 2D picture. The results of impact echo tests were plotted in a 2D format and the irregularities in the concrete were identified based on the shear wave intensity as shown in Table 3-2.

Table 3-2: Criteria for concrete quality based on shear wave speed.

Speed (m/s)	Concrete Quality
X<2000	Bad
2000>X>3000	Moderate
3000>X>4000	Very Good

Impact Echo contours of a sample roof slab (SP5) is presented in Figure 3-24**.** The contours show very weak reflection of the shear waves around the openings. On the contrary, as we move from the openings the shear wave reflection was stronger. This shows that the concrete around the opening is weak and, in some cases, it may be delaminated. The shear wave velocity in these regions was in the range of 200 to 800 m/s. In the sound areas, the shear wave velocity noted was more than 2000 m/s indicating that the concrete is in good condition. The yellow colors indicating very good quality concrete can also be seen (> 3000 m/s). The ultrasonic impact echo results are in good agreement with the hammer survey carried out to determine delamination of concrete.

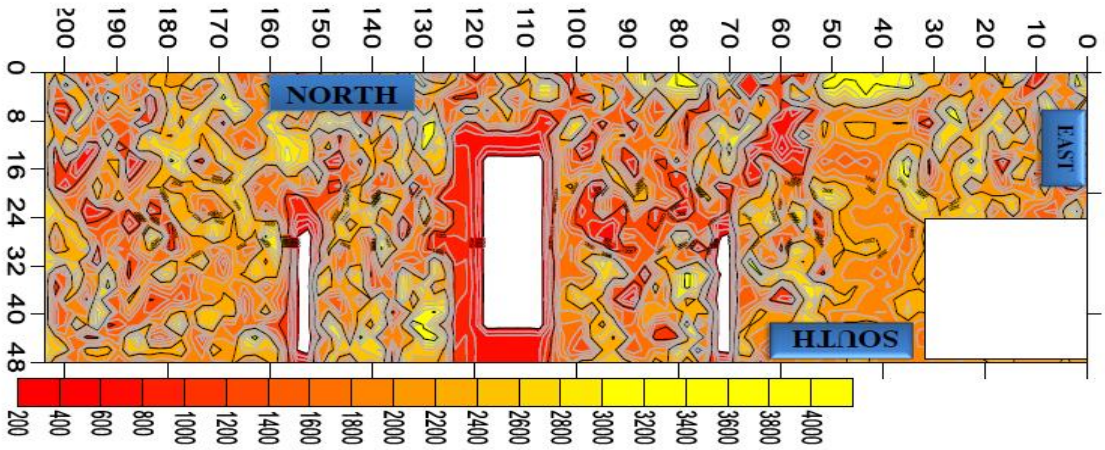

Figure 3-24: Impact Echo contours of roof slab SP5.

3.3.7 Corrosion Potential

The potential monitoring is the most commonly used method for detecting reinforcement corrosion in concrete structures based on ASTM C876. The corrosion potentials were measured at a grid spacing of 2 x 2 feet, both in the longitudinal and transverse directions on the top of the roof slab. These measurements provide information on the state of passivity of the reinforcing steel. Interpretation of the half-cell potential values, vis-a-vis the corrosion status, is shown in Table 3-3.

Table 3-3:. Corrosion potential and their interpretation according to ASTM C876.

Potential, V (Vs $Cu/CuSO_4$)	Probability of Corrosion
<-0.35	>95 %
-0.20 to -0.35	approx. 50 %
>-0.20	< 5 %

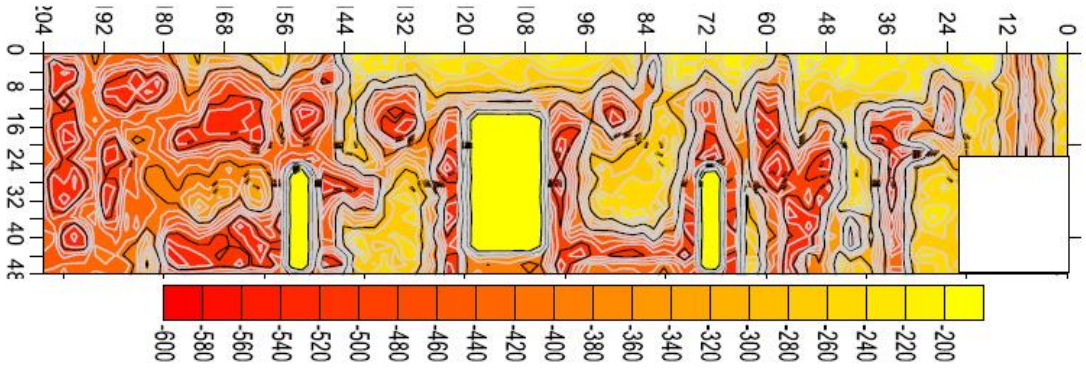

Figure 3-25: Corrosion potential mapping for roof slab SP5.

The corrosion potential measurements carried out on a typical roof slab (Figure 3-25) were more negative than the threshold value of -350 mV (Max -500 mV) in wide areas indicating high probability of corrosion throughout the roof slab and more prominent around the openings. The contours show that the western portion of roof slab has higher potentials.

Higher potential indicates that there is an active corrosion of reinforcing steel in these areas particularly near the openings and in some areas away from it. This is also manifested by cracking and delamination of concrete. Corrosion potentials recorded were less negative than the threshold value of -350 mV in many areas, indicating that the reinforcing steel in these areas is still in passive state of corrosion.

3.3.8 Ground Penetration Radar Survey

Ground Penetrating Radar (GPR) is an effective method for mapping the subsurface anomalies up to a depth of 5 meters. These anomalies show electrical properties that are distinctive compared to the surrounding media. The GPR emits a short duration electromagnetic (EM) pulse from a transmitter antenna, which propagates in the subsurface until it encounters a material having different electrical and magnetic properties, resulting in partial reflection of wave recorded by a receiver antenna. The other part of the wave refracts to the next media according to the Snell's law. The receiver antenna is recording the amplitude of the reflected waves and their traveling time which can be transformed into depth if the EM wave's velocity is known. The velocity is known for common materials but can also be calculated from diffracted waves. As compared with other geophysical methods, GPR has many advantages, including lightweight and portability. One major limitation of the application of GPR in concrete testing is the depth of penetration versus resolution.

The GPR employed in this project is a high frequency 1600 MHz GPR, which can penetrate into the concrete to a depth of 500 mm. The overall thickness of the roof slab is 400 mm. GPR was also used to locate reinforcement in the concrete slab before extracting cores. The GPR

scans 2D and 3D were carried out at accessible places on the top of the slab. The GPR data was processed using RADAN software.

After the visual observations, accessible rectangular areas were identified and lines were marked to conduct survey with GPR. In each area GPR line scans were run two feet apart and analyzed to identify any anomalies in the substrate.

The GPR survey scans of the roof slab were conducted using Structure Scan Mini Radar from GSSI and the data was analyzed using RADAN software. The subsurface anomalies shown in Figure 3-27. Figure 3-26 presents a mapping of the corrosion over the roof slab. Dark red colored contours indicate severe reinforcement corrosion, whereas, yellow and green represent moderate and no corrosion, respectively. According to these results, severe to moderate corrosion of reinforcing steel noted on the slab. These results are in good agreement with the other non-destructive techniques. GPR clearly identifies the corrosion state of the top reinforcement in the slab.

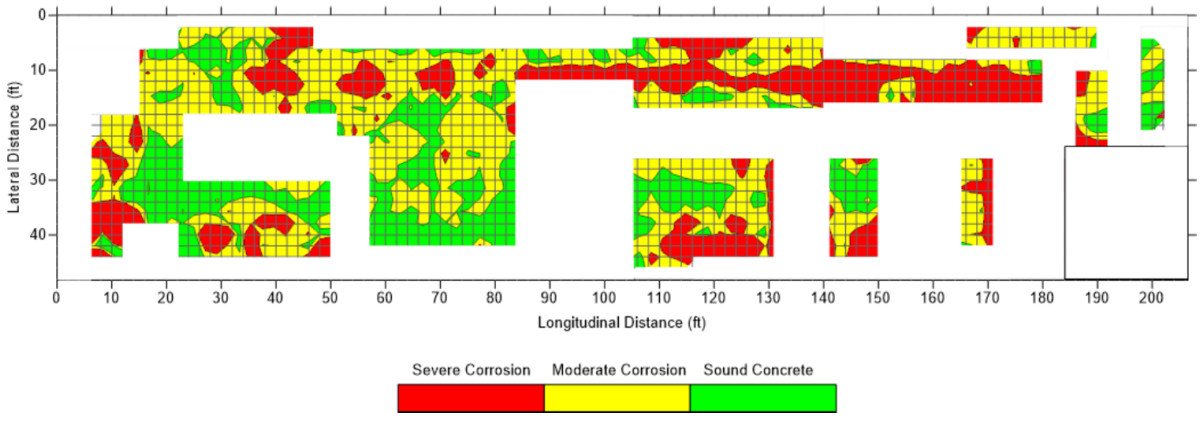

Figure 3-26: Estimated corrosion of reinforcing steel of the roof slab with GPR (white areas are either opening or inaccessible) SP5.

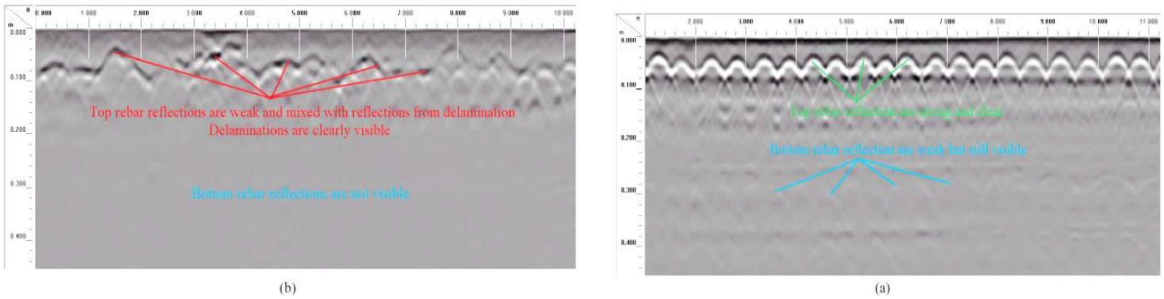

Figure 3-27: Reflection from a) normal and b) corroded reinforcing steel with GPR

GPR survey, impact echo as well as corrosion potential mapping suggested delamination due to corrosion of reinforcing steel at several locations at the top of the roof slab. GPR and other techniques provide an excellent indication of the reinforcement corrosion and delamination in the top reinforcement of the roof slab. It does also give an indication of deterioration in the bottom reinforcement in only the locations where the top layer of the steel is not corroded. A mapping of repairs carried out on the roof slab shows that in many locations they exist at the same location as the top slab.

3.3.9 Petrographic Analysis of Concrete

Specimens extracted from the vapor zone and the from submerged zone (bottom of wall) were subjected to petrographic examination according to ASTM C856. The petrographic examination of the hardened concrete was performed to determine, aggregate gradation, water to cement ratio and cement content. The hardened concrete cored specimens from the West wall, outer and inner surfaces of concrete specimens extracted from the cores are shown in Figure 3-28.

Figure 3-28: Sample retrieved from the west wall for petrographic examination

According to the results of the petrographic examination of the hardened concrete the following are the observations:

1. The coarse aggregates are moderately hard, light brown/cream LIMESTONE, including detrital quartz grains (partially coated by iron oxides/hydroxides) and opaque minerals. Some of the limestone aggregate particles exhibit evidence of calcination.

2. The course aggregate particles, particularly those near the outer surface (those within the outer 100 mm) exhibit internal stress cracks and regular sulfur infilled cracks.

3. The fine aggregate are natural sand, 4.75 mm nominal maximum sized, subrounded to sub-angular, evenly distributed and randomly orientated particles. Fine aggregate particles, particularly those near the outer surface (those within the outer 100 mm) regular sulfate infilled cracks.

4. The concrete exhibited multiple sub-parallel cracks running through both the cement matrix and coarse aggregate particles. Most cracks are infilled with hardened sulfur, although some cracks are still open. It is likely that the cracks could result from a combination of sulfate

attack, extreme temperature gradient and stresses, and cracks resulting from reinforcement corrosion (Figure 3-29).

5. The outer surface of the concrete exhibited a surface coating that appears largely intact.

6. The inner (fracture) end surface of the core exhibited a white sulfur coating. More probably, it is due to the formation of the gypsum.

7. The air voids are 3 mm maximum, typically <2 mm sized, irregular, evenly distributed and randomly orientated entrapped air voids. The estimated excess void is %0.5.

8. The cement pastes typically exhibited low micro porosity, indicative of an overall original water/cement ratio in the low range. It is likely that the high temperatures that the concrete has been subject to have driven off some of the pore waters.

9. The uncarbonated cement matrix exhibited rare, small sized, portlandite crystallites that were evenly distributed. It is possible that the intense temperature that the concrete has been subject to has led to dehydration of any original portlandite.

10. The outer surface of the concrete was coated by a multi-layered coating (approximately 2mm thick). The coating appeared to comprise crushed igneous rock fragments bound by a cementitious binder. The binder was well-bonded to the underlying concrete, although it did de-bond during the thin-section making process.

11. Figure 3-30 shows the photomicrograph obtained from the concrete cores. Cracks through the cement matrix, coarse aggregate and fine aggregate filled with sulfur is clearly evident.

The petrographic examination of concrete shows nominal 19mm, crushed limestone/dolomite coarse aggregate and quartzitic sand fine aggregate, bound by a probable Portland-type cement matrix. It is likely that the dark color of the cement matrix is the result of chemical alteration and some degree of polymerization. The coarse aggregate particles, particularly those near the outer surface (those within the outer 100 mm) exhibit internal stress cracks and also regular sulfur infilled cracks. The concrete exhibits multiple cracks and air voids infilled with sulfur that run sub-parallel to the outer surface. These cracks run through the cement matrix and coarse and fine aggregate particles. The cracking, could be a combination of sulfate attack, extreme temperature gradient and stresses, and cracks resulting from reinforcement corrosion. The outer surface of the concrete exhibited a surface coating that appears largely intact. The inner (fracture) end surface of the core exhibited a white sulfur coating.

Figure 3-29: View of the core extracted from the West wall of SP5 showing multiple cracks

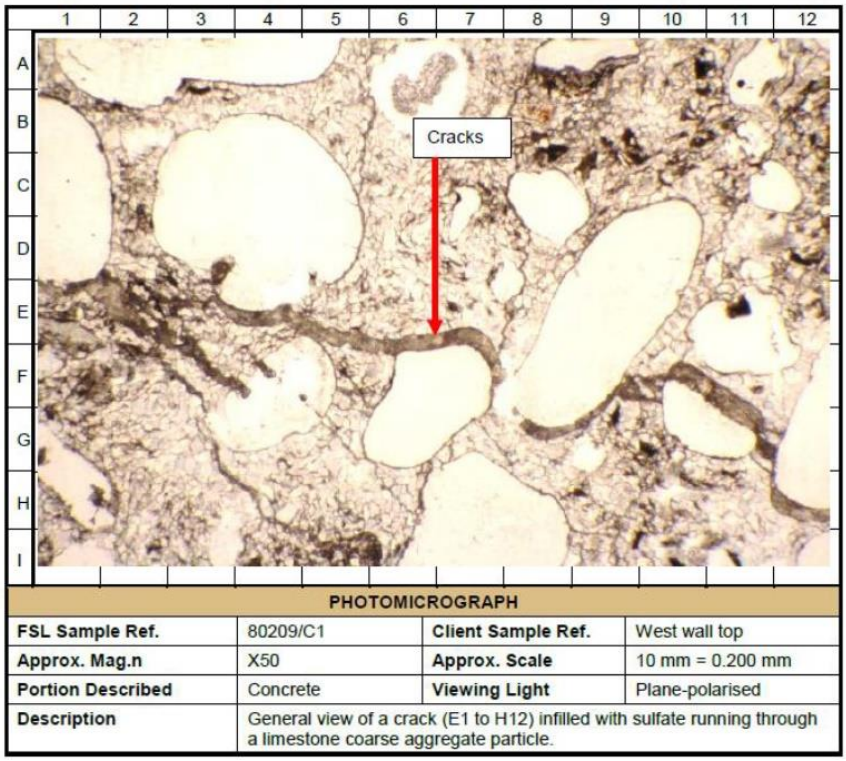

PHOTOMICROGRAPH			
FSL Sample Ref.	80209/C1	**Client Sample Ref.**	West wall top
Approx. Mag.n	X50	**Approx. Scale**	10 mm = 0.200 mm
Portion Described	Concrete	**Viewing Light**	Plane-polarised
Description	General view of a crack (E1 to H12) infilled with sulfate running through a limestone coarse aggregate particle.		

Figure 3-30: Petrographic analysis indicating crack filled with sulfur running through limestone

3.4 Concluding Remarks

Visual surveys indicate sever deterioration on the sulfur pits structures mainly in the form of cracking, delamination and active corrosion. The deterioration mechanism is different between the walls, roof slab and the foundation. Considering the walls, tests indicated high sulfate content in concrete (5-10 times allowable), however there has not been wide damage in the form of expansion typically associated with sulfate attack. In all sulfur pits surveyed the walls have similar pattern of cracking parallel lines that are caused by thermal expansion as the structure is subjected to elevated temperature of 130-160^{o}C. similar observations have been found for the foundations. In both foundations and walls the compressive strength has

increased significantly due to ingress of sulfur (densification of the matrix) reaching 4 times the original specified concrete compressive strength (24.5MPa).

Roof slab is the part which has undergone extensive damage in almost all the sulfur pits in the form of cracking, delamination and active corrosion. Visual as well as hummer sounding and impact echo all have indicated delamination which has been confirmed after removal of part of the roof slab (Figure 1-1). The removed part has also confirmed the active corrosion which reduced the reinforcing steel by more than %50 and caused delamination due to expansion. The chloride level is typically known to be the major cause of corrosion in reinforced concrete structures, however it was within allowable limits at the roof slabs. The second well known contributor to corrosion is carbonation (carbon dioxide and lead to the formation of calcium carbonate $CaCO_3$). Carbonation reduces the pH value of the concrete matrix and destroy the passivation around steel reinforcement which leads to corrosion. However, carbon dioxide is not expected to be present in a sulfur storage tank. Also, petrography analysis did not indicate formation of $CaCO_3$. This brings the investigation toward another source that might leads to reduction of the pH value in the concrete matrix. Among the components of the molten sulfur there exist certain percentage of sulfuric acid as a residual from the recovery process, in addition to the acidic gases and fumes that could possibly be the cause of this pH reduction. At elevated temperature and in the presence of moisture and molten sulfur more of this sulfuric acid fumes might form. This has been supported by the fact that most of the damage has been observed in the roof slabs as well as the top part of the walls.

This research is intended to investigate the damage caused by sulfuric acid at both normal and elevated temperature on eight different types of concrete incorporating the use of sulfate resistant cement, Calcium Aluminate Concrete, SCMs and Alkali Activated Concrete.

CHAPTER 4

EXPERIMENTAL PROGRAM

4.1 Methodology

In this experimental program the performance of eight different types of concrete will be investigated in accelerated testing by exposure to sulfuric acid at different conditions over a period of 12 weeks. The concrete types investigated are Ordinary Portland Cement (OPC) and Sulfate Resistant Portland Cement (SRPC), Supplementary Cement Materials (GGBFS, FA, SF), Alkali Activated Polymer Concrete, Calcium Aluminate Concrete (CAC) and Ultra High-Performance Concrete (UHPC). Performance of each type of concrete will be investigated based on physical and mechanical properties in addition to material characterization. Results of various test will be analyzed and correlated collectively to understand the mechanism of damage.

4.2 Materials

The concrete types investigated as part of this experimental program are described and designated in Table 4-1. Detailed mix design is provided in Table 4-2. XRF test of raw materials provides the percentage of elements oxides is shown in Table 4-3. Raw materials chemical composition as identified by EDS is provided in Table 4-4. SEM and XRD analysis of the raw materials are shown in Figure 4-4 to Figure 4-10.

Table 4-1: Description of the concrete types investigated part of the experimental program

Mix type	Designation	Remark	Group
Ordinary Portland Cement (OPC)	M1		Conventional
Sulfate Resistant Portland Cement (SRPC)	M2		
Supplementary Cement Materials	M3 (GGBFS)		SCMs
	M4 (FA)		
Alkali Activated Polymer Concrete	M5	GGBFS and FA activated with NaOH and Na_2SiO_3	Polymer
	M8	Commercial Acid Resistant Polymer based	
Aluminate Concrete (CAC)	M7	Commercial dry mixed concrete	Special Concrete
Ultra-High-Performance Concrete (UHPC)	M6	Reinforced with steel fibers	

Concrete cylinder samples of 3x6in and 4x8in sizes in addition to paste cubes of 2x2in were cast and cured for 28 days and tested for initial physical and mechanical properties including compressive and tensile strength, modulus of elasticity, mass, absorption, density, air voids and material analysis (SEM, EDX, XRD, FTIR). Exposed as well as cured samples retrieved at 2, 4, 8 and 12 weeks were observed and tested for compressive and tensile strength, mass loss, penetration/corrosion depth and visual appearance. Material analysis (SEM, EDX, XRD, FTIR) was conducted again at the end of exposure period of 12 weeks.

To evaluate the performance of the various concrete mixes to sulfuric acid, samples were exposed to sulfuric acid and monitored for 12 weeks. Exposure conditions are as follows:

- Exposure of concrete and past specimens to %5 sulfuric acid

- Exposure of concrete and past specimens to %5 sulfuric acid at high temperature (100^{o}C)
- Exposure of concrete to %10 sulfuric acid
- Exposure of concrete with higher w/c ratio to %5 sulfuric acid at ambient and high temperature

Two protective coating systems were investigated as part of this research. The first is a novel developed application using a liner of Glass Fiber Reinforced Plastic (GFRP) with high grade vinyl ester resin to sustain the elevated temperature. The second is commercially available high-performance industrial polymer coating based on three-dimensional high cross link structure through Ether bonds (C-O-C). Coating was performed by the manufacturer specialized team.

Concentration of the sulfuric acid was monitored through pH measurements as well as through titration with a base (NaOH). The titration process is based on chemical reaction between acid (H_2SO_4) and a base (NaOH) in the presence of a color indicator (phenolphthalein). Base is added to the acid until color change to pink indicating a neutralized solution (Figure 4-1: Titration process to determine sulfuric acid concentration). Acid was added regularly to keep the sulfuric acid concertation constant at %5.

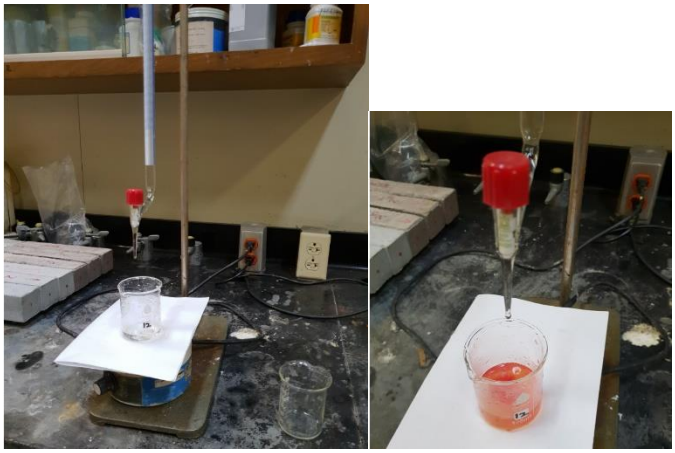

Figure 4-1: Titration process to determine sulfuric acid concentration

Table 4-2: Concrete Mix Proportions

	Concrete Component (kg/m3)							
Mix No.	Cement	GGBSF	FA	SF	W/binder ratio	Sand	Aggregate	Superplasticizer (L)
M1	370				0.4 & 0.6	776	1121	3.7
M2	370 V				0.4 & 0.6	776	1121	3.7
M3	165	340		45	0.3& 0.5	696	1006	5.5
M4	335		160	37	0.3 & 0.5	629	1119	6.0
M5		340	145		(34 L water +65L NaOH and 162L Na_2SiO_3			3.7
M6	900			220	0.15	1005	171 St. Fib	11.2
M7	Pre packed				%9.30			
M8	Pre packed				0.4		405	
P1	370				0.4			3.7
P2	370 V				0.4			3.7
P3	165	340		45	0.3			5.5
P4	335		160	37	0.3			6.0
P5		340	145					3.7

Figure 4-2: Concrete cylinder Specimens before exposure to sulfuric acid. M1 to M8 from left

Figure 4-3: Paste cube Specimens before exposure to sulfuric acid. P1 to P5 from left

Table 4-3: Raw Materials Chemical Oxides Composition, XRF

	Al2O3	SiO2	P2O5	K2O	CaO	TiO2	Fe2O3
SF	0.0038	96.16	0.6826	0.509	0.6179	0.00271	0.07951
CAC	44.58	4.711	1.045	0.3196	37.12	1.649	4.701
FLY ASH	16.13	39.39	0.8329	1.131	1.087	1.584	6.67
GGBFS	11.3	31.31	0.889	0.54	41.93	0.423	0.6528
SRPC	3.651	19.27	0.9553	0.6609	64.51	0.195	4.048
OPC	4.366	17.3	0.95	0.61	63.19	0.27	2.92
ARC	7.7	28.56	0.83	0.6	16.51	0.56	3.64

Table 4-4: Raw Materials Chemical Composition, EDS

	Ca	**Si**	**Fe**	**Al**	**S**	**Mg**	**Na**	**K**
M1	62	24	3.9	4.3	2.6	2.2	0.4	0.3
M2	56.6	35	2.6	2.1	2	1.4	0.2	0.1
M3	37.4	47.2	1.3	5.7	2.9	3.1	0.6	
M4	53.2	28	6.9	8.5	1.2	0	1.9	0.4
M5	17.7	60.9	3.6	9.3	0.6	1.6	4.2	2.1
M6	49.7	40.2	4.3	1.9	0.9	0.8	0.6	1.5
M7	50.8	4.3	4.2	39.8	0	0.5	0.2	0.2
M8	39.6	34	9.4	11.7	1.3	2.2	0	1.7

Ordinary Portland Cement (OPC)

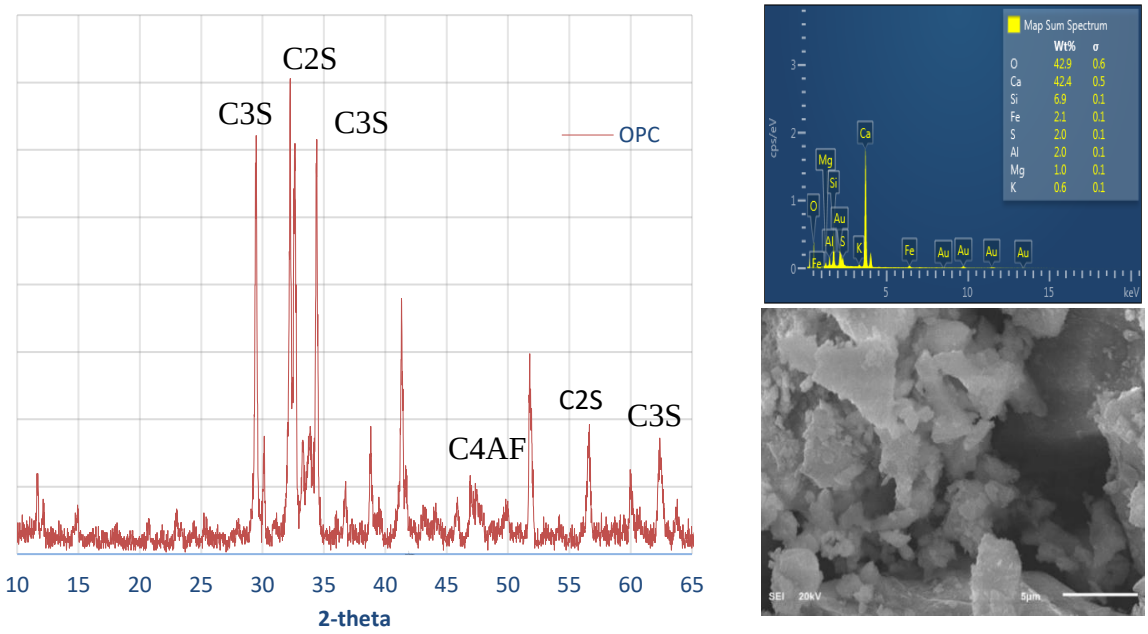

Figure 4-4: Material Analysis of OPC raw cement

Sulfate Resistant Portland Cement (SRPC)

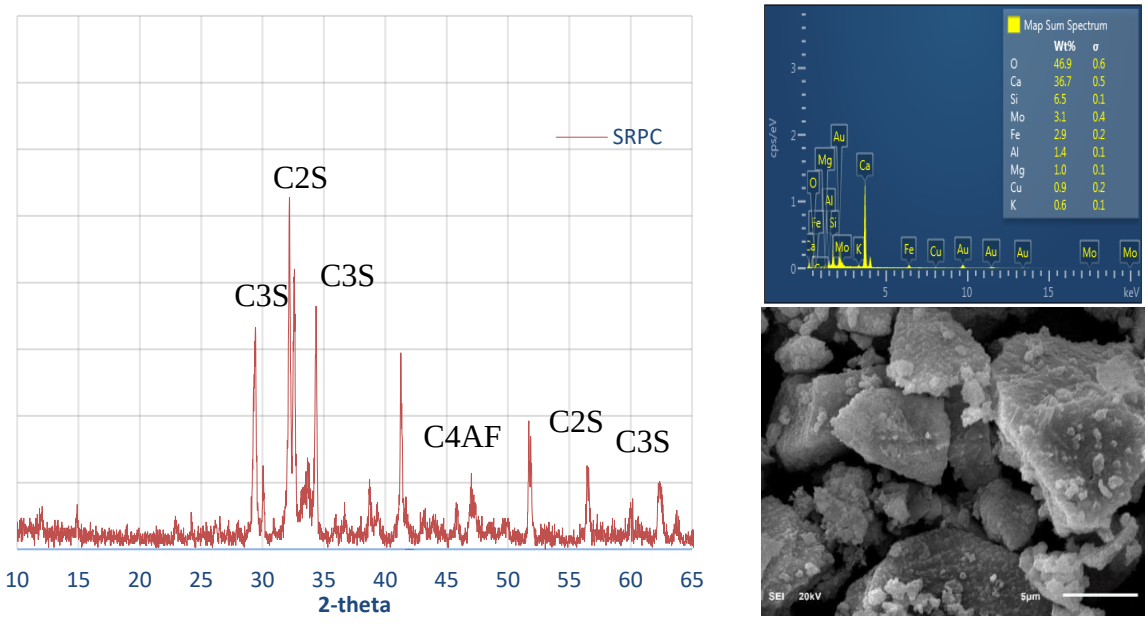

Figure 4-5: Material Analysis of SRPC Cement

FLY ASH (FA)

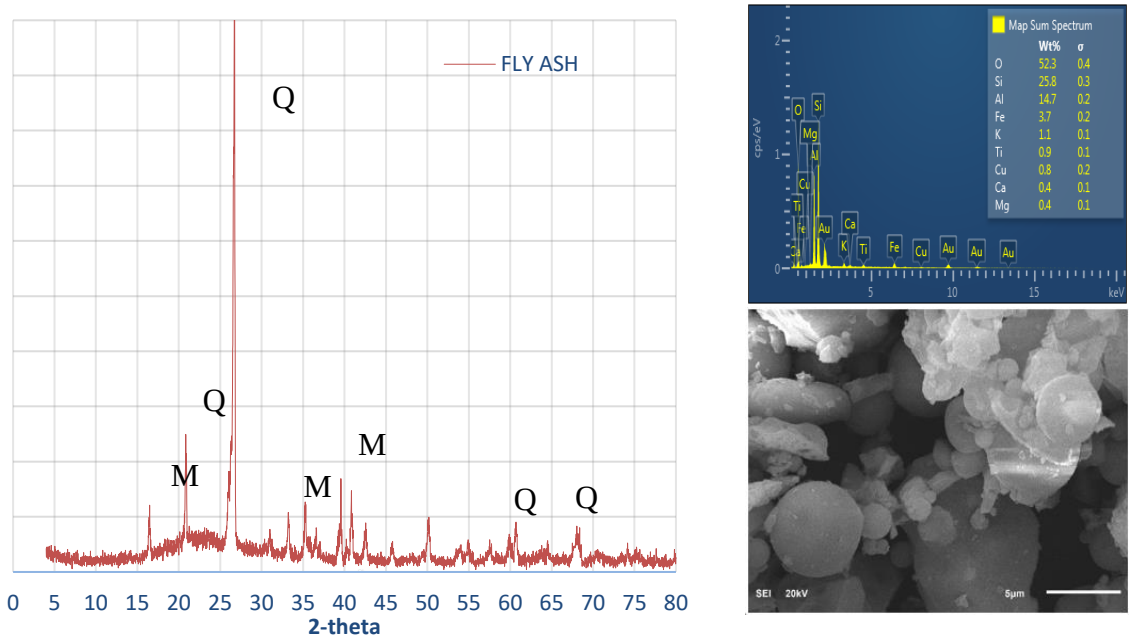

Figure 4-6: Material Analysis of FLY ASH

Ground Granulated Blast-Furnace Slag (GGBFS)

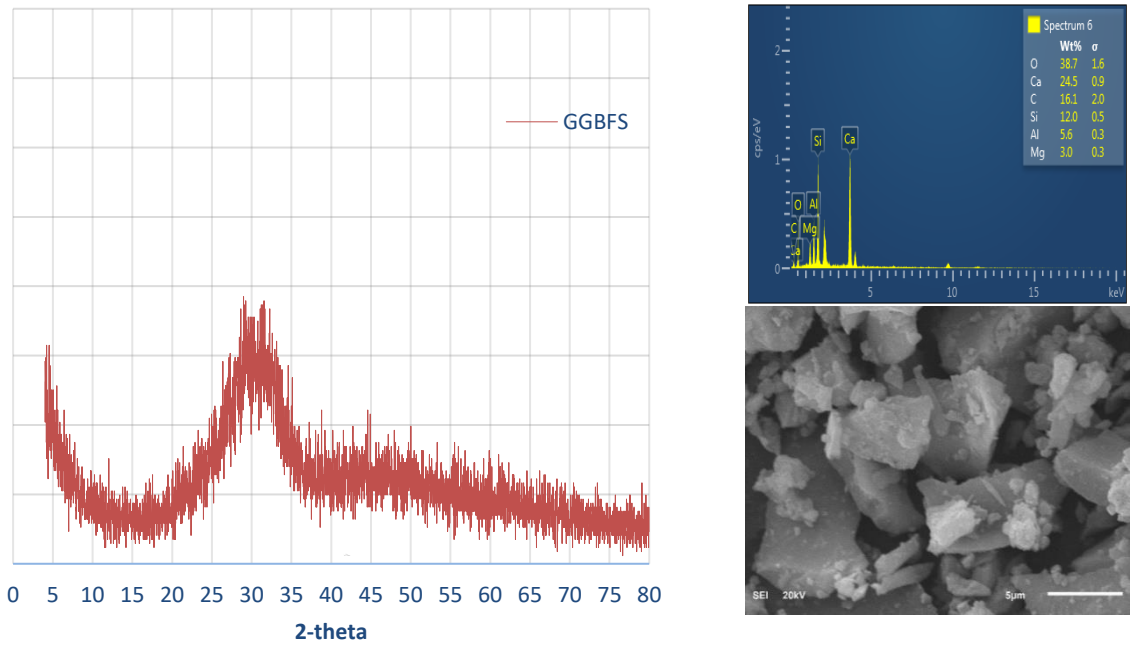

Figure 4-7: Material Analysis of GGBFS

SILICA FUME

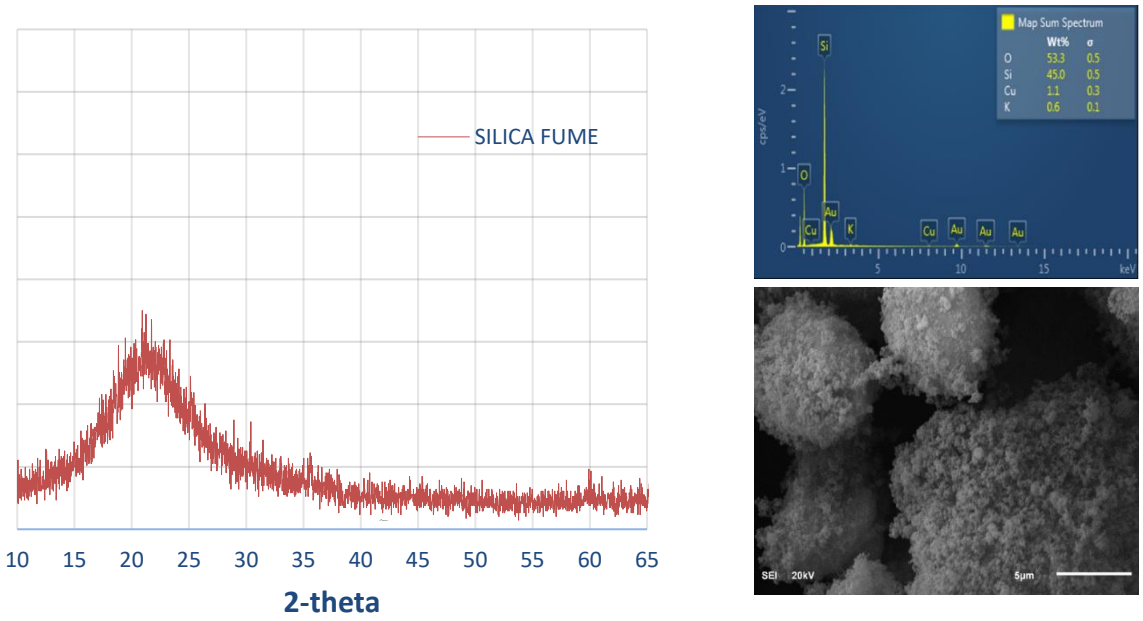

Figure 4-8: Material Analysis of Silica Fume

Calcium Aluminate Cement

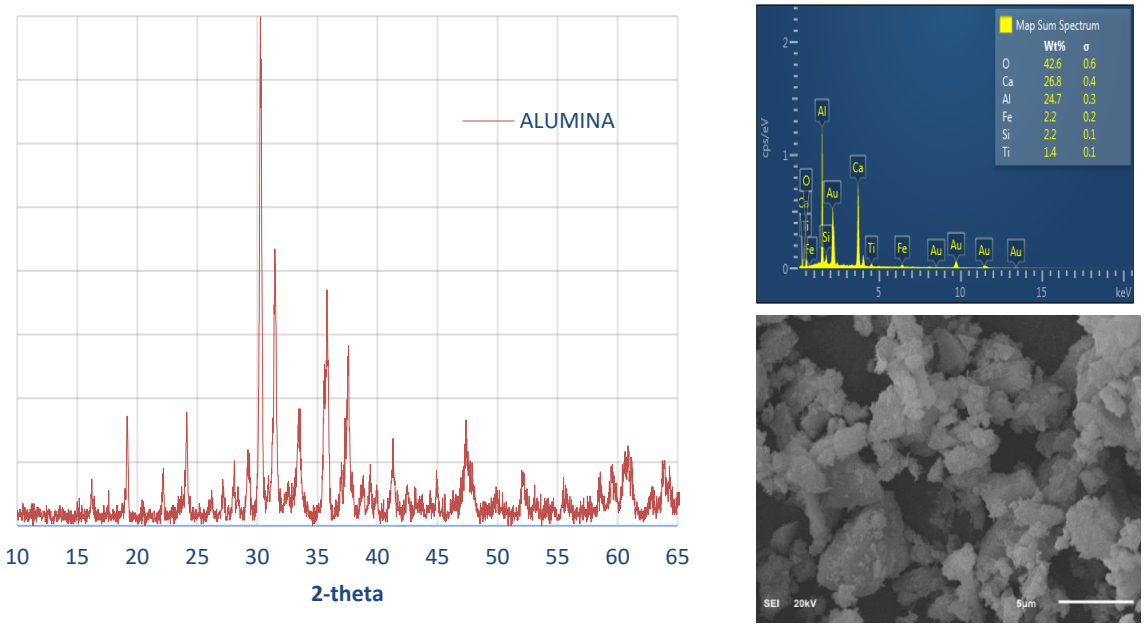

Figure 4-9: Material Analysis of Calcium Aluminate Cement

Alkali Activated Concrete (Pre-Packed)

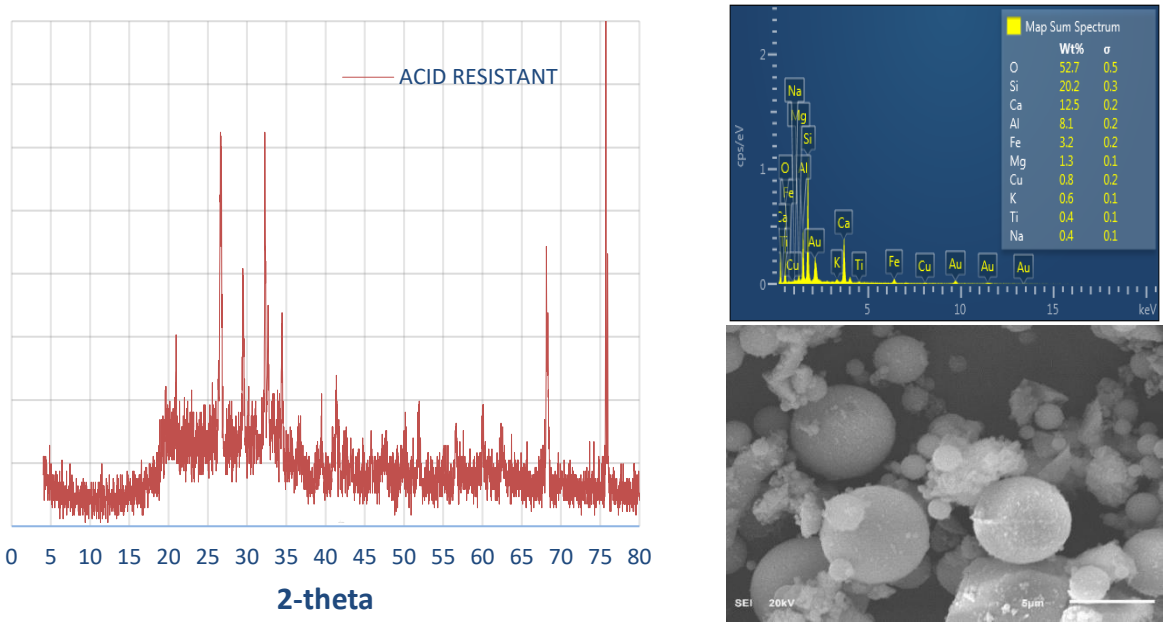

Figure 4-10: Material Analysis of AAC

Polymer concrete include concrete mixes with Fly Ash and GGBFS (M5). Alkali activated concrete based on FA, GGBFS and SF with %10 OPC and enhanced with polymer fibers (M8). M5 mix included use of Laboratory grade Na_2SiO_3 and NaOH as alkali activators. The percentage composition of Na_2O %8.7, SiO_2 %29, H_2O %62. All the available water was from added water. Fly ash and GGBFS were first mixed together and then fine and course aggregates were added and mixed thoroughly. Activator in the liquid form was then added and mixed again with the additional water being added during mixing together with the superplasticizer. material was consolidated in the mold with aid of vibration table. Molds were removed the second day and samples were left to cure at room temperature (24^oC).

Figure 4-11: Concrete Mixing and slump measurement

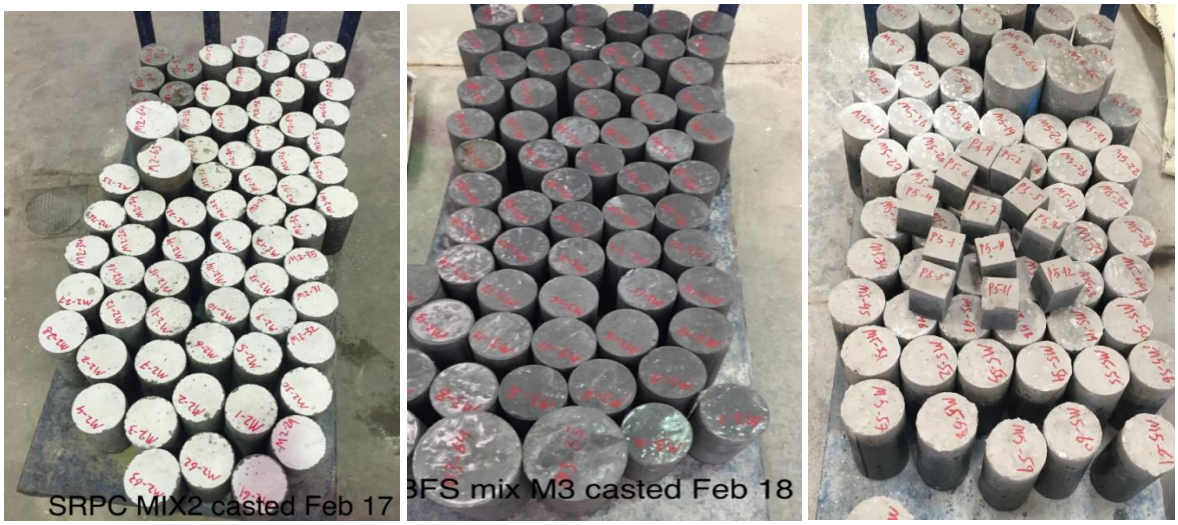

Figure 4-12: Demolded Concrete specimens ready for curing

Figure 4-13: Special mixer used for the UHPC concrete and spread measurement

Figure 4-14: Curing of concrete samples at 24C

Experimental setup for the elevated temperature exposure was established after evaluation and testing of several combination of coated carbon steel and polymers. Most of them have failed to withstand the high temperature combined with acidity. A specially manufactured Glass Fiber Reinforced Polymer (GFRP) tank shown in Figure 4-15. was manufactured for testing samples exposed to acid at elevated temperature (100^{o}C). The GFRP was based on Vinyl ester resin which has the resistance to %5 sulfuric acid. GFRP gratings and support tubes were used to stack the samples. External heating jacket was used to achieved the required temperature. Figure 4-15 illustrate the experimental setup for high temperature exposure.

Samples exposed to sulfuric acid at ambient temperature were placed in polypropylene containers. Figure 4-16 to Figure 4-18. illustrate the experimental setup for exposure at ambient temperature.

Figure 4-15: Experimental Setup for exposing concrete samples to sulfuric acid at elevated temperature

Figure 4-16: Concrete Specimens exposed to sulfuric acid after 4 weeks of exposure. M1, M2, M3 and M4

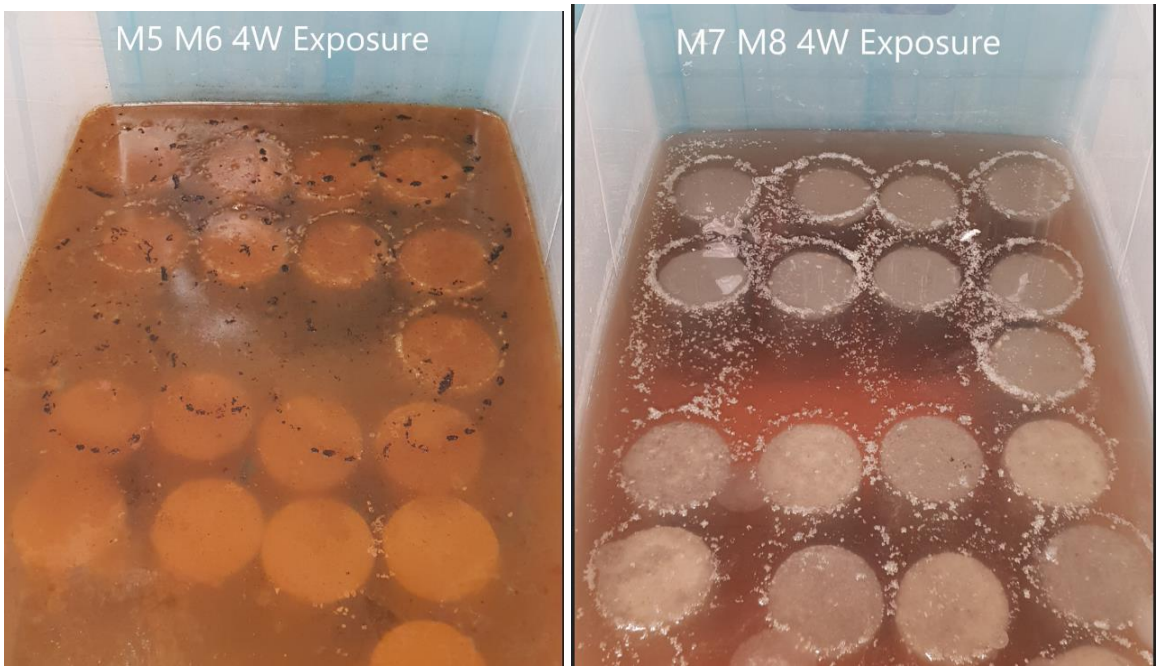

Figure 4-17: Concrete Specimens exposed to sulfuric acid after 4 weeks of exposure. M5, M6, M73 and M8

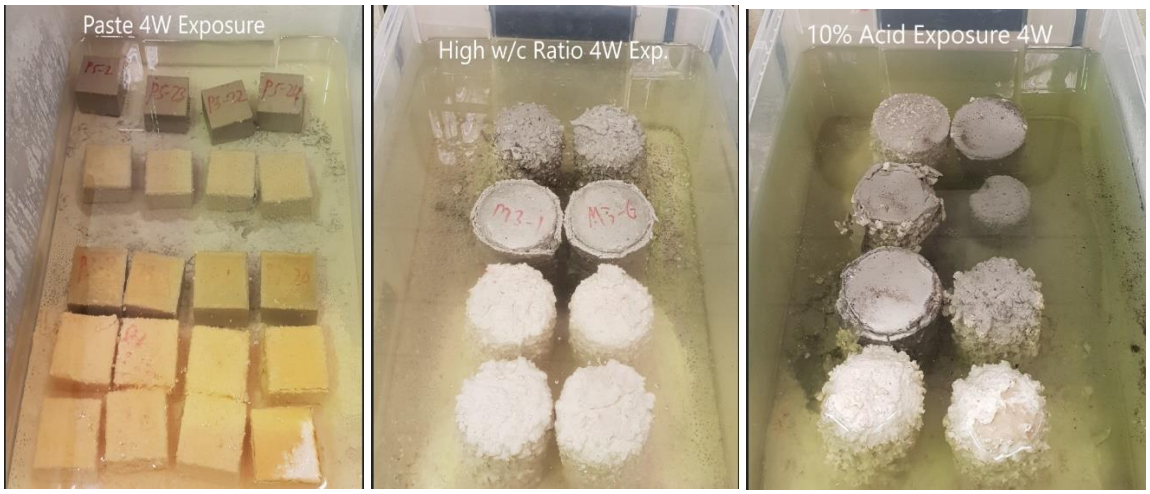

Figure 4-18: high w/c Concrete and paste Specimens exposed to sulfuric acid after 4 weeks of exposure and samples exposed to %10 sulfuric acid concentration

Figure 4-19: Concrete Specimens retrieved from the acid exposure and brushed to remove the loose outer layer. 2, 4 and 8 weeks.

4.3 Testing Methods

Preliminary testing of the mechanical properties including compressive strength, tensile strength, modulus of elasticity, rapid chloride permeability, migration, density, permeability and air voids. In addition to the material analysis (SEM, EDX, XRD and FTIR).

4.3.1 Density Air Voids and Absorption

Density, Absorption and Voids were measured according to ASTM C-642. Oven-dry mass was first determined after drying specimens in an oven at a temperature of 100 to 110°C for a period not less than 24 h.

Figure 4-20: Concrete specimens placed in ventilated oven to obtain the oven dry mass

Saturated mass after immersion (SSD) was determined after Immersing the specimen in water at approximately 21°C for 48 h. Saturated mass after boiling was then determined after placing the specimen in water and boil for 5 h. Finally, immersed apparent mass of concrete specimens were determined by suspending the specimens in water. Calculation of the density, air voids and absorption were then determined in accordance to ASTM C-642.

4.3.2 Mass Reduction

Mass of concrete was monitored by measuring weight of the samples before and after exposure to sulfuric acid. Mass loss expressed as a percentage of original mass at different exposure time for specimens from all mixtures exposed to the sulfuric acid solutions in accordance to the following equation:

$$ML = \frac{Mi - Mf}{Mi} X100$$

Where ML is the mass loss percentage, Mi is the initial mass measured after 28 days curing, and Mf is the final mass measured after exposure to sulfuric acid.

4.3.3 Compressive and Tensile Strength

Compressive strength was conducted in accordance to ASTM C39. Split tensile strength was conducted in accordance to ASTM C496. Average of 3 Cylinders 3x6in size was considered for compressive strength. Samples were capped with sulfur to ensure smooth surface. Samples tested for 7 days, 28 days before starting the exposure to sulfuric acid. Exposed samples were retrieved and tested for periods of 2, 4, 8 and 12 weeks. Each retrieved samples include both water cured (continuous curing) and acid exposed in order to make comparison.

$$f'c\ Loss = \frac{f'ci - f'ca}{f'ci}$$

Where f'c loss is the percentage reduction in compressive strength, f'ci is the compressive strength of unexposed samples (water curing), f'ca is the compressive strength after exposure to sulfuric acid.

Figure 4-21: Crushed Concrete Specimens after two weeks of exposure to sulfuric acid

4.3.4 Modulus of Elasticity

Modulus of elasticity was tested in accordance to ASTM C 469-02. Two sets of tests were conducted using strain gauges as well as LVDTs to establish the stress-strain curves. Data logger was used to record the data.

Figure 4-22: Concrete Specimens tested for modulus of elasticity after curing. LVDT and train gauges and data acquisition

4.3.5 Permeability and Migration Coefficients

To evaluate the penetrability of the pore structure of the concrete mixtures, the rapid chloride penetrability test (RCPT) was performed in accordance to according to ASTM C1202 (2012). Concrete disks cut from 4”x8” cylinders (100×50 mm disk size) were utilized for this test. Average of three samples for each mix. Concrete disks were placed in vacuum for 2hr + soaked in water for more than 24 hr. Using 30g/l NaCl and 10 g/l NaOH with 60 V electric potential and run for 6 hrs. Permeability of each type of concrete was classified in accordance to the criteria provided by ASTM-1202 shown in Table 4-5.

Table 4-5. Chloride ion penetrability classification. ASTM 1202-12

Coulombs	Chloride Ion Permeability
>4000	High
4000-2000	Moderate
2000-1000	Low
1000-100	Very low
<100	Negligible

Figure 4-23: 50 mm desks cut from 6"x12" Concrete Cylinders to conduct RCPT and Migration tests

Figure 4-24: Setup measure Rapid Chloride Permeability (RCPT)

Migration coefficients were measured in accordance to NT Build 492. Germann Instrument was used with setting time duration and applied voltage as per manufacturer's recommendation shown in Table 4-6. After completion of the applied electric potential, the

sample is cut and sprayed with silver nitrate to indicate the depth of penetration. Migration coefficient is then calculated as per the following equation (NT Build 492):

$$D_{nssm} = \frac{0.0239(273+T)L}{(U-2)t}\left(x_d - 0.0238\sqrt{\frac{(273+T)L\,x_d}{U-2}}\right) \quad (4)$$

where:

D_{nssm}: non-steady-state migration coefficient, $\times 10^{-12}$ m^2/s;

U: absolute value of the applied voltage, V;

T: average value of the initial and final temperatures in the anolyte solution, °C;

L: thickness of the specimen, mm;

x_d: average value of the penetration depths, mm;

t: test duration, hour.

Table 4-6: Voltage and duration for Migration coff. Measurement. NT Build 492

Initial current I_{30V} (with 30 V) (mA)	Applied voltage U (after adjustment) (V)	Possible new initial current I_0 (mA)	Test duration t (hour)
$I_0 < 5$	60	$I_0 < 10$	96
$5 \le I_0 < 10$	60	$10 \le I_0 < 20$	48
$10 \le I_0 < 15$	60	$20 \le I_0 < 30$	24
$15 \le I_0 < 20$	50	$25 \le I_0 < 35$	24
$20 \le I_0 < 30$	40	$25 \le I_0 < 40$	24
$30 \le I_0 < 40$	35	$35 \le I_0 < 50$	24
$40 \le I_0 < 60$	30	$40 \le I_0 < 60$	24
$60 \le I_0 < 90$	25	$50 \le I_0 < 75$	24
$90 \le I_0 < 120$	20	$60 \le I_0 < 80$	24
$120 \le I_0 < 180$	15	$60 \le I_0 < 90$	24
$180 \le I_0 < 360$	10	$60 \le I_0 < 120$	24
$I_0 \ge 360$	10	$I_0 \ge 120$	6

4.3.6 Acid Penetration (Corrosion Depth)

After each period of exposure, the acid affected layer as defined by the layer through which acid penetrated was measured by testing the pH cross the depth of the concrete sample (sample

from split tensile test is utilized). Phenolphthalein color indicator was used to evaluate the pH. Phenolphthalein is colorless below 8 and pink Above 10. Corrosion depth is defined as the acid affected layer plus the depth of dissolved layer (reduction in specimens' diameter). The behavior of the various types of concrete is different for both acid affected layer and dissolved layer and sometimes inversely related. This will be demonstrated in the discussion of corrosion depth for each group below. The concept of corrosion depth is illustrated in Figure 4-25.

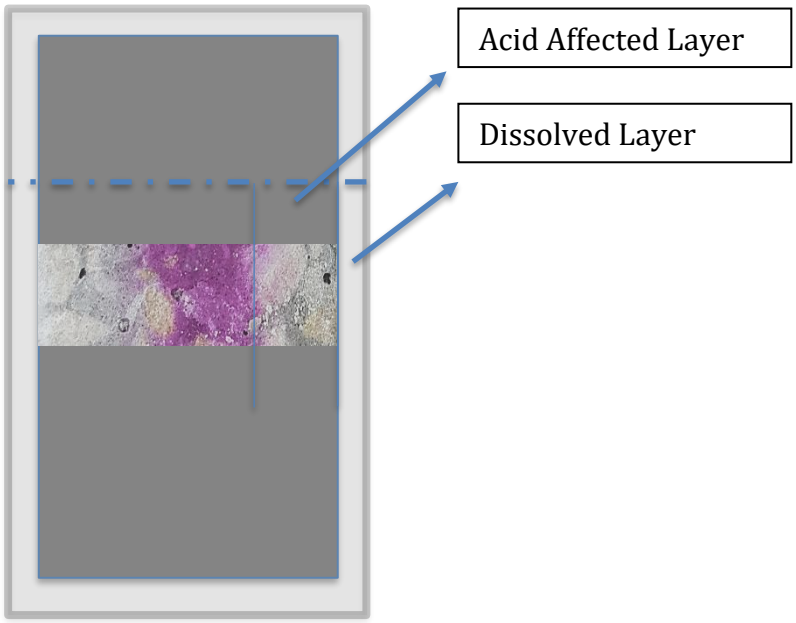

Figure 4-25 Illustration of the Corroded Layer Concept

4.3.7 Material Characterization

Characterization is an essential aspect of materials research that involves the determination of the composition and microstructure of the material. Various techniques have been utilized by researchers in the characterizing of cementitious materials, the reactions occurring in the cement hydration process, the hardened concrete microstructure and knowledge of the

evolution of the different mechanical and durability properties. Many research studies have examined the microstructure of cementitious materials subjected to sulfuric acid (Shamila, 2016). Primarily focused in identification of formed reaction products to explain changes of mechanical and structural properties of concrete. Each of these techniques describes different aspects of the material. This experimental program involves extensive microstructural studies for the 8 different concrete mixes before and after exposure to %5 sulfuric acid solution, at normal and elevated temperature. These studies are conducted to understand the change in chemical composition for each type of concrete under such environment and consequently its relation to the degradation of the mechanical properties. The techniques used and the specific purpose of their use are as follows:

XRF (X-ray fluorescence) determines the elemental composition of materials in oxides form. Oxides such as CaO, SiO_2, Al_2O_3, Fe_2O_3 are examples of very important elements of the cementitious material composition that can be detected by this technique.

XRD determines the compounds crystalline phases such as Portlandite, Calcite, Quarts, gypsum, ettringite, CSH, C_2S and C_3S. Phases that are amorphous in nature are difficult to detect by this Tanique. A Bruker D8 Advance powder diffractometer (XRD) instrument was utilized in this study. Powder Samples were taken from the surface of specimens.

Figure 4-26: XRD ULTIMA IV, XRF SPECTRO XEPOS – KFUPM_RI

SEM and EDS provide magnified images and morphology of the microstructure in addition to quantitate estimation of the elemental composition such as Ca, Fe, Na, Si and Al. The observations were carried out through microscope JOEL JSM-6610LV (Figure 4-27). Analysis was conducted on fresh fractured surface after coating with Au.

Figure 4-27: SEM-EDS JOEL JSM-6610LV – KFUPM_RI

Fourier-transform infrared spectroscopy (FTIR) describes the material composition based on the type of bonds detected. It is useful to identify amorphous materials that are not detected by XRD.

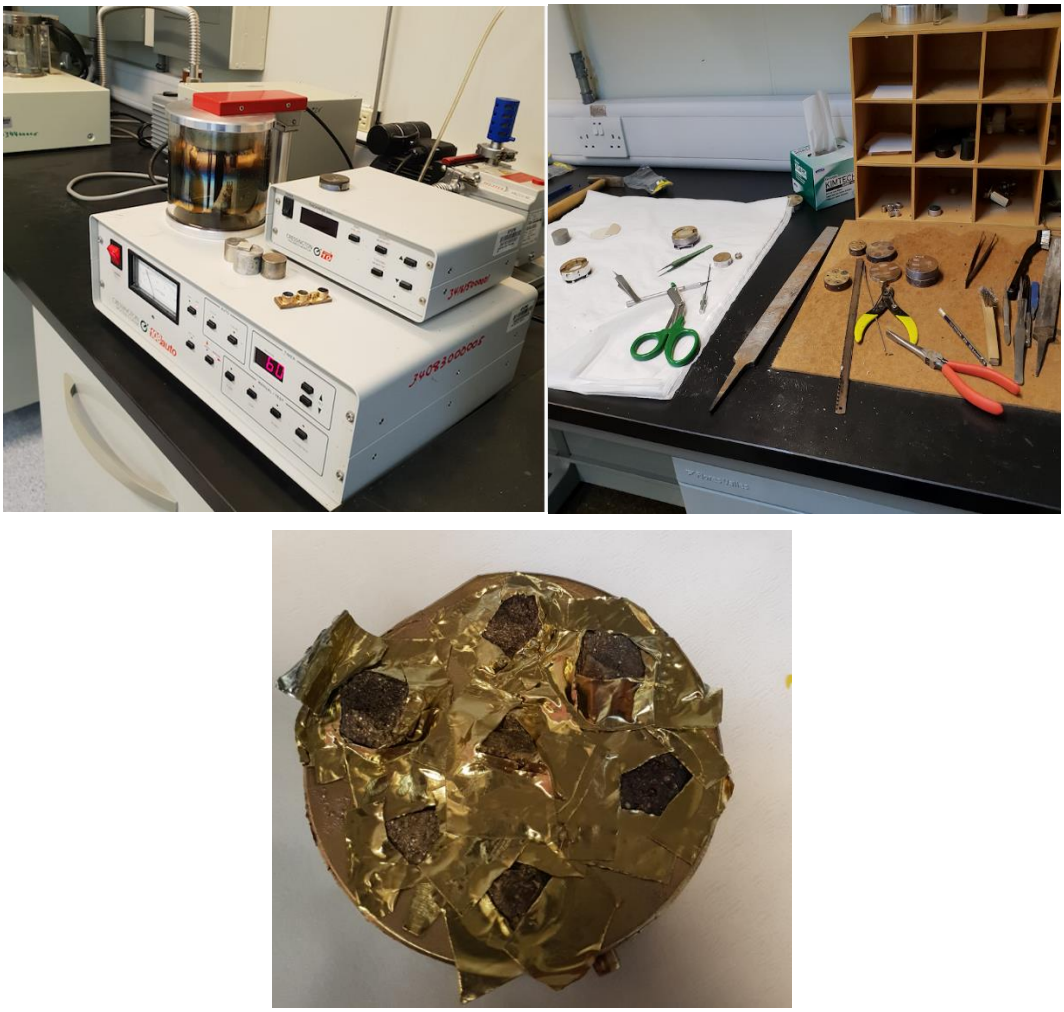

Figure 4-28: samples preparation and Au coating to conduct SEM, EDS

CHAPTER 5

RESULTS AND DISCUSSION

5.1 Density Air Voids and Absorption

Density, water absorption and volume of permeable voids were measured according to ASTM C-642. Oven-dry mass was determined after drying specimens at a temperature of 100 to 110 °C for 24 hrs. Saturated mass was determined after immersing the specimen in water at approximately 21 °C for 48 h. Saturated mass after boiling was then determined after placing the specimen in water and boil for 5 h. Apparent mass of concrete specimens was measured for samples immersed in water. Table 5-1 shows the measured mass values for all concrete types.

Table 5-1: Measured Mass of concrete specimens

	Oven-Dry Mass g (A)	Saturated Mass After Immersion g (B)	Saturated Mass After Boiling g (C)	Immersed Apparent Mass g (D)
Mix no	24hrs in oven	SSD after 48 hrs in Water	SSD After boiling 24 hrs	
M1	1625.4	1687.4	1691.5	985.4
M2	1667.4	1725.9	1738.2	1027
M3	1684.1	1714.5	1718.7	1009.9
M4	1631.7	1675.8	1678.8	984.4
M5	1535.4	1636.2	1664.4	946.1
M6	1633	1641.5	1647.8	958.2
M7	1941.8	2009.7	2019.3	1281.4
M8	1448	1471.4	1486.8	772.2

Absorption, density and voids were calculated after measuring the weight in accordance to the method described in to ASTM C-642 and presented in Table 5-2.

In general, the density of all groups was in the range 2011-2630kg/m3. The lower density obtained in M8 is due to the less aggregates proportion used in this mix (binder to aggregate ratio 0.675 vs 0.3 in M5). The Alumina Aggregates used within the CAC (M7) concrete has contributed to this increase in density. Denser concrete matrix in the SCM group (M3, M4) resulted in a relatively higher density than conventional concrete.

It can be clearly seen that M5 had significantly higher absorption and volume of permeable voids (%12.93) as compared to all other groups, and specifically compared to the polymer concrete M8 (%4.7). Higher calcium content in M8 lead to more hydration and formation of C-S-H gel that filled the pores (Yep 2005, Borges 2016, Buchwald 2009). the Calcium Aluminate Concrete (M7) comes second highest in volume of permeable voids with %7.47 and then OPC (M1), SRPC (M2), Followed by the SCM group GGBFS (M3) and FA (M4) with %3.61 and %4.81 respectively. The lowest among all in absorption and volume of voids was the UHPC with only %1.89.

Volume of permeable voids results are in line with the rapid chloride permeability test. In the case of polymer concrete group, it indicates total charge passing through M5 samples of 1100 Coulombs which is classified as “low” in accordance to ASTM C-1202 vs 284 in M8 which is classified very low. Similar result was obtained by (Rajamane et. al. 2011)

Table 5-2: Density Air Voids and Absorption

	Absorption after immersion, %	Absorption after Immersion and Boiling	Bulk Density, Dry T/M3	Bulk Density After Immersion (g1) T/M3	Bulk Density after immersion and boiling	Apparent density T/M3	Volume of permeable pore space (voids), %
M1	4.25%	4.50%	2.292	2.390	2.396	2.556	6.51%
M2	3.81%	4.55%	2.338	2.427	2.444	2.616	7.23%
M3	2.12%	2.37%	2.369	2.419	2.425	2.510	3.61%
M4	3.09%	3.27%	2.341	2.413	2.418	2.535	4.81%
M5	6.84%	8.68%	2.132	2.278	2.317	2.616	12.93%
M6	0.70%	1.09%	2.364	2.380	2.390	2.426	1.89%
M7	3.55%	4.04%	2.630	2.724	2.737	2.943	7.47%
M8	2.37%	3.44%	2.011	2.059	2.081	2.161	4.71%

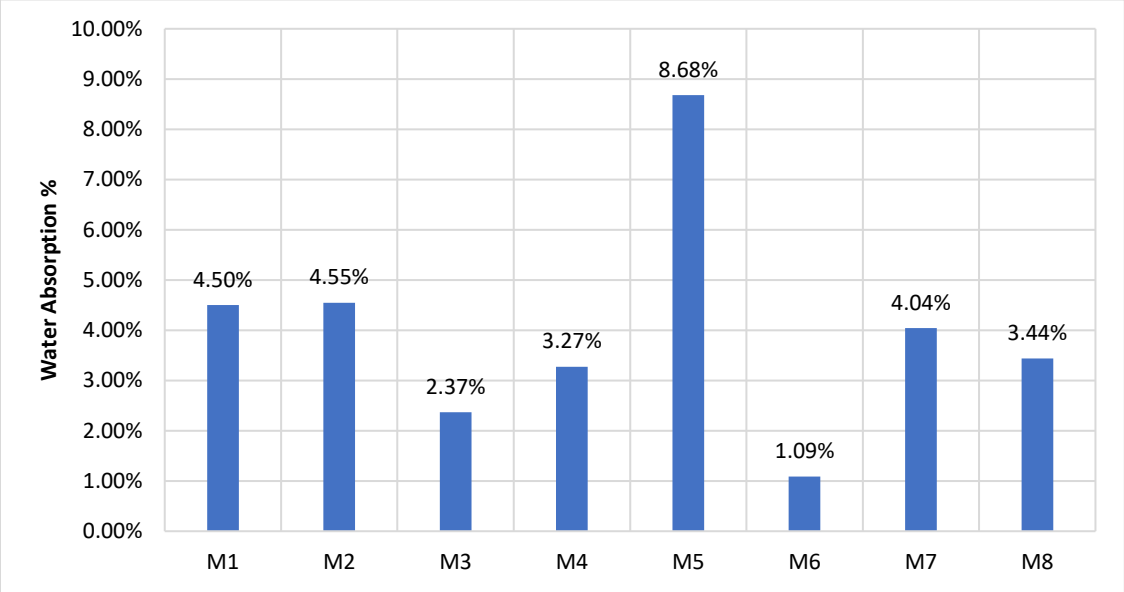

Figure 5-1: Concrete Absorption after immersion and boiling. M1-M8

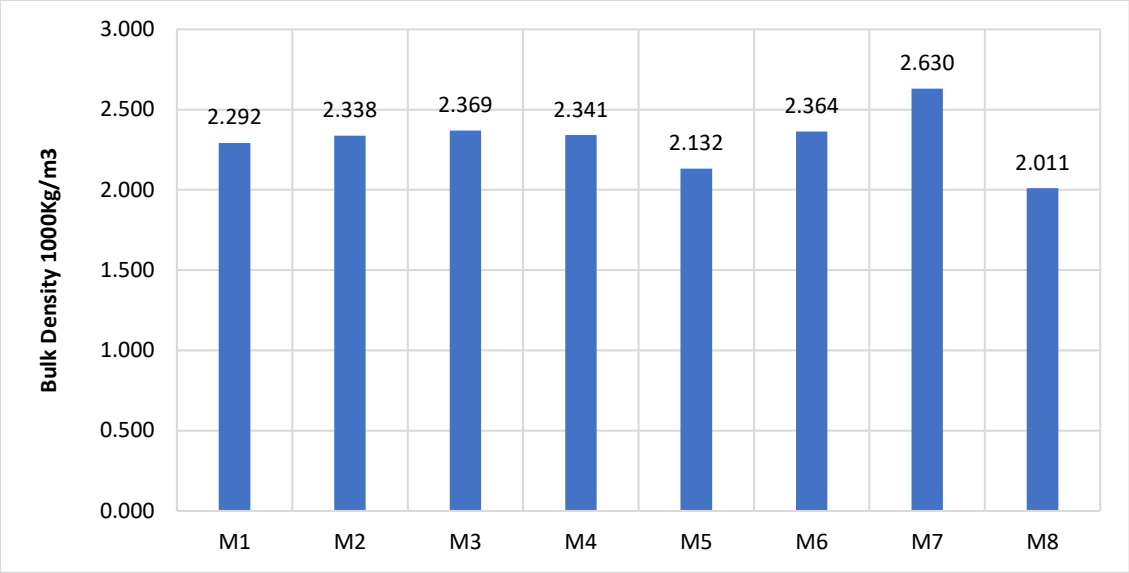

Figure 5-2: Concrete Density

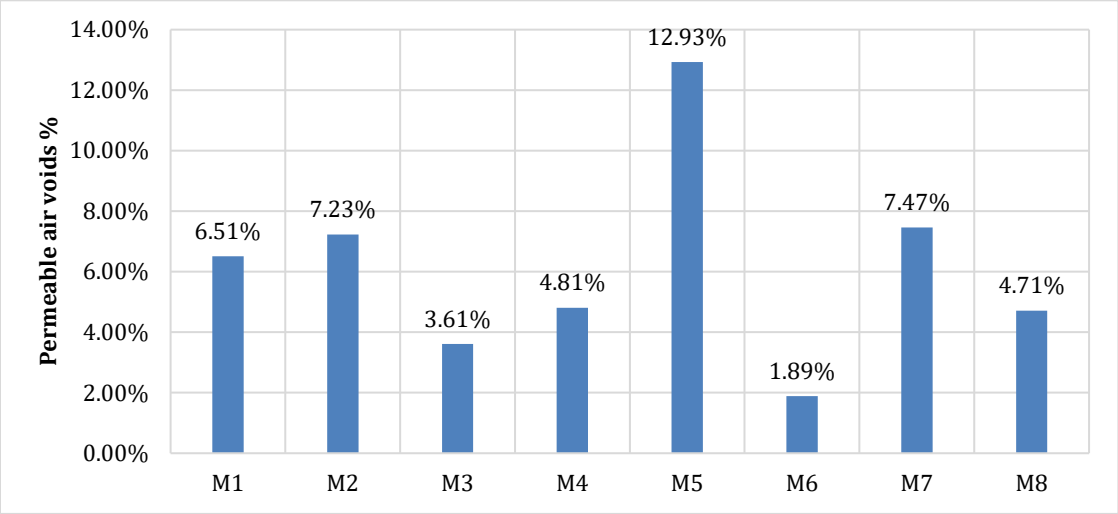

Figure 5-3: Volume of permeable pore space (voids), %

5.2 Permeability and Migration Coefficients

Results of the RCPT indicates that the highest permeability was found in the conventional concrete group M1 and M2 with a rating of "Moderate" per ASTM C1202 classification

(Table 5-3). UHPC on the other hand had the lowest permeability with a rating “negligible, followed by the SCM group M3 and M4 “very low” and followed by CAC and polymer “low and very low” rating.

Table 5-3: Concrete Permeability rating per ASTM C-1202

	COLUMBS	Rating per ASTM C1202
M1	2284	Moderate
M2	3552	Moderate
M3	138	Very Low
M4	272	Very Low
M5	1100	Low
M6	32	Negligible
M7	1003	Low
M8	284	V. Low

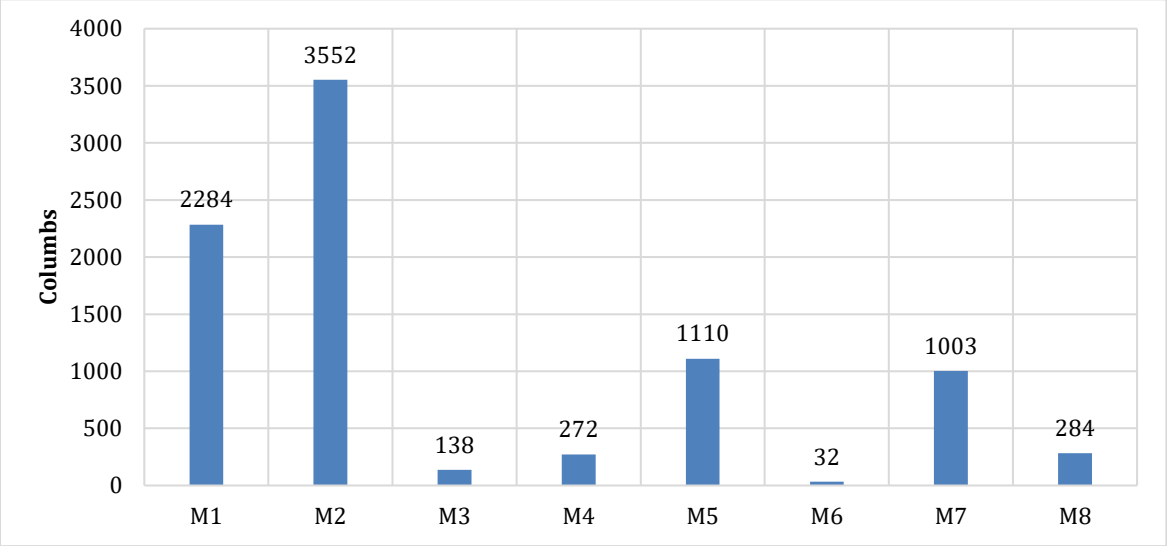

Figure 5-4: Charge Passes (Columbus) FOR Rapid Chloride Permeability (RCPT)

Migration coefficients calculated per NT Build 492 are provided in Table 5-4. The results indicate that the highest penetration and diffusion coefficients was found in the conventional concrete group OPC (M1) and SRPC (M2) mixes with diffusion coff. of 15.489x10^-12 m2/s and 15.018 x10^-12 m2/s for M1 and M2 respectively. UHPC on the other hand had the lowest

0.399 x10^-12 m2/s, followed by the SCM group M3 and M4, CAC and polymer in range of 1.0-1.83 x10^-12 m2/s. In general, the incorporation of different types of SCMs such as silica fume, GGBFS and fly ash had a significant effect on reducing permeability. Similar findings were reported by (Mahmud Amin, 2017). Mahmoud explained this by the SCMs role in refining the pore structure of concrete and enhancing its discontinuity. Measurements and calculation of diffusion coefficient are provided in Table 5-4.

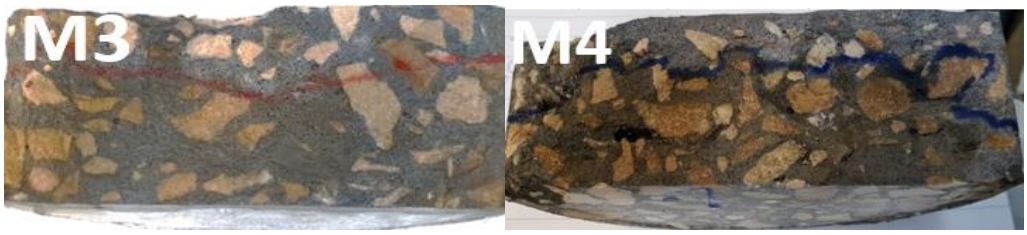

Figure 5-5: Discs retrieved from the cell, cut and sprayed with silver nitrate solution to measure the penetration depth

Table 5-4: Measurements and calculation of Migration coefficients

	Initial current	Volt	initial temp.	final temp.	Avg. Temp.	penetration depth (mm)	Time (hrs)	Avg Diff. Coff x10^-12 m2/S
M1	50	30	23	25	24	40	24	15.489
	54	30	23	25	24	39.5	24	
M2	50	30	23	26	24.5	38	24	15.018
	46	30	24	26	25	39	24	
M3	3.1	60	22	24	23	12	48	1.004
	3.2	60	22	24	23	10	48	
M4	6.6	60	23	25	24	20	48	1.689
	6	60	23	25	24	16	48	
M6	19	60	22	23	22.5	3	24	0.399
	13	60	22	24	23	2	24	
M7	20	60	24	26	25	9	24	1.826
	25	60	24	26	25	11	24	
M8	4.5	60	22	24	23	8	24	1.526
	6	60	22	24	23	9	24	

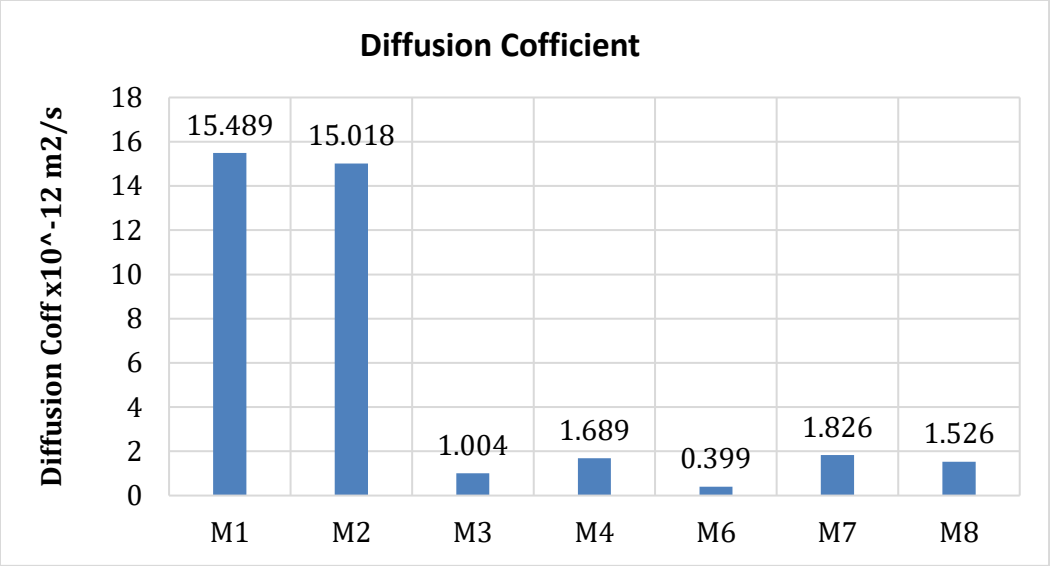

Figure 5-6: Calculated Diffusion Coff x10^-12 m2/s per NT BULD 492

5.3 Modulus of Elasticity

Modulus of elasticity results revealed wide variation among the different types of concrete. The calculated modulus of elasticity for all groups are provided in Table 5-5. The stress vs strain curves are provided in Figure 5-7-5.15. The highest modulus was obtained for the CAC M7 group of 58.9 GPa followed by UHPC M6 group 52.3 GPa. The lowest was the polymer concrete M5 with 8.18 GPa. Lower modulus obtained in M5 is an indicator of decreased hardness caused by the incorporation of low calcium content and less formation of C-S-H in polymer concrete as reported by Buchwald (2009).

Table 5-5: Calculation of modulus of elasticity

	Max Stress	S2	S1	ε1	ε2	E (GPa)
M1	53.94	21.58	1.82	0.00005	0.00053	41.33
M2	58.04	23.22	4.17	0.00005	0.00041	53.05
M3	63.42	25.37	6.80	0.00005	0.00042	50.88
M4	66.61	26.64	2.35	0.00005	0.00054	50.09
M5	18.81	7.53	0.68	0.00005	0.00089	8.18
M6	91.42	36.57	2.40	0.00005	0.00070	52.32
M7	89.05	35.6	3.2	0.00005	0.0006	58.94
M8	38.09	15.23	1.50	0.00005	0.00076	19.32

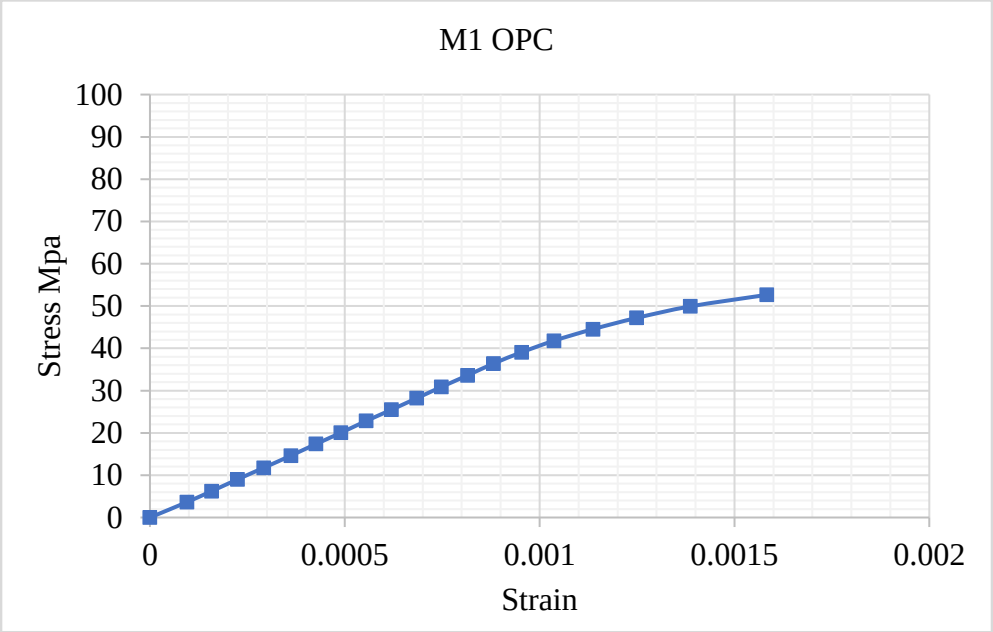

Figure 5-7: Stress-Strain Curve (M1-OPC)

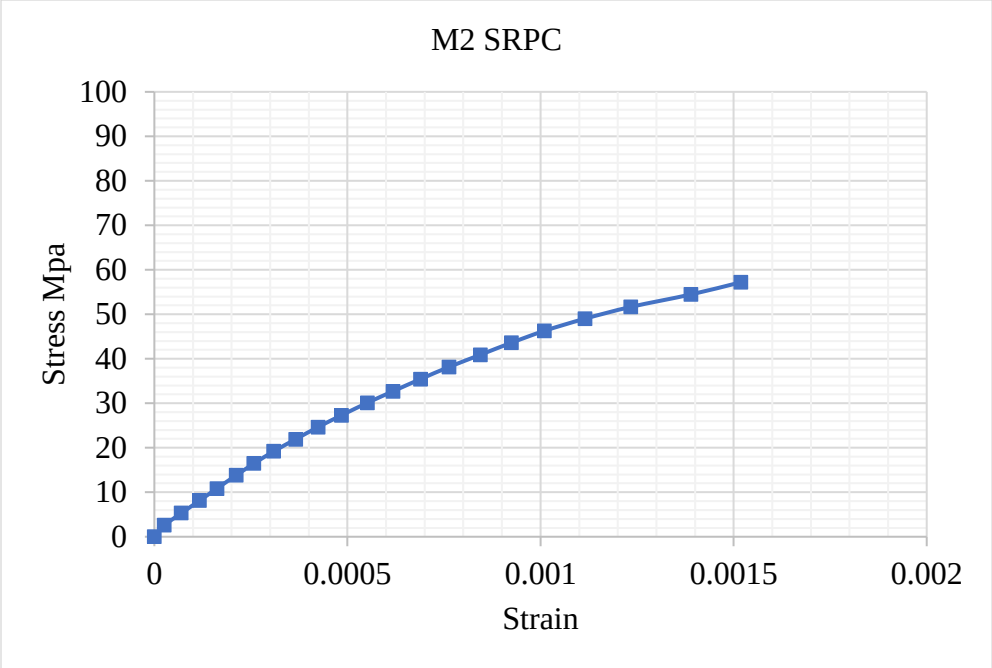

Figure 5-8: Stress-Strain Curve (M2-SRPC)

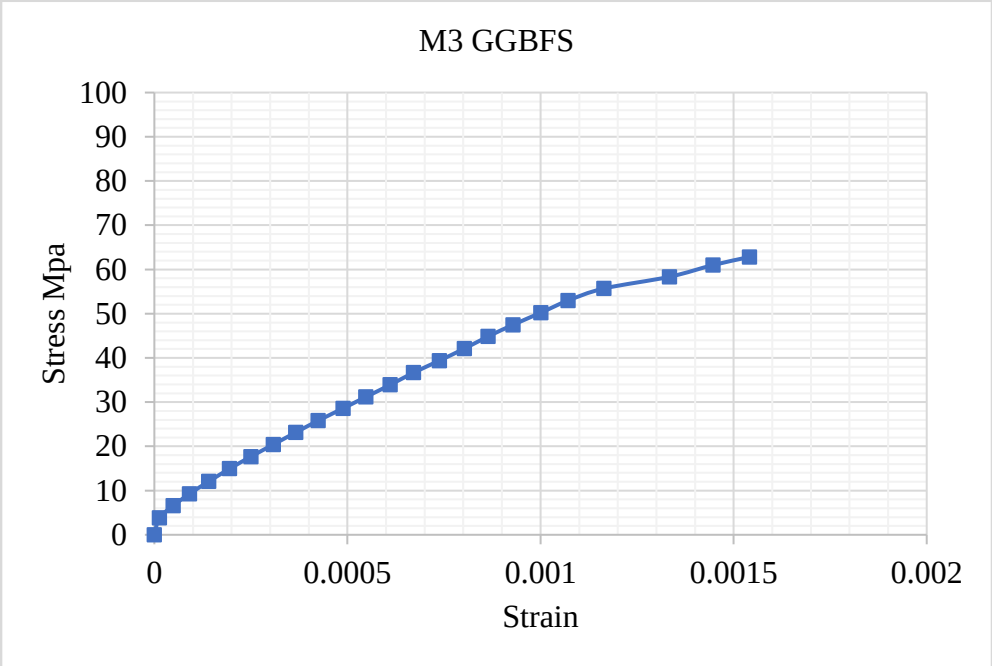

Figure 5-9: Stress-Strain Curve (M3-GGBFS)

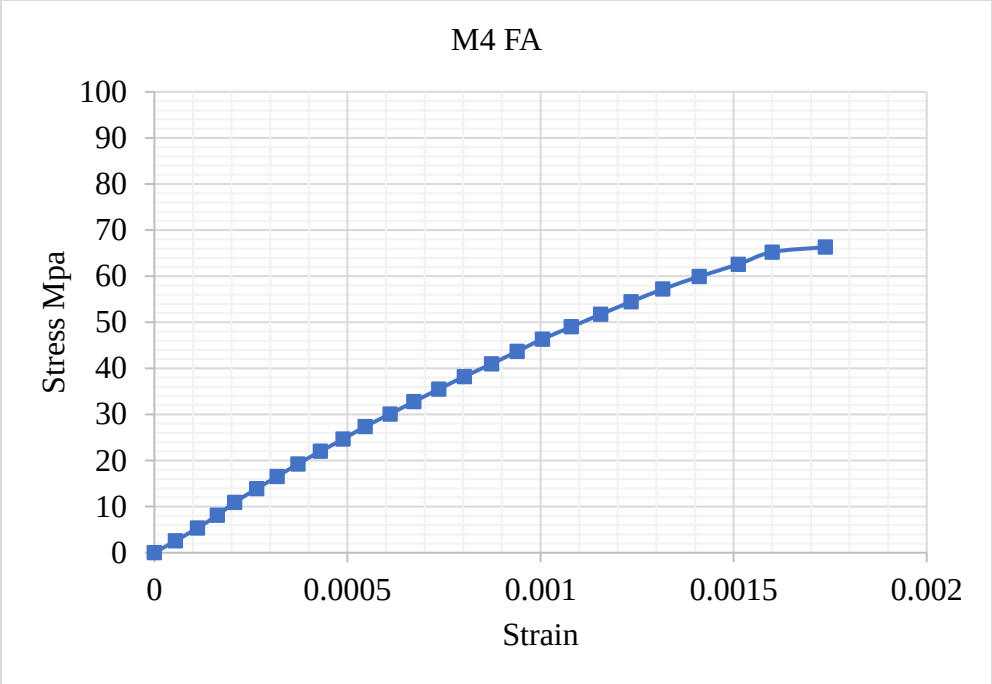

Figure 5-10: Stress Strain Curve (M4-FA)

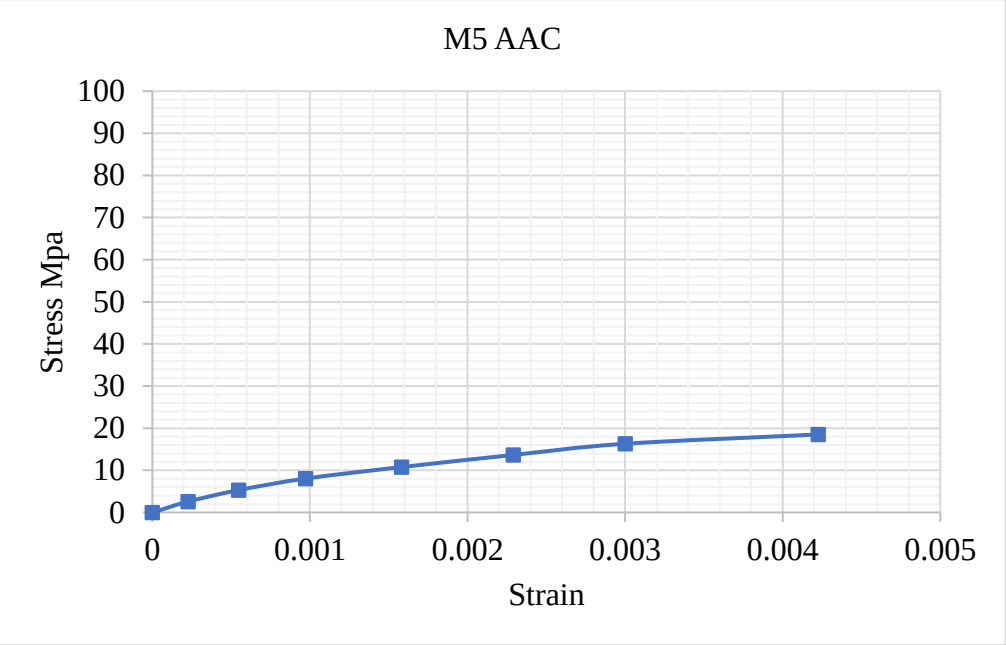

Figure 5-11: Stress-Strain Curve (M5-AAC)

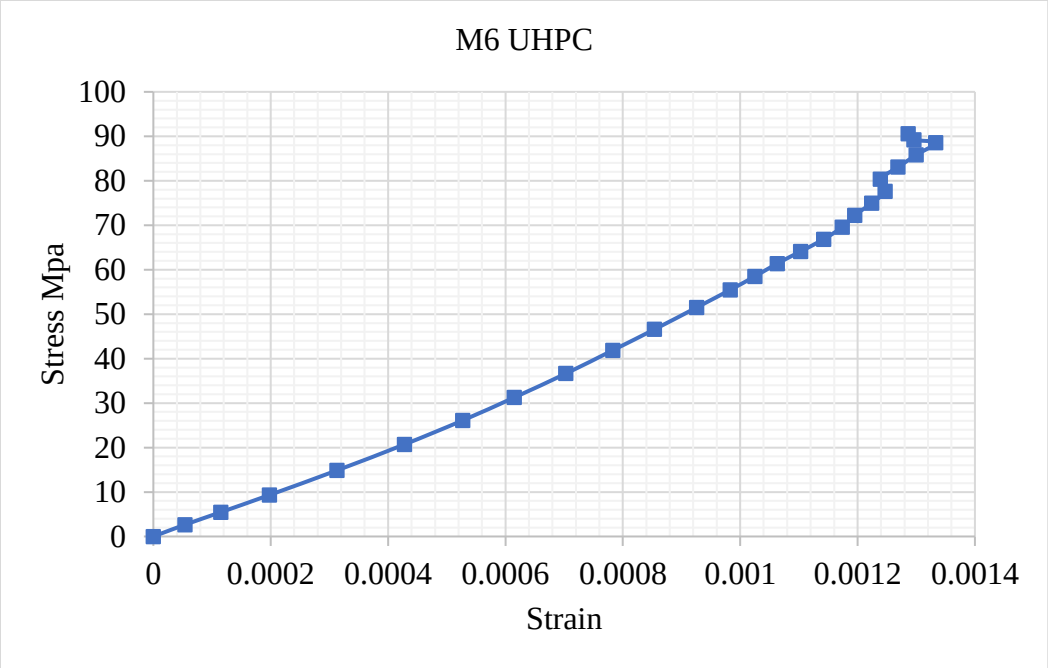

Figure 5-12: Stress-Strain Curve (M6-UHPC)

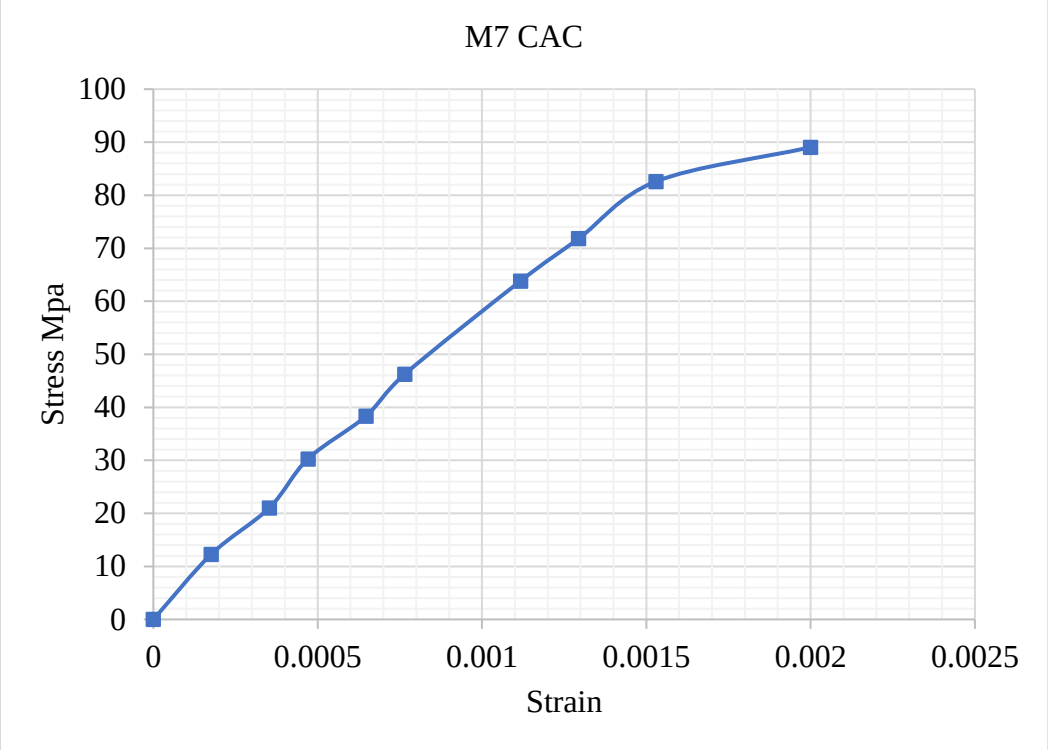

Figure 5-13: Stress-Strain Curve (M7-CAC)

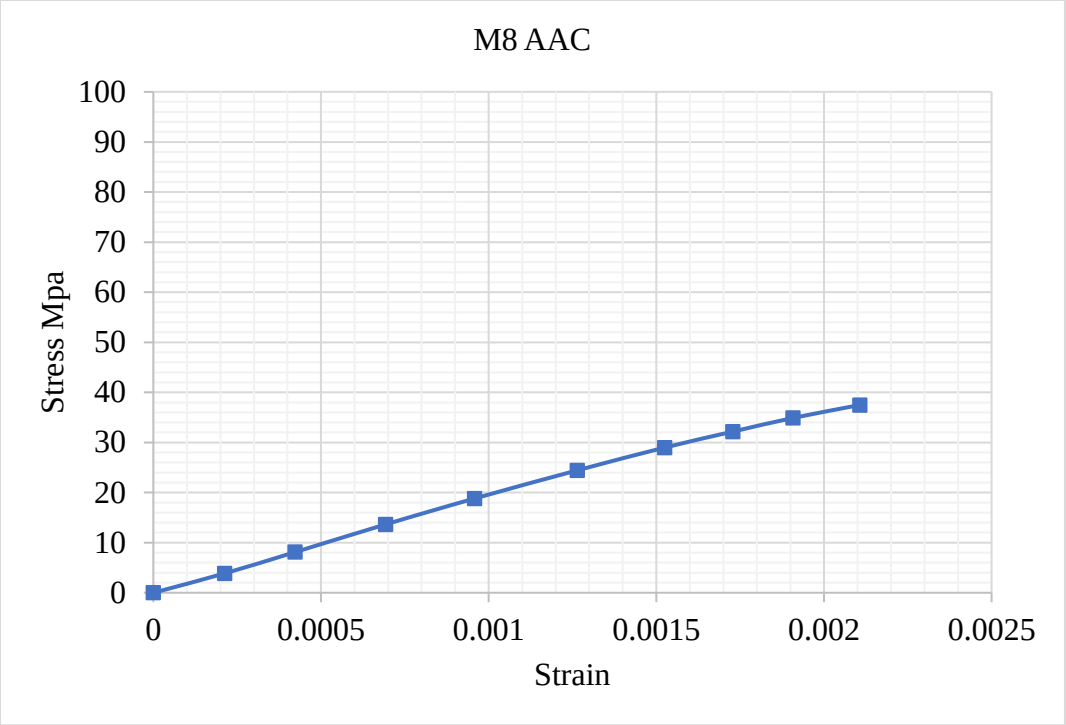

Figure 5-14: Stress-Strain (M8-AAC)

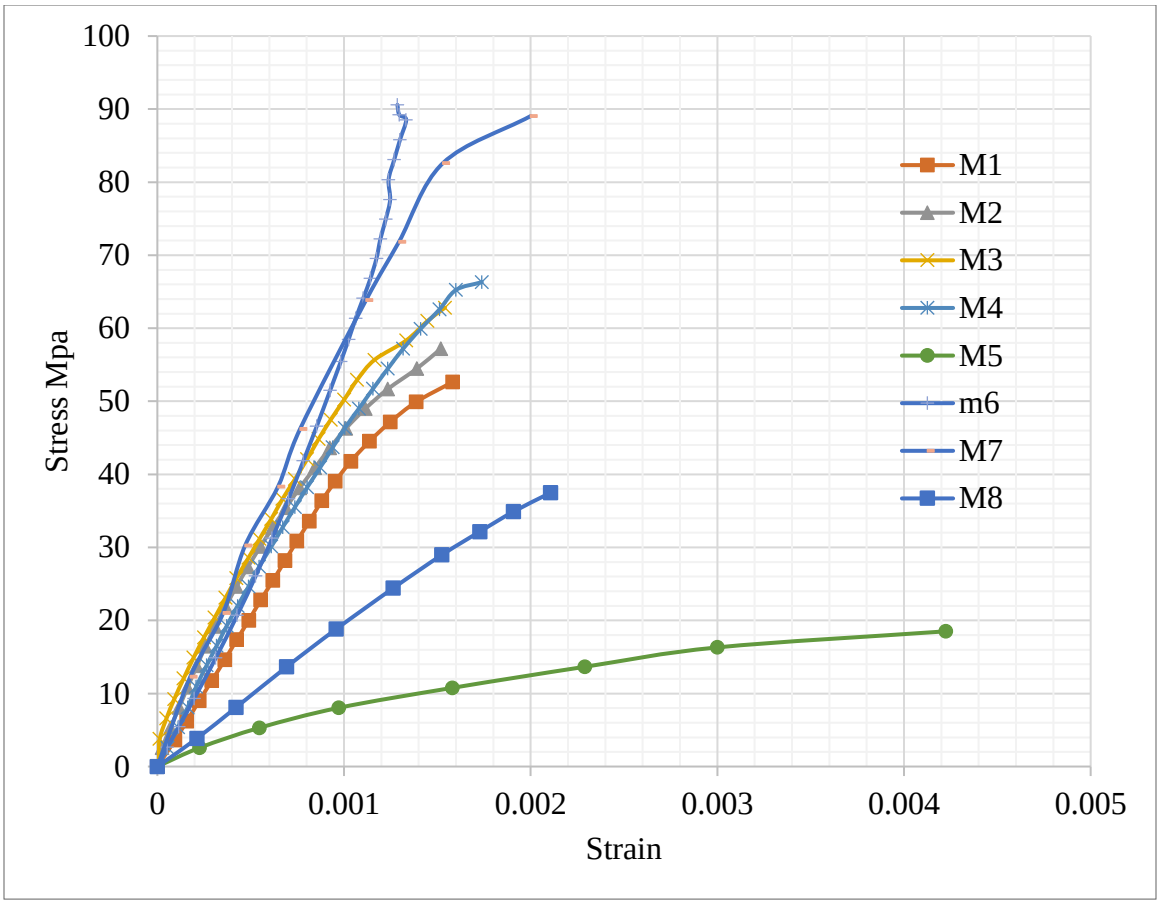

Figure 5-15: Stress-Strain Curve (all concrete types)

5.4 Visual Monitoring

Throughout the exposure period, the changes in the appearance of the specimens were monitored visually. Samples retrieved at periods of 2, 4, 8 and 12 weeks were brushed and washed and photographed. Figure 5-16-5.28 shows the changes on surface appearance of all concrete specimens over the 12 weeks period of exposure to sulfuric acid.

Within few days, white powder material (identified as gypsum by XRD) deposited progressively on the surface of all specimens in conventional concrete group M1-OPC and M2-SRPC. Very soft and easily removable corroded layer expanded gradually to reach the

aggregate which loosen and fall apart. Visual appearance of high w/c ratio specimens and those exposed to high temperature from this group demonstrated similar pattern in color as well as deposited soft layer.

No notable change in color among specimens in the SCM group M3-GGBFS and M4-FA. M3 showed more resistant to disintegration during the early few weeks with only visually observable crack, while M4 showed quick deposition of the outer layer in dark gray color which also was identified by XRD as gypsum. Similar pattern was observed for specimens exposed to high temperature from this group in terms of color as well as deposited soft layer.

Polymer concrete group (M5 and M8) also showed no sign of change in color. The outer layer remained intact and starting disintegrating after 8 weeks. Microcracks were noticed in both types and more prominent in the high temperature exposure.

The special concrete groups involving M6-UHPC and M7-CAC did not show sign of color change as well. The UHPC demonstrated large softening of the outer layer in dark gray color, with no signs of cracks. CAC on the other hand showed only very minor outer layer softening which did not even cause aggregate loosening.

The specimens coated with high performance polymer coating demonstrated large degradation of the coating material when exposed to sulfuric acid at high temperature followed by degradation of the concrete. Specimens coated with GFRP liner on the other hand remained on perfect condition with no sign of liner disintegration.

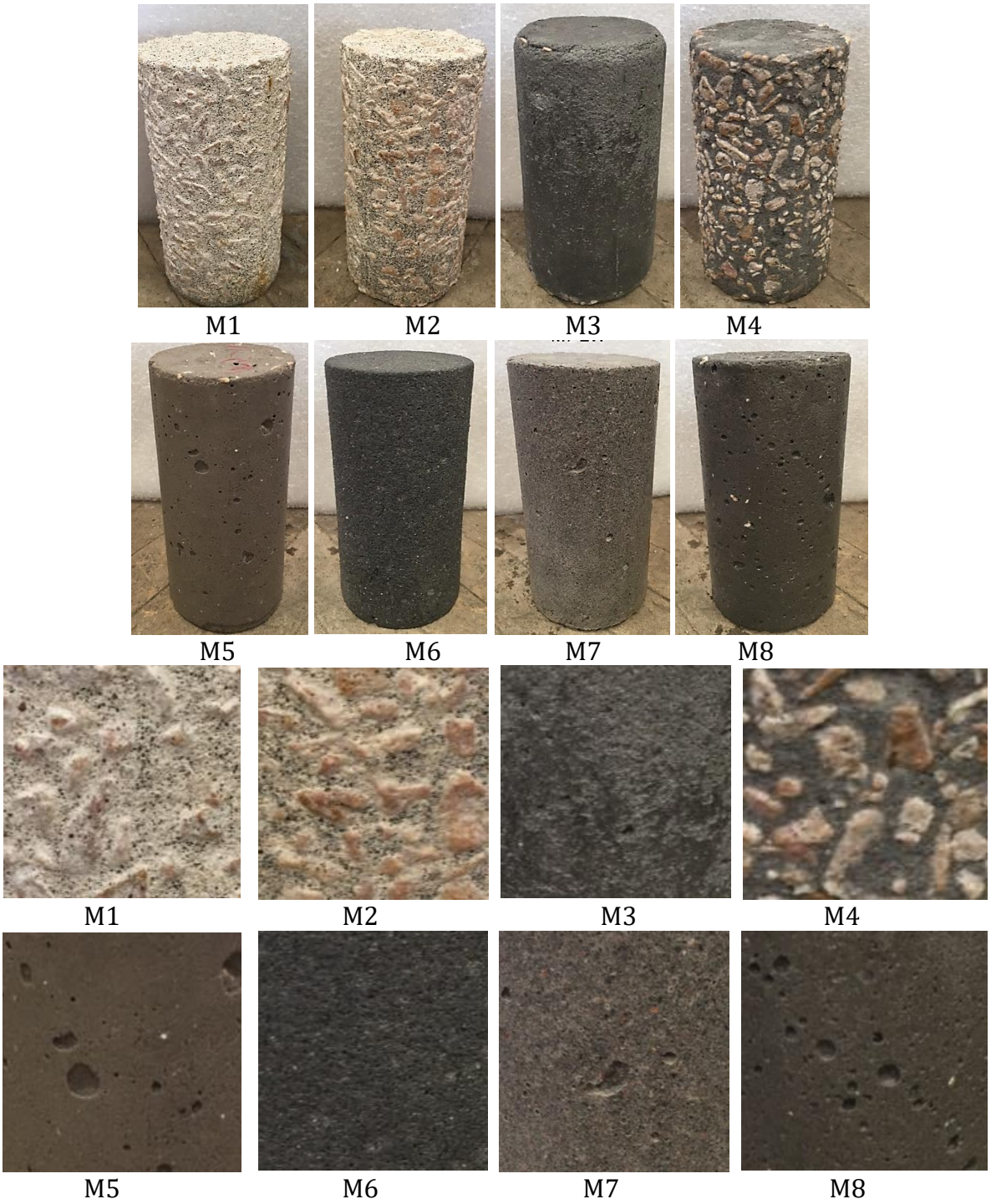

Figure 5-16: Visual Appearance after 2 weeks of exposure to %5 sulfuric acid. Specimens and enlarge sections.

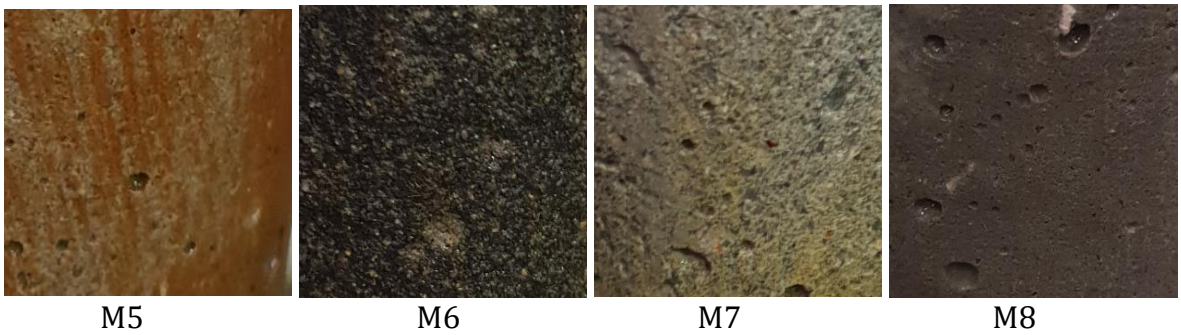

Figure 5-17: Visual Appearance after 4 weeks of exposure to %5 sulfuric acid. Specimens and enlarge sections.

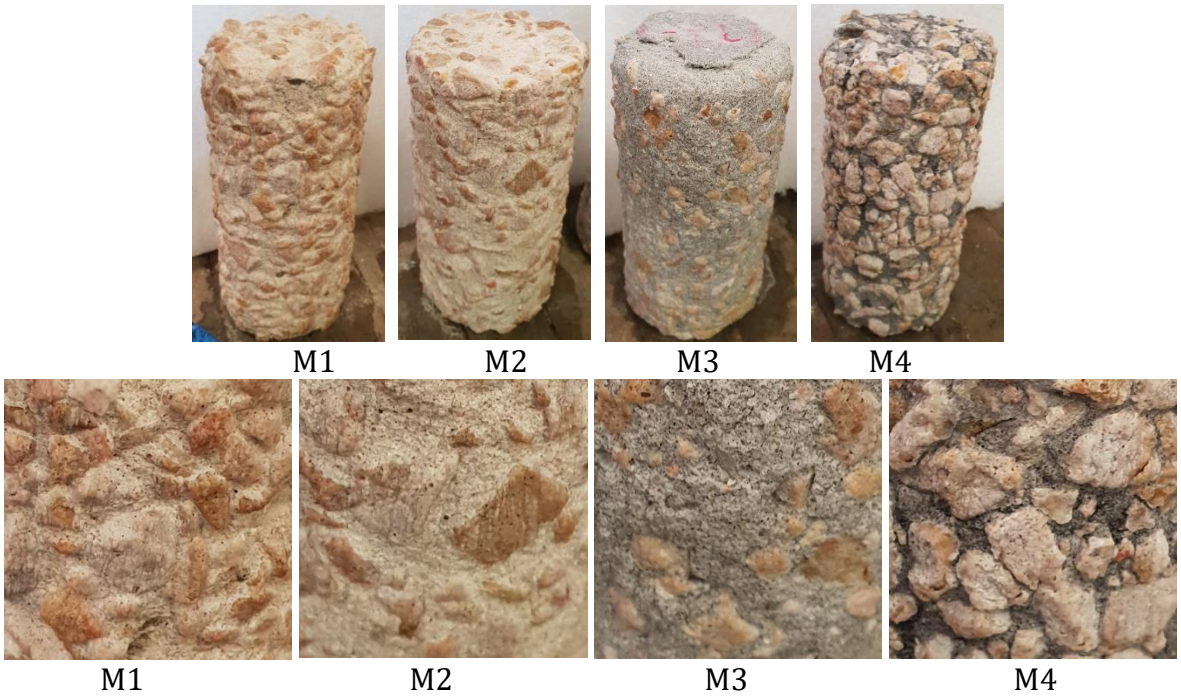

Figure 5-18: Visual Appearance of concrete specimens with high w/c ratio after 4 weeks of exposure to %5 sulfuric acid. Enlarge sections from the specimens.

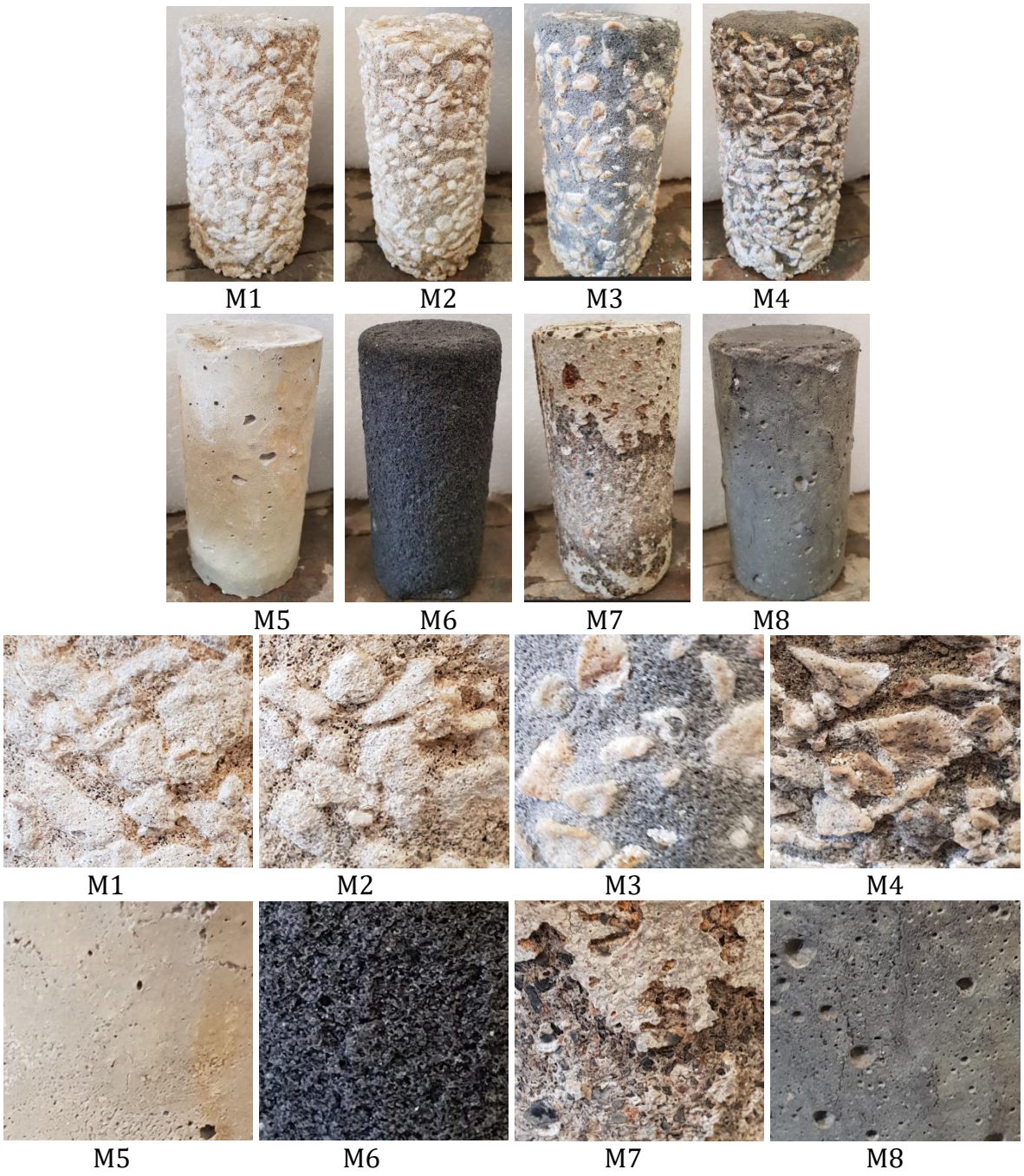

Figure 5-19: Visual Appearance after 4 weeks of exposure to %5 sulfuric acid at elevated temperature. Specimens and enlarge sections.

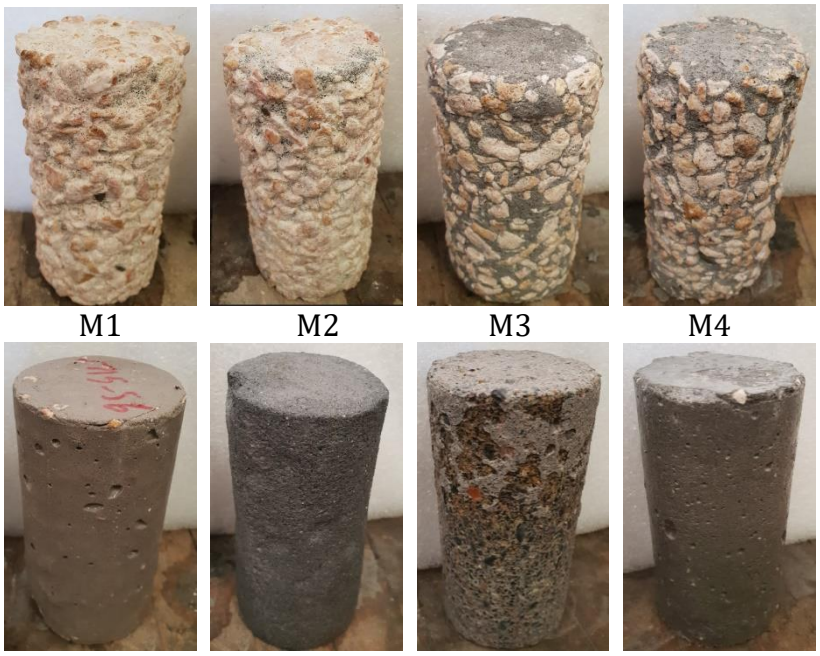

Figure 5-20: Visual Appearance after 8 weeks of exposure to %5 sulfuric acid.

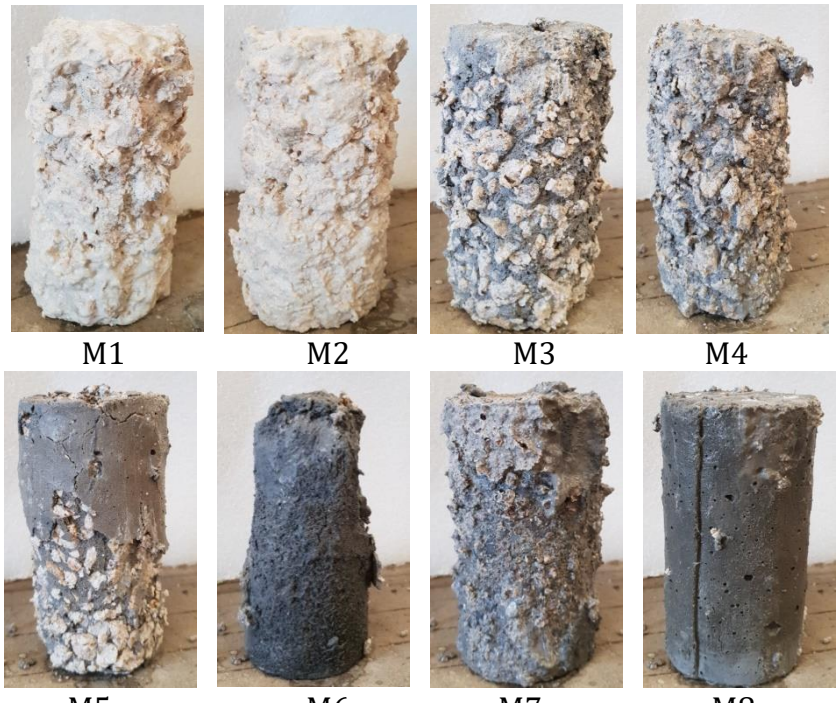

Figure 5-21: Visual Appearance after 12 weeks of exposure to %5 sulfuric acid.

M1 M2 M3 M4

Figure 5-22: Visual Appearance of concrete specimens with high w/c ratio after 12 weeks of exposure to %5 sulfuric acid.

M5 M6 M7 M8

M1 M2 M3 M4

Figure 5-23: Visual Appearance after 12 weeks of exposure to %10 sulfuric acid.

Figure 5-24: Visual Appearance paste cube specimens after 12 weeks of exposure to %5 sulfuric acid.

Figure 5-25: Visual Appearance of concrete specimens placed in the vapor zone after 12 weeks of exposure to %5 sulfuric acid at elevated temperature.

M4 M3 M2 M1

Figure 5-26: Visual Appearance of concrete specimens with high w/c ratio after 12 weeks of exposure to %5 sulfuric acid at elevated temperature.

Figure 5-27: GFRP coated concrete specimens after 12 weeks exposure to %5 sulfuric acid at elevated temperature

Figure 5-28: Concrete Specimens coated with industrial polymer coating after 4 weeks of exposure to %5 sulfuric acid at elevated temperature

5.5 Mass Loss

Mass was measured for samples before and after exposure to sulfuric acid. Mass loss as a percentage of original mass at different exposure time for specimens from all mixtures exposed to the %5 sulfuric acid solutions are calculated and presented in Table 5-6 and shown in Figure 5-29 to Figure 5-36.

Conventional Concrete Group (M1, M2)

The outer layer white color converted to gypsum and deposited leaving the aggregate exposed and over time loosening and removed. Similar observation was reported by (Hill et al 2003) and (Yang et. al 2012). For the first 4 weeks both mixes have undergone a slow reduction in mass in the range of %6.5 and %5.8 for M1 and M2 respectively. The pattern increased sharply in over the period from 4 to 12 months reaching %21.4 and %20.6. Similar results

were also reported in the previous studies as well. (Thokchom 2014 and Mehta 2017). The %10 acid concentration significantly increased the mass loss to %31.5 in the case of M1 vs %27.4 in M2. This is expected as the increase of acid concentration lead to more ions exchange and bleaching of Ca^{++} ions to react and form gypsum. This was demonstrated by the studies conducted with higher concentration acid such as (Hewayde et al 2007, Freidin 1999, Aydin et al 2005, Shamila 2016) as compared to those with less concentration (Yuan et al 2013, Shengyuan et. al 2012, Chang et al 2005, Hill et al 2003).

At elevated temperature %5 acid exposure on the other hand both M1 and M2 demonstrated an accelerated mass loss similar to the %10 exposure normal temperature, losing %31.7 and %27.4 for M1 and M2 respectively after 12 weeks. This can be explained by the acceleration of the reaction (kinetics) at high temperature.

The effect of increased w/c cement ratio was prominent at the early stage of exposure (4 weeks) were the mass loss %11.8 compared to %6.5 in M2 and %8.8 compared to %5.8 in M2. This difference has diminished over time and no significant difference was observed after 12 weeks of exposure. In Yuan's study (2013) he observed that the degradation rate for samples with high porosity is greater than that with low porosity. He attributed this to the diffusion of sulfate is very fast and too sensitive to the porosity. (Kawai et. Al. 2005) on the other hand reported preferential effect of increased porosity.

Polymer Concrete Group (M5, M8)

Unlike Portland cement, no gypsum deposition was observed on the surface of the specimens. Some Expansion and microcracks were found. The outer layer remained intact in the case of M8 and started softening and pealing after 8 weeks in M5. Similar observation was reported

by (ALI 2005) and (Yang et. al 2012). For the first 60 days both mixes have undergone an increase in mass which continue for the case of M8 and reached %3.3 at 90 day. The pattern reserved sharply in M5 to become %11.9 mass loss When specimens were exposed to sulfuric acid solution, the pores absorbed the solution and therefore increased mass. Similar results were also reported in the previous studies (Thokchom 2014 and Mehta 2017). The %10 acid concentration significantly increased the mass loss to %21 in the case of M5 while M8 demonstrated %1 mass gain.

At elevated temperature on the other hand M5 followed similar pattern of initial increased mass but significantly higher reduction at 90 days of %21. However, in the case of M8 it has experienced the only mass loss in all exposure conditions at elevated temperature after 90 days (%3).

All polymer concrete specimens have undergone increase in volume (2mm in diameter) at 8 weeks. Soroka (1979) reported the same pattern at 28days and explained this increase in volume by the absorption of acid. (Davidovits 1994) reported the high resistance of geopolymer concrete with average mass loss of %6.5 in comparison to %45 for conventional concrete specimens in an acidic environment

Table 5-6: Mass Reduction (%)

Mix No.	2W	4W	8W	12W	4W H. Temp	4W H W/C	12W H. W/C	12W 10%	12W H.Temp	12W H. Temp H. W/C ratio
M1	6.5	6.2	12.4	21.4	9.3	11.8	22.1	31.5	31.7	28.4
M2	5.8	5.9	12.3	20.6	8.8	8.8	21.3	27.4	27.3	27.7
M3	-3.1	3.3	11.1	21.9	8.8	7.4	39.2	23.3	36.1	39.6
M4	6.3	6.5	15.2	28.2	10.8	11.3	31.5	31.3	36.4	47.2
M5	-0.4	-0.6	-0.9	11.9	-1.4			21.0	5.9	
M6	6.7	8.5	18.5	31.0	13.6			52.9	76.0	
M7	-0.3	-0.6	0.7	6.1	-2.1			13.3	13.7	
M8	-0.7	-1.3	-2.6	-3.3	-5.3			-1.0	-3.3	
P1				21.1					69.4	
P2				14.0					60.7	
P3				37.6					81.7	
P4				32.2					100.0	
P5				1.7					48.4	

SCMs Group M3-GGBFS, M4-FA

Some expansion and microcracks were found on the surface starting from the first week. The outer layer gray color converted to gypsum and deposited leaving the aggregate exposed and over time loosening and removed. For the first 4 weeks both mixes have undergone a slow reduction in mass in the range of %3.3 and %6.5 for M3 and M4 respectively. The pattern increased sharply over the period from 4 to 12 months reaching %21.9 and %28.2. The %10 acid concentration increased the mass loss to %23.3 in the case of M3 vs %31.3 in M4. This is expected as the increase of acid concentration lead to more ions exchange and bleaching of Ca^{++} ions to react and form gypsum.

At elevated temperature 5% acid exposure on the other hand both mixes followed similar pattern in mass loss as the 10% normal temperature, losing %36.1 and %36.4 for M3 and M4

respectively after 12 weeks. This can be explained by the acceleration of the reaction (kinetics) at high temperature.

The effect of increased w/c cement ratio was prominent in the case of M3 where the mass loss was %7.4 in 4 weeks and %39.2 at 12 weeks. This is significantly higher than the mass compared to the same mix with lower w/c ratio which was %21.9. M4 on the other hand lost %8.8 and %31.5 for 4 and 12 weeks respectively which is not far from the low w/c ratio.

Special Concrete Group M6-UHPC and M7-CAC

The two concrete types under this group performed in a totally different manner. UHPC, although has the highest performance among all groups in the mechanical properties, it performed negatively in term of mass stability when exposed to sulfuric acid. Mass loss especially at high temperature where it lost %76 in mass. The outer layer gray color converted to gypsum and deposited uniformly. This is attributed to the fact that this mix did not include aggregate which did not experience reduction in mass throughout the other mixes. Moreover, higher reaction surface presented in UHPC had led to accelerated reaction. The high inclusion of silica fume reduced significantly the permeability and diffusion coefficients but it did not prevent or reduce the reaction with sulfuric acid. UHPC had a 12 weeks mass reduction of %31 and %52.9 for the acid concentration exposure of %5 and %10 respectively.

CAC on the other hand demonstrated the best performance among all groups in term of integrity and mass reduction. The outer surface remains highly intact with only small amount of soft layer deposition which again determined by XRD to be gypsum. 12 weeks mass reduction of %6.1, and %13.7 at high temperature. No signs of color change or cracking was identified. Unlike Portland cement, the hydration product of CAC is based on CAH (Calcium

Aluminate Hydrate) phases which are not easy to break by sulfuric acid. Moreover, absence of calcium hydroxide (the most vulnerable phase to acid attack) made it resistant to sulfuric acid.

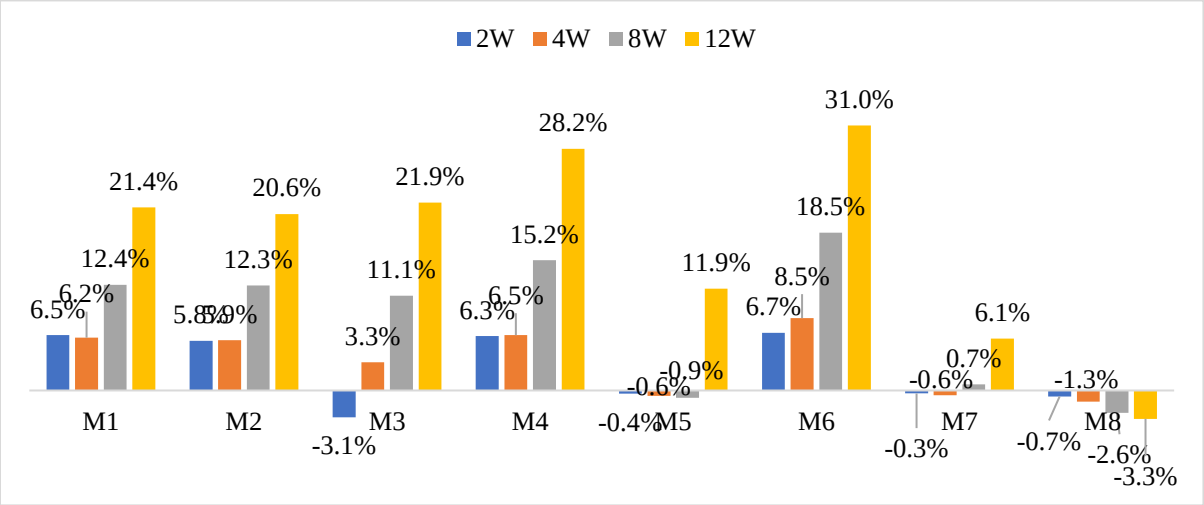

Figure 5-29:Mass Reduction After Exposure to %5 Sulfuric Acid

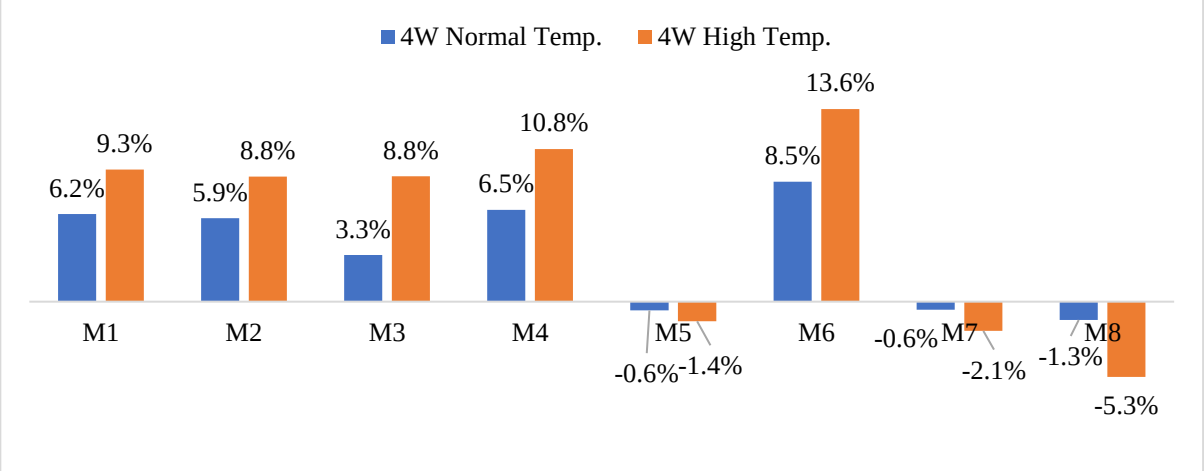

Figure 5-30: Mass Reduction After 4W Exposure to %5 Sulfuric Acid Normal vs High Temp

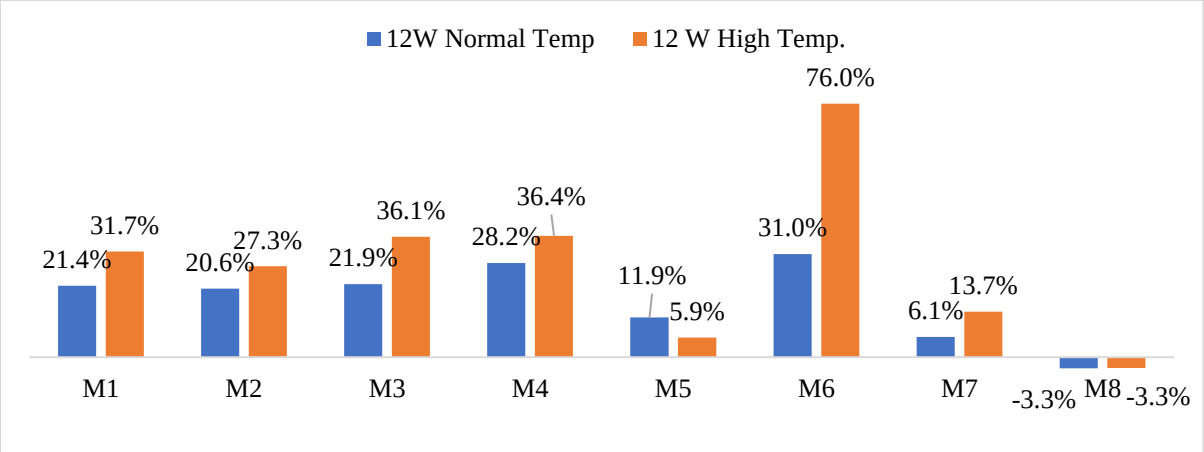

Figure 5-31: Mass Reduction After 12W Exposure to %5 Sulfuric Acid Normal vs High Temp

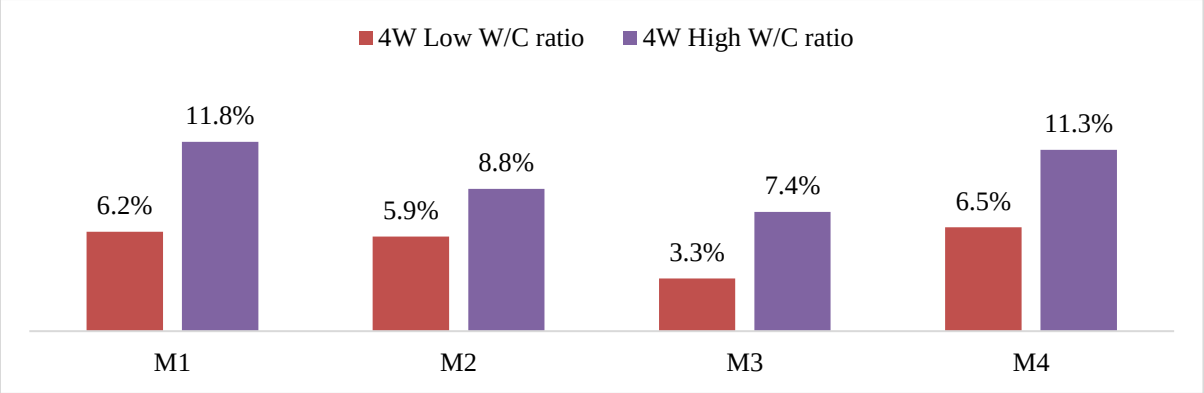

Figure 5-32: Mass Reduction After 4W Exposure to %5 Sulfuric Acid Low vs High w/c ratio

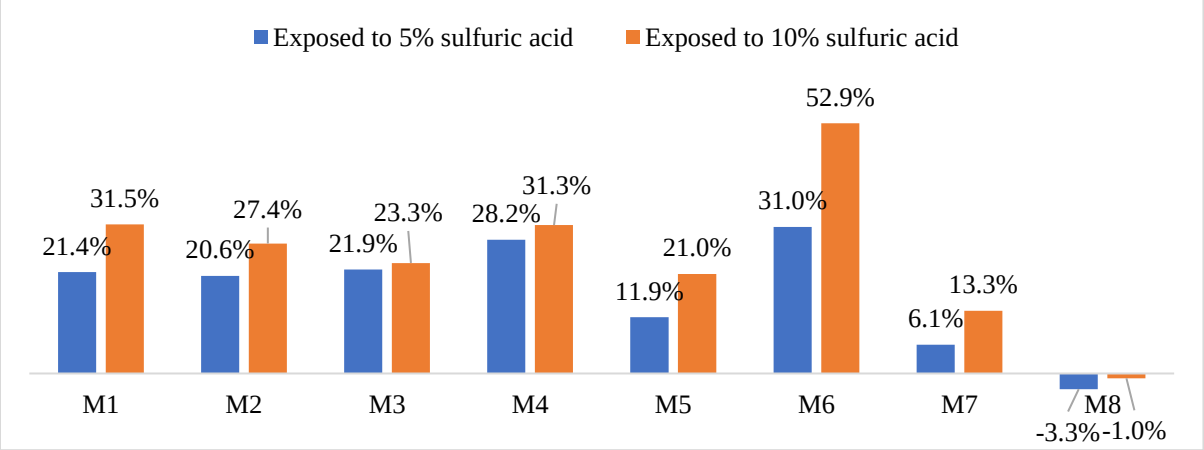

Figure 5-33: Mass Reduction After 12W Exposure to %5 vs %10 Sulfuric Acid at Normal Temp.

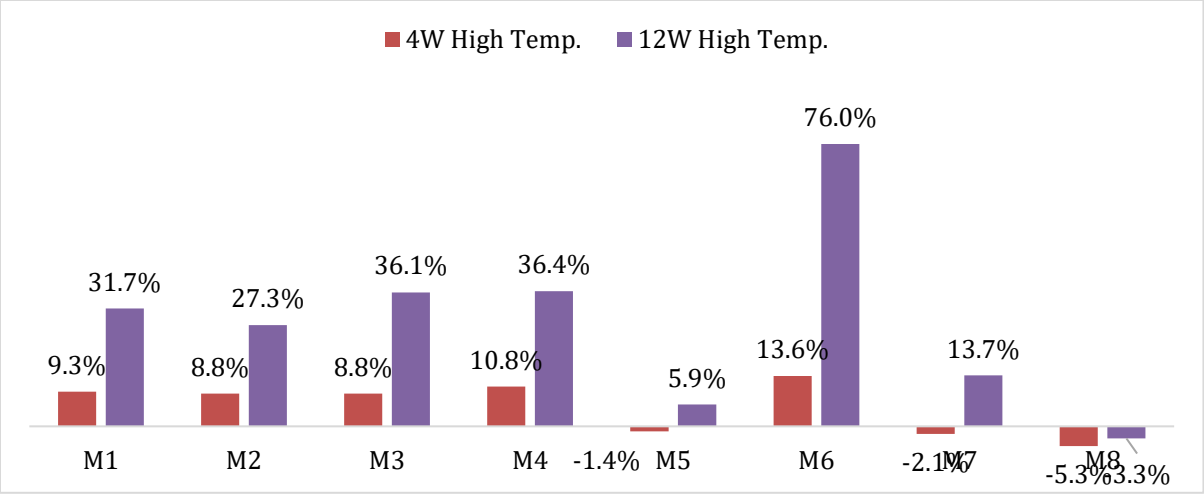

Figure 5-34: Mass Reduction After Exposure to %5 Sulfuric Acid at High Temp

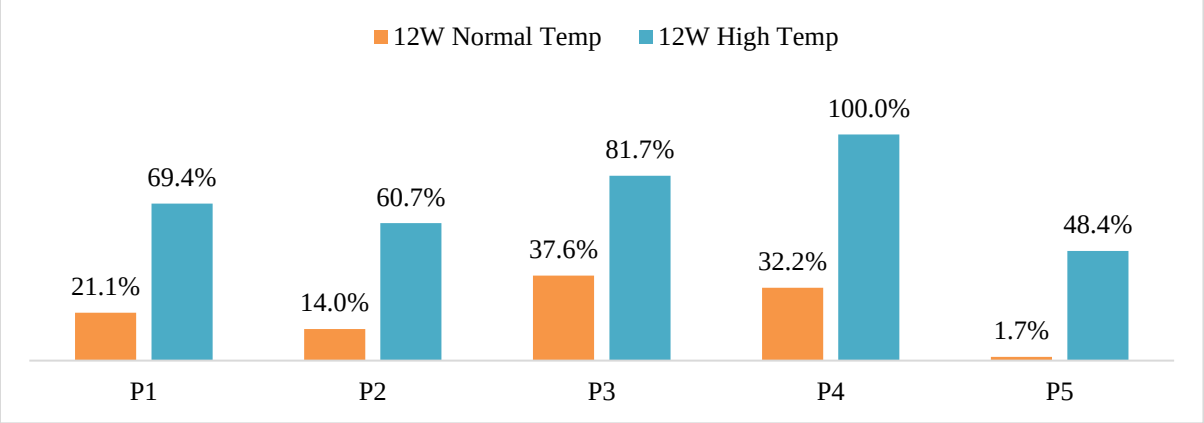

Figure 5-35: Mass Reduction in Paste After 12W Exposure to %5 Sulfuric Acid Normal vs High Temp

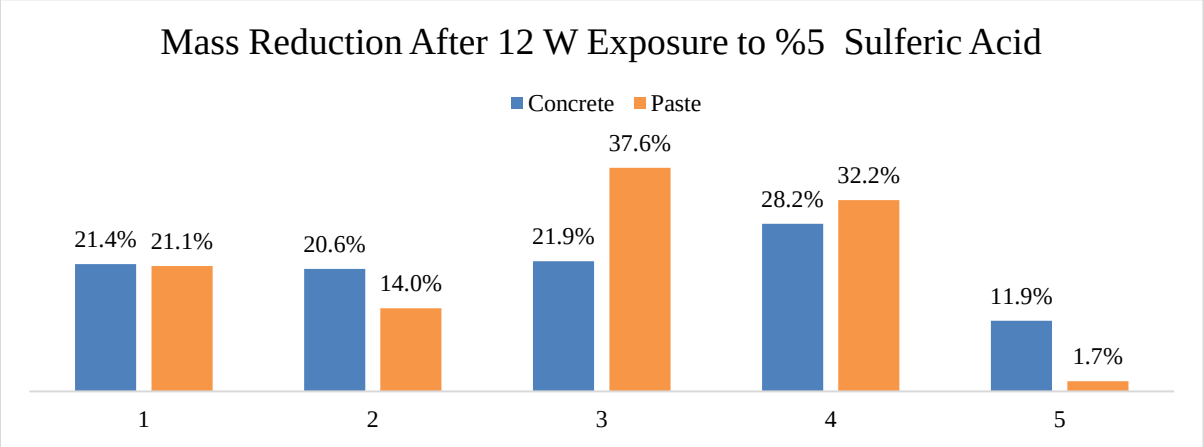

Figure 5-36: Mass Reduction After 12 W Exposure to %5 Sulfuric Acid

5.6 Compressive Strength

Compressive strength was conducted in accordance to ASTM C39. Average of 3 Cylinders 3x6in size was considered. Samples were capped with sulfur to ensure smooth surface. Samples tested for 7 days, 28 days before starting the exposure to sulfuric acid. Exposed samples were retrieved and tested for periods of 2, 4, 8 and 12 weeks. Each retrieved sample include both water cured (reference) and acid exposed in order to make comparison. Compressive strength results of the water cured samples are shown in Figure 5-37-5.45 and Table 5-7. Results for samples under acid exposure at normal and high temperature are provided in Table 5-8 and Table 5-9.

Table 5-7: Compressive Strength of sample under curing

	7days	28 days	2W curing	4W curing	8W curing	12W curing
	7	28	42	56	84	112
M1	41.70	49.96	53.401	54.00	52.99	56.5
M2	38.84	43.39	49.325	52.00	55.26	56.0
M3	63.21	81.36	84.000	85.00	84.02	82.8
M4	47.60	68.32	69.000	71.00	77.23	77.0
M5	24.43	22.00	22.760	20.00	19.25	20.2
M6	94.59	101.6	105.0	100.78	100.55	100.0
M7	51.70	74.08	70.000	66.00	62.00	60.0
M8	22.10	28.56	37.209	40.00	39.63	39.4

Table 5-8: Compressive Strength of sample exposed to %5 sulfuric acid at normal temperature

	28 days	2W Acid	4W Acid	8W Acid	12W Acid
M1	49.96	47.7	50.0	47.0	26.7
M2	43.39	45.1	45.0	45.5	32.1
M3	81.36	57.3	62.0	45.7	39.7
M4	68.32	57.3	62.4	48.0	22.4
M5	22.00	21.0	20.8	18.3	16.3
M6	101.6	101.6	87.0	79.0	54.7
M7	74.08	57.4	74.8	57.1	55.1
M8	28.56	35.7	35.4	34.9	38.6

Table 5-9: Compressive Strength of sample exposed to %5 sulfuric acid at high temperature

	28 days	4W Acid H.temp	12W Acid H.temp
M1	49.96	42.79	21
M2	43.39	44.61	20
M3	81.36	62.78	25
M4	68.32	55.39	16
M5	22.00	24.91	14
M6	101.6	93.87	19
M7	74.08	54.81	45
M8	28.56	41.50	32

Conventional Concrete Group (M1-OPC, M2-SRPC)

Compressive strength of unexposed specimens at 28 days of curing were 50.3 MPa and 43.2 MPa for M1 and M2 respectively as shown in Figure 5-38 and Figure 5-39. Compressive strength of exposed specimens at ambient temperature indicated a significant reduction from 56.4MPa to 26.7MPa (%53) in the case of M1 after 12 weeks while reduction was from 56.0 to 32.14 (%39) in the case of M2. At elevated temperature (100^{o}C) on the other hand indicated a drop in strength by %63.0 and %62.0 for M1 and M2 respectively. Loss of compressive strength is attributed to the softening of the corroded outer layer and the breakage of the CSH hydrated cement phase which is the primary contributor to the strength of concrete in addition to the cracking due to formation of expansive products formed by sulphate reaction with

aluminate phases. Similar observation of mass loss was reported by Mehta (2017). Hewayde et. Al (2007) has attributed the strength reduction to the loss of cement paste and its structural integrity, weakening of the concrete matrix, as well as a reduction in the specimen's diameter. Xie (2004) attributed it to changing crystal structure and internal expansion. There is a direct but not proportional relationship between mass loss and compressive strength in the case of M1 (R2=0.8) and M2 (R2=0.9) as indicated in Figure 5-48 and Figure 5-49. In the case of M1 mass loss %21.4 vs a compressive strength loss of %53. While in the case of M2 mass loss of %20.6 vs a compressive strength of %39. This explains the fact that the degradation extends far beyond the outer surface.

Alkali Activated Polymer Concrete Group (M5, M8)

Compressive strength of unexposed specimens at 28 days of curing were 23 MPa and 28 MPa for M5 and M8 respectively. Compressive strength of exposed specimens at ambient temperature indicated a small reduction from 20MPa to 16MPa (%20) in the case of M5 after 12 weeks while reduction was very minor in the case of M8 (%2). At elevated temperature (100^{o}C) on the other hand indicated a drop in strength of %30, and %12.5 for M5 and M8 respectively. Figure 5-42 and Figure 5-45 illustrate the compressive strength loss for M5 and M8. Incorporation of OPC cement (%10) in M8 lead to the improved strength as compared to the case of M5 which only included GGBFS and FA.

The availability of more calcium content in the form of OPC in M8 lead to significantly higher compressive strength of unexposed specimens. The increase in calcium content initiates the hydration mechanism which results in the formation of calcium-based hydrated products C-S-H. Moreover, liberation of more heat during hydration provide better curing which further

increased the geo-polymeric alumina-silicate bonds. Improvement in the microstructure with less porosity has also contributed to the increase compressive strength (Skyara et. Al 2006).

The strong alumina-silicate bonds which are not easily broken by acid resulted in better performance in term of strength. (Mehta 2017, Bakharev 2005). No direct relationship between mass loss and compressive strength loss identified as illustrated in Figure 5-52 and Figure 5-55.

SCMs Group (M3-GGBFS, M4-FA)

In general, incorporation of supplementary cementitious materials (SEMs), including GGBFS, FA, and SF had led to increased compressive strength of water cured concrete specimens. Compressive strength of unexposed specimens at 28 days of curing were 81.36 MPa and 68.32 MPa for M3 and M4 respectively as shown in Figure 5-40 and Figure 5-41. The advantage of added SCMs is either due to the pores filling effect by very fine particles or due to pozzolanic reaction in which they react with calcium hydroxide to form a reaction product that is similar in composition and properties to C-S-H as discussed in Section 2.3.

Compressive strength of exposed specimens at ambient temperature indicated a significant reduction from by %52 and %67 in M3 and M4 respectively after 12 weeks. At elevated temperature (100^{o}C) on the other hand indicated a drop-in strength %70 and %76 for M3 and M4 respectively. Loss of compressive strength is attributed to the softening of the corroded outer layer and the breakage of the CSH hydrated cement phase which is the primary contributor to the strength of concrete. There is direct proportional relationship between mass loss and compressive strength in the case of M4 (R2=0.9) while M4 did not establish clear relationship (R2=0.3) as indicated in Figure 5-50 and Figure 5-51.

Special Concrete Group (M6-UHPC, M7-CAC)

UHPC had the highest performance among all groups in the mechanical properties with compressive strength of 101.6 MPa at 28 days curing (Figure 5-43). This has been achieved by the incorporation of SF and steel fibers in the concrete mix. However, this concrete was among the highest in reduction in compressive strength, losing %74 after 12 weeks acid exposure at high temperature. As explained before this concrete had performed the worst in term of mass stability when exposed to sulfuric acid. It did not establish clear relationship between mass and compressive strength (R2=0.09) as indicated in Figure 5-53.

CAC came third among the highest compressive strength among all groups in the mechanical properties with compressive strength of 74.08 MPa at 28 days curing (Figure 5-44). In addition, CAC demonstrated great resistant to sulfuric acid with only %8.0 reduction after 12W exposure and %25 after 12W exposure at high temperature. Figure 5-46 and Figure 5-47 illustrate the compressive strength loss for both concrete types. As explained before, absence of calcium hydroxide in the hydration product of CAC increased resistance to acid. It did not establish clear relationship between mass and compressive strength (R2=0.06) as indicated in Figure 5-54.

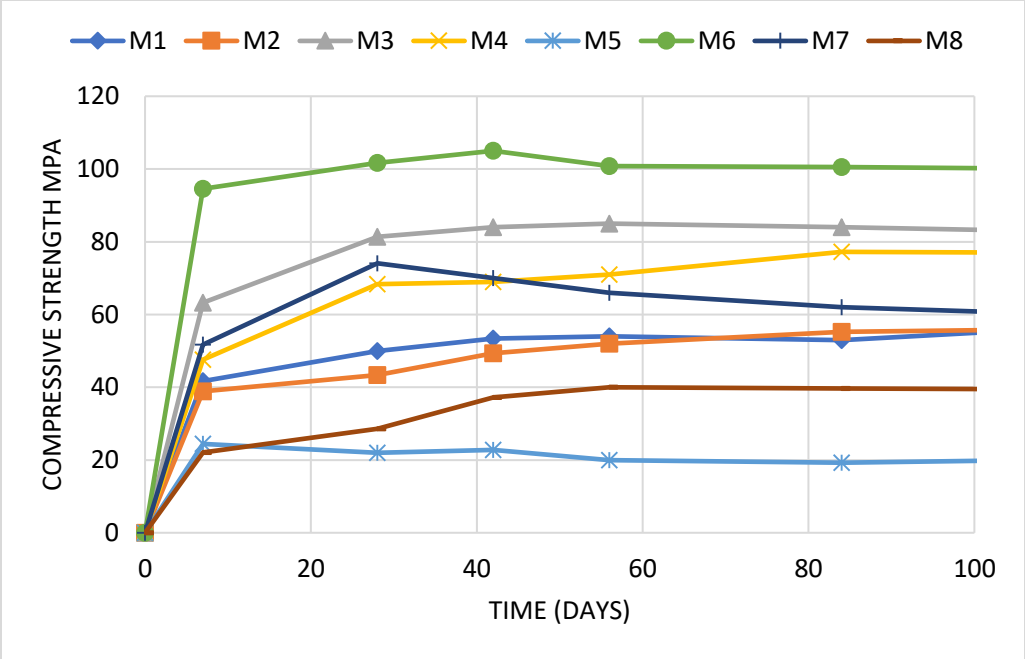

Figure 5-37: Compressive strength of concrete specimens under continuous water curing. M1-M8

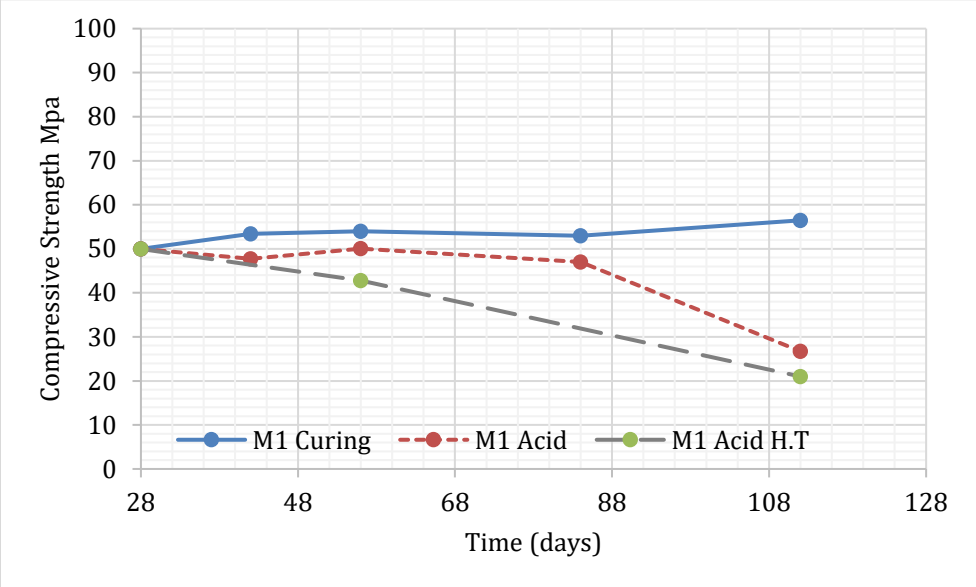

Figure 5-38: Compressive Strength of M1-OPC under water curing and under sulfuric acid exposure at normal (NT) and elevated temperature (HT)

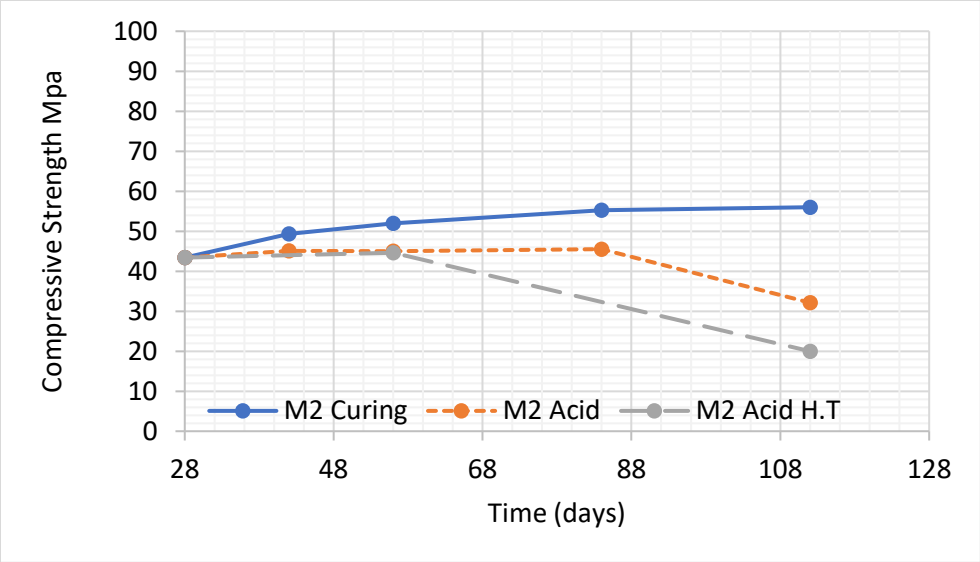

Figure 5-39: Compressive Strength of M2-SRPC under water curing and under sulfuric acid exposure at normal (NT) and elevated temperature (HT)

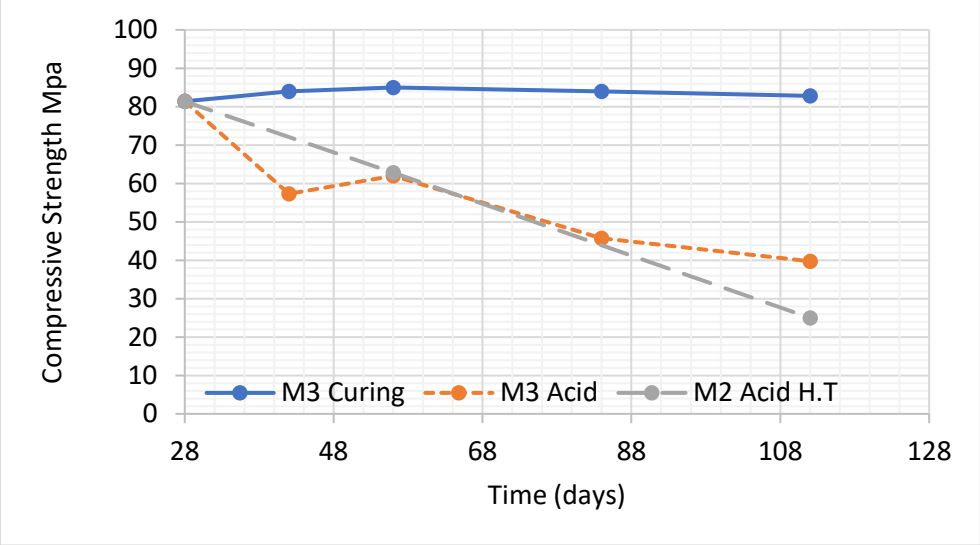

Figure 5-40: Compressive Strength of M3-GGBFS under water curing and under sulfuric acid exposure at normal (NT) and elevated temperature (HT)

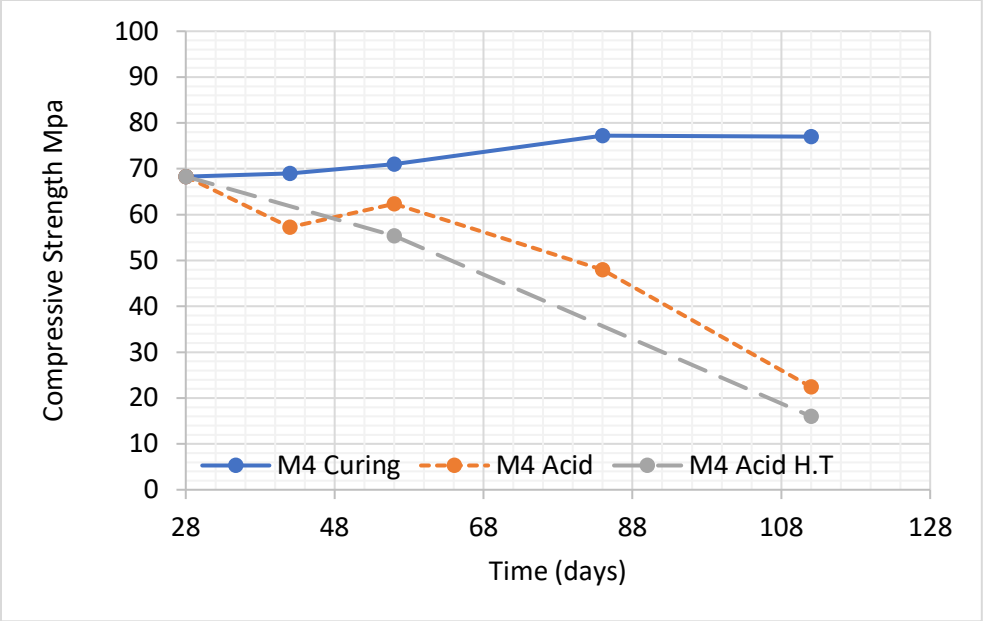

Figure 5-41: Compressive Strength of M4-FA under water curing and under sulfuric acid exposure at normal (NT) and elevated temperature (HT)

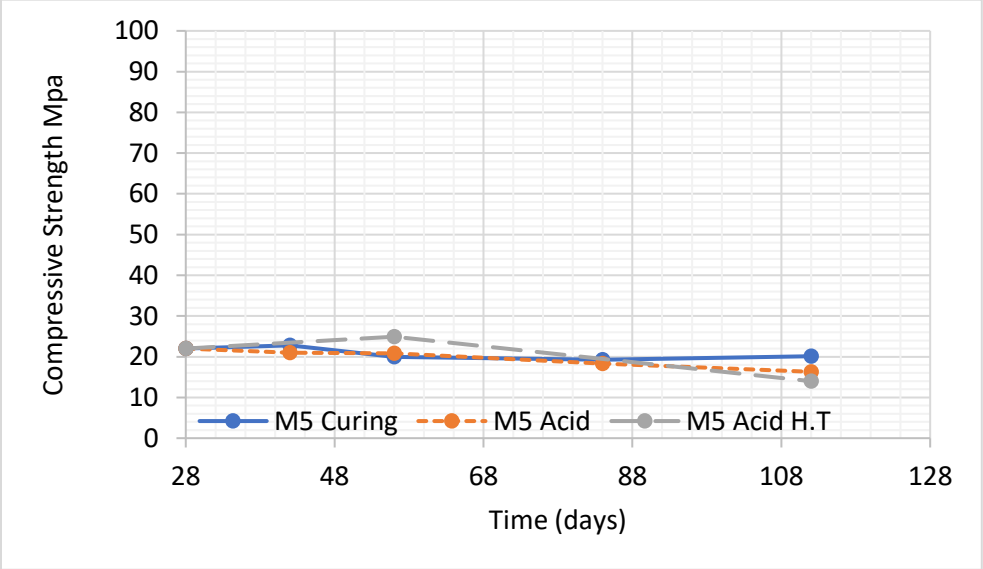

Figure 5-42: Compressive Strength of M5-AAC under water curing and under sulfuric acid exposure at normal (NT) and elevated temperature (HT)

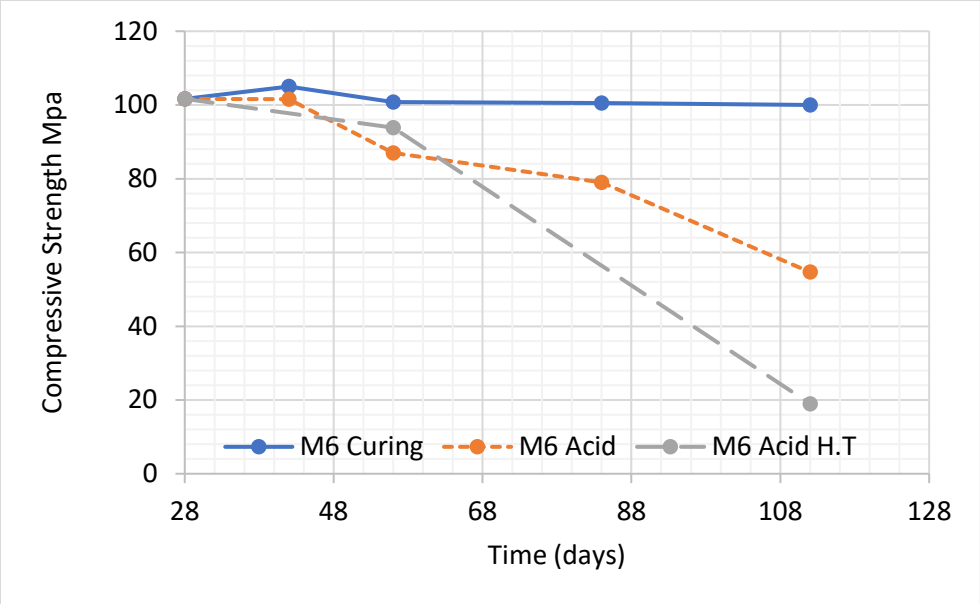

Figure 5-43: Compressive Strength of M6-UHPC under water curing and under sulfuric acid exposure at normal (NT) and elevated temperature (HT))

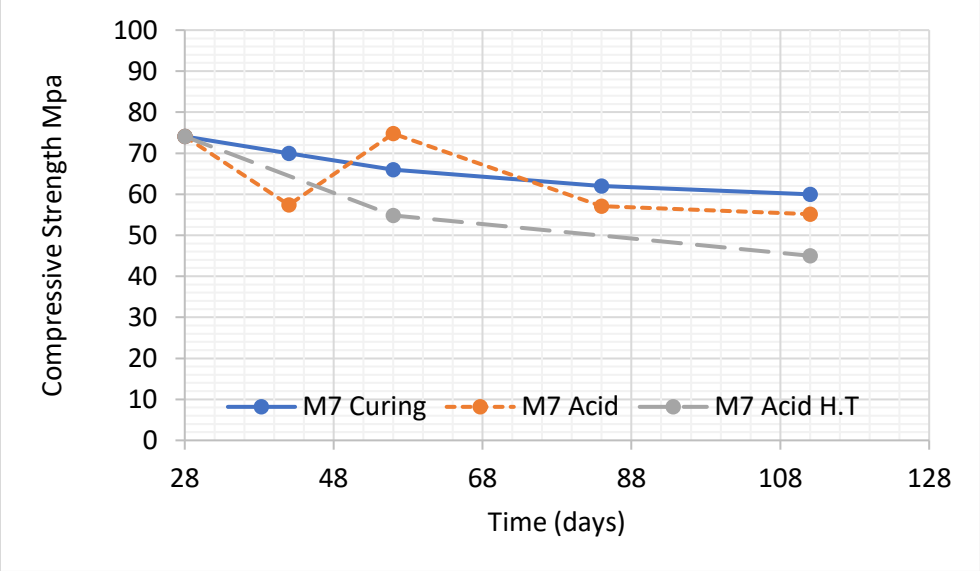

Figure 5-44: Compressive Strength of M7-CAC under water curing and under sulfuric acid exposure at normal (NT) and elevated temperature (HT)

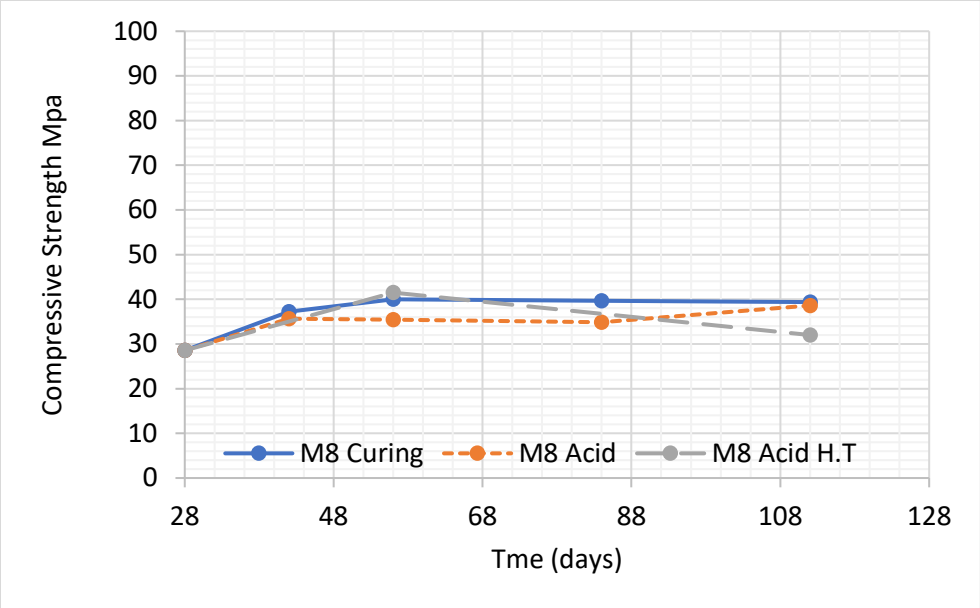

Figure 5-45: Compressive Strength of M8-Acid Resistant under water curing and under sulfuric acid exposure at normal (NT) and elevated temperature (HT)

Table 5-10: Compressive strength Loss (%) after exposure to sulfuric acid

	2W	4W	4W H.T	8W	12W	12W HT
M1	11	7	21	11	53	63
M2	9	10	14	18	39	62
M3	34	27	26	46	52	70
M4	12	16	20	38	67	76
M5	8	-11	-25	5	19	31
M6	3	5	7	21	24	74
M7	8	4	27	26	8	25
M8	4	7	-4	12	2	19

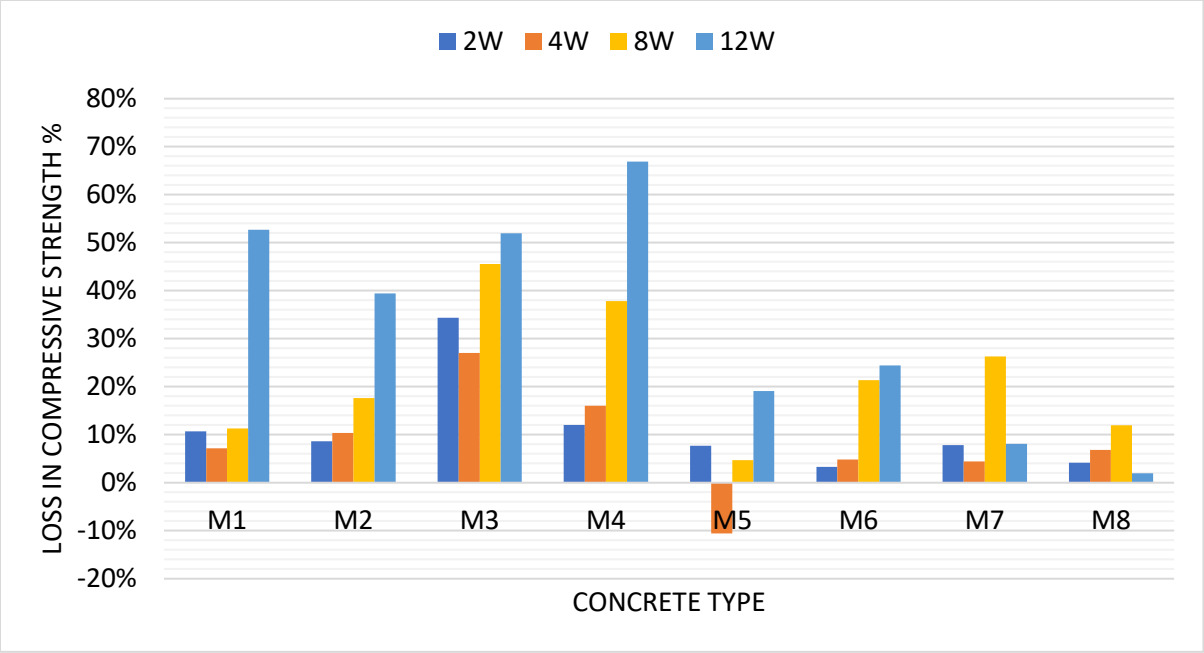

Figure 5-46: % Loss of Compressive Strength-Normal Temp

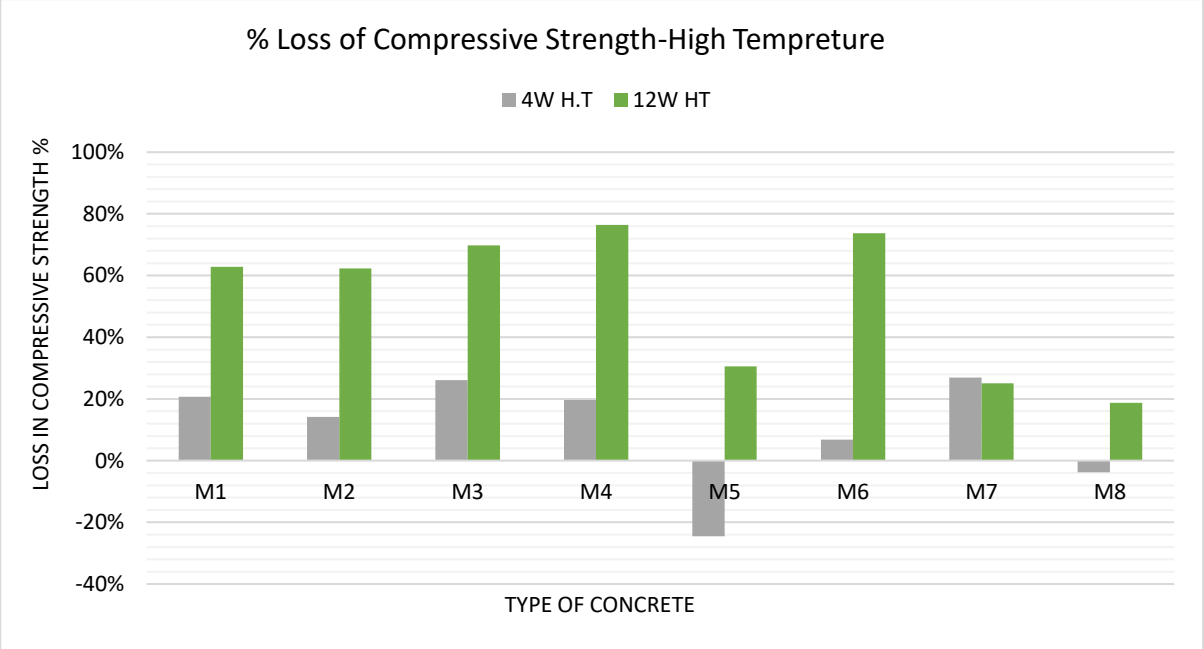

Figure 5-47: % Loss of Compressive Strength-High Temperature

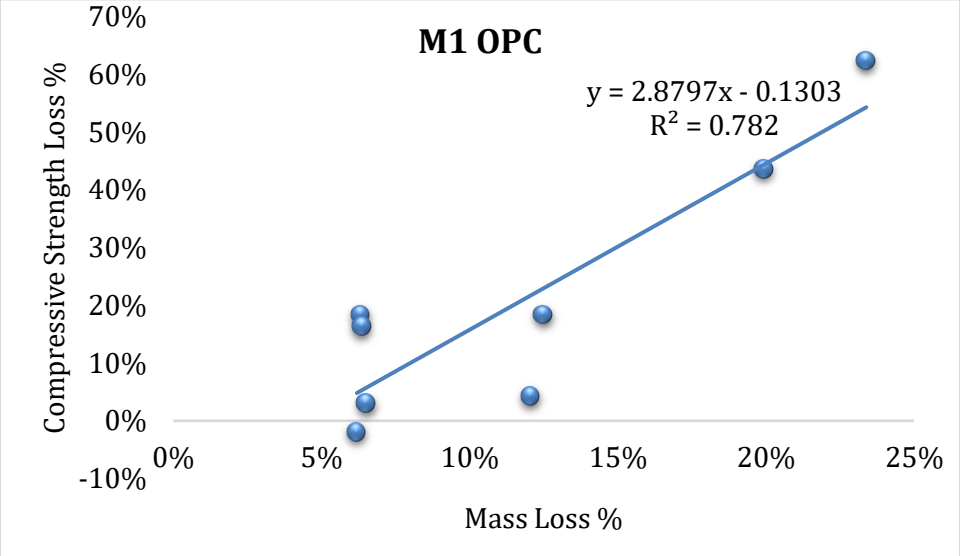

Figure 5-48: Correlation between % loss of mass and strength, (M1).

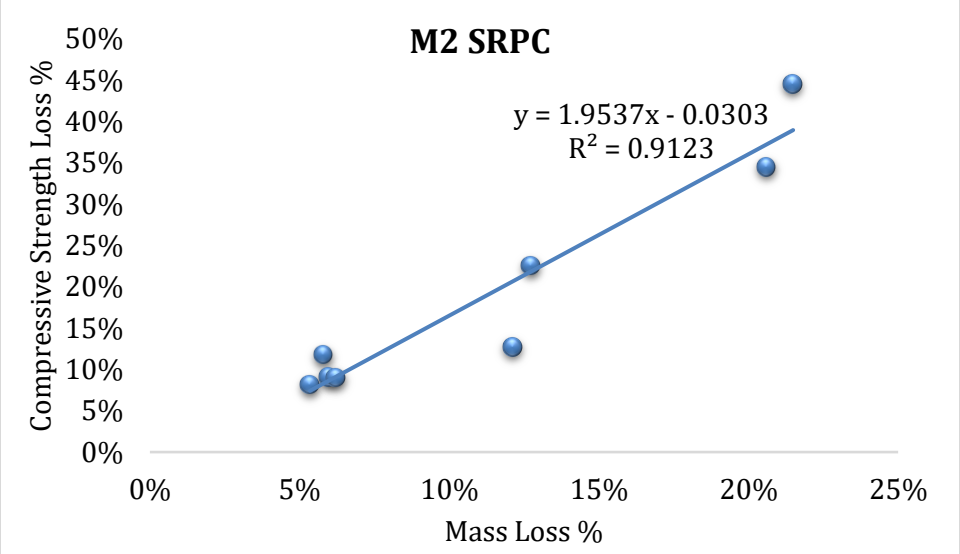

Figure 5-49: Correlation between % loss of mass and strength, M2.

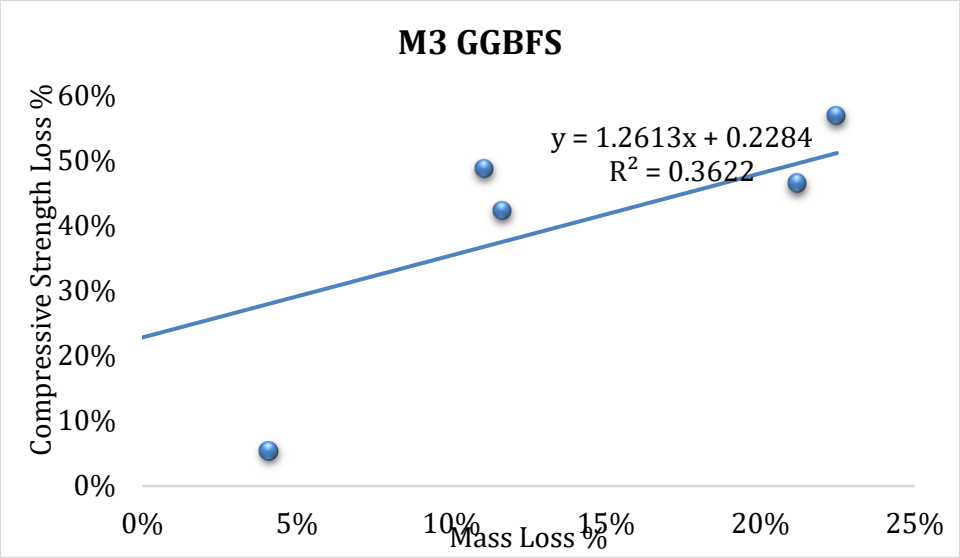

Figure 5-50: Correlation between % loss of mass and strength, M3.

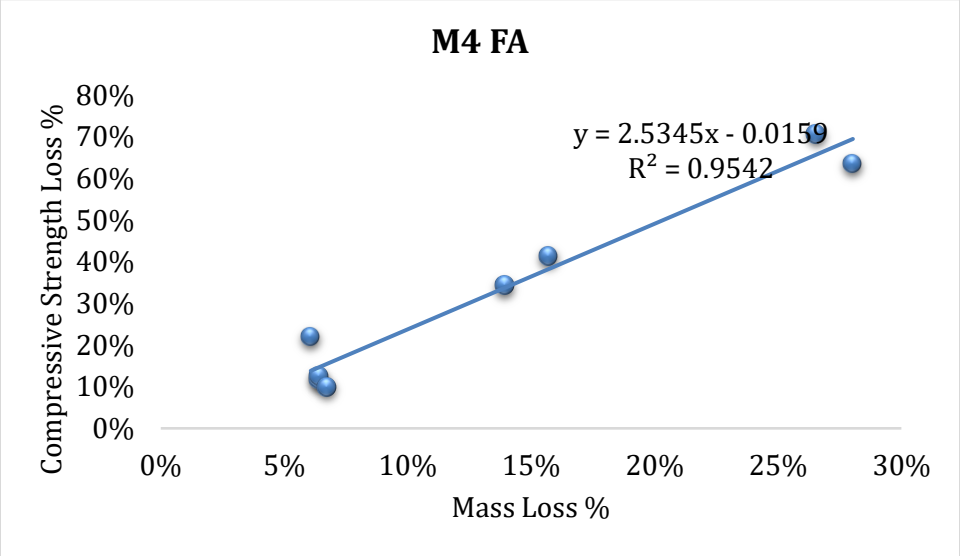

Figure 5-51: Correlation between % loss of mass and strength, M4

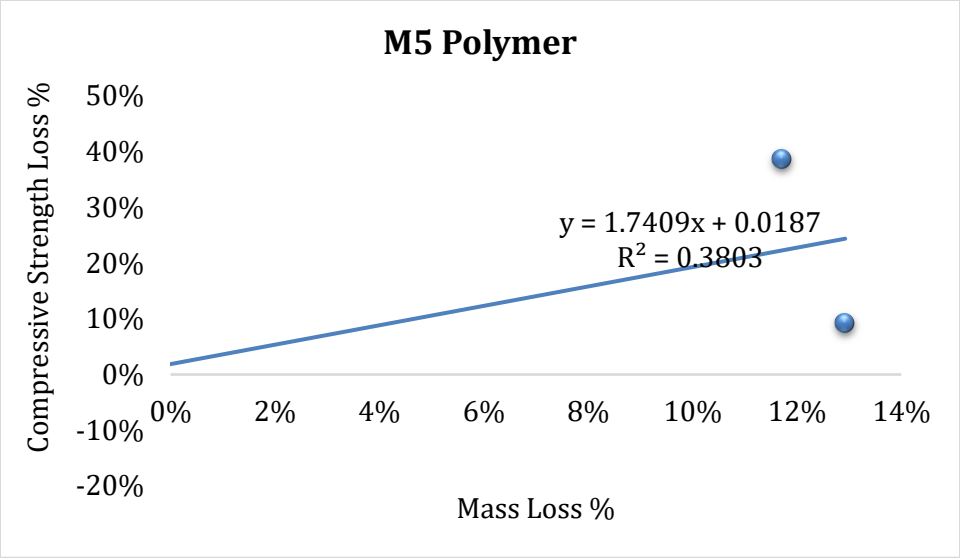

Figure 5-52: Correlation between % loss of mass and strength, M5

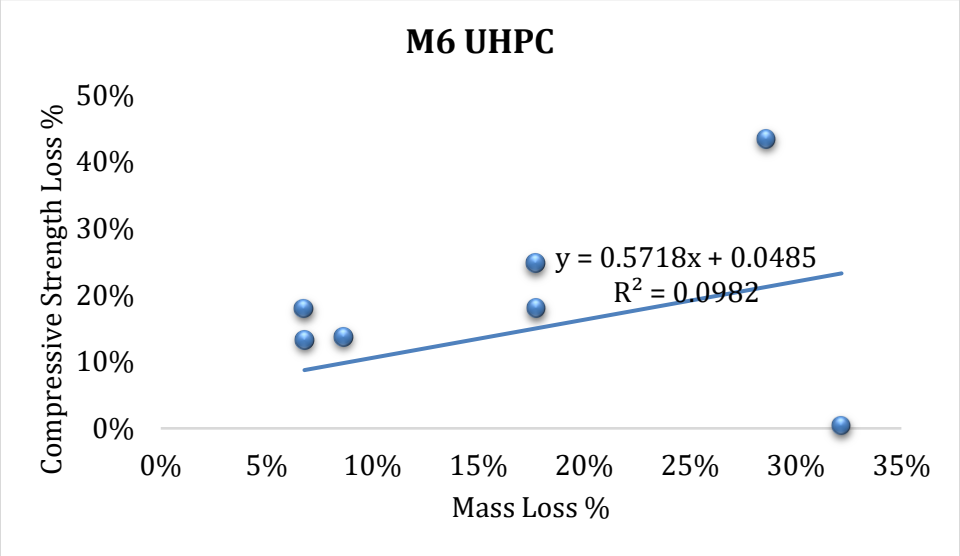

Figure 5-53: Correlation between % loss of mass and strength, M6

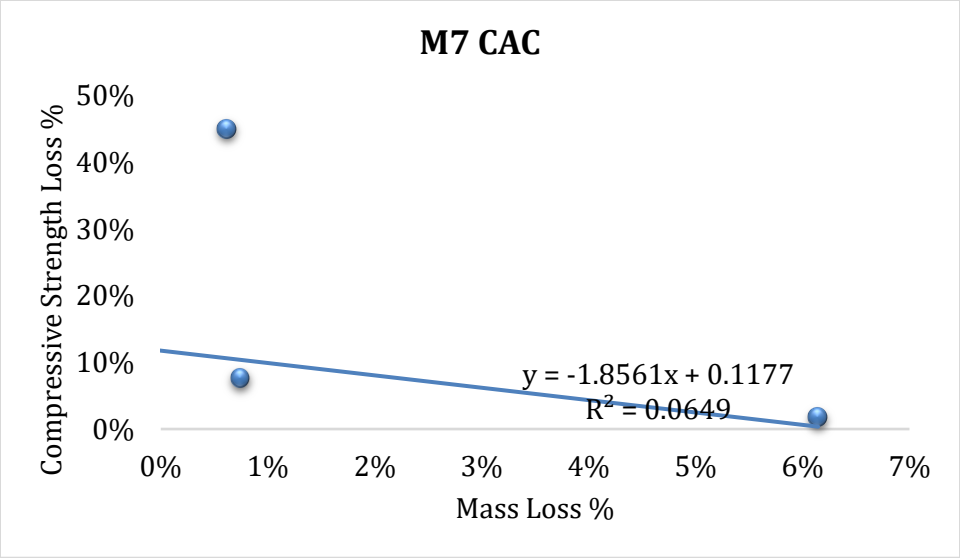

Figure 5-54: Correlation between % loss of mass and strength, M7

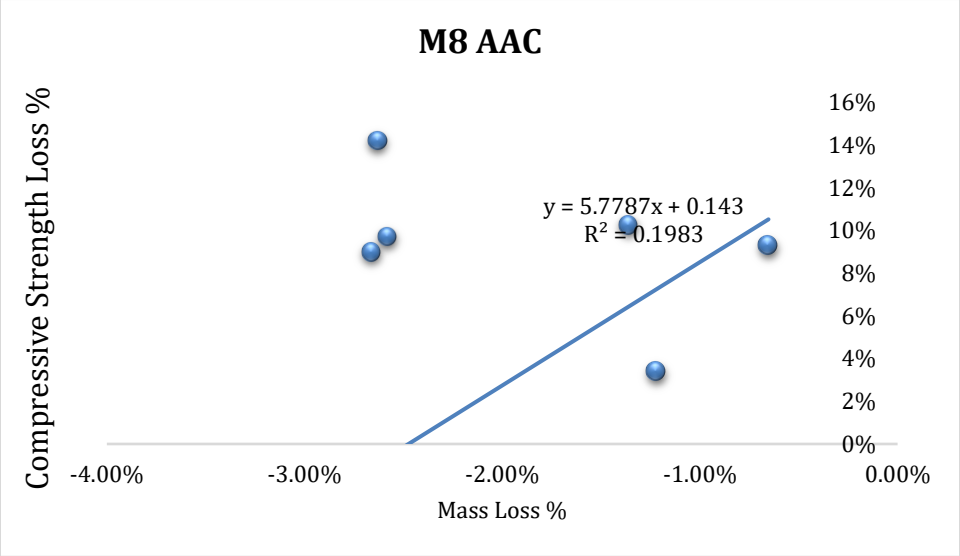

Figure 5-55: Correlation between % loss of mass and strength, M8

5.7 Split Tensile Strength

Split tensile strength was conducted in accordance to ASTM C496. Results of tensile strength for all concrete types before and after exposure to sulfuric acid are provided in Figure 5-57.

The results presented are for the exposure up to 8 weeks. As the specimen's outer surface loose, the paste and expose aggregate, it becomes rough which make it difficult to evenly distribute the load. A rubber mat was used to allow uniform load distribution over the surface. However, after 8 weeks of exposure it became difficult to accommodate and obtain accurate and reliable results.

Results of the split tensile strength before exposure to acid are consistent with the compressive strength results. Reduction in split tensile strength after exposure ranges from %18 to %34 was found in the conventional and SCM groups. In the case of UHPC it was %13, while in CAC and AAC concrete demonstrated an increase in split tensile strength in the range %5 to %22.

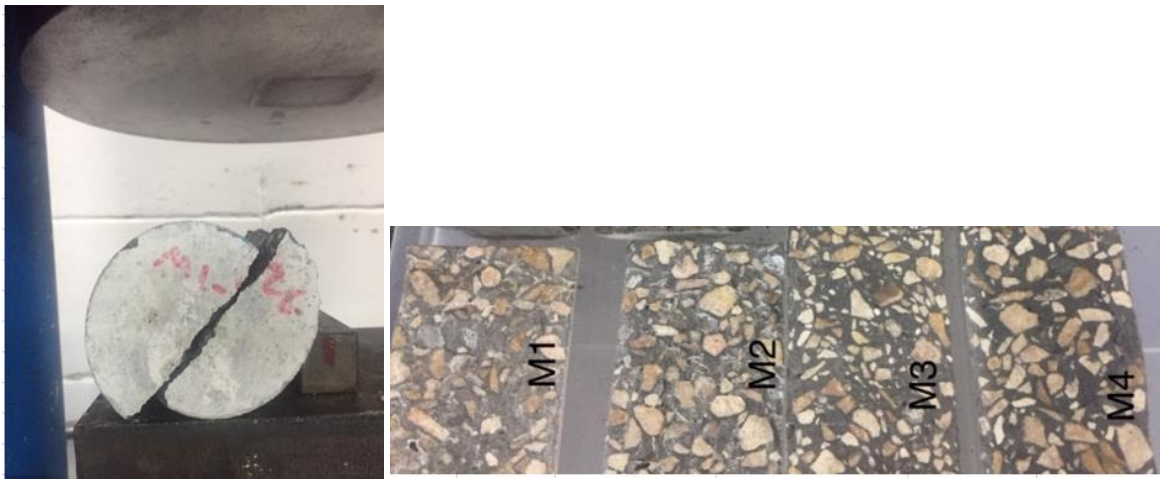

Figure 5-56: Split tensile strength of concrete specimens

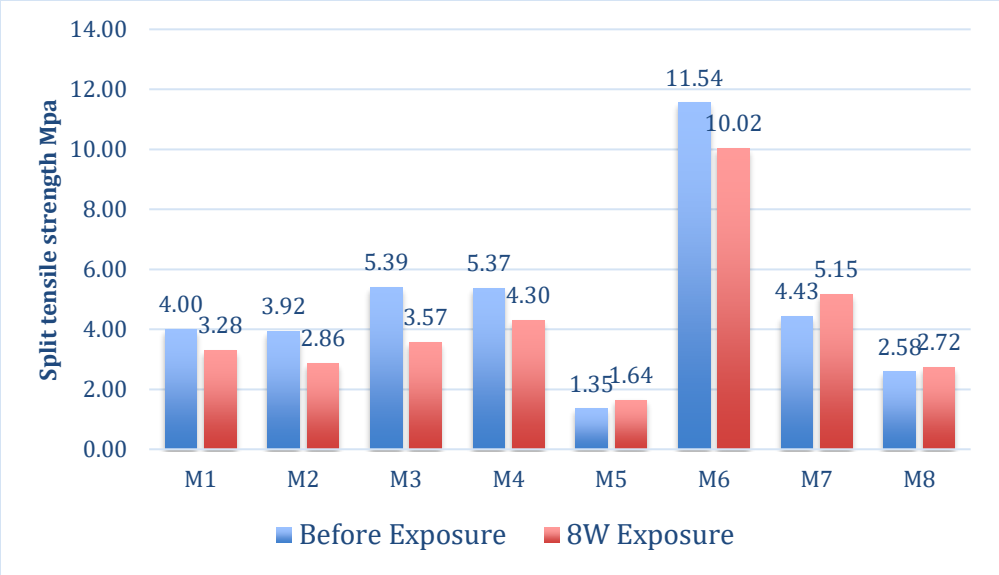

Figure 5-57: Split tensile strength of concrete under water curing and under sulfuric acid exposure

5.8 Acid Penetration (Corrosion Depth)

After each period of exposure, the acid affected layer as defined by the layer through which acid penetrated was measured by testing the pH cross the depth of the concrete sample (sample from split tensile test is utilized). Phenolphthalein color indicator was used to evaluate the pH, Phenolphthalein is colorless below 8 and pink Above 10. Corrosion depth is defined as the acid affected layer plus the depth of dissolved layer (reduction in specimens' diameter). The behavior of the various types of concrete is different for both acid affected layer and dissolved layer and sometimes inversely related. This will be demonstrated and the discussion of corrosion depth for each group below. The concept of corrosion depth was discussed in section 4.3.6 and illustrated here in Figure 5-58.

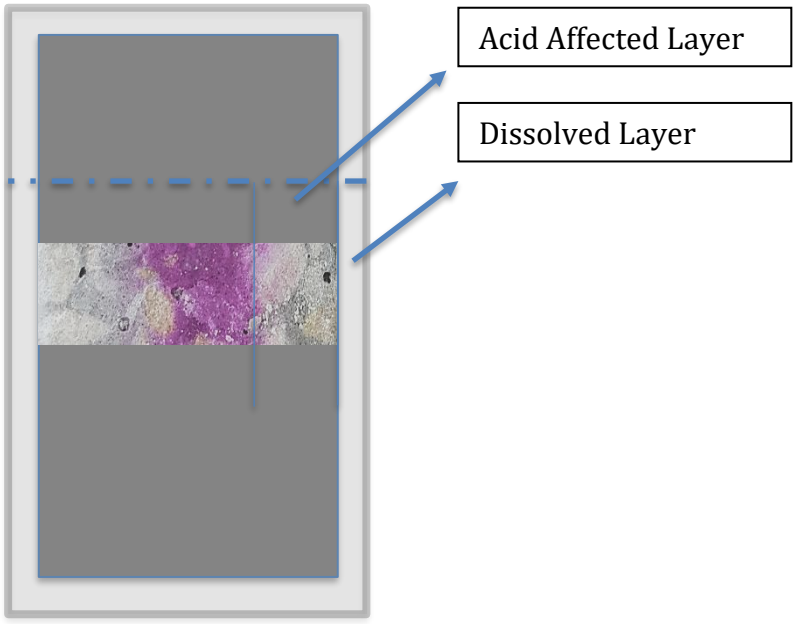

Figure 5-58: Illustration of the Corroded Layer Concept

Conventional Concrete Group (M1, M2)

From the penetration analysis as shown in Figure 5-59, it is clearly noticed that the pH affected region is just the extreme outer surface meaning that the sulfuric acid doesn't penetrates into concrete. The reaction between the various phases in concrete and the sulfuric acid takes place only in the surface portion of specimens. Similar finding was reported by (Ueda et al. 1996). Corrosion depth provided in Figure 5-63 indicates a similar pattern for both M1 and M2 with a maximum corrosion depth of 7mm and 8mm for M1 and M2 respectively, occurred at 12 weeks exposure to %5 sulfuric acid at high temperature.

SCMs Group (M3-GGBFS, M4-FA)

Incorporation of SCMs did not change the mechanism of acid penetration into the concrete. Figure 5-60 indicates that the pH affected region is just the extreme outer surface and that

acid doesn't penetrate into concrete. Corrosion depth provided in Figure 5-64 indicates a similar pattern for both M3 and M4 with a maximum corrosion depth of 7mm and 7.5mm for M3 and M4 respectively, occurred at 12 weeks exposure to %5 sulfuric acid at high temperature.

Polymer Concrete Group (M5, M8)

Unlike other types of concrete, the behavior of alkali activated polymer concrete was different in the manner that it had stronger resistance to dissolution of the outer layer, however this type of concrete experienced the highest acid penetration. This can be clearly seen from the penetration depth (Figure 5-61). Overall corrosion depth was 25mm for M5 and 15mm for M8 (Figure 5-65).

Special Concrete Group M6-UHPC, M7-CAC

From the penetration analysis as shown in Figure 5-62, it is clearly noticed that the pH affected region is just the extreme outer surface meaning that the sulfuric acid hardly penetrated into hardened cement. However, corrosion depth manifested by the dissolution of outer layer was very significant in the case of M6-UHPC which is the highest compared to all other groups. Corrosion depth provided in Figure 5-66 indicates an 18mm corrosion depth in M6 after 12 weeks exposure to %10 sulfuric acid while the maximum corrosion depth in CAC-M7 was only 2.5mm, which is the lowest among all other groups as well.

M1-OPC Ambient Temperature M2-SRPC

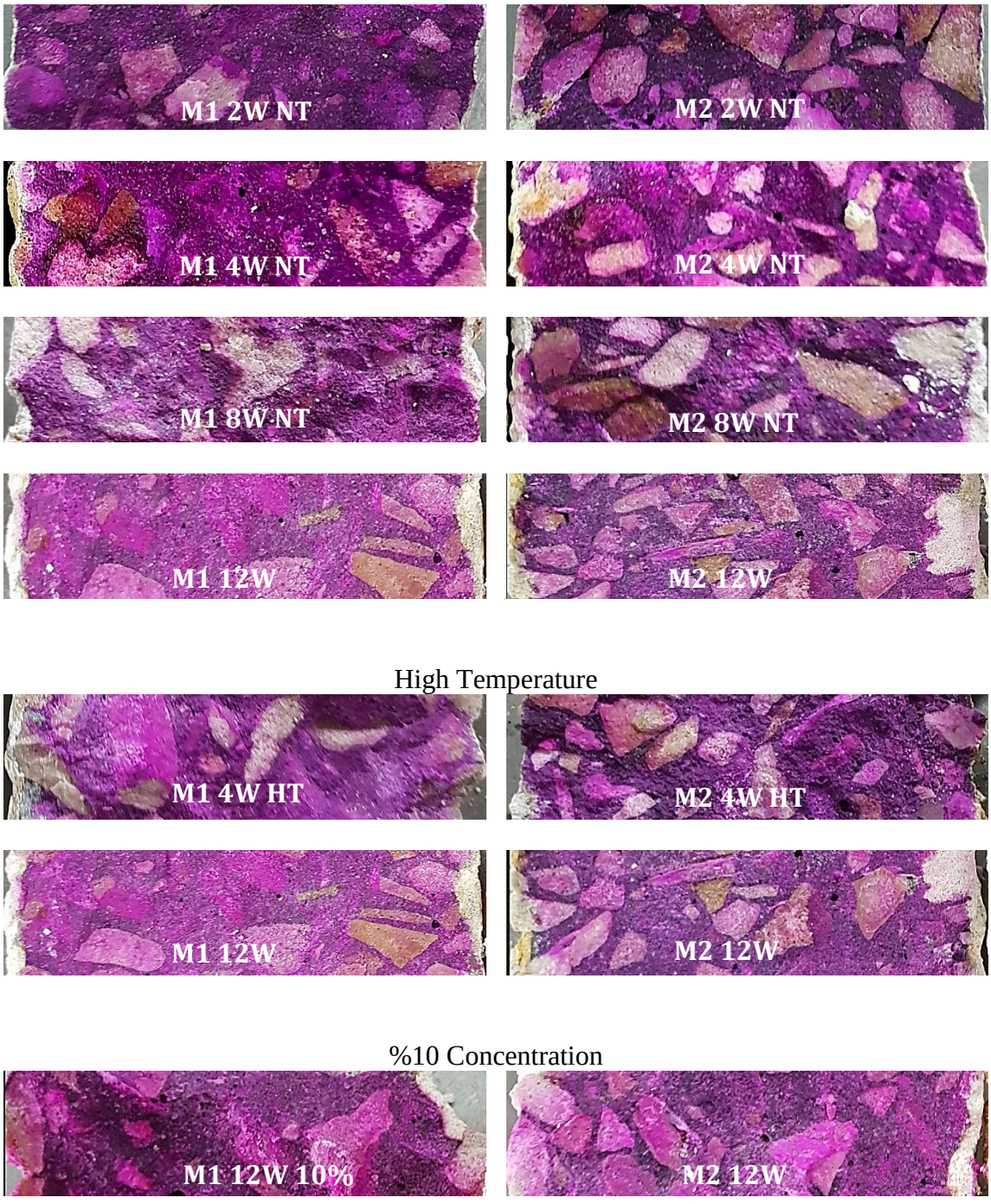

Figure 5-59:Corroded layer of concrete sample M1(left) and M2 (Right) after 2, 4, 8 and 12 Weeks at Ambient and high Temperature and at %10 concentration exposure indicated by sprayed phenolphthalein

M3-GGBFS Ambient Temperature M4-FA

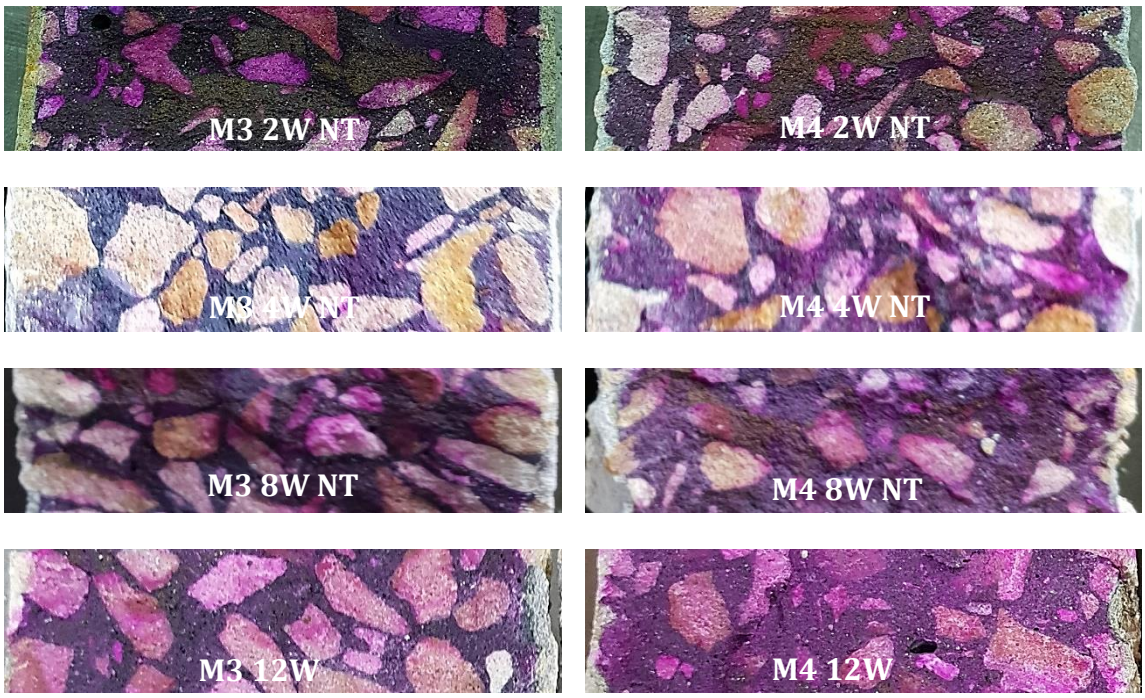

High Temperature

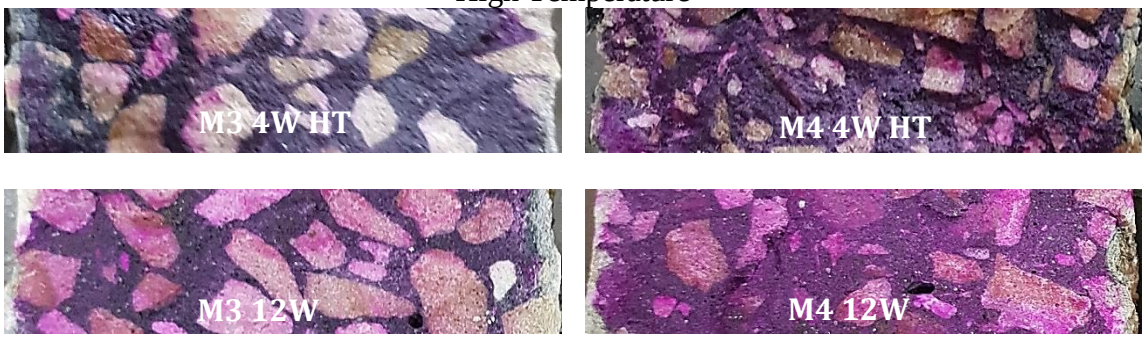

%10 Concentration

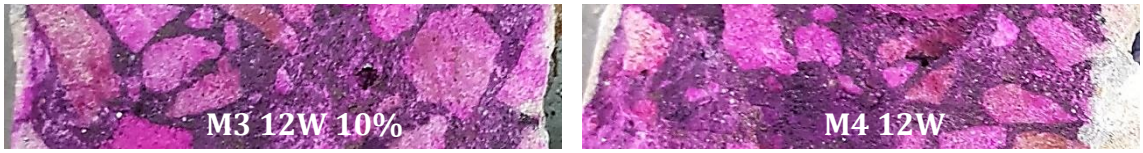

Figure 5-60:Corroded layer of concrete sample M3(left) and M4 (Right) after 2, 4, 8 and 12 Weeks at Ambient and high Temperature and at %10 concentration exposure indicated by sprayed phenolphthalein

M5-AAC Ambient Temperature M8-Acid Resistant

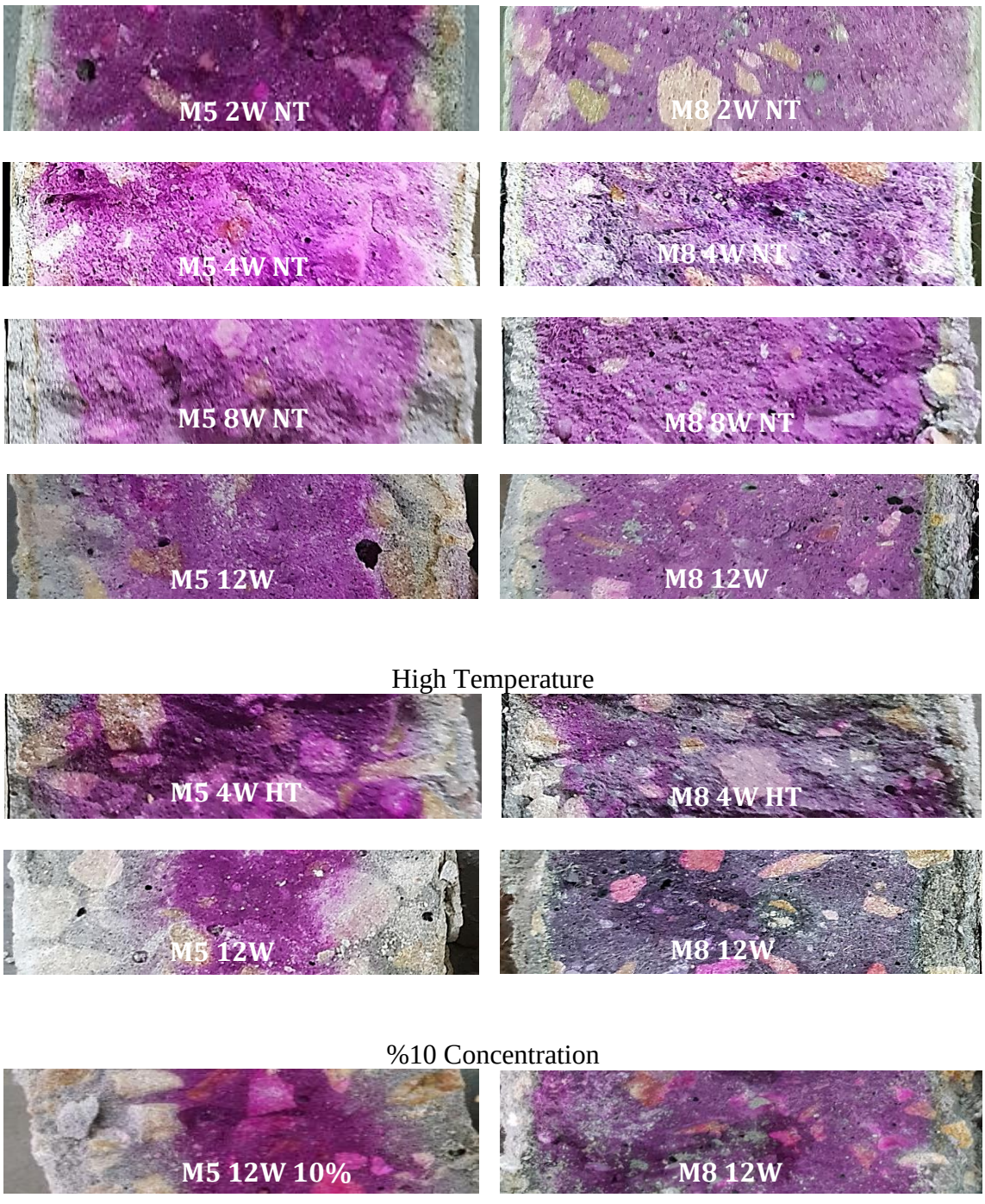

Figure 5-61:Corroded layer of concrete sample M5(left) and M8 (Right) after 2, 4, 8 and 12 Weeks at Ambient and high Temperature and at %10 concentration exposure indicated by sprayed phenolphthalein

M6-UHPC Ambient Temperature M7-CAC

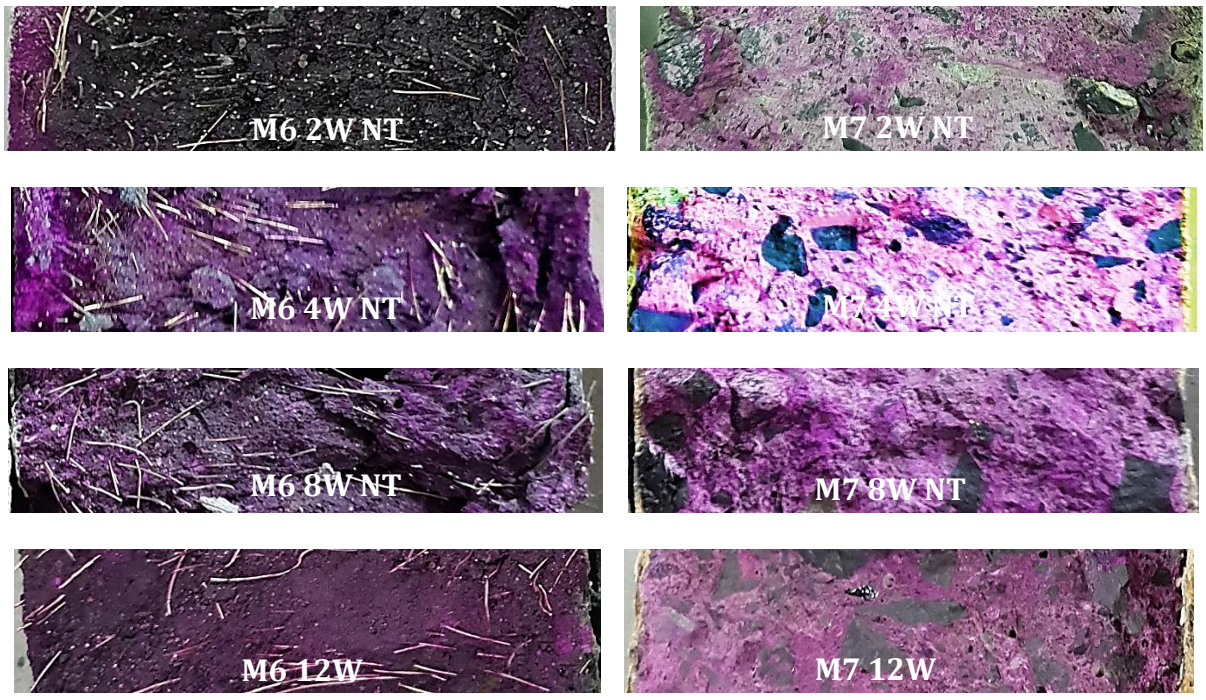

High Temperature

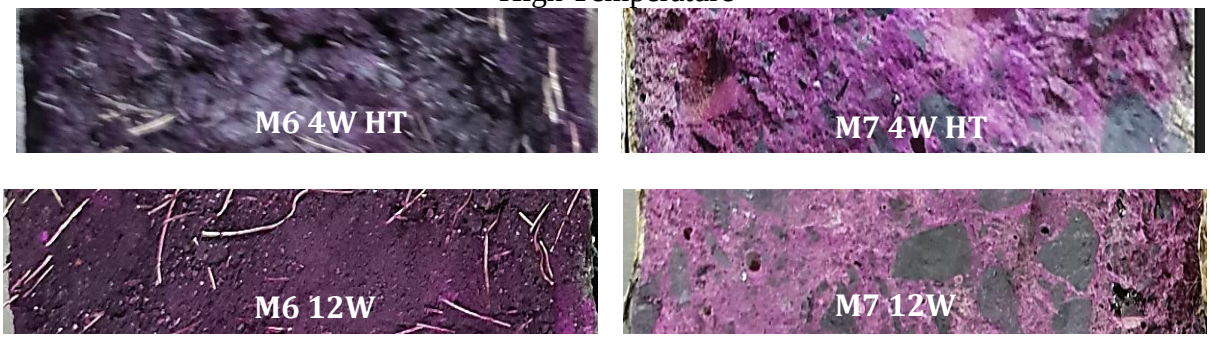

%10 Concentration

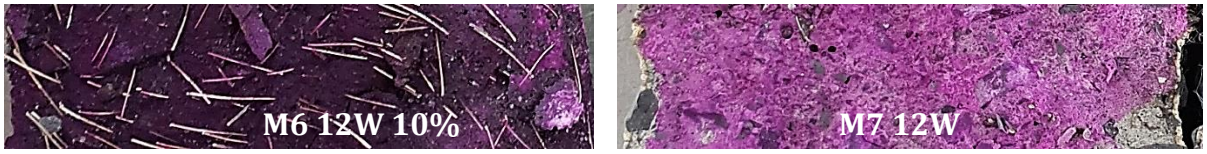

Figure 5-62:Corroded layer of concrete sample M6(left) and M7 (Right) after 2, 4, 8 and 12 Weeks at Ambient and high Temperature and at %10 concentration exposure indicated by sprayed phenolphthalein

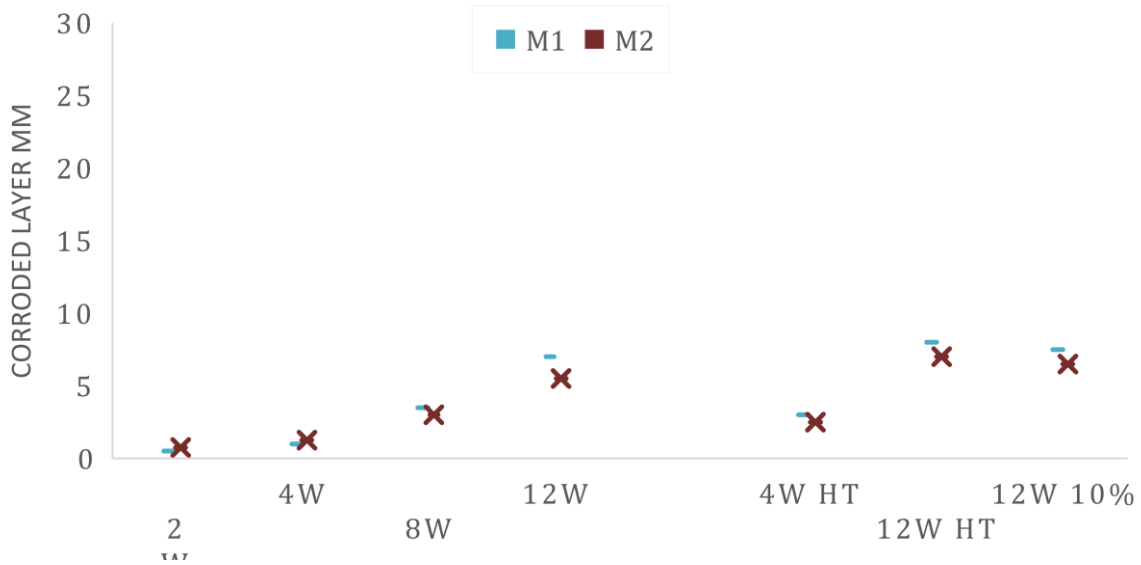

Figure 5-63: Corroded depth for M1 and M2 specimens after 2, 4, 8 and 12 Weeks at Ambient and high Temperature and at %10 concentration exposure

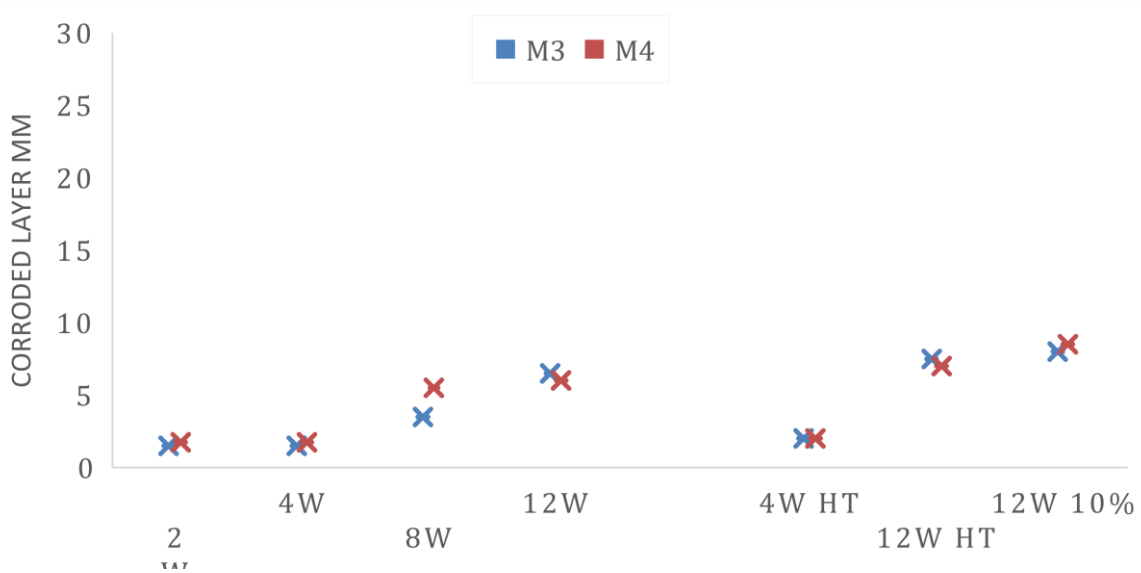

Figure 5-64: Corroded depth for M3 and M4specimens after 2, 4, 8 and 12 Weeks at Ambient and high Temperature and at %10 concentration exposure

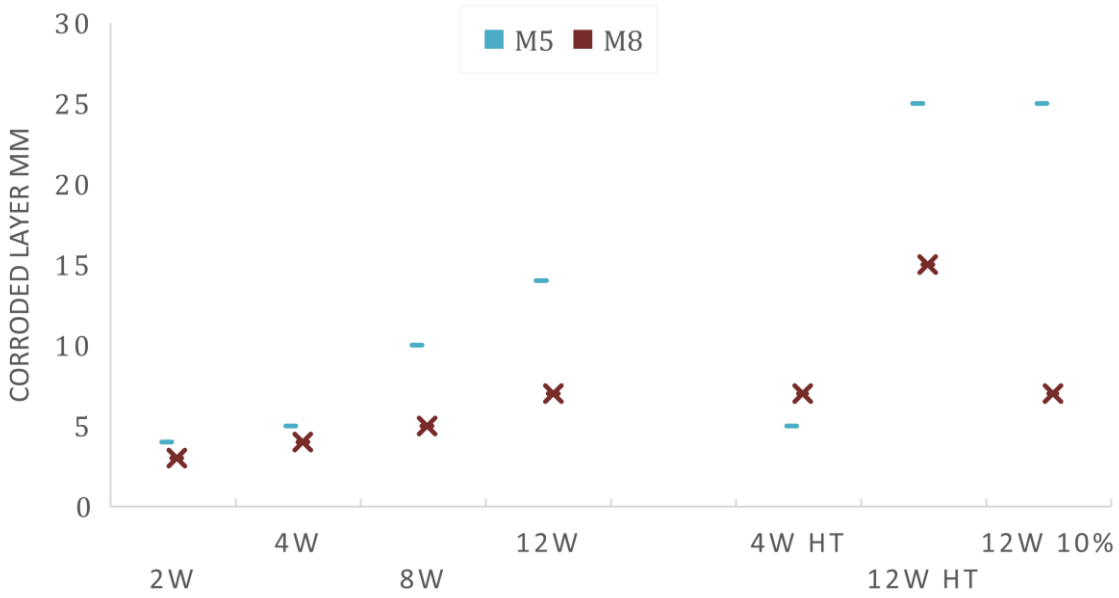

Figure 5-65: Corroded depth for M5 and M8 specimens after 2, 4, 8 and 12 Weeks at Ambient and high Temperature and at %10 concentration exposure

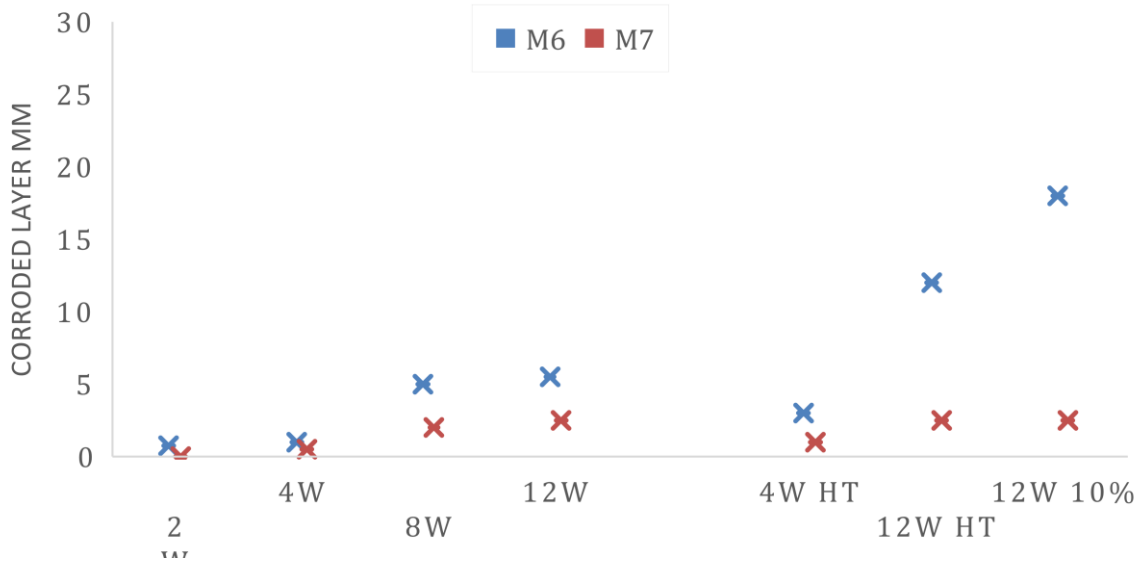

Figure 5-66: Corroded depth for M6 and M7 specimens after 2, 4, 8 and 12 Weeks at Ambient and high Temperature and at %10 concentration exposure

5.9 Material Characterization – SEM and EDS

Samples obtained from each type of concrete before exposure to sulfuric acid in addition to samples obtained from the outer surface of specimens after 12 weeks of exposure were investigated with the aid of scanning electron microscopy (SEM/EDX), X-ray diffraction (XRD), infrared spectroscopy (FTIR). Moreover, samples obtained from the specimens exposed at elevated temperature and paste were analyzed to understand the variation in microstructure due to variation in these parameters.

Examinations made by SEM and EDX were conducted on small pieces cut from the specimens before and after exposure to acid. For the exposed specimens the pieces were taken from the corroded microstructure at regions very close to the acid-exposed surface. SEM and EDX are presented in Figure 5-67 . In general, the results confirmed the presence of gypsum crystals in the corroding outer layer in almost all the mix groups. This gypsum and its expansive reaction seem to be responsible for aggregates becoming loose and falling out in acid affected layers. Sulfur content has significantly increased. Similar finding was reported by (ALI2005) confirming that all the sulfur and calcium in the corroded layer are present in the form of gypsum. Moreover, formation of microcracks and increased porosity of the outer layer was observed in the SEM images in line with other reported results by (Zhang 2018).

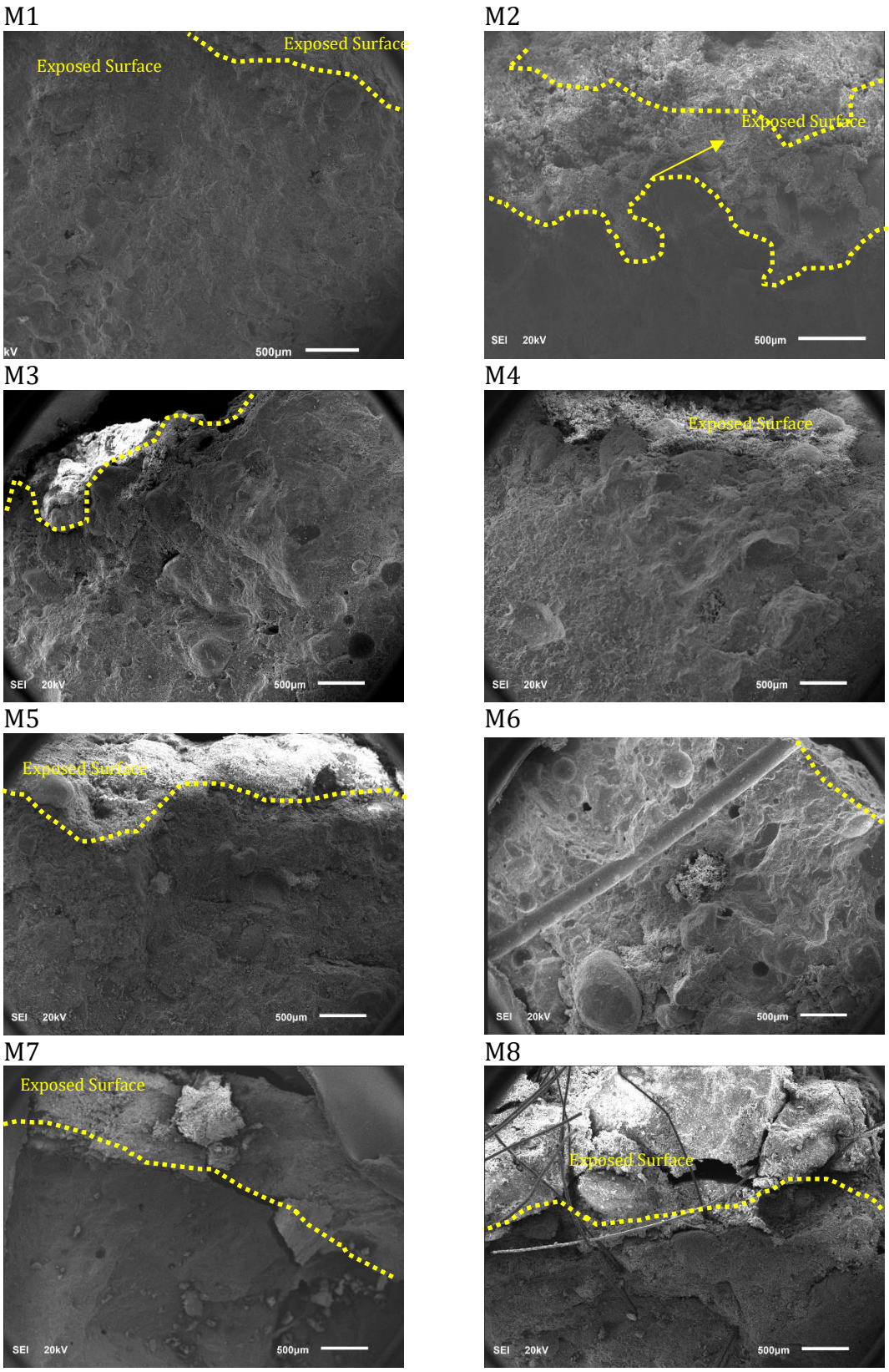

Figure 5-67: low magnification SEM image for exposed concrete specimens showing the interface between affected and intact concrete layer

Table 5-11: EDX before and after exposure to sulfuric acid

Before Exposure

	Ca	Si	Fe	Al	S	Mg	Na	K	NA/AL	AL/Si	Ca/Si
M1	62	24	3.9	4.3	2.6	2.2	0.4	0.3	0.09	0.18	2.58
M2	56.6	35	2.6	2.1	2	1.4	0.2	0.1	0.10	0.06	1.62
M3	37.4	47.2	1.3	5.7	2.9	3.1	0.6		0.11	0.12	0.79
M4	53.2	28	6.9	8.5	1.2	0	1.9	0.4	0.22	0.30	1.90
M5	17.7	60.9	3.6	9.3	0.6	1.6	4.2	2.1	0.45	0.15	0.29
M6	49.7	40.2	4.3	1.9	0.9	0.8	0.6	1.5	0.32	0.05	1.24
M7	50.8	4.3	4.2	39.8	0	0.5	0.2	0.2	0.01	9.26	11.81
M8	39.6	34	9.4	11.7	1.3	2.2	0.2	1.7	0.02	0.34	1.16

After Exposure

	Ca	Si	Fe	Al	S	Mg	Na	K	NA/AL	AL/Si	Ca/Si
M1	35.8	18.1	3.1	2.7	30.5	0.6	0.3	0	0.11	0.15	1.98
M2	39.2	20.4	1.5	1.4	35.7	0.4	0.8	0.5	0.57	0.07	1.92
M3	30	15	3	4	30	1.5	1	0.5	0.25	0.27	2.00
M4	49.9	7.7	4.6	3.7	34	0	0.1	0	0.03	0.48	6.48
M5	12.6	49	3.4	16.4	12.7	0.5	0.8	1.3	0.05	0.33	0.26
M6	40.4	50.9	1	2.4	3.4	0.8	0	1.1	0.00	0.05	0.79
M7	36.2	1.9	16.9	9.7	32.3	0.3	0.7	0	0.07	5.11	19.05
M8	17.2	49.3	4	4.9	26	0.4	0.4	1.2	0.08	0.10	0.35

Conventional Concrete Group (M1, M2)

Sulfur content has significantly increased from 1.7 to 30.5 in M1 and from 2.0 to 35.7 in M2. (Table 5-11). Na/Al and Al/Si ratio in uncorroded sample is 0.09 and 018 for M1 and 0.1 and 0.06 for M2 respectively. Higher Al/Si in M1 is expected since OPC has a higher Aluminum (C_3A) content than SRPC. Ca/Si ratio on the other hand is 2.58 for M1 and 1.62 in M2 uncorroded layer. This ratio dropped to 1.98/1.92 after exposure, confirming the ions exchange and bleaching of ca ions to react and form gypsum. This was demonstrated by the studies conducted by (Hewayde et al 2007, Arrifin 2013, Aydin et al 2005). Shamila 2016 attributed this to decalcification.

Polymer Concrete Group (M5, M8)

The results confirmed the presence of gypsum crystals in the corroding outer layer surrounded by phases mainly containing silica and aluminum gel (Figure 5-72). Sulfur content has significantly increased from 0.5 to 9.8 in M5 and from 3.5 to 26 in M8. SEM Images indicate the formation of a barrier gel in polymer concrete mixes. Similar finding was reported by Shamila 2016. Polymer and carbon fibers in M8 clearly shown in SEM image. These fibers remained intact and were not affected by the acid, which might have contributed to holding the outer layer of the concrete intact. Na/Al and Al/Si ratio of the detected N-A-S-H type gel in uncorroded sample is 0.45 and 0.15 respectively. The measured ratio is inconsistent with results reported by Zhang 2018 where the range of Na/Al ratio and Al/Si ratio distributed over a range of 0.26 and 0.66, respectively (Table 5-11). This could be explained by the variation of these elements in the fly ash and GGBFS raw material. M8 which contains more Ca had a higher Ca/Si of 1.16 compared to 0.29 in M5. The Ca/Si ration dropped to 0.35 and 0.26 in M8 and M5 respectively after exposure to sulfuric acid. Al/Si ratio increased in M5 and decreased M8. Similar finding was reported by (Zhang 2018) which he had confirmed by the FTIR analysis. He explained that by the fact of aluminum removal from gel structure due to the protons attack on the Si–O–Al bonds (Allahverdi 2001). SEM and EDX od unexposed samples indicated large number of voids and microcracks which create weak links in the microstructure in M5. M8 on the other hand has a relatively denser matrix with fewer cracks. EDS analysis also confirmed the existence of additional calcium based hydrated products in M8 specimens. Mehta 2016 reported that with increasing OPC (as fly ash replacement) Ca/Al ratio and Ca/Si ratio increased.

SCMs Group (M3-GGBFS, M4-FA)

SEM images from fracture surfaces of the exposed specimens indicated that the surface of concrete underwent significant deterioration due to sulfuric acid attack with clear gypsum formation on the surface. Sulfur content has significantly increased from 2.9 to 30 in M3 and from 1.2 to 34 in M4. Ca/Si and Al/Si ratio in uncorroded sample are 0.79 and 0.12 for M3 and 1.9 and 0.3 for M4 respectively (Table 5-11). Higher Al/Si and less Ca/Si when compared to OPC M1 is expected. However, this ratio has not dropped after exposure to sulfuric acid which is supposed to happen though ions exchange and bleaching of ca ions to react and form gypsum. SEM and EDX of unexposed samples indicated a relatively dense matrix. Calcium based hydrated products (C-S-H) was seen which is primary contributor to strength properties.

Special Concrete Group (M6-UHPC, M7-CAC)

SEM images from fracture surfaces of the exposed specimens indicated clear presence of gypsum formation on the surface. SEM and EDX of unexposed samples indicated relatively dense matrix. Ca/Si ratio dropped from 1.2 to 0.69 and while Al/Si ratio remained at 0.05. Higher Al/Si and less Ca/Si when compared to OPC M1 is expected.

5.10 Material Characterization – XRD

The X-ray diffractogram (XRD) of the material before exposure to acid indicates peaks corresponding to CSH, portlandite (P), quarts (Q), Calcite (C) and gypsum (G) phases. Gypsum phase ($CaSO_4.2H_2O$) dominated the diffractogram of exposed specimens both at low and at high temperature as well as paste samples. These peaks identified at 11.5, 29.2, 33.3, 37.2 2-theta. Gypsum was identified in all the samples (Figure 5-68-5.80) as the key reaction product between the sulfuric acid solution and hydrated cement paste (Girardi and Maggio

2011). Common peaks of calcite are likely occurred from the coarse aggregate contained a fraction of carboniferous aggregate, while the sources of quartz in the diffractograms originated from sand.

Conventional Concrete Group (M1, M2)

XRD diffractogram of M1and M2 samples (Figure 5-68, Figure 5-69) before exposure to acid indicates phases of portlandite, CSH, and Quartz. After exposure to acid the main phase identified in XRD is gypsum with small low intensity peaks of quartz and CSH. The formation of gypsum has been reported in previous works when the OPC containing calcium-rich material were exposed to sulfuric acid. This is due to the reaction between the dissolved calcium cation and the sulfate anion. the calcium present in pore solution or part from portlandite, CSH or CaO is the major source of gypsum formation. (Hill et al. 2003).

Polymer Concrete Group (M5, M8)

The X-ray diffractogram of the material before exposure showing phases of Quartz and Mullite (3Al2O3.2SiO2), similar to that of fly ash used. Peaks corresponding to C–S–H phase that occurs in systems with a high content of Ca (Figure 5-73, Figure 5-76). Similar finding was reported by Zhang 2018, Lloyd et al 2012 and Mehta 2016). Peaks corresponding to C-S-H, N-A-S-H and C-A-S-H were identified as also reported in previous studies in polymer concrete (Salami et. al 2017, Borges 2016 and, Buchwald 2009). Although it involves strong aluminum-silicate bonds which will take longer time to break, the ultimate reaction taking place will result in formation of gypsum. These bonds provided higher resistant to sulfuric acid and therefore contributed to the high mass and strength stability of polymer concrete as compared to conventional concrete.

SCMs Group (M3-GGBFS, M4-FA)

The X-ray diffractogram of concrete incorporating fly ash and GGBFS showed the presence of phases such as CSH, Quartz, CASH. Melilite which is a crystalline compound generally present in unhydrated fly ash (McCarthy et al. 1984, Mahmud 2017)). Portlandite peaks with less intensity is an indication of less content in the specimens incorporating SCMs was due pozzolanic activity, resulting in production of additional/secondary C-S-H gel as discussed in previous sections. Similar finding was reported by (Mahmud 2017).

Some researchers (Mahmoud 2017, Li et al. 2000, Fang 2017) reported that the activity of fly ash (pozzolanic reaction with portlandite) will be hindered if the pH drops below 13. Thus, it appears that the unreacted fly ash found in the reaction zone of the specimen's act as an inert filler for samples exposed to sulfuric, unless the concrete is cured for long period of time (>56 days), long enough for pozzolanic reaction to take place. The ultimate phases identified after exposure to sulfuric acid both at low and high temperature was mainly gypsum with low quantity of calcite, quartz and CSH.

Special Concrete Group M6-UHPC, CAC M7 CAC

XRD diffractogram of UHPC samples (Figure 5-68) before exposure to acid indicates phases of portlandite, CSH, and Quartz. Phases identified in CAC on the other hand indicated presence of calcium aluminate hydrate phases. After exposure to acid the main phase identified in XRD is gypsum with small low intensity peaks of quartz and CSH in the case of UHPC.

M1 (ordinary portland cement)

Before Exposure

After Exposure

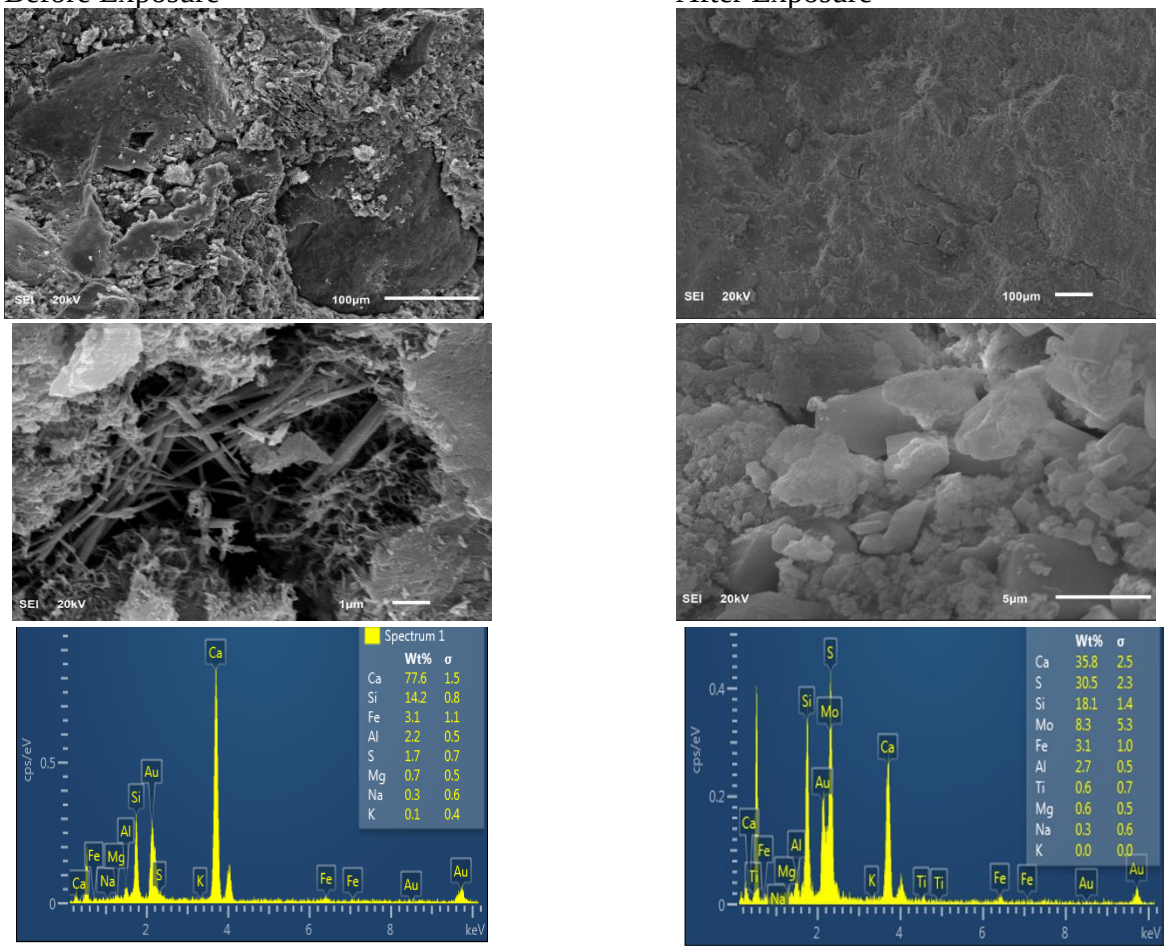

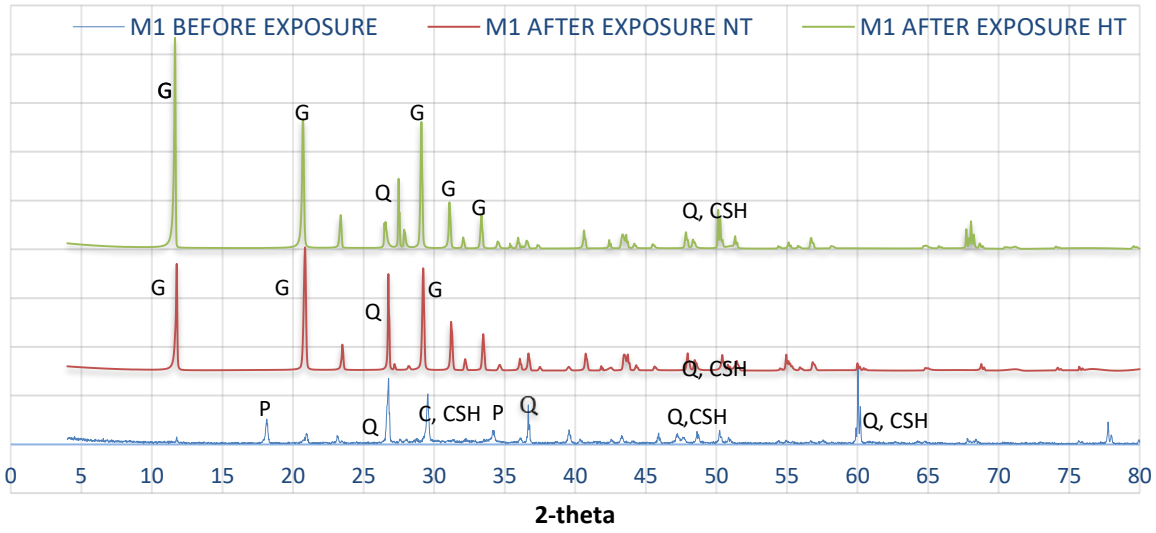

Figure 5-68: SEM, EDX and XRD Unexposed sample, (b)sample exposed to %5 acid at normal temperature, and (c). sample exposed to %5 sulfuric acid at high temperature, M1.

M2 (sulfate resistant cement)

Before Exposure

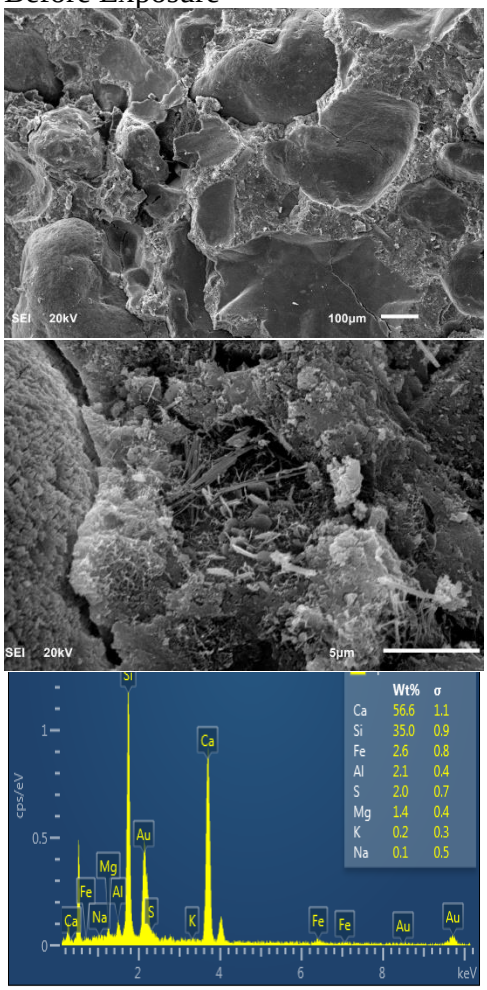

After Exposure

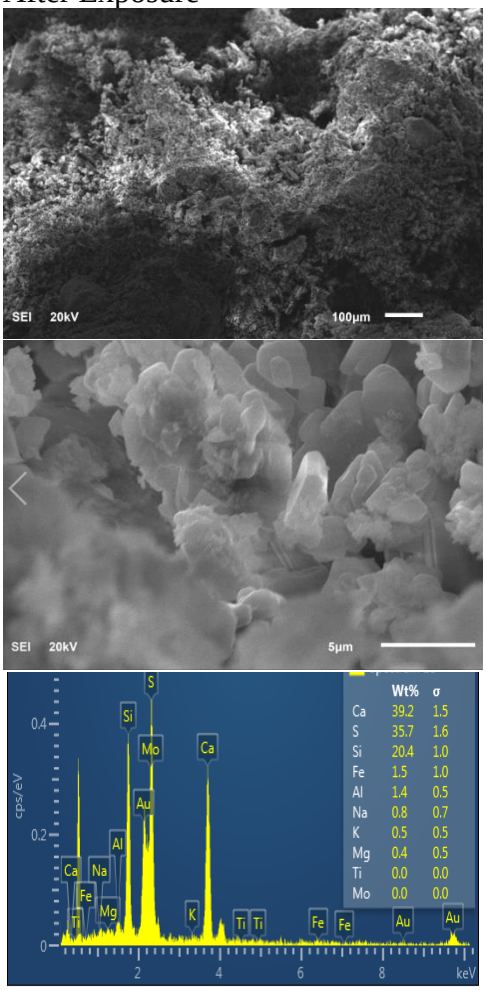

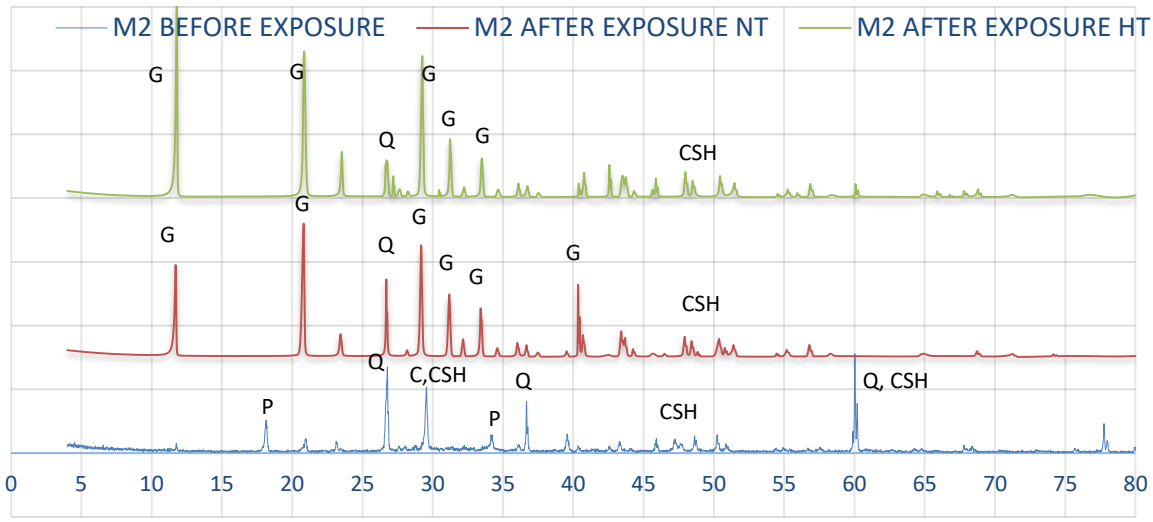

Figure 5-69: SEM, EDX and XRD Unexposed sample, (b)sample exposed to %5 acid at normal temperature, and (c). sample exposed to %5 sulfuric acid at high temperature. M2

M3 (GGBFS)

Before Exposure

After Exposure

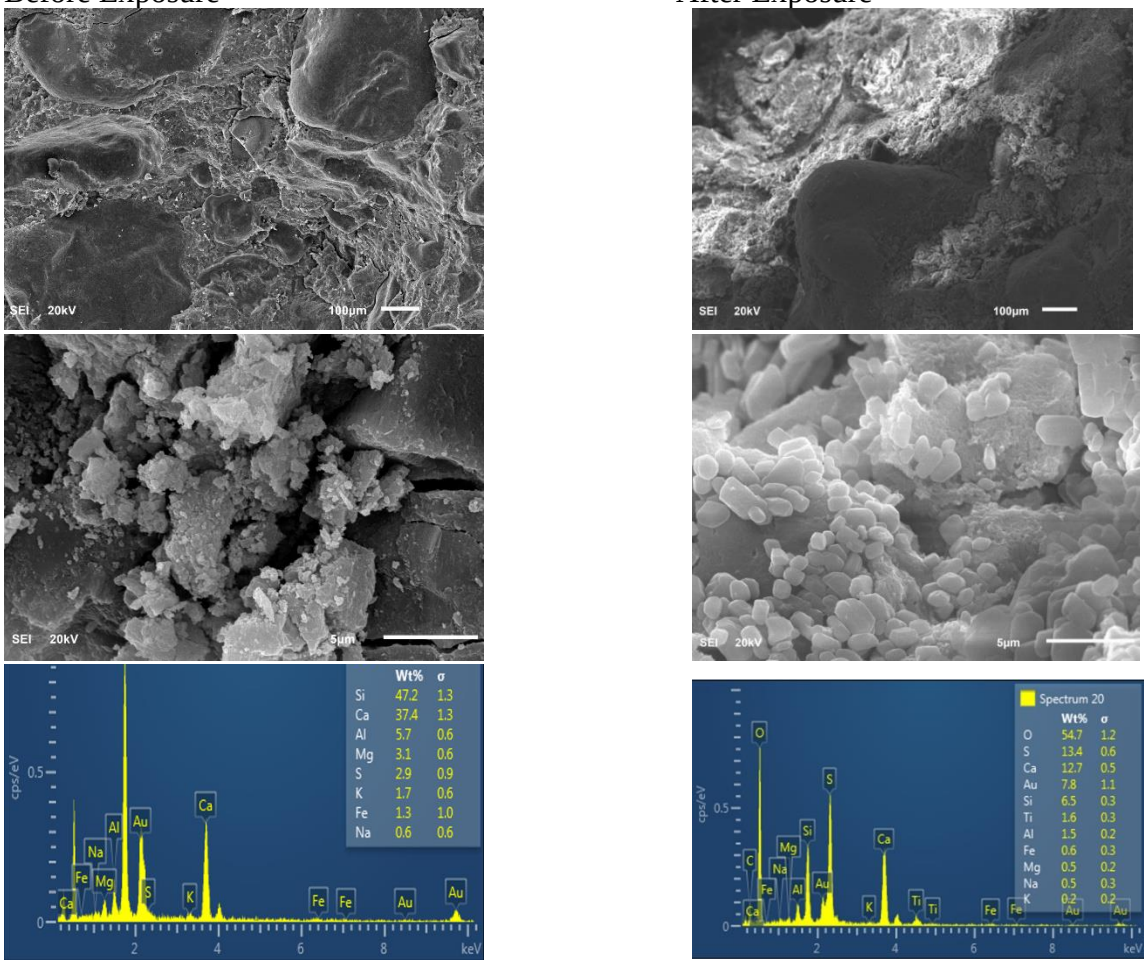

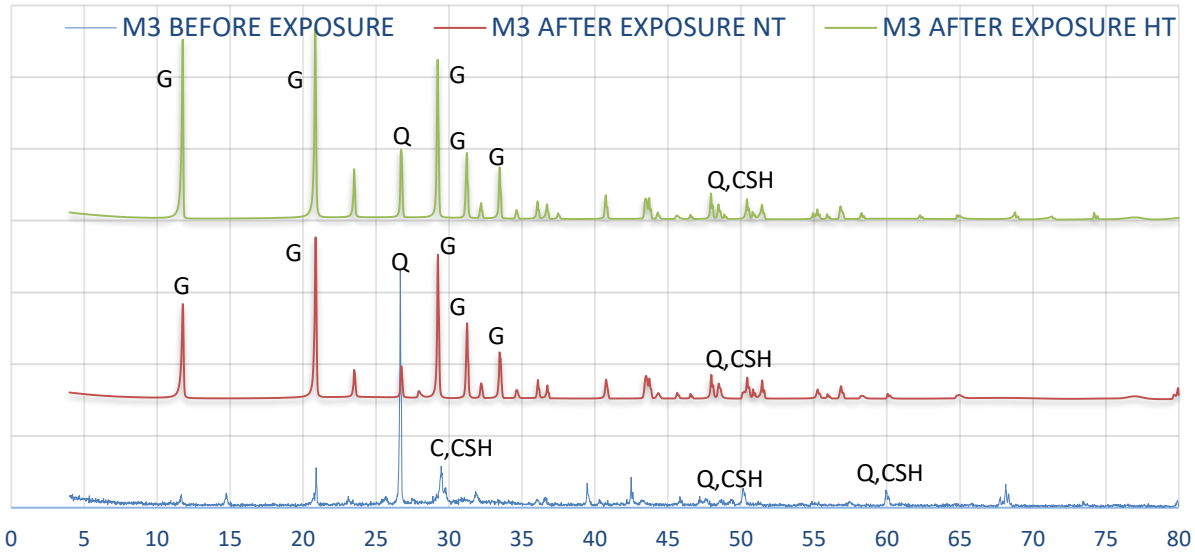

Figure 5-70: SEM, EDX and XRD Unexposed sample, (b)sample exposed to %5 acid at normal temperature, and (c). sample exposed to %5 sulfuric acid at high temperature. M3

M4 (Fly Ash)

Before Exposure

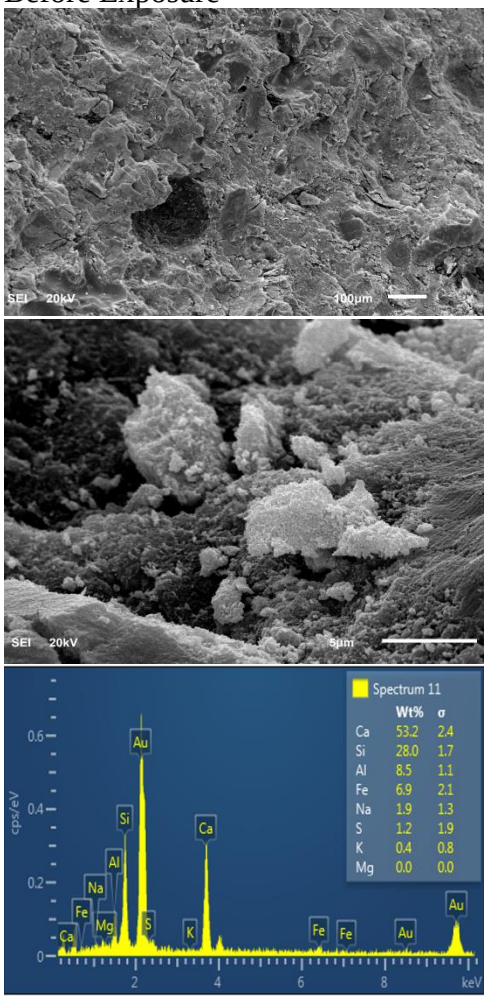

After Exposure

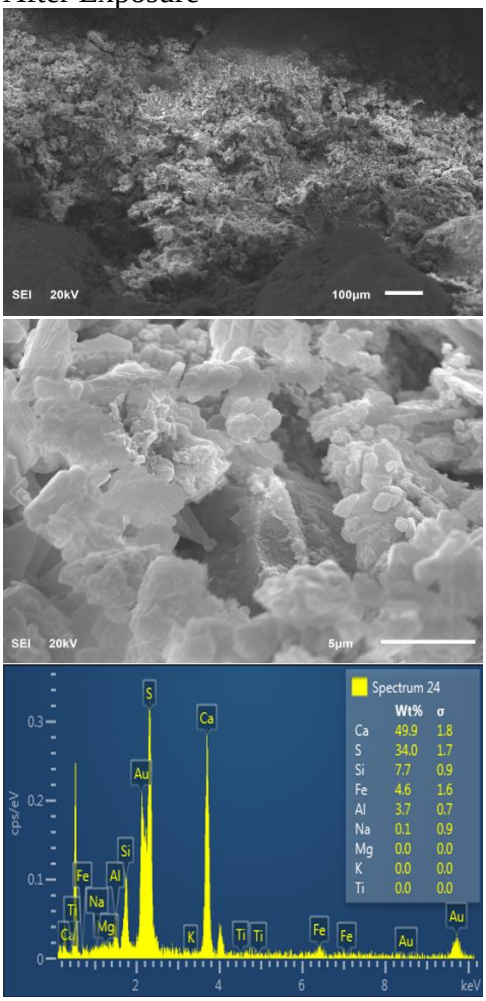

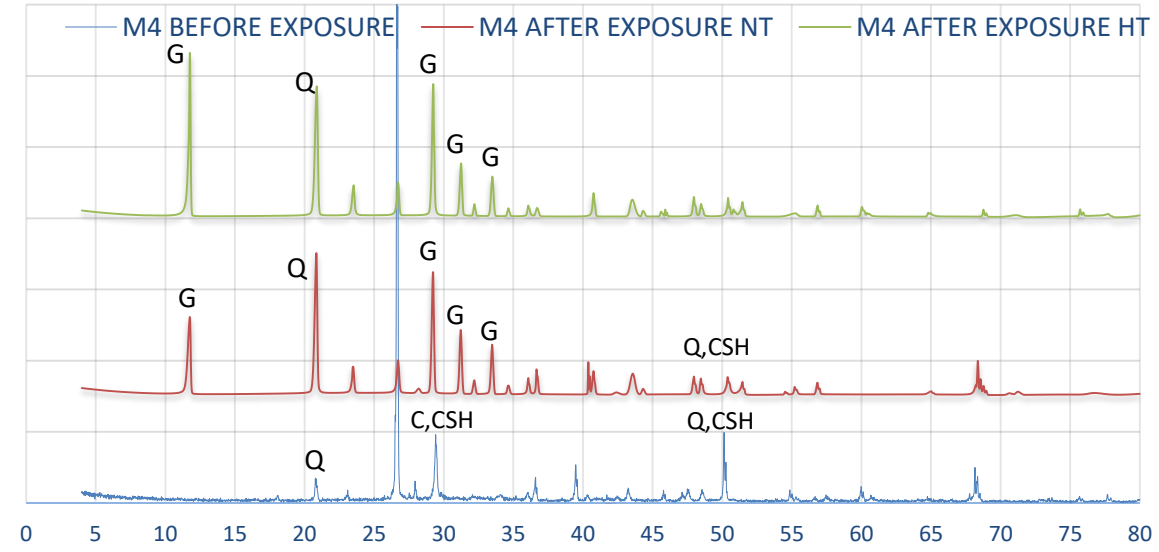

Figure 5-71: SEM, EDX and XRD Unexposed sample, (b)sample exposed to %5 acid at normal temperature, and (c). sample exposed to %5 sulfuric acid at high temperature. M4

M5 (Polymer-AAC)

Before Exposure

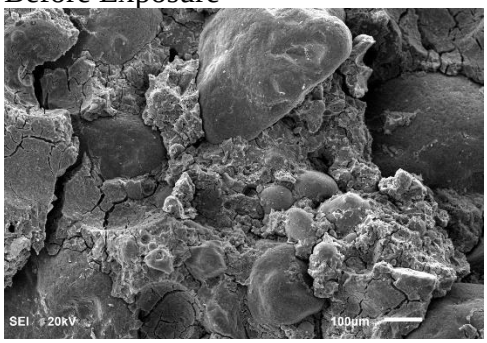

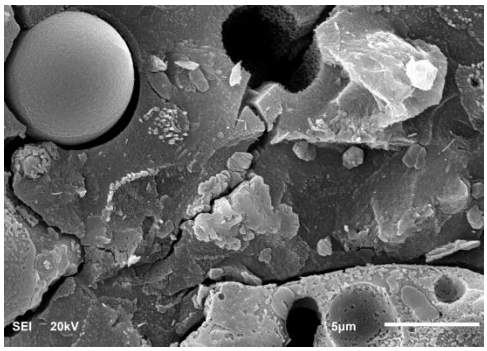

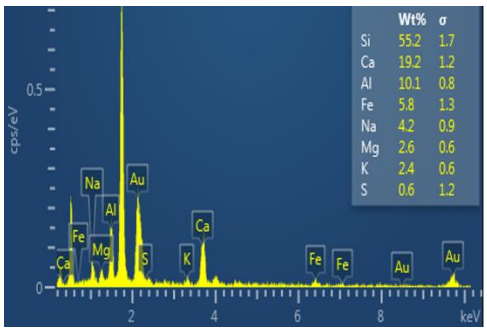

After Exposure

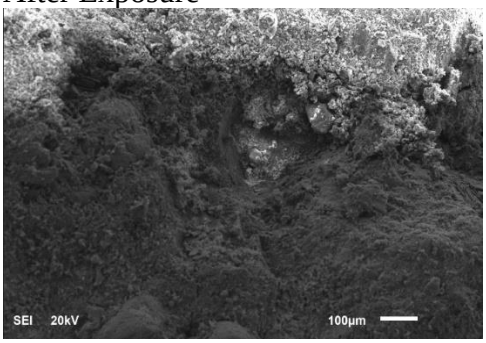

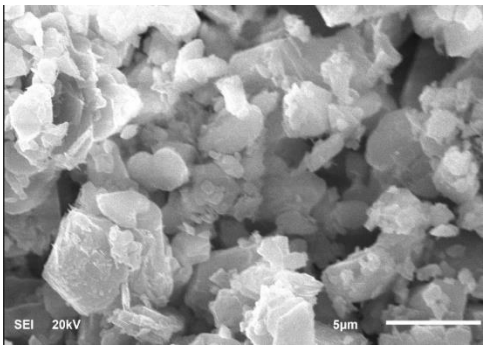

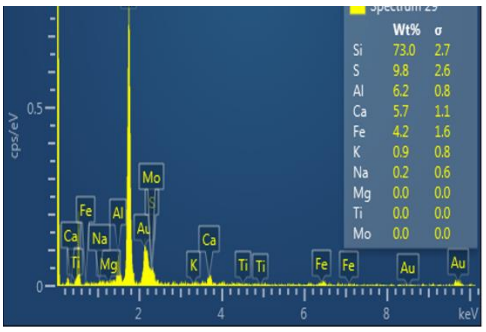

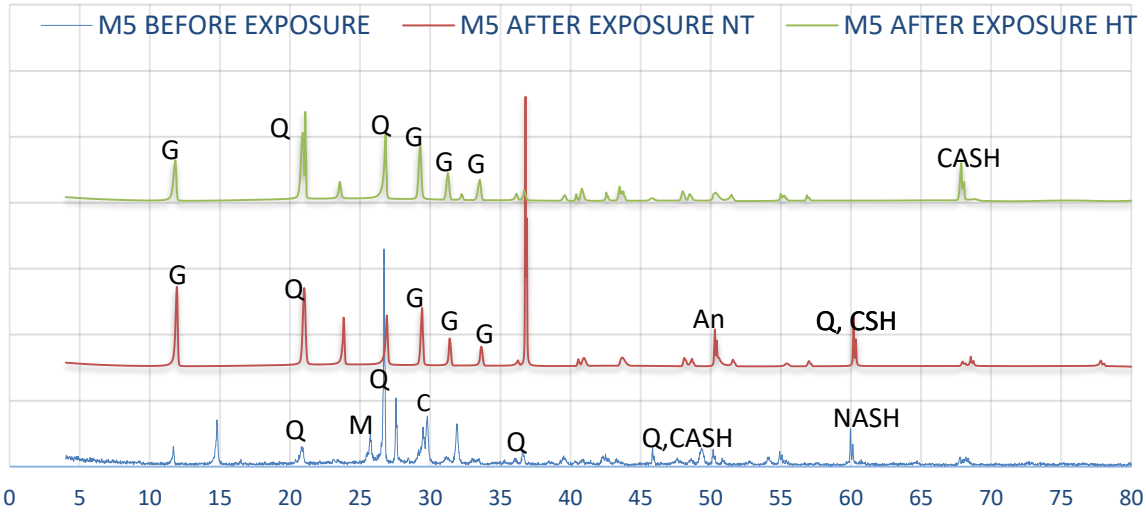

Figure 5-72: SEM, EDX and XRD Unexposed sample, (b)sample exposed to %5 acid at normal temperature, and (c). sample exposed to %5 sulfuric acid at high temperature. M5

M6 (UHPC)

Before Exposure

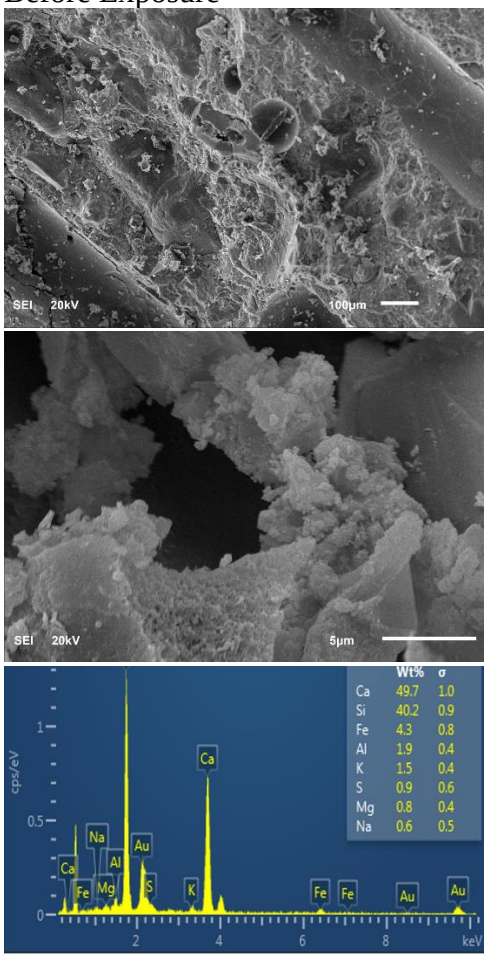

After Exposure

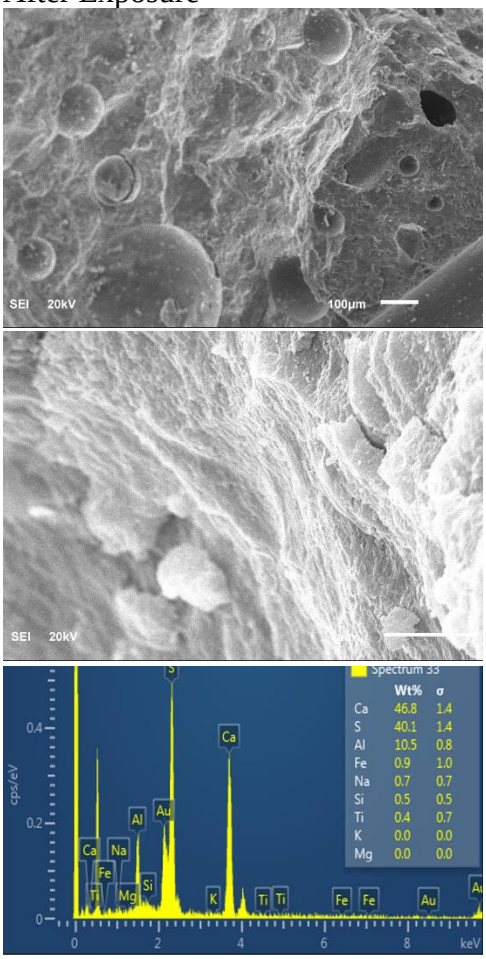

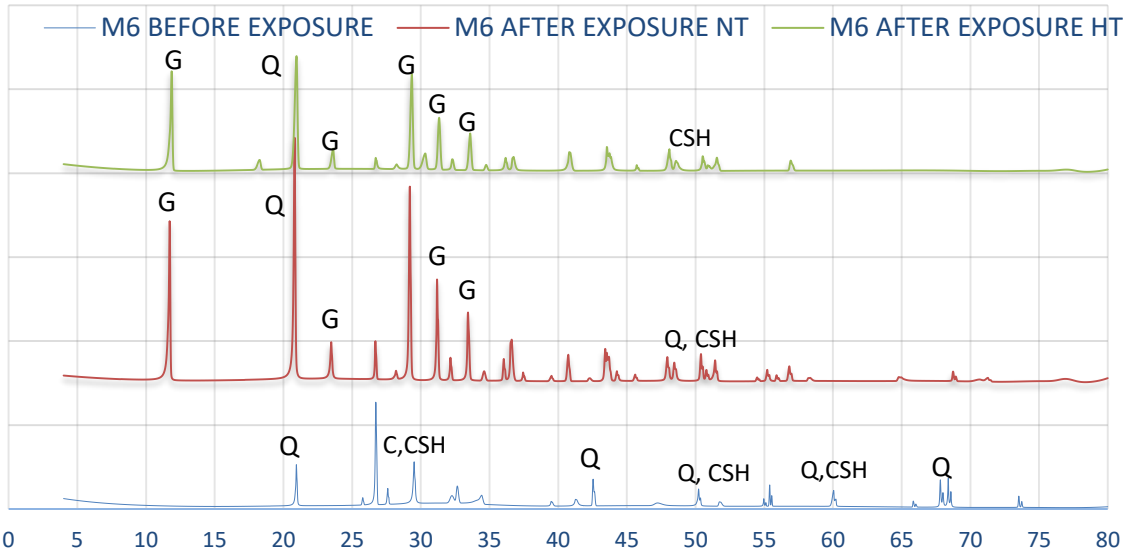

Figure 5-73: SEM, EDX and XRD Unexposed sample, (b)sample exposed to %5 acid at normal temperature, and (c). sample exposed to %5sulfuric acid at high temperature. M6

M7 (CAC)

Before Exposure

After Exposure

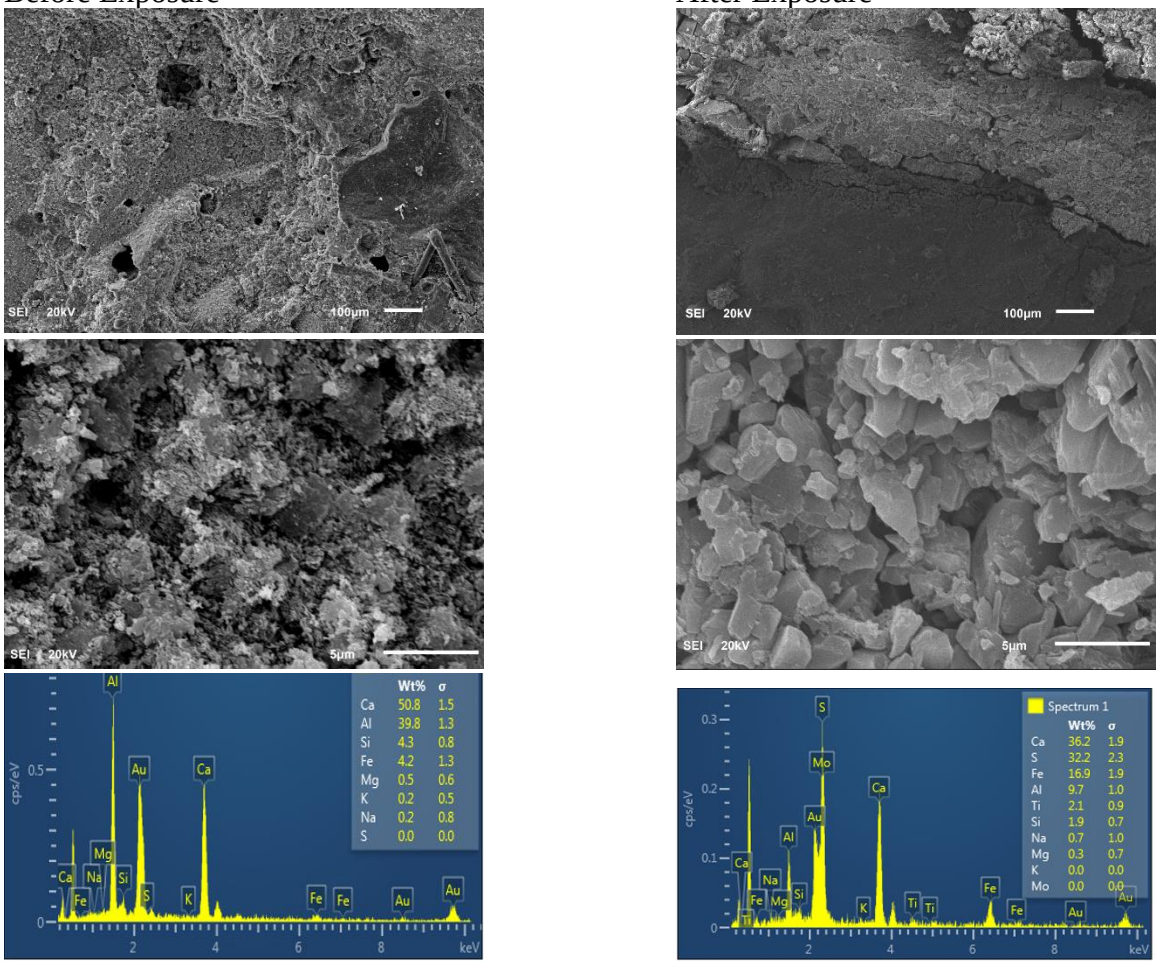

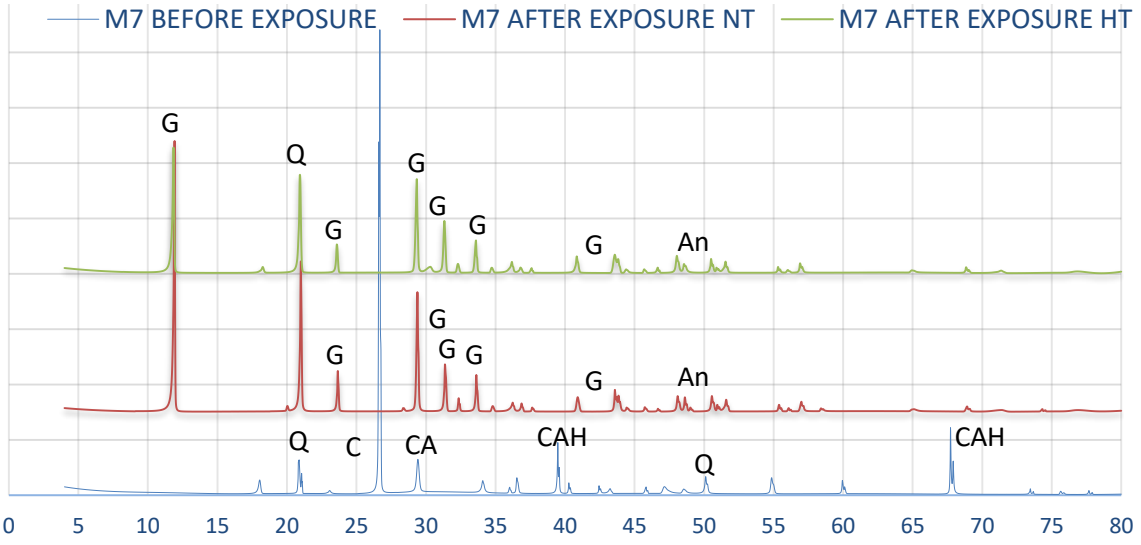

Figure 5-74: SEM, EDX and XRD Unexposed sample, (b)sample exposed to %5 acid at normal temperature, and (c). sample exposed to %5 sulfuric acid at high temperature. M7

M8 (Polymer-Acid Resistant)

Before Exposure

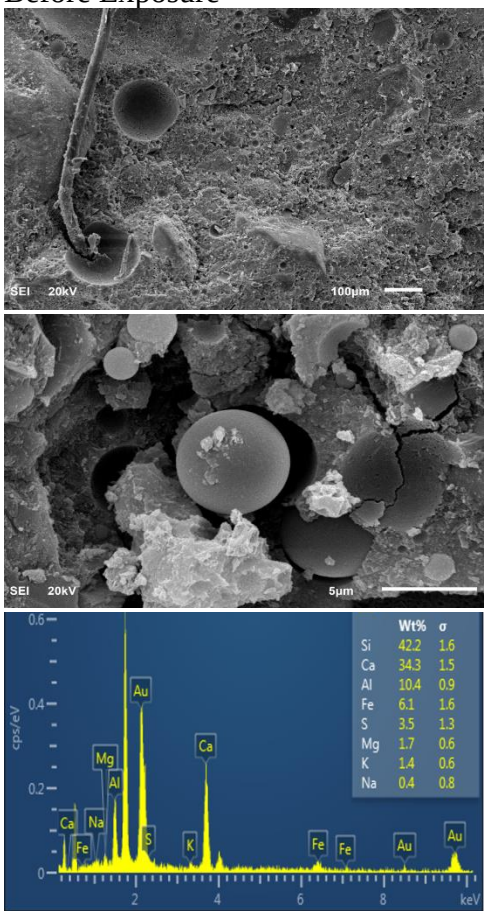

After Exposure

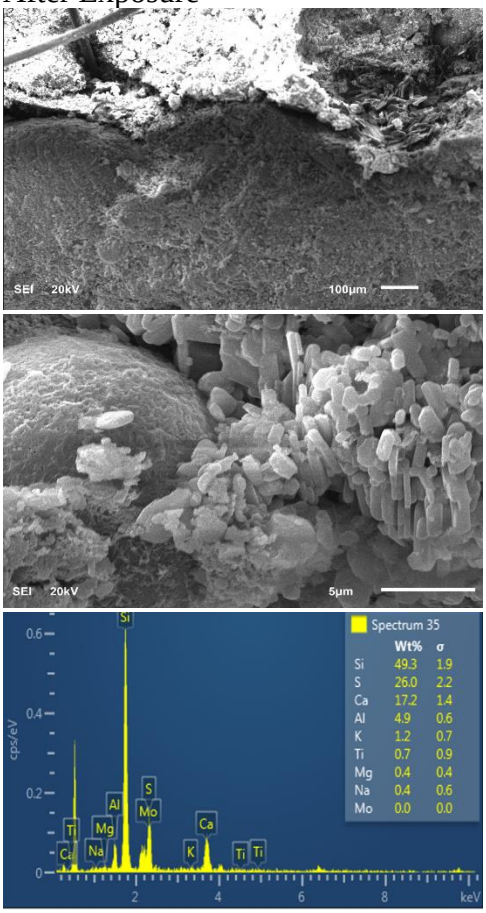

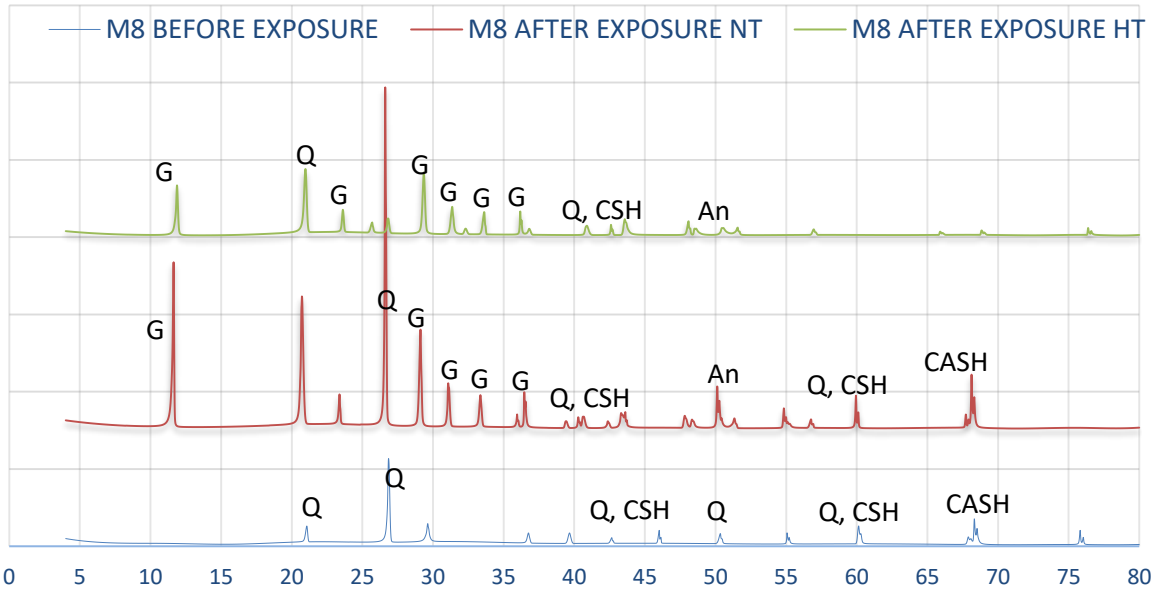

Figure 5-75: SEM, EDX and XRD Unexposed sample, (b)sample exposed to %5 acid at normal temperature, and (c). sample exposed to %5 sulfuric acid at high temperature. M8

P1 (OPC Paste)

Before Exposure

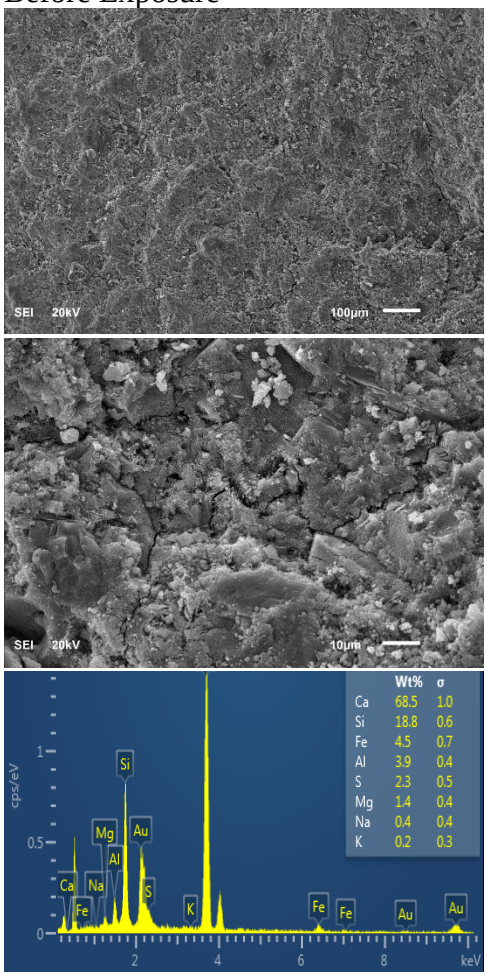

After Exposure

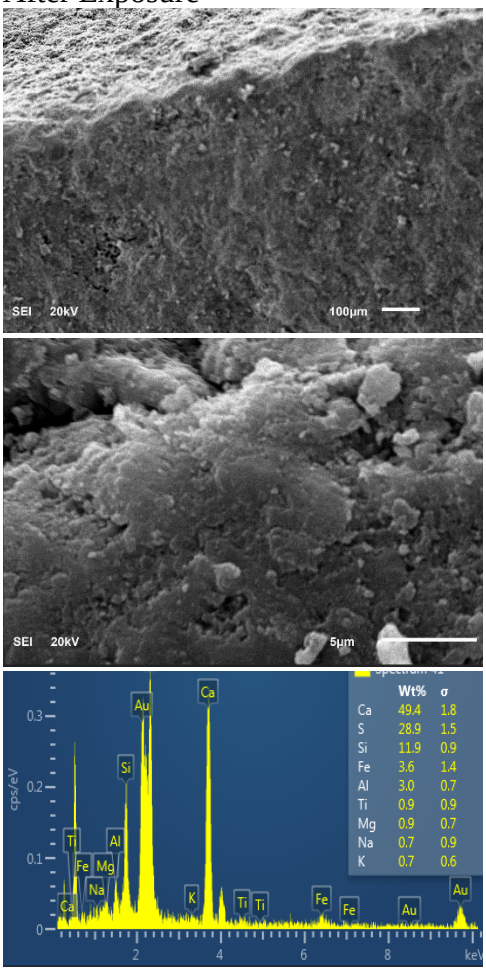

Figure 5-76: SEM, EDX Unexposed sample, (b)sample exposed to %5 acid at normal temperature, and (c). sample exposed to %5 sulfuric acid at high temperature. P1

P2 (SRPC Paste)

Before Exposure

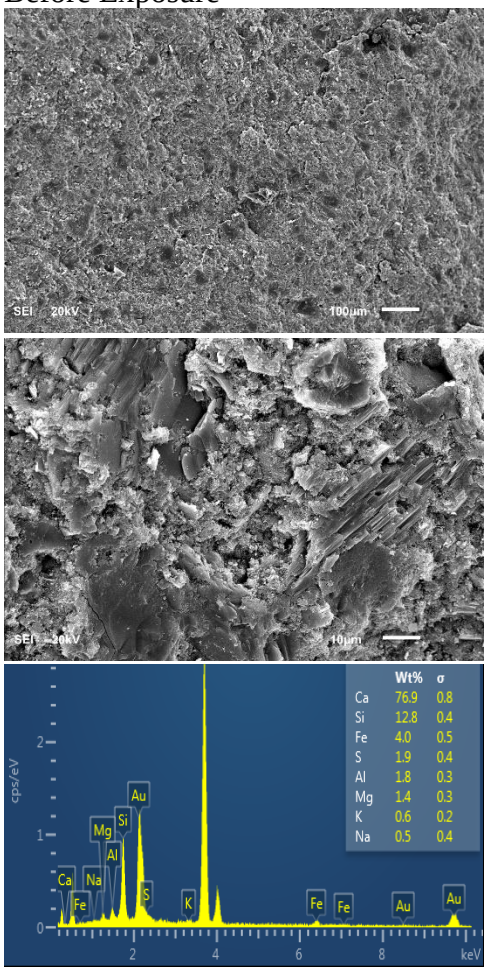

After Exposure

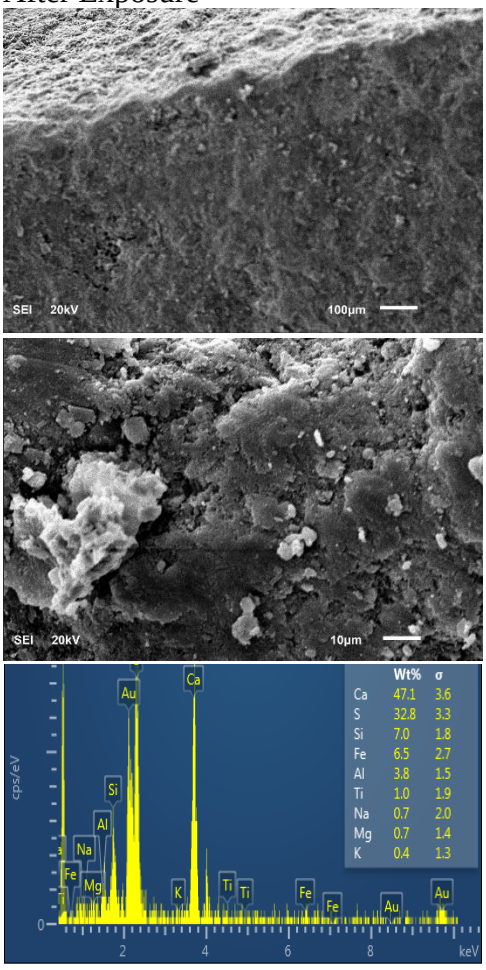

Figure 5-77: SEM, EDX Unexposed sample, (b)sample exposed to %5 acid at normal temperature, and (c). sample exposed to %5 sulfuric acid at high temperature. P2

P3 (GGBFS Paste)

Before Exposure

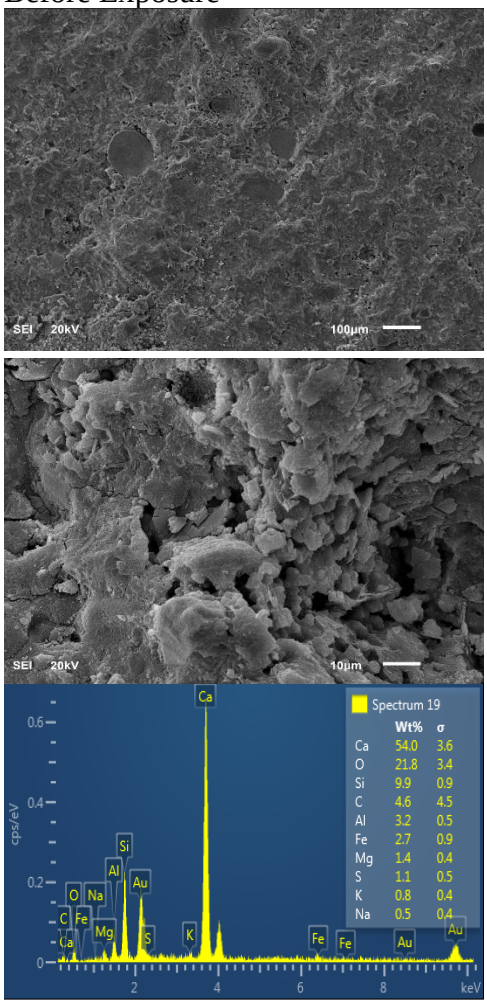

After Exposure

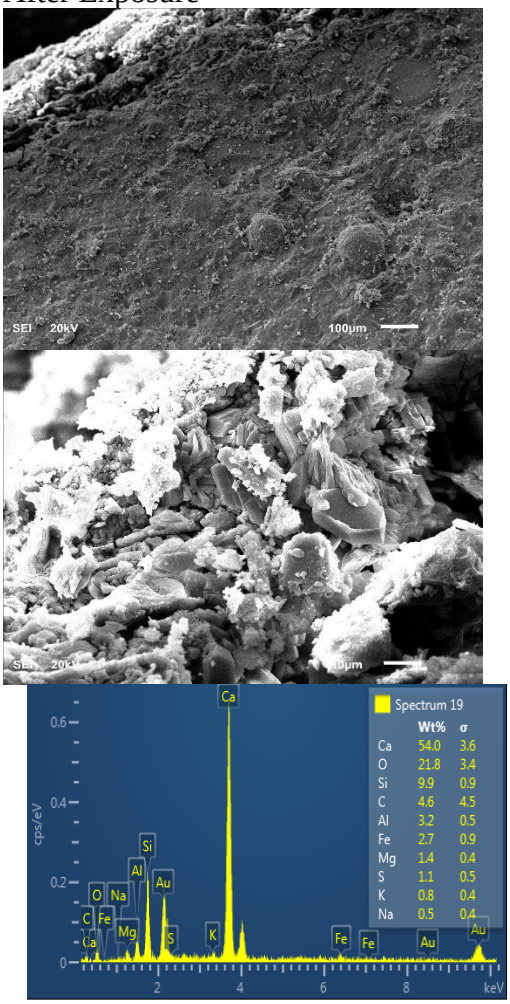

Figure 5-78: SEM, EDX Unexposed sample, (b)sample exposed to %5 acid at normal temperature, and (c). sample exposed to %5 sulfuric acid at high temperature. P3

P4 (FA Paste)

Before Exposure

After Exposure

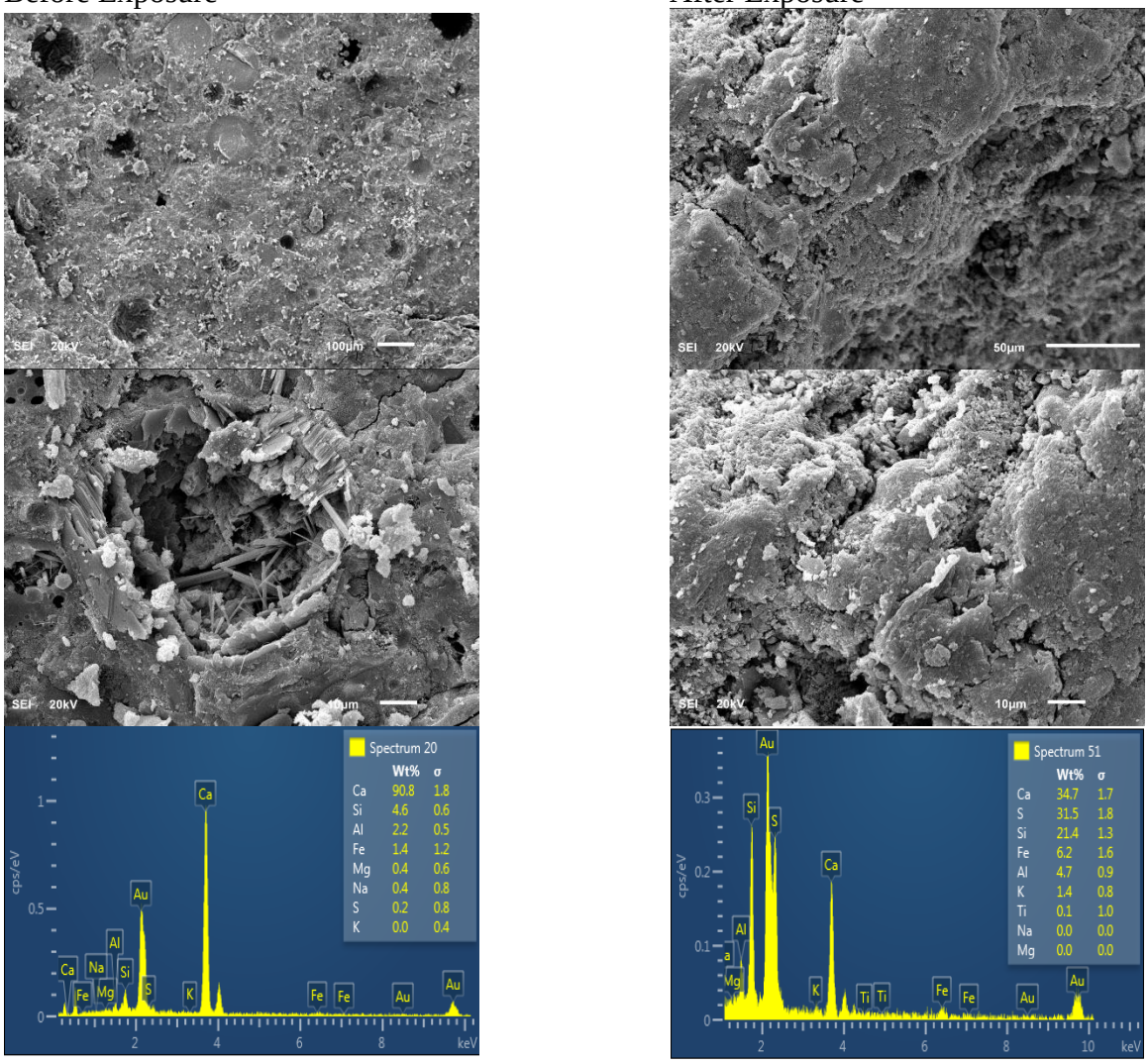

Figure 5-79: SEM, EDX Unexposed sample, (b)sample exposed to %5 acid at normal temperature, and (c). sample exposed to %5 sulfuric acid at high temperature. P4

P5 (Polymer Paste)

Before Exposure

After Exposure

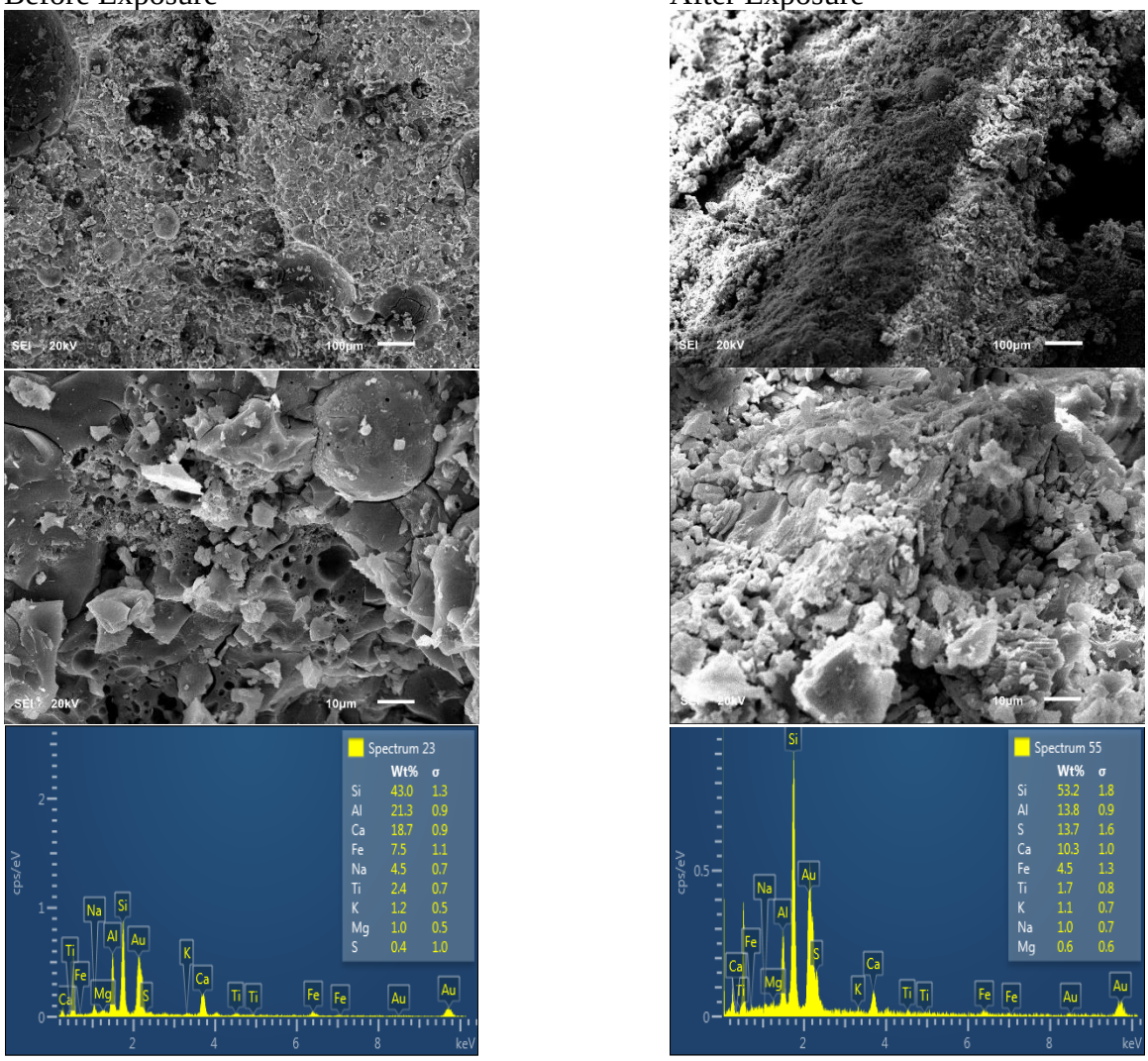

Figure 5-80: SEM, EDX Unexposed sample, (b)sample exposed to %5 acid at normal temperature, and (c). sample exposed to %5 sulfuric acid at high temperature. P5

5.11 Material Characterization – FTIR

As a further confirmation of the formed phases identified in XRD, Infrared (FTIR) spectroscopy technique was used which provides insights into the molecular framework of the sample structures. Powder samples obtained from the specimens before exposure and after from the outer surface after 12 weeks of exposure were tested by FTIR. The IR spectra of all concrete specimens before and after exposure to sulfuric acid is presented in Figure 5-81-5.88. Peaks at around 600 cm-1,620 cm-1 and 1100 cm-1 are indicative of SO_4^{2-} groups, which belong to sulfate phases such as ettringite and gypsum (Stark 2003). Th Peaks at 600 and 670 corresponds specifically to S-O bond of SO_4^{2-} while peaks at 1620, 3400 and 3540 corresponds to hydrogen bonded hydroxyl group of H_2O molecules in dehydrated gypsum (Yang 2018). Other metal oxides presented in the sample have bands of M-O bonds at 465, 550 and 660 cm−1. This includes the bands for the SiO2 in quartz at 550. It is worth mentioning that the characteristics of IR bands associated with quartz includes (i) Si–O asymmetrical bending vibration at 465 cm−1; (ii) Si–O symmetrical stretching vibration at 780–800 cm−1; (iii) Si–O symmetrical bending vibration at 695 cm−1; and (iv) Si–O asymmetrical stretching vibration at IR Frequency of 1080–1175 cm−1. The bands between 1400 and 1450 cm−1 correspond to the symmetric stretching vibration of calcium carbonate. This could be present from the limestone aggregates.

Spectroscopy of all samples after exposure to sulfuric acid indicates a similar product formed in both ambient and elevated temperature exposure condition. Th Peaks formed and identified at 600 and 670 and 1100 corresponds to S-O bond of SO_4^{2-} while peaks at 1620, 3400 and

3540 corresponds to hydrogen bonded hydroxyl group of H_2O molecules in dehydrated gypsum. This further confirm the results obtained by XRD.

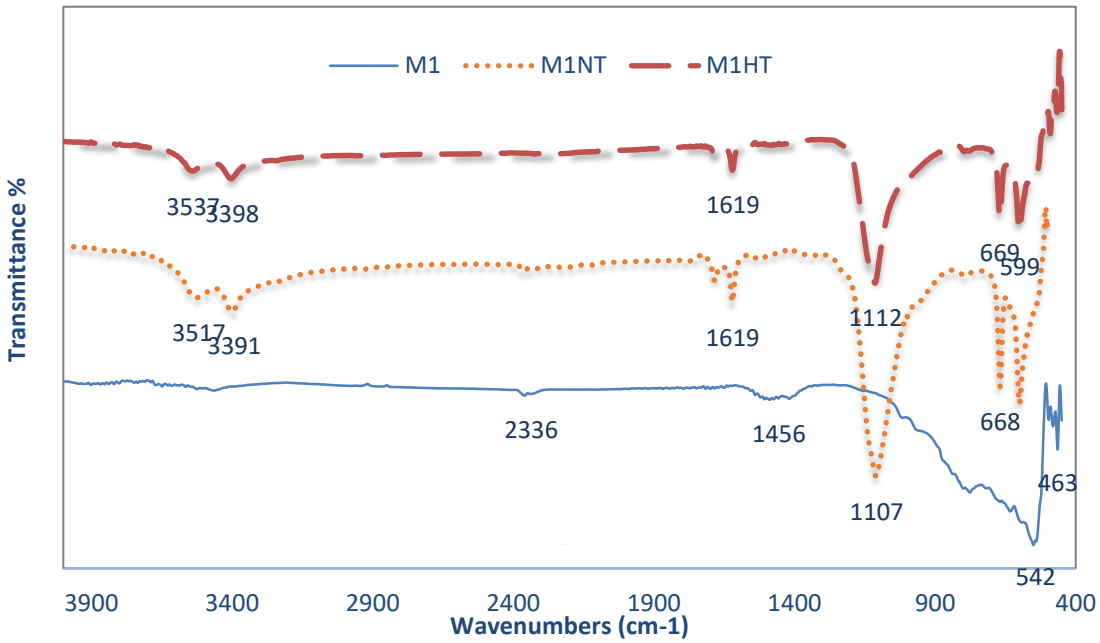

Figure 5-81: FTIR spectra of Unexposed sample, (b)sample exposed to %5 acid at normal temperature, and (c). sample exposed to %5 sulfuric acid at high temperature. M1

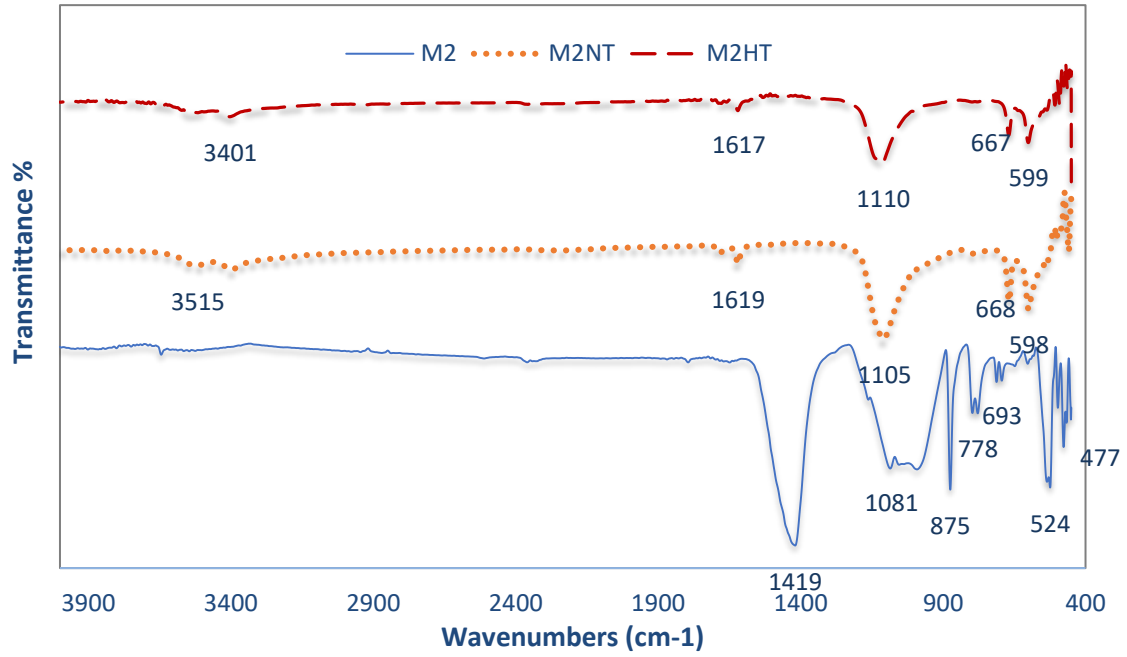

Figure 5-82: FTIR spectra of a)Unexposed sample, (b)sample exposed to %5 acid at normal temperature, and (c). sample exposed to %5 sulfuric acid at high temperature. M2

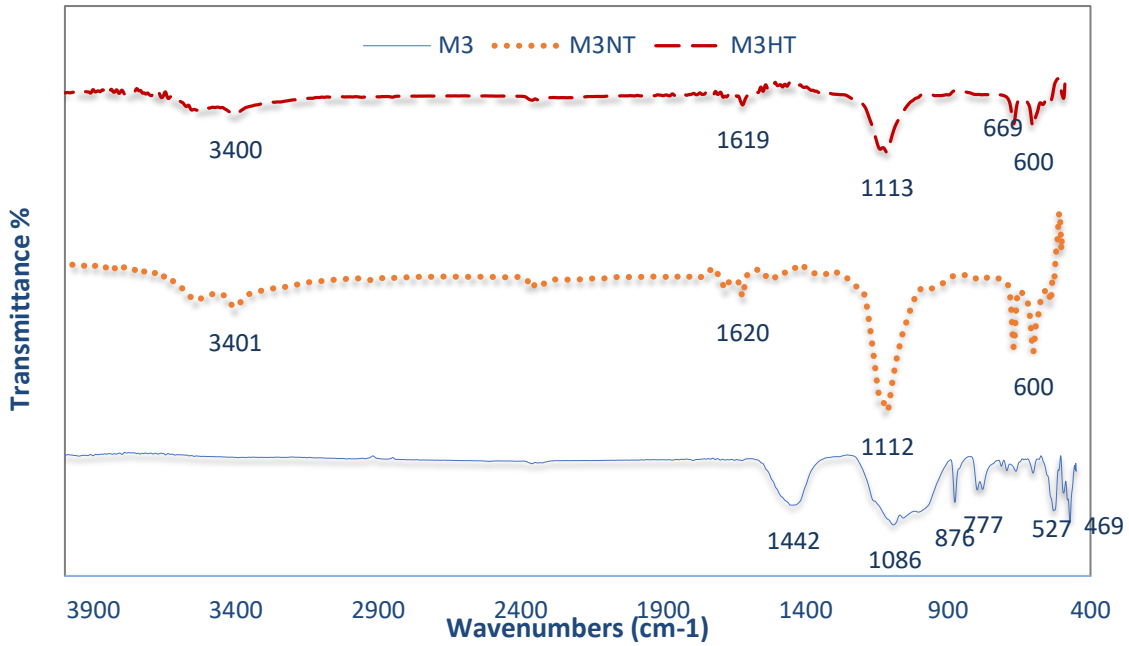

Figure 5-83: FTIR spectra of Unexposed sample, (b)sample exposed to %5 acid at normal temperature, and (c). sample exposed to %5 sulfuric acid at high temperature. M3

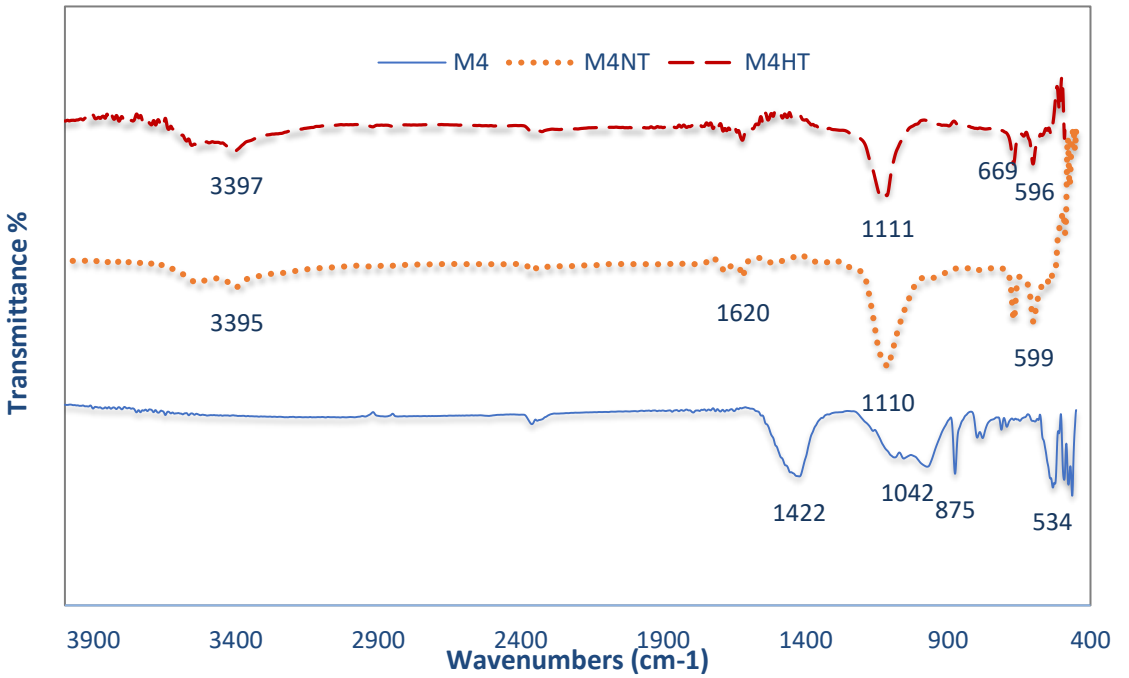

Figure 5-84: FTIR spectra of Unexposed sample, (b)sample exposed to %5 acid at normal temperature, and (c). sample exposed to %5 sulfuric acid at high temperature. M4

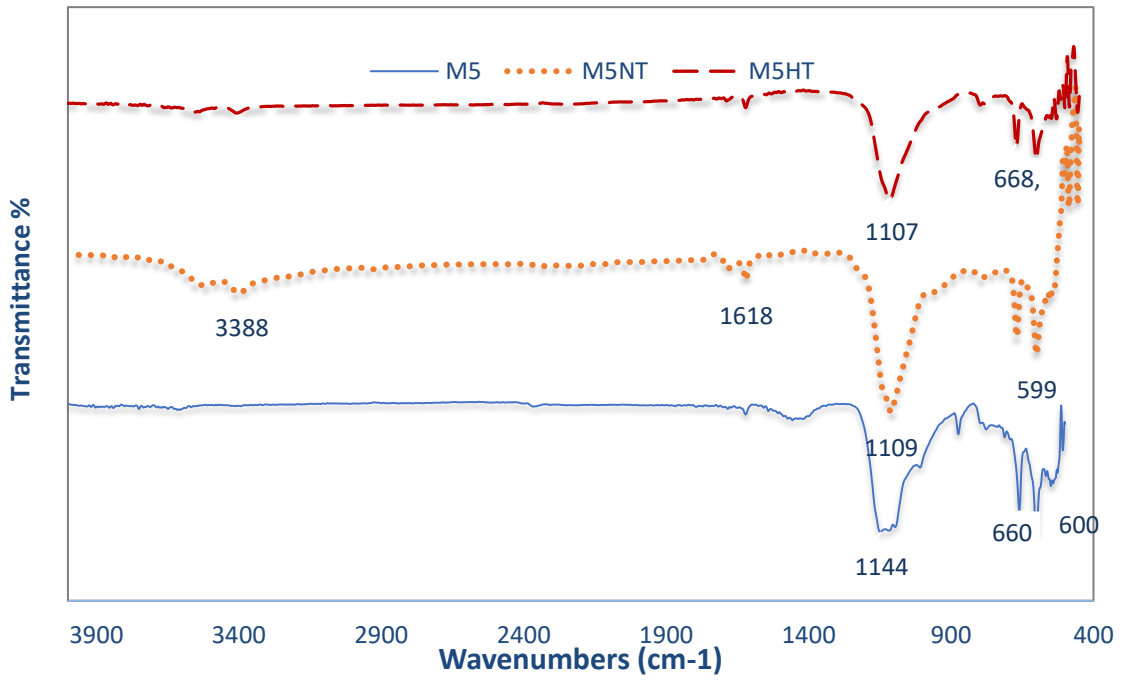

Figure 5-85: FTIR spectra of Unexposed sample, (b)sample exposed to %5 acid at normal temperature, and (c). sample exposed to %5 sulfuric acid at high temperature. M5

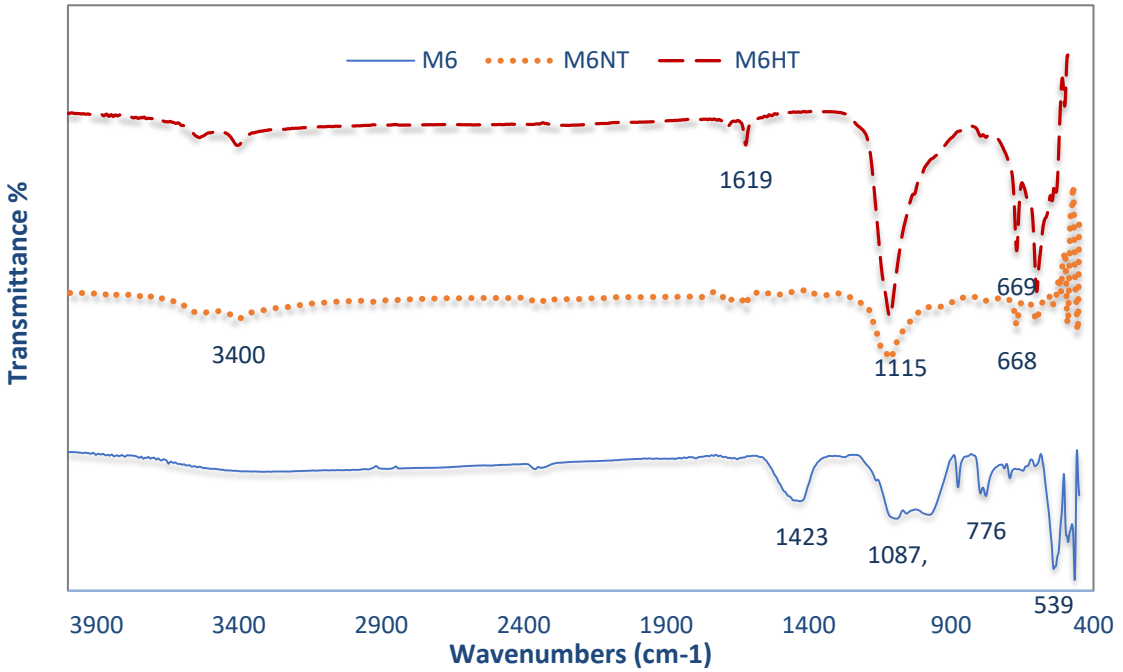

Figure 5-86: FTIR spectra of Unexposed sample, (b)sample exposed to %5 acid at normal temperature, and (c). sample exposed to %5 sulfuric acid at high temperature. M6

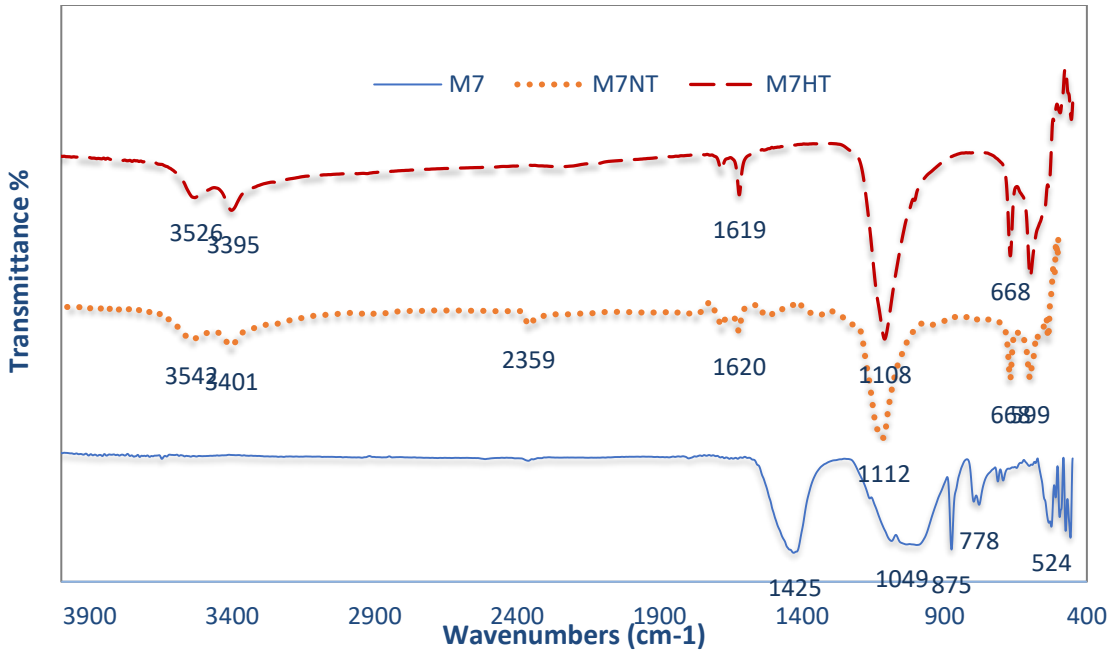

Figure 5-87: FTIR spectra of Unexposed sample, (b)sample exposed to %5 acid at normal temperature, and (c). sample exposed to %5 sulfuric acid at high temperature. M7

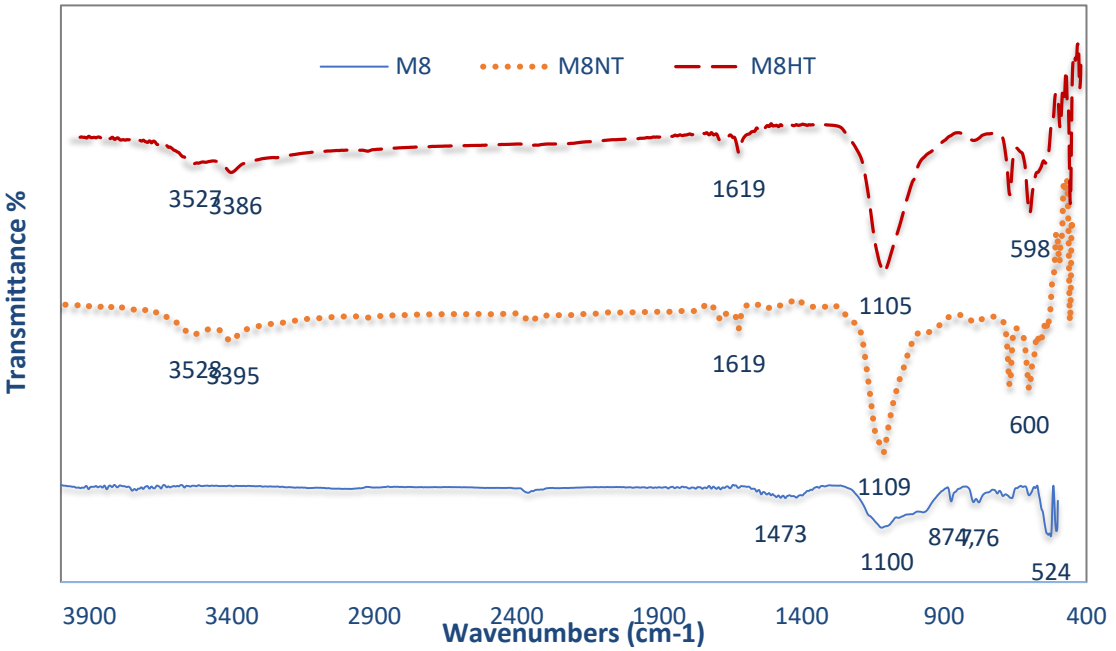

Figure 5-88: FTIR spectra of Unexposed sample, (b)sample exposed to %5 acid at normal temperature, and (c). sample exposed to %5 sulfuric acid at high temperature. M8

CHAPTER 6

MODELING DEGRADATION OF CONCRETE

6.1 Description of the Damage Model

The diffusion-reaction-damage model developed by Tixier and Mobasher (2003) was adopted to simulate the combined sulfate and sulfuric acid attack. The model is based on diffusion of sulfate ions in accordance to Ficks law, coupled with reaction taking place between calcium aluminates and sulfate to form gypsum and ettringite. The reaction results in an increase in volume and subsequently create internal tensile stresses/strains. When these exceed the concrete tensile strength, it cracks and subsequently reduce stiffness. These cracks further increase the diffusion at the crack location (layer). Because of change in diffusivity throughout the depth of concrete, the problem is treated as a moving boundary. Parameters considered are as follow:

Initial Material Properties	Computed material parameters
Geometry of the concrete structure	Mechanical properties
Cement content and composition	Capillary porosity
w/c ratio	C3A and Sulfate content cross the depth
Degree of hydration	Reduced Stiffness
Diffusion, D	Linear Expansion
Sulfate surface concentration	Internal strains
E, F't	
Diffusion of cracked/uncracked (D1/D2)	
Reaction Rate	

The model is extended to take in consideration the effect of increased porosity at the surface due to acid effect (dissolution of portlandite and decomposition of CSH). The numerical simulation was conducted by a MATLAB program and solved as a 2D problem. A parametric study was conducted to simulate the effect of variation of various parameters and to analyze the behavior of the diffusion, reaction and damage mechanisms. These parameters include diffusion, diffusion of cracked/uncracked material, volume of pores that can be filled with expansive material, C_3A content, reaction rate, modulus of elasticity.

calcium aluminate phases are represented in the model Pi with i=1..3, and defined as P1=C_4AH_{13}, P2=C_4ASH_{12} calcium aluminate monosulfate hydrate and P3= C_3A. The relative proportions are calculated based on material input data. Volumetric calculations are calculated based on stoichiometry with the following reactions taking place.

$C_4AH_{13}+3C\underline{S}H_2+14H \rightarrow C_6A\underline{S}H_{32}+CH$

$C_4A\underline{S}H_{12}+2C\underline{S}H_2+16H \rightarrow C_6A\underline{S}H_{32}$

$C_3A+3C\underline{S}H_2+26H \rightarrow C_6A\underline{S}H_{32}$

$$\frac{\Delta V_P}{V_P}=\frac{(m_V^{C_6A\bar{S}_3H_{32}})^{-1}}{(m_V^{P_i})^{-1}+a(m_V^{C\bar{S}H_2})^{-1}}-1, \quad \text{with } m_V^k=\frac{d^k}{M^k}$$

where dk, Mk, and m_v^k are respectively the density, molar mass, and molar volume of a given compound. The reacted and unreacted aluminate phase are denoted as Car and are calculated as function of time and space. Cau(x,t), according to

$$C_{ar}(x,t)=C_a-C_{au}(x,t)$$

Volumetric strain is calculated based on the total reacted aluminate phases

$$\varepsilon_V^0(x,t) = C_{ar} \sum_P \left(\frac{\Delta V}{V} \right)_P$$

The capillary porosity, ϕ, is estimated according to the Powers model approach (Hoglund 1992) with w/c as the water/cement ratio, Vc the volumetric fraction of cement in the concrete, and a_α the degree of hydration of the cement. Capillary porosity plays an important role in accommodating the expansive material. The percentage of this porosity that can be filled is controlled through the input parameter "% of porosity that can be filled with expansive material", the higher this value the more time it will take for the damage to take place. This is incorporated into the model through time delay to the evolution of volumetric strain.

$$\Phi = \max\left(V_c \frac{\frac{w}{c} - 0.39\alpha}{\frac{w}{c} + 0.32}, 0 \right)$$

$$\varepsilon_V^t(x,t) = \varepsilon_V^0(x,t) - f\Phi$$

$$\varepsilon(x,t) = \frac{1}{3}\varepsilon_V^t(x,t)$$

Degradation in stiffness is introduced through a damage function ω applied to the uniaxial strain. In the linear elastic range ω=0, meaning there is no damage. In the non-linear elastic range cracks initiate imposing a damage to the stiffness calculated as function of the crack density ω =16/9*Cd, εth is threshold strain

$$C_d = 0.16 \times \left(1 - \frac{\varepsilon_{th}}{\varepsilon} \right)^{2.3}$$

$E = E_0 \times (1-\omega)$

In the post peak zone where, maximum stress is reached the damage function is expressed by the relation presented by Nemat-Nasser and Hori (1993)

$$\frac{\sigma}{f_t'} = \sqrt{\frac{\tan(\pi\omega_0/2)}{\tan(\pi\omega/2)}}; \quad \frac{w}{w_0} = \frac{\sigma}{f_t'}\left(\frac{\log(\sec\pi\omega/2)}{\log(\sec\pi\omega_0/2)}\right) - 1$$

Where ω_0 is the accumulated damage at the peak stress. The deformation at peak is w0 and obtained as $w_0=\varepsilon_p x H$, where H is the gauge length of the specimen and ε_p is the strain at peak. Modulus of elasticity is calculated as:

$$E = \frac{\sigma}{\varepsilon - \varepsilon_0}, \text{ with } \varepsilon_0 = \varepsilon_p - \frac{f_t'}{E_0}$$

Average expansion throughout the cross section based on average E can be expressed as:

$$\Delta = \sigma_r\left(\frac{1}{\overline{E}} - \frac{1}{E_0}\right)H$$

Diffusion-reaction:

$$\frac{\partial U}{\partial T} = D\frac{\partial^2 U}{\partial X^2} - kU$$

The sulfate concentration is represented as U and the diffusion constant as D. Parameter k represents the rate of take up of sulfates and may be considered as the solubility rate. Numerical solution is obtained using finite difference.

6.2 Parametric Study

A parametric study was conducted to simulate the effect of variation of various parameters and to analyze the behavior of the diffusion, reaction and damage mechanisms. These parameters include diffusion, diffusion of cracked/uncracked material, volume of pores that

can be filled with expansive material, Surface concentration of SO_4^{2-} mol/m3 and modulus of elasticity. Initial input parameters are presented in Table 6-1:

Table 6-1: Initial Input Parameters

Thickness of the specimen (meters) L	0.075
Length of the specimen (meters) H	0.15
diffusion coefficient of uncracked material_(m^2/s)_D2	9.00E-13
Ratio of diffusion coefficient for a cracked material to the uncracked D1/D2_(>1);	20
Sulphate boundary concentration_(mol/m^3_of_material),_U0;	500
Cement dosage_(kg/m^3_of_material),Cement content;	370
BSG of cement, MVC;	3.15
water/cement ratio, wc;	0.4
Degree of hydration of cement, DRcement;	0.9
Fraction of capillary porosity that can be filled, phi frac;	0.45
C3A content of cement, CC3Ai;	0.06
Gypsum content of cement, Gypsum;	0.06
Degree of reaction of C3A, DRC3A;	0.9
Rate constant of reaction between sulfates and aluminates (m^3/mol.s),_k;	3.00E-10
Young's modulus of material (MPa),_E0;	41000
Tensile strength of material (MPa), ft;	4
Residual hydrostatic expansive stress in the pore microstructure_(MPa), residual stress;	10

Variation of various parameters

Case	Diffusion Coefficient (m^2/s)	Diffusion coefficient of cracked/uncracked	Surface concentration of SO42- mol/m3	%of capillary voids filled	Modulus of Elasticity (GPa)
1	2E-13	5	10	0.1	10
2	4E-13	6	25	0.2	15
3	6E-13	7	50	0.3	20
4	8E-13	8	100	0.4	25
5	1E-12	9	200	0.5	30
6	3E-12	10	300	0.6	35
7	5E-12	12	500	0.7	40
8	7E-12	14	550	0.8	45
9	8E-12	18	600	0.9	50
10	9E-12	20	650	0.99	55

The effect of variation in the diffusion coefficient (D2) is illustrated in Figure 6-1 Strain profile, degradation of elastic modulus, penetration depth, linear expansion and sulfate concentration with variation in diffusion (D2) parameter. The simulation indicates that a higher diffusion coefficient will result in higher diffusion of sulphate ions toward the inside of the specimens. Sulfate content of 350 mol/m3 at the full depth of specimens was indicated in the case of highest diffusion (9E-12(m^2/s) vs 25 mol/m3 in the case of lowest diffusion (1E-13(m^2/s)) Consequently, more sulphate ions available to react with calcium aluminate phases leads to more expansion that can be seen in the larger volumetric strain and linear expansion developed. Looking at the penetration depth which is an indication of the cracked depth, it also reveals that higher diffusion result in faster penetration and consequently faster degradation of stiffness (700 days for full degradation in case with lowest diffusion vs 100 days for the case of highest diffusion). It can be concluded that the diffusion parameter has a detrimental effect on the modeling of the sulphate and sulfuric acid attack on concrete.

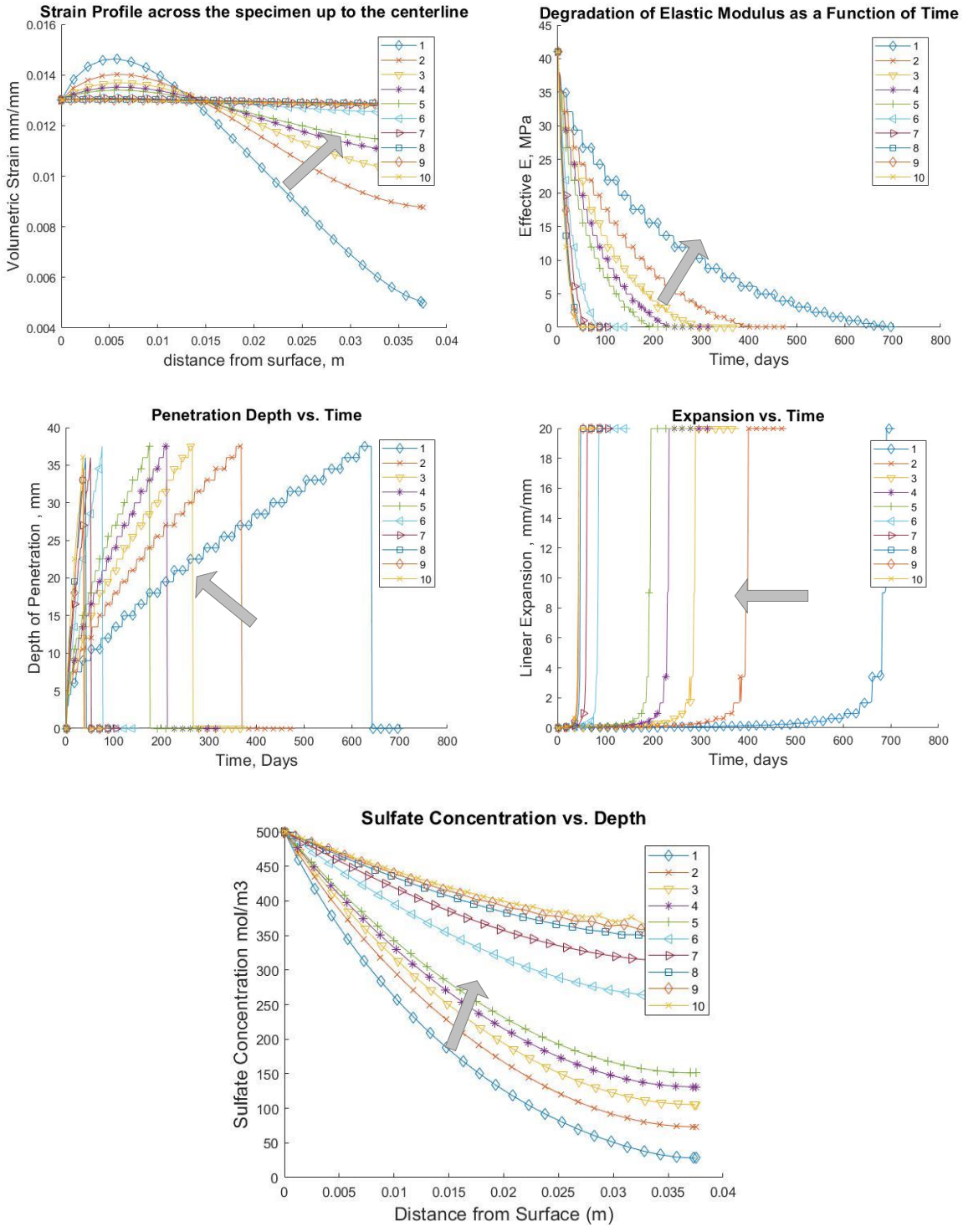

Figure 6-1 Strain profile, degradation of elastic modulus, penetration depth, linear expansion and sulfate concentration with variation in diffusion (D2) parameter.

The effect of variation in the ratio of diffusion coefficient of cracked/uncracked (D1/D2) material illustrated in Figure 6-2. The simulation indicates that a higher diffusion coefficient will result in higher diffusion of sulphate ions toward the inside of the specimens. However, it is not as significant as the diffusion coefficient. Sulfate content of 75 mol/m3 was indicated in the case of highest D1/D2 (20) vs 10 mol/m3 in the case of lowest diffusion D1/D2 (5). More sulphate ions available to react with calcium aluminate phases leads to more expansion that can be seen in the larger volumetric strain and linear expansion developed. Looking at the penetration depth which is an indication of the cracked depth, it also reveals that higher diffusion result in faster penetration and consequently faster degradation of stiffness (900 days for full degradation in case with lowest D1/D2 vs 350days for the case of highest D1/D2). It can be concluded that the diffusion parameter has an important effect on the modeling of the sulphate and sulfuric acid attack on concrete but less significant when compared to the diffusion parameter D2.

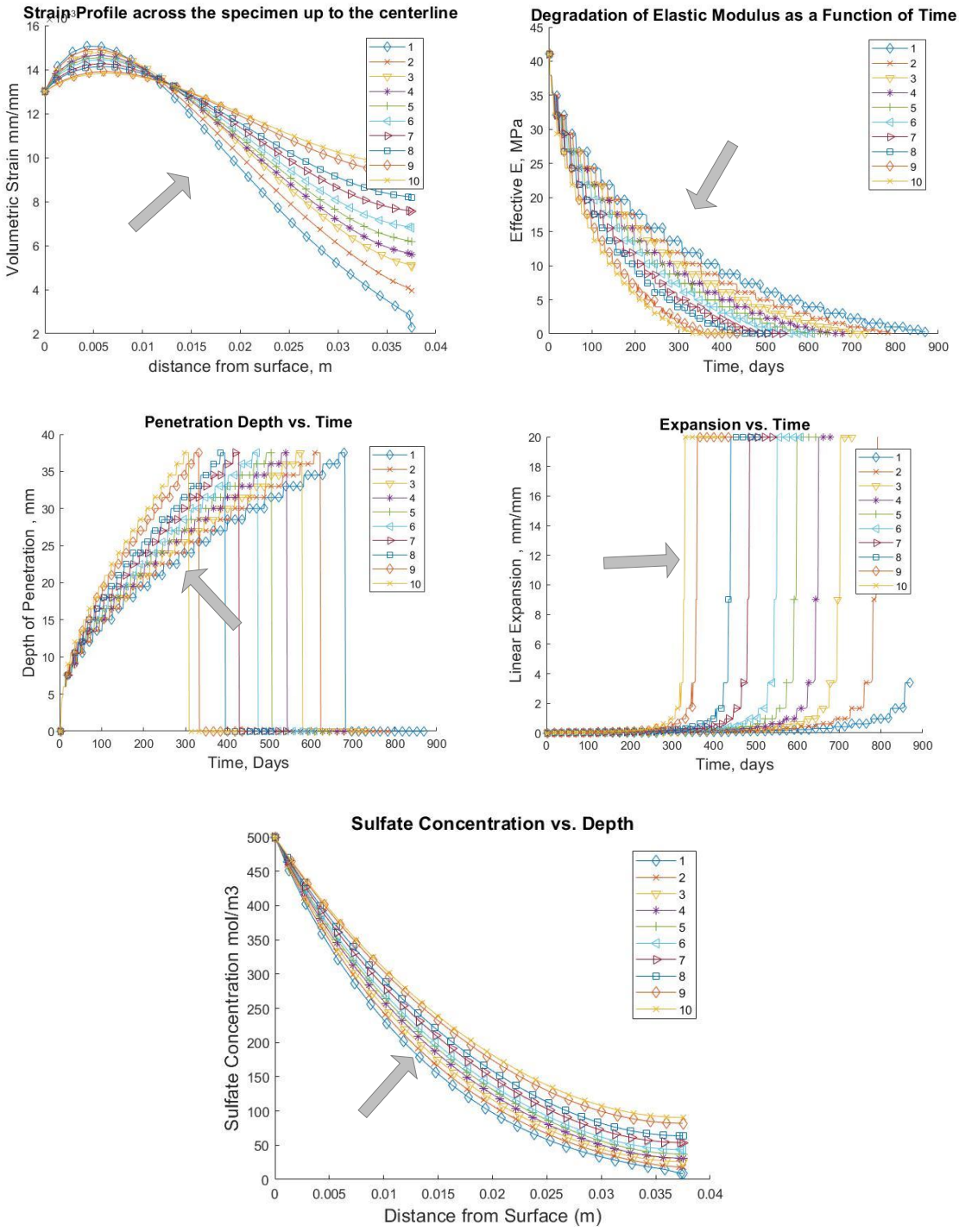

Figure 6-2 : Strain profile, degradation of elastic modulus, penetration depth, linear expansion and sulfate concentration with variation in diffusion cracked to uncracked (D1/D2) material parameter.

The effect of variation in the surface concentration of sulfate ions is illustrated in Figure 6-3. The simulation indicates higher sulfate content only at intermediate depth that doesn't extend toward the full extent of specimen's depth. This can be explained by the fact that penetration will be controlled by the reaction rate. Sulfate content of in the range of 0-30 mol/m3 was indicated at the full depth. At intermediate depth more sulphate ions available to react with calcium aluminate phases leads to more expansion that can be seen in the larger volumetric strain and linear expansion developed. Looking at the penetration depth which is an indication of the cracked depth, it also reveals that higher diffusion result in faster penetration and consequently faster degradation of stiffness (900 days for full degradation in case with highest surface concentration vs 1300 days for the case of lowest surface concentration). It can be concluded that the surface concentration of sulphate ions has an important effect on the modeling of the sulphate and sulfuric acid attack on concrete that is more significant at intermediate depth.

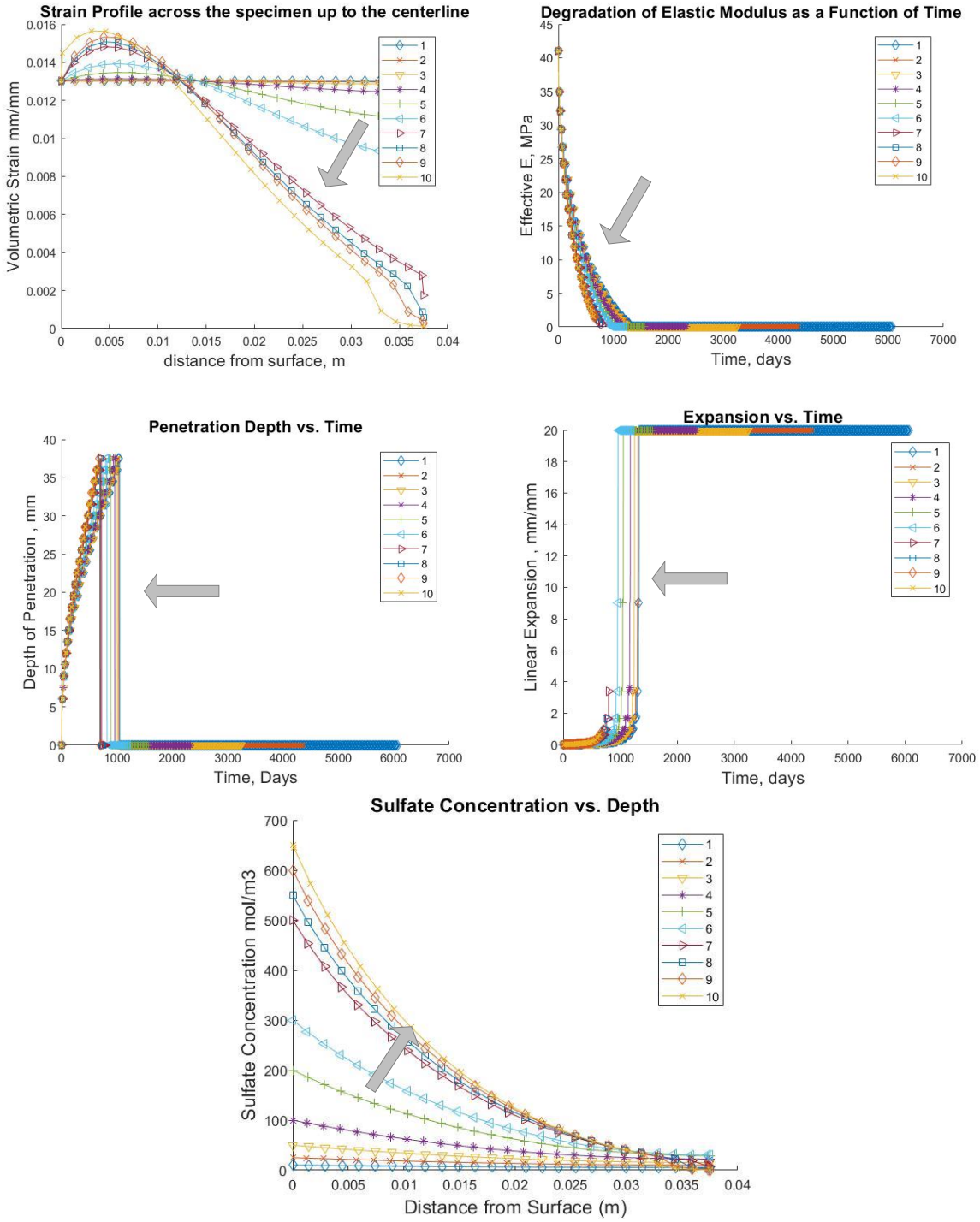

Figure 6-3:Strain profile, degradation of elastic modulus, penetration depth, linear expansion and sulfate concentration with variation surface concentration of sulphate parameter.

Capillary voids provide space of expansive products to fill (buffer effect). Once these pores are filled the expansion and degradation of the concrete will take place. Effect of variation in the surface concentration of sulfate ions is illustrated in Figure 6-4. The simulation indicates that providing higher percentage of the capillary voids to be filled with expansive material will significantly slow down the degradation process. Looking at the penetration depth which is an indication of the cracked depth, it also reveals that capillary voids result in slower penetration and consequently slower degradation of stiffness (2200 days for full degradation in case with highest volume of capillary voids (0.99) vs 500 days for the case of capillary voids (0.1). It can be concluded that the Capillary voids of sulphate ions has an important effect on the modeling of the sulphate and sulfuric acid attack on concrete that is more significant at intermediate depth.

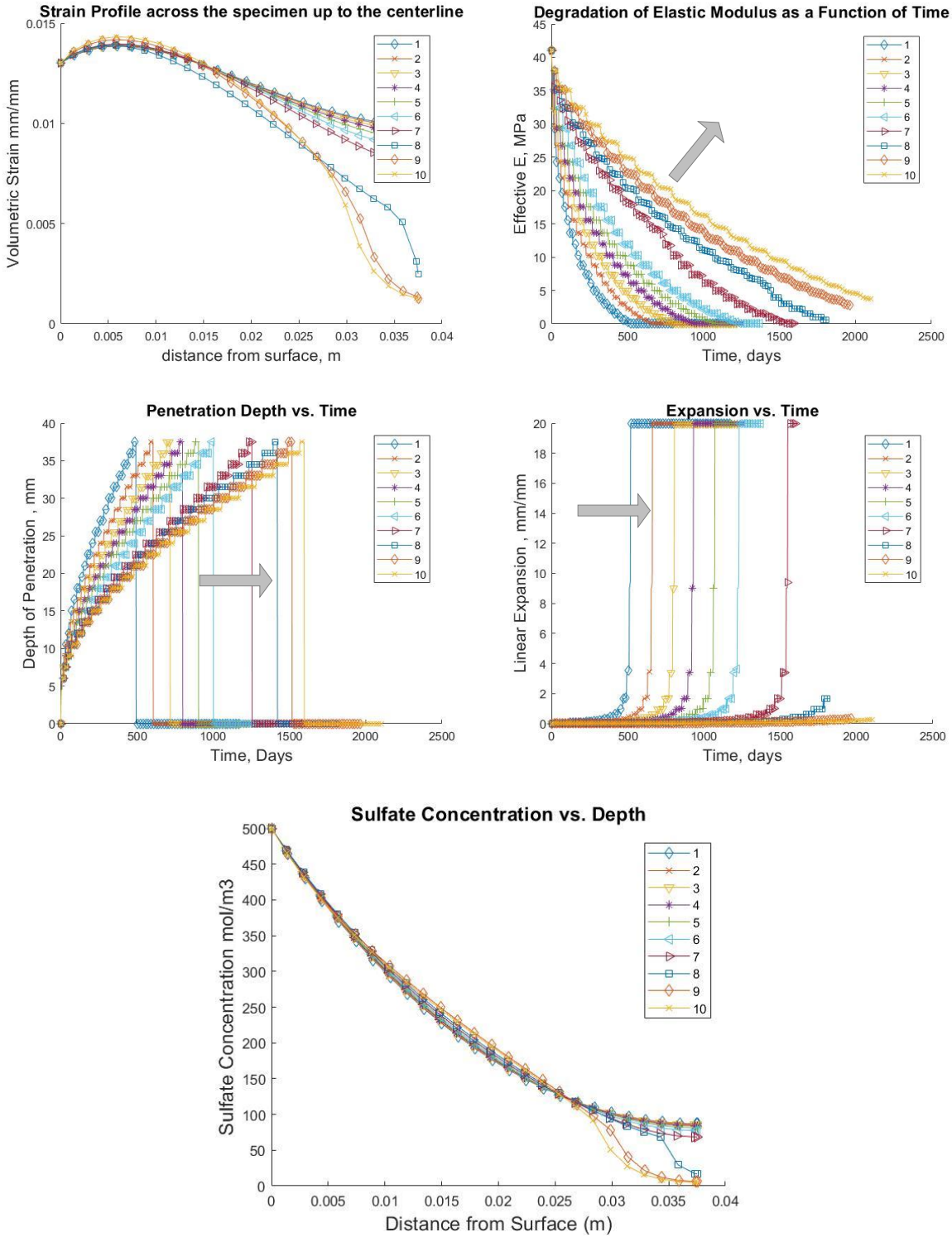

Figure 6-4: Strain profile, degradation of elastic modulus, penetration depth, linear expansion and sulfate concentration with variation in capillary voids parameter.

Modulus of elasticity play an important role in the damage propagation through the concrete matrix. Since the damage is triggered by expansion and development of internal strains, a more rigid material will behave more like brittle material allowing less deformation to take place before failure. Inversely a more flexible material will withstand more deformation before failure. Variation of the elastic modulus parameter revealed an important effect on the damage of concrete attacked by sulphate and sulfuric acid. This can be observed in Figure 6-5 which shows that the material with highest stiffness failed at a faster time than the flexible material. Looking at the penetration depth which is an indication of the cracked depth, it also reveals that lower elastic modulus result in slower degradation (4000 days for full degradation in case with lowest modulus (10GPa) vs 2200 days for the case of highest modulus (55GPa). It can be concluded that the modulus of elasticity has an important effect on the modeling of the sulphate and sulfuric acid attack on concrete.

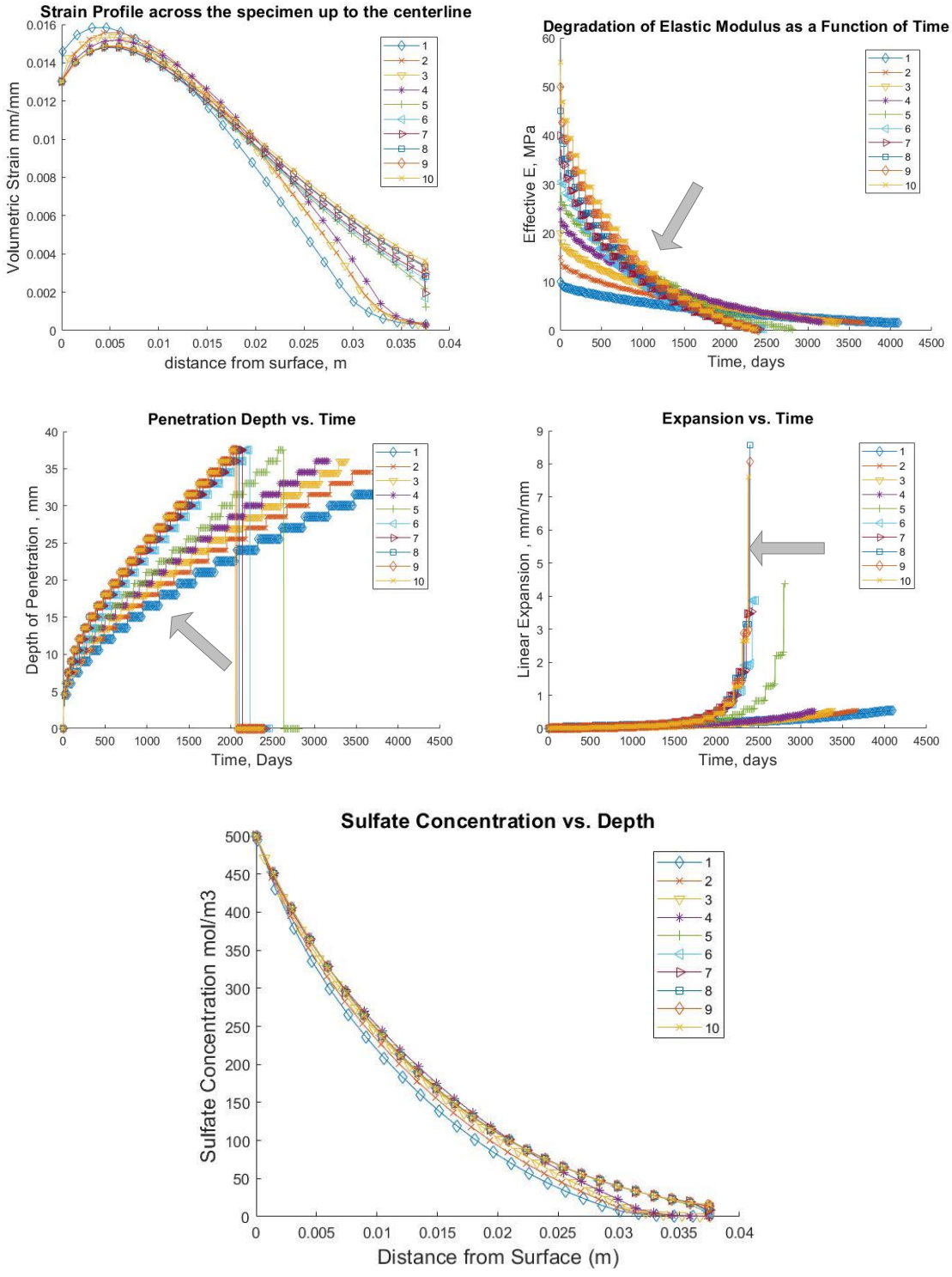

Figure 6-5: Strain profile, degradation of elastic modulus, penetration depth, linear expansion and sulfate concentration with variation in modulus of elasticity.

6.3 Modeling the Experimental Work

After conducting the parametric study and understanding the behavior of the material and the damage due to various parameters, a calibrated model was developed to simulate and compare with the actual data obtained from the experimental work. Ordinary Portland cement (M1) concrete was selected to be compared with simulation. Simulation for a period of 12 weeks was considered.

The following input parameters were specified for the model.

Thickness of the specimen (meters) L	0.075
Length of the specimen (meters) H	0.15
diffusion coefficient of uncracked material_(m^2/s)_D2	9.00E-13
Ratio of diffusion coefficient for a cracked material to the uncracked D1/D2_(>1);	20
Sulphate boundary concentration_(mol/m^3_of_material),_U0;	500
Cement dosage_(kg/m^3_of_material),Cement content;	370
BSG of cement, MVC;	3.15
water/cement ratio, wc;	0.4
Degree of hydration of cement, DRcement;	0.9
Fraction of capillary porosity that can be filled, phi frac;	0.35
C3A content of cement, CC3Ai;	0.06
Gypsum content of cement, Gypsum;	0.06
Degree of reaction of C3A, DRC3A;	0.9
Rate constant of reaction between sulfates and aluminates (m^3/mol.s),_k;	3.00E-10
Young's modulus of material (MPa),_E0;	41000
Tensile strength of material (MPa), ft;	4.5
Residual hydrostatic expansive stress in the pore microstructure_(MPa), residual stress;	10

The model predicted reasonably the sulfate content through the depth of the concrete specimen as compared with the data obtained from experiment (Figure 6-6). The model has slightly over estimated the penetration depth as compared with the depth of damaged encountered in the experiment. The compressive strength loss of concrete type M1 was %52.1, corresponding to a theoretical loss of 20mm in the concrete cylinder diameter. (Figure 6-7-6.9)

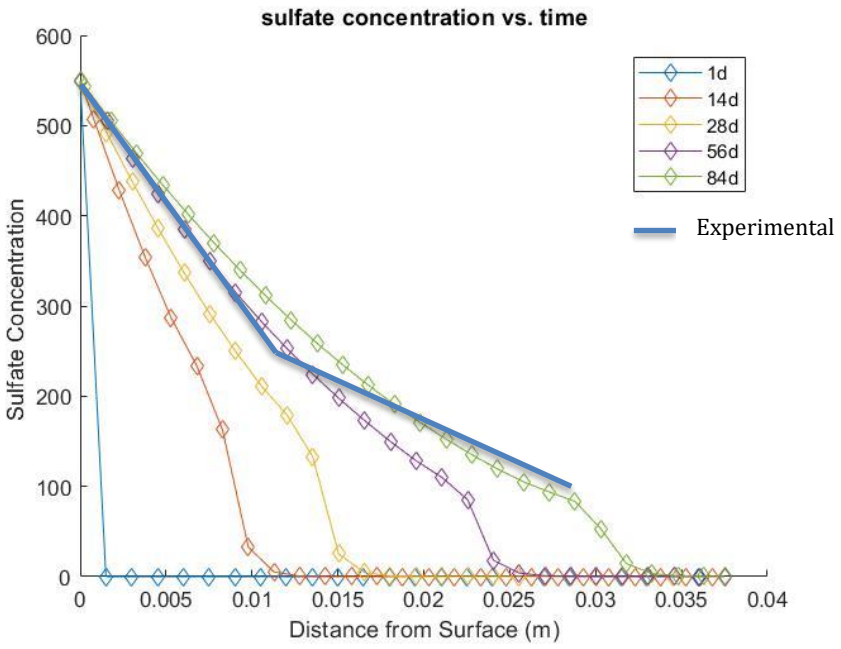

Figure 6-6: Comparison between simulated and measure sulfate content in type M1-OPC concrete after 12 weeks of exposure

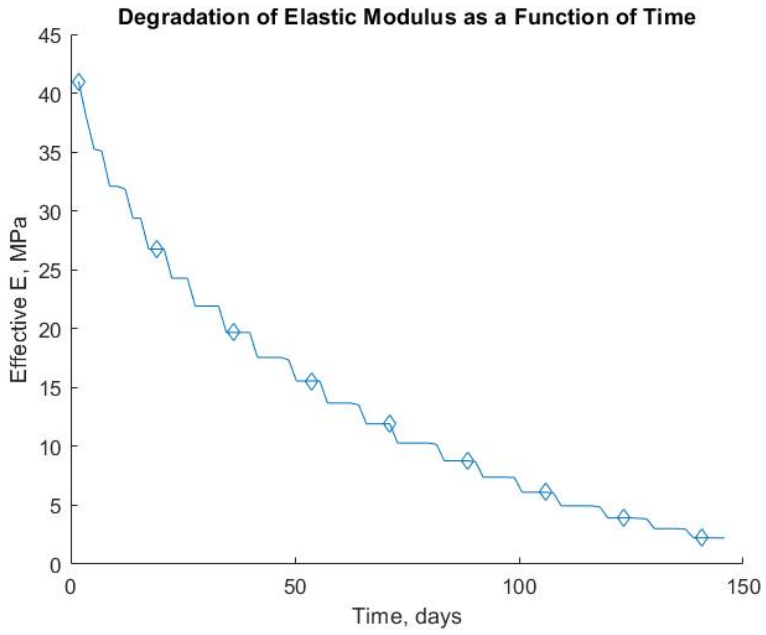

Figure 6-7: Simulated degradation of elastic modulus

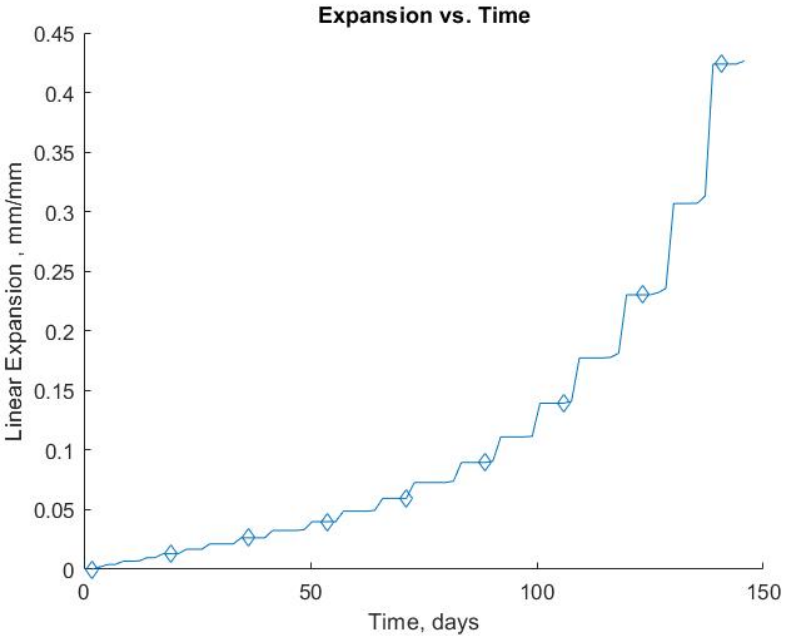

Figure 6-8:simulated linear expansion

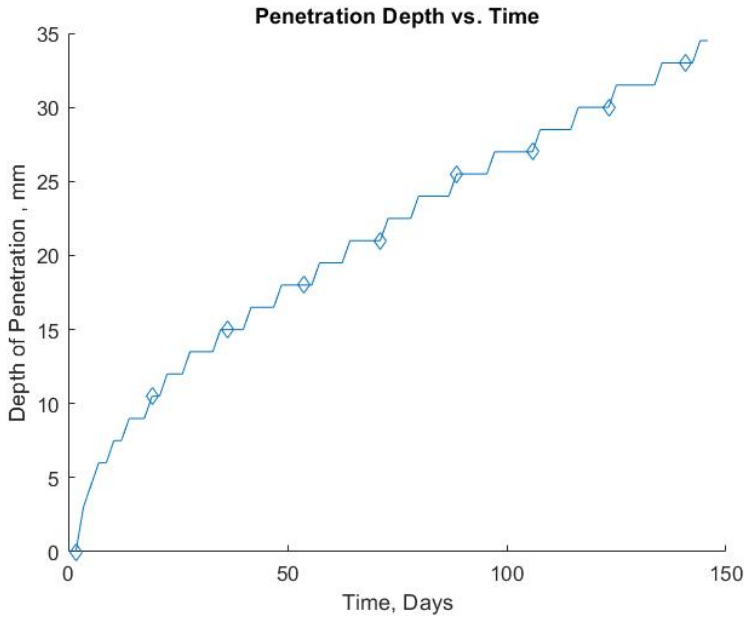

Figure 6-9: Simulated depth of penetration

CHAPTER 7

CONCLUSIONS AND RECOMMENDATIONS

Sulfur Pit is an essential part of oil and gas processing facilities where the sulfur after extraction from the hydrocarbons in Sulfur Recovery Units is stored and maintained in liquid phase at temperatures ranging from 130 °C to 160 °C. The molten sulfur reacts with water vapor in a sealed sulfur pit resulting in the formation of acidic vapors in the pit. These acidic vapors are primarily sulfurous and sulfuric acid vapors. These acidic vapors at high temperature results in damage to the concrete slab and walls above the zone of sulfur immersion in the sulfur pit. Literature review of the mechanisms of various forms of sulfate and sulfuric acid attack was conducted and previous work on performance of various types of concrete developed for sulfuric acid exposed structure mainly focused on sewage transmission and treatment facilities. Sulfur pit is a specialized concrete structure subjected to combined sulfur/sulfuric acid exposure at high temperature which has not been addressed.

In order to determine the damage mechanism, a detailed analysis of the field investigations carried out on existing sulfur pit structures was conducted and the exposure environment and loading to which a sulfur pit structure is subjected was ascertained. Results of visual inspection, semi-destructive testing (SDT), nondestructive testing (NDT) and laboratory tests on concrete core and powder samples from the pits were analyzed. Based on the analysis of field investigations, it has been determined that sulfuric acid vapors is a major cause of concrete deterioration in sulfur pits and it accelerates the reinforcement corrosion process by damaging the concrete cover to the reinforcement.

A comprehensive experimental program was established to evaluate the performance of eight different types of concrete in an accelerated testing scheme, by exposure of concrete specimens to dilute sulfuric acid solution under normal and high temperature conditions. The concrete mixes investigated includes using Ordinary Portland Cement (OPC) concrete, Sulfate Resistant Portland Cement (SRPC) concrete, concrete with Supplementary Cement Materials (GGBFS, FA, SF), Alkali Activated Polymer Concrete, Calcium Aluminate Concrete (CAC) and Ultra High-Performance Concrete (UHPC).

Moreover, two protective coating systems were investigated as part of this research. The first system uses a Glass Fiber Reinforced Plastic (GFRP) liner with high grade vinyl ester resin to sustain the elevated temperature. The second system is a commercially available high-performance industrial polymer coating based on three-dimensional high cross link structure through Ether bonds (C-O-C). To evaluate the performance of the various concrete mixes subjected to dilute sulfuric acid, concrete cylinder samples were exposed to %5 sulfuric acid solution at normal and elevated temperature for a period of 12 weeks. Concrete specimens retrieved at selected ages were tested for mechanical properties and microstructural investigations.

Numerical modeling using diffusion-reaction damage was developed as an extension of the Tixier and Mubasher's model (2003) to predict the behavior of concrete subject to sulfuric acid. Parametric study was conducted to understand the effect of variation in different parameters on the deterioration of concrete. Subsequently, the actual deterioration of ordinary Portland cement as obtained from experimental work was simulated and compared.

7.1 Conclusions from Field Investigation

1. Visual Surveys indicate severe deterioration of concrete structural element in the sulfur pits mainly in the form of cracking, delamination and reinforcing steel corrosion, being more prominent in the ceiling of the sulfur pit.
2. The deterioration mechanism varies in the walls, roof slab and the foundation. A significant increase in compressive strength (2 to 3 times the original specified compressive strength) is indicated in the base slab and the portion of the walls which are immersed in molten sulfur. Petrography examination indicated microcracks filled with sulfur which could be the reason for such increase in strength.
3. No significant damage and corrosion were observed in the base slab and portions of walls immersed in molten sulfur. However, in all sulfur pits surveyed, the walls have similar pattern of cracking parallel lines that are caused by thermal expansion as the structure is subjected to elevated temperature up to 160 ^{o}C.
4. Ceiling of the roof slab, which is subjected to sulfuric acid vapor fumes undergone extensive damage in almost all the sulfur pits in the form of cracking, delamination and active corrosion of reinforcing steel. Portions of roof slab have collapsed in some sulfur pits. pH reduction in roof slabs could be attributed to the sulfuric acid vapors.
5. The top part of the walls in the sulfur pit, which are also subjected to sulfuric acid vapors show similar deterioration.

7.2 Conclusions from the Experimental Program

1. From the eight concrete mixes investigated in the experimental program, the best performance in terms of mechanical properties and resistance to chemical attack and acid penetration was the calcium aluminate concrete.
2. SCMs group did not show any improvement as compared to conventional concrete as has been indicated by many researchers. The beneficial effect of enhance concrete microstructure provided by pozzolanic reaction and pores filling effect diminishes at high concentration sulfuric acid exposure
3. Alkali activated concrete investigated extensively in the literature for its resistance to sulfuric acid, demonstrated a relatively high resistance to sulfuric acid in terms of retained mass and strength in this research also. However, it has also been demonstrated that the deep acidification depth, makes it unfavorable from the reinforcement corrosion protection aspect.
4. Although UHPC concrete had the highest performance in mechanical properties and minimum permeability as indicated by absorption test, RCPT and NT BULD 492 it demonstrated the maximum loss in strength and mass.
5. Material characterization techniques (SEM, EDX, XRD and FTIR) provided valuable insights toward understanding the changes in material after exposure to sulfuric acid. In general, the acid reaction with concrete takes place at the extreme outer surface and the ultimate product formed is gypsum.
6. The reaction speed depends on the chemical composition of the concrete and their relative resistance to the acid.

7. Portlandite is the fastest reacting phase to form gypsum, followed by calcium silicate hydrate phase, Quartz and calcite. These are typical phases found at different percentage in conventional concrete and SCMs.
8. Polymer concrete on the other hand contain aluminum silicate bonds formed through the polymerization process which are not easy to break which makes it more resistance to acid. Likewise, Calcium aluminate concrete contains calcium aluminate hydrate (CAH) phases which are not easily broken by sulfuric acid.
9. The effect of exposure to sulfuric acid at elevated temperature was increase in rate of the deterioration (kinetics of the reaction). Loss of mass and strength in samples exposed to %5 sulfuric acid at elevated temperature is very comparable to that of samples exposed to %10 sulfuric acid at an ambient temperature (25 ^{o}C).
10. Glass Fiber Reinforced Plastic (GFRP) applied as a coating material has shown great resistance to sulfuric acid at normal and at elevated temperature (No sign of damage). On the other hand, high-performance industrial polymer coating based on three-dimensional high cross link structure through Ether bonds (C-O-C) failed in just 4 weeks when applied on concrete exposed to sulfuric acid at high temperature.

7.3 Conclusions from the Numerical Modeling

1. Numerical modeling using diffusion-reaction damage was developed as an extension to Tixier and Mubasher's model (2003) to predict the behavior of concrete subject to sulfuric acid.
2. The model is based on the combined sulfate and sulfuric acid attack taking place concurrently, with acid acting on the surface. Sulfate ions penetrates through the concrete and causes expansion

3. The parametric study provided an insight into the understanding of the degradation mechanism and the effect of variation in different parameters on the performance of concrete.
4. The model provided reasonable prediction of the sulfate diffusion when compared to actual data from experimental work but overestimated the cracking and degradation of concrete of the elastic modulus.

7.4 Recommendations

1. Calcium Aluminate Cement Concrete (CAC) demonstrated high resistance to sulfuric acid and demonstrated best performance among all concrete mixes investigated in the experimental program. CAC is therefore recommended for sulfur storage structures. CAC can be utilized for construction of the structural system provided that the ultimate long-term compressive strength of CAC after "conversion" is specified.
2. More economical solution would be to use CAC as a liner (75mm thick) inside a conventional reinforced concrete sulfur storage structure for the walls, columns and foundation.
3. Externally applied Glass Fiber Reinforced Plastic (GFRP) liner with high grade resin to is a potential candidate for protection of concrete in a sulfur pit as a liner. However, further investigations need to be carried out this system.

7.5 Future Work

1. Long term study should be considered to expose and monitor the performance of concrete specimens in molten sulfur inside an actual sulfur storage tank and monitor frequently over several number of years.
2. Exploring the viability and investigating of the performance of Glass Fiber Reinforced Plastic (GFRP) manufactured sulfur storage tanks in molten sulfur environment.
3. Further investigation of the GFRP liner as a protection system in sulfur storage structures.

References

[1] Marchand, E. Samson, Y. Maltais, J.J. Beaudoin, “Theoretical analysis of the effect of weak sodium sulfate solutions on the durability of concrete”, Cement & Concrete Composites vol.24, pp. 317-329, June 2002

[2] E. Samson, J. Marchand, “Modeling the transport of ions in unsaturated cement-based materials”, computers and structures, vol.85, no.23-24, pp.1740-1756, Dec 2007

[3] Yang Lu, Edward Garboczi2, Dale Bentz3, Jeffrey Davis “Modeling of Chloride Transport in Cracked Concrete: A 3-D Image– based Microstructure Simulation”, COMSOL Conference, Nov. 2012

[4] Dale P. Bentz, W. Spencer Guthrie, Scott Z. Jones, and Nicos S. Martys, “Predicting Service Life of Steel-Reinforced Concrete Exposed to Chlorides, Concrete International, vol. 36, no.9, pp. 55-64, Jan. 2014

[5] A. Campos, C.M. López, A. Aguado, “Diffusion–reaction model for the internal sulfate attack in concrete”, Construction and Building Materials, vol.102, pp.531-540, Jan. 2016

[6] Kamile Tosun, Burak Felekoglua, Bülent Baradan, Akın Altun, “Effects of limestone replacement ratio on the sulfate resistance of Portland limestone cement mortars exposed to extraordinary high sulfate concentrations”, Construction and Building Materials, vol.23, no.7, pp.2534-2544, Jul. 2009

[7] Tai Ikumi, Sergio H.P. Cavalaro, Ignacio Segura, Albert de la Fuente, Antonio Aguado, “Simplified methodology to evaluate the external sulfate attack in concrete structures”, Materials and Design, vol.89, pp. 1147-1160, Jan., 2016

[8] P. Henocq a, E. Samson a, J. Marchand, “Portlandite content and ionic transport properties of hydrated C3S Paste”, Cement and Concrete Research, vol.42, no.2, Feb. 2012

[9] J. Beaudoina, S. Catinaudb, J. Marchand, “Volume stability of calcium hydroxide in aggressive solutions”, Cement and Concrete Research, vol.31, no.1, pp. 149-151, Jan. 2001

[10] N. Cefis, C. Comi, “Damage modelling in concrete subject to sulfate attack”, Frattura ed Integrità Strutturale, vol.8, no.29, pp. 222-229, Jul. 2014

[11] Adam Neville, “The confused world of sulfate attack on concrete”, Cement and Concrete Research, vol34, no.8, pp. 1275-1296, Aug. 2004

[12] Qingke Nie, Changjun Zhou, Huawei Li, Xiang Shu, Hongren Gong, Baoshan Huang, “Numerical Simulation of Fly Ash Concrete Under Sulfate Attack”, Construction and Building Materials, vol.84, no.1, pp. 261-268, June. 2015

[13] M. K. Rahman, H. A. Khalifah, M. K. Ammar, E. Abu-Aisheh, “Condition Assessment and Finite Element Modelling of a Sulfur Pit Structure in the Sulfur Recovery Unit of a Gas Plant”, 4th SCMT Conference, 2016

[14] Fernando B. Mainier, Paulo César Fernandes de Almeida, Bruna Nani, Lisiane H. Fernandes, Marcone Freitas dos Reis, “Corrosion Caused by Sulfur Dioxide in Reinforced Concrete”, Open Journal of Civil Engineering, vol.5, no.4, pp. 379-389, Dec. 2015

[15] C. M. Hansson, A. Poursaee, S. J. Jaffer, “Corrosion of Reinforcing Bars in Concrete”, The Masterbuilder., Dec 2012

[16] Baird, C. and Cann, M. Environmental Chemistry, Macmillan. 2005

[17] AASHTO LRFD Bridge Design Specifications, sixth edition, American Association of State Highway and Transportation Officials, Washington, DC, 2013

[18] Bertolini, L., Elsener, B., Pedeferri, P., and Polder, R., “Corrosion of Steel in Concrete”, Prevention, Diagnosis, Repair, Wiley-VCH, 2004

[19] Vahid Jafari Azad, Chang Li, Circe Verba, Jason H. Ideker, O.Burkan Isgor, “A COMSOL–GEMS interface for modeling coupled reactive-transport geochemical processes”, Computers & Geosciences, vol.92, Jul. 2017

[20] Lothenbach, B., Matschei, T., Moschner, G., Glasser, F., “Thermodynamic Modelling of the Effect of Temperature on the Hydration and Porosity of Portland Cement”.Cem.Concr.Res. vol.38, no.1, pp. 1-18. Jan. 2008

[21] Bentz D., Garboczi, E., Lu, Y., Martys, N., Sakulich, A., and Weiss, J. “Modeling of the Influence of Transverse Cracking on Chloride Penetration into Concrete” Cement and Concrete Composites, vol.38, pp. 65-74, Apr. 2012

[22] Shamila Salek, Bijan Samali, Timothy Murphy, Richard Wuhrer And Georgius Adam, “Comparative Study between Microstructure of a Novel Durable Concrete and Normal Concrete Subjected to Harsh Environments”. 9th International Conference on Fracture Mechanics of Concrete and Concrete Structures. 2016

[23] Robin E. Beddoe, Horst W. Dorner “Modelling Acid Attack on Concrete: Part I. The Essential Mechanisms”, Cement and Concrete Research, vol.35, no.12, pp. 2333-2339, Dec. 2005

[24] Robin E. Beddoe, “Modelling Acid Attack on Concrete: Part II. A Computer Model”, Cement and Concrete Research, vol.38, pp. 20-35, Oct. 2016

[25] Haifeng Yuan, Patrick Dangla, Patrice Chatellier, Thierry Chaussadent, “Degradation Modelling of Concrete Submitted to Sulfuric Acid Attack”, Cement and Concrete Research, vol.53, pp. 267-277, Nov. 2013

[26] M.T. Bassuoni, M.L. Nehdi, “Resistance of Self-Consolidating Concrete to Sulfuric Acid Attack”, Cement and Concrete Research, vol.37, no.7, pp. 1070-1084. Jul. 2007

[27] J. Daczko, D. Johnson, S. Amey, “Decreasing Concrete Sewer Pipe Degradation Using Admixtures”, Mater. Perform. Vol.36, no.1, pp. 51-56, Jan. 1997

[28] N. Fattuhi, B. Hughes, “Ordinary Portland Cement Mixes with Selected Admixtures Subjected to Sulfuric Acid Attack”, ACI Mater. J., vol.85, no.6, pp. 512-518, Nov. 1988

[29] S. Ehrich, L. Helard, R. Letourneux, J. Willocq, E. Bock, “Biogenic and Chemical Sulfuric Acid Corrosion of Mortars”, ASCE J. Mater. Civ. Eng., vol.11, no.4, pp. 340-344, 1999

[30] N. Fattuhi, B. Hughes, “SRPC and Modified Concretes Subjected to Severe Sulphuric Acid Attack”, Mag. Concr. Res., vol.40, no.144, pp. 159-166, 1988

[31] K. Torii, M. Kawamura, “Effects of Fly Ash and Silica Fume on The Resistance of Mortar to Sulfuric Acid and Sulfate Attack”, Cem. Concr. Res., vol.24, no.2, pp. 361-370. 1994

[32] D. Roy, P. Arjunan, M. Silsbee, “Effect of Silica Fume, Metakaolin, And Low-Calcium Fly Ash on Chemical Resistance of Concrete”, Cem. Concr. Res., vol.31, no.12, pp. 1809-1813, 2001

[33] J. Monteny, N. De Belie, E. Vincke, W. Verstraete, L. Taerwe, “Chemical Microbiological Tests to Simulate Sulfuric Acid Corrosion of Polymer Modified Concrete”, Cem. Concr. Res., vol.31, no.9, pp. 1359-1365, 2001

[34] E. Vincke, E. Wanseele, J. Monteny, A. Beeldens, N. De Belie, L. Taerwe, D. Van Gemert,W. Verstraete, “Influence of Polymer Addition on Biogenetic Sulfuric Acid Attack of Concrete”, Int. Biodeterior. Biodegrad., vol.49, no.4, pp. 283-292, 2002

[35] S. Ehrich, L. Helard, R. Letourneux, J. Willocq, E. Bock, “Biogenic and Chemical Sulfuric Acid Corrosion of Mortars”, ASCE J. Mater. Civ. Eng., vol.11, no.4, pp. 340-344, 1999

[36] P.C. Hewlett, Lea’s, “Chemistry of Cement and Concrete”, Arnold, UK, 1998.

[37] T. Durning, M. Hicks, “Using Microsilica to Increase Concrete's Resistance to Aggressive Chemicals”, Concr. Int., vol.13, no.3, pp 42-48, 1991

[38] P.K. Mehta, “Studies on Chemical Resistance of Low Water/Cement Ratio Cements”, Cem. Concr. Res., vol.15, no.6, pp. 969-978, 1985

[39] J. Monteny, N. De Belie, L. Taerwe, “Resistance of Different Types of Concrete Mixtures to Sulfuric Acid”, Mater. Struct., vol.36, no.258, pp. 242-249, May 2003

[40] Z. Chang, X. Song, R. Munn, M. Marosszeky, “Using Limestone Aggregates and Different Cements for Enhancing Resistance of Concrete to Sulphuric Acid Attack, Cem. Concr. Res., vol.35, no.8, pp. 1486-1494, Aug. 2005

[41] A. Tamimi, “High Performance Concrete Mix for an Optimum Protection in Acidic Conditions”, Mater. Struct., vol.30, no.197, pp. 188-191, Apr. 1997

[42] E. Attiogbe, S. Rizkalla, “Response of Concrete to Sulfuric Acid Attack, ACI Mater. J., vol.85, no.6, pp. 481-488, Dec. 1988

[43] W.H. Harrison, “Sulphate Resistance of Buried Concrete”, Building Research Establishment Report, 1992.

[44] J.P. Skalny, I. Odler, J. Marchand, Sulfate Attack on Concrete, Spon, London, 2001.

[45] H.F.W. Taylor, “Discussion of Sulfate Attack Mechanisms”, Materials Science of Concrete Special Volume, Amer. Ceramic Society, Ohio, pp. 33-34, 1999

[46] H.F.W. Taylor, Cement Chemistry, Second edition, Thomas Telford, London, 1997.

[47] R.P. Khatri, V. Sirivivatnanon, J.L. Yang, “Role of Permeability in Sulphate Attack”, Cem. Concr. Res., vol.27, no.8, pp. 1179-1189, Aug. 1997

[48] J.F. Young, S. Mindess, R.J. Gray, A. Bentur, The Science and Technology of Civil Engineering Materials, Prentice-Hall, New Jersey, 1998.

[49] R.J. Detwiler, P.C. Taylor, L.J. Powers, W.G. Corley, J.B. Delles, B.R. Johnson, “Assessment of Concrete in Sulfate Soils”, ASCE J. Perform. Constr. Facil. vol.14, no.3, pp. 89-96, 2000

[50] K.E. Kurtis, P.J.M. Monteiro, J.I. Brown, W. Meyer-Ilse, “Expansive Reactions in Concrete Observed by Soft X-Ray Transmission Microscopy”, Mater. Res. Soc. Symp. Proc. 524 pp. 3-9, 2001

[51] M.A. Shazali, W.A. Al-Kutti, M.K. Rahman, A.H. Al-Gadhib, M.H. Baluch, “COMSOL Multiphysics Modeling of Chloride Binding in Diffusive Transport of Chlorides in Concrete”, COMSOL Multiphysics User's Conference 2009.

[52] F. Girardi, R. Di Maggio, “Resistance of Concrete Mixtures to Cyclic Sulfuric Acid Exposure and Mixed Sulfates: Effect of The Type of Aggregate”, Cement & Concrete Composites, vol.33, no.2, pp. 276-285, Feb. 2011

[53] F. Girardi, W. Vaona, R. Di Maggio, “Resistance of Different Types of Concretes to Cyclic Sulfuric Acid and Sodium Sulfate Attack”, Cement & Concrete Composites, vol.32, no.8, pp. 595-602, Sep. 2010

[54] Ankur Mehta, Rafat Siddique, “Sulfuric Acid Resistance of Fly Ash Based Geopolymer Concrete”, Construction and Building Materials, vol.146, pp. 136-143, Aug. 2017

[55] Anwar Khitab, Muhammad Tausif Arshad, Faisal Mushtaq Awan, Imran Khan, “Development of an Acid Resistant Concrete: A Review”, International Journal of Sustainable Construction Engineering & Technology, vol.4, no.2, Nov. 2013

[56] J. Hill, E.A. Byars, J.H. Sharp, C.J. Lynsdale, J.C. Cripps, Q. Zhou "An Experimental Study of Combined Acid and Sulfate Attack on Concrete", Cement & Concrete Composites, vol.25, pp. 997-1003, 2003

[57] HW Dorner and RE Beddoe, “Prognosis of Concrete Corrosion Due to Acid Attack” 9DBMC, 2002

[58] M.A.M. Ariffin a, M.A.R. Bhutta b, M.W. Hussin b, M. Mohd Tahir b, Nor Aziah c, “Sulfuric Acid Resistance of Blended Ash Geopolymer Concrete”, Construction and Building Materials, vol.43, pp. 80-86, 2013

[59] Henchi, K.; Samson, E.; Chapdelaine, F.; and Marchand, J., “Advanced Finite-Element Predictive Model for the Service Life Prediction of Concrete Infrastructures in Support of Asset Management and Decision-Making,” Computing in Civil Engineering, L. Soibelman and B. Akinci, eds., American Society of Civil Engineers, Reston, VA, pp. 870-880. 2007.

[60] Jumate E. and Manea, D.L., “X-Ray Diffraction Study of Hydration Processes in The Portland Cement”, Journal of Applied Engineering Sciences, vol. 14, no.1, pp.79-86, Jan. 2011

[61] Osama Hodhod a, Gamal A. Salama, “Analysis of Sulfate Resistance in Concrete Based on Artificial Neural Networks and USBR4908-Modeling”, Ain Shams Engineering Journal, vol. 4, pp. 651-660 2013

[62] Higgins, D. D. and Crammond, N. J., "Resistance of Concrete Containing Ggbs to the Thaumasite Form of Sulfate Attack." Cement & Concrete Composites, vol.25, pp. 921-929, 2003

[63] Fang Qing, Li Beixing, Yin Jiangang, Yuan Xiaolu, “Microstructural and Microanalytical Study on Concrete Exposed to the Sulfate Environment”, Materials Science and Engineering, 269 012070. Nov, 2017

[64] Janina Setinaa, Alona Gabreneb, Inna Juhnevicac, “Effect of Pozzolanic Additives on Structure and Chemical Durability of Concrete”, 11th International Conference on Modern Building Materials, Structures and Techniques, MBMST, 2013

[65] Mehta 2017 Ankur Mehta, Rafat Siddique, “Sulfuric acid resistance of fly ash based geopolymer concrete”, Construction and Building Materials, vol.146, pp.136-143, Aug. 2017

[66] Martina Kovalčíková, Adriana Eštoková, Jozef Oravec, Alena Luptáková, “Investigation of the Precipitates on the Concrete Surface due to Sulphate Exposure”, SSP - Journal of Civil Engineering, vol.11, no.2, 2016

[67] Yudong Xie, Xujian Lin, Weijie Pan, Tao Ji, Yongning Liang, Hongru Zhang, “Study on Corrosion Mechanism of Alkali-Activated Concrete with Biogenic Sulfuric Acid”, Construction and Building Materials, vol.188, pp. 9-16, Nov. 2018

[68] Ali Allahverdi, František Škvára, “Sulfuric Acid Attack on Hardened Paste of Geopolymer Cements Part 1. Mechanism of Corrosion at Relatively High Concentrations”, Ceramics – Silikáty, vol.49, no.4, pp. 225-229, 2005

[69] Babatunde Abiodun Salami, Megat Azmi Megat Johari, Zanial Arifin Ahmad and Mohammed Maslehuddin, “POFA-Engineered Alkhali-activated Cementitious Composite Performance in Acid Environment, Journal of Advanced Concrete Technology, vol 15 pp. 684-699, 2017

[70] Pacheco Torgal, F. Labrincha, J. Leonelli, C. Palomo, A. and Chindaprasit, P “Handbook of Alkali Activated Cements, Mortars and Concretes” Elsivir. 2014

[71] C.K. Yip, G.C. Lukey, J.S.J. van Deventer, "The coexistence of Geopolymeric Gel and Calcium Silicate Hydrate at Early Stage of Alkaline Activation", Cem. Con. Res, vol.35, pp. 1688-1697, 2005

[72] A. Buchwald, R. Tatarin, D. Stephan, "Reaction Progress of Alkaline-Activated Metakaolin-Ground Granulated Blast Furnace Slag Blends", J. Mater. Sci., vol.44, no.20, pp. 5609-5617, Oct. 2009

[73] Kaempfer, W., Berndt, M., "Polymer-Modifed Mortar with High Resistance to Acid and to Corrosion by Biogenous Sulfuric Acid". Proceedings of the Ninth ICPIC Congress, Bologna (Italy), pp. 681- 687, 1998

[74] De Belie N., Monteny J., "Resistance of Concrete Containing Styrol Acrylic Acid Ester Latex to Acids Occurring in Livestock Housing". Cement and Concrete Research, vol.28, no.11, pp. 1621-1628, 1998

[75] De Belie, N., Verschoore, R., Van Nieuwenburg, D., "Resistance of Concrete with Limestone Sand or Polymer Additions to Feed Acids". Transactions of the ASAE vol.41, no.1, pp. 227-233, 1998

[76] Bakharev T, "Resistance of Geopolymer Materials to Acid Attack". Cement and Concrete Research, vol.35, no.4, pp. 658-670, 2005

[77] Thokchom, S., Ghosh, P. and Ghosh, S. "Resistance of Fly Ash Based Geopolymer Mortarts in Sulfuric Acid" ARPN Journal of Engineering and Applied Science, vol.4, no.1, pp. 65-70, 2009

[78] Z. Huajun, Z. Zuhua, D. Fenggan, C. Yalong, "The Effects of Phase Changes on The Bonding Property of Geopolymer To Hydrated Cement, Constr. Build. Mater. Vol.48, pp.124-130, 2013

[79] U. Rattanasak, P. Chindaprasirt,U. Rattanasak, P. Chindaprasirt, "Influence of Na(OH) Solution on the Synthesisof Fly Ash Geopolymer", Miner. Eng., vol.22 pp. 1073-1078, 2009

[80] P. Chindaprasirt, W. Chalee, C. Jaturapitakkul, U. Rattanasak, "Comparative Study on the Characteristics of Fly Ash and Bottom Ash Geopolymers", Waste Manage., vol.29, pp. 539-543, 2009

[81] T. Suwan, M. Fan, "Influence of OPC Replacement and Manufacturing Procedures on the Properties of Self-Cured Geopolymer", Constr. Build. Mater., vol.73, pp. 551-561, 2014

[82] Pangdaeng, T. Phoo-ngernkham, V. Sata, P. Chindaprasirt, “Influence of Curing Conditions on Properties of High Calcium Fly Ash Geopolymer Containing Portland Cement as Additive”, Mater. Des., vol.53, pp. 269-274, 2014

[83] Ravi Sharma, D.P. Bisen, Usha Shukla and B.G. Sharma, “X-ray Diffraction: A Powerful Method of Characterizing Nanomaterials”, Recent Research in Science and Technology, vol.4, no.8, pp. 77-79, 2012

[84] N.P. Rajamane, M.C Nataraja, N. Lakshmanan and J.K Dattatreya, “Rapid chloride permeability test on geopolymer and Portland cement Concretes”, Indian Concret Journal., vol85, no.10, pp. 21-26, Oct. 2011

[85] S. Thokchom, “Fly Ash Geopolymer Pastes in Sulphuric Acid”, Int. J. Eng. Innov. Res., vol.3, no.6, pp. 943-947, 2014

[86] J. Davidovits, “High-Alkali Cements for 21st Century Concretes”, Symposium on Concrete Technology: Past, Present and Future, University of California, Berkeley, 1994

[87] X.J. Song, Marosszeky, M.M. Brungs, R. Munn, “Durability of Fly Ash-Based Geopolymer Concrete Against Sulphuric Acid Attack”, International Conference on Durability of Building Materials and Components, Lyon, France, 2005.

[88] S. Alonso, A. Palomo, “Alkaline Activation of Metakaolin and Calcium Hydroxide Mixtures: Influence of Temperature, Activator Concentration and Solids Ratio, Mater. Lett., vol.47, pp. 55-62, 2001

[89] P. Rovnaník, “Effect of Curing Temperature on The Development of Hard structure Of Metakaolin-Based Geopolymer”, Constr. Build. Mater., vol 24, pp. 1176-1183, 2010

[90] J.S.J. Van Deventer, J.L. Provis, P. Duxson, G.C. Luckey, “Reaction Mechanisms in the Geopolymeric Conversion of Inorganic Waste to Useful Products”, J. Hazard. Mater., vol.139, pp. 506-513, 2007

[91] F. Skvara, L. Kopecky, J. Nimeeek, Z. Bittnar, “Microstructure of Geopolymer Materials Based on Fly Ash”, Ceram. Silik., vol.4, pp. 208-215, 2006

[92] Yu Yang, Tao Ji, Xujian Lin, Caiyi Chen, Zhengxian Yang, “Biogenic Sulfuric Acid Corrosion Resistance of New Artificial Reef Concrete”, Construction and Building Materials, vol.158, pp. 33-41, Jan. 2018

[93] Wei Zhang , Xiao Yao, Tao Yang, Zuhua Zhang, “The Degradation Mechanisms of Alkali-Activated Fly Ash/Slag Blend Cements Exposed to Sulphuric Acid”, Construction and Building Materials 186 1177–1187. 2018

[94] R.R. Lloyd, J.L. Provis, J.S.J. van Deventer, “Acid Resistance of Inorganic Polymer Binders -Corrosion Rate”, Mater. Struct. 45. 2012

[95] Allahverdi, F. Skvara, “Nitric Acid Attack on Hardened Paste of Geopolymeric Cements – Part 2”, Ceram. Silik. 45 (2001) 143–149.

[96] Van Driessche, A., Benning, L. G., Ossorio, M., Rodriguez-Blanco, J., D Bots. P. and Garciua-Ruiz, J. M, “Bassanite, a Stable Crystalline Precursor Phase During Gypsum Precipitation at Room Temperature”, Rivista de la Sociedad Espanola de Mineralogia, 16, 172-173. 2012

[97] Lesbani, A. Sitompul, S.O.C. Mohadi, R. Hidayati, N. Characterization and Utilization of Calcium Oxide (Cao) Thermally Decomposed From Fish Bones as A Catalyst in The Production of Biodiesel From Waste Cooking Oil. Makara J. Technol. 121–126. 2016

[98] Imtiaz, A.; Farrukh, M.A. Khaleeq-ur-rahman, M. Adnan, R. Micelle-assisted “Synthesis of Al2O3 ·CaO Nanocatalyst: Optical Properties and Their Applications in Photodegradation of 2,4,6-Trinitrophenol”. Sci. World J., 641420. 2013

[99] Gonzalez M., E. Hernandez, J. A. Ascencio, F. Pacheco, S. Pacheco, and R. Rodriguez, "Hydroxyapatite Crystals Grown on a Cellulose Matrix Using Titanium Alkoxide as a Coupling Agent," Journal of Materials Chemistry, Vol. 13, pp. 2948-2951. 2003

[100] P.K. Mehta, “Studies on Chemical Resistance of Low Water/Cement Ratio Cements”, Cem. Concr. Res. 15 (6) 969–978. 1985

[101] Hewayde, E, Nehdi, ML, Allouche, E & Nakhla, G, “Using Concrete Admixtures for Sulfuric Acid Resistance”, in Proceeding of institutions of Civil Engineers-Construction Materials vol. 160. 2007

[102] Freidin, C. 1999, “Behavior of Silica-Concrete Based on Quartz Bond in Sulphuric Acid”, Cement and Concrete Composites, vol. 21, no. 4, pp. 317-23.

[103] Shengyuan, Y, Zhigang, S, Xiang, L & Yunchuan, ZH., “Comparative Study on Theory Model and Test Result for Dilute sulfuric Acid to Erode Concrete”, Procedia Earth and Planetary Science, vol. 5, pp. 188-97.2012

[104] Yuan, H, Dangla, P, Chatellier, P & Chaussadent, T, 'Degradation Modelling of Concrete Submitted to Sulfuric Acid Attack', Cement and Concrete Research, vol. 53, pp. 267-77.2013

[105] Stark D.C. “Occurrence of Thaumasite in Deteriorated Concrete”. Cement and Concrete Composites, 25, 1119–1121. 2003

[106] Hyeoneun Park, Yeonung Jeong, Jae-Hong Jeong and Jae Eunoh, “Strength Development and Hydration Behavior of Self-Activation of Commercial Ground Granulated Blast-Furnace Slag Mixed with Purified Water”, Materials 2016.

[107] Hyung-Seok Kim, Joo-Won Park, Yong-Jun An, Jong-Soo Bae and Choon Han, “Activation of Ground Granulated Blast Furnace Slag Cement by Calcined Alunite” Materials Transactions, Vol. 52, No. 2 (2011) pp. 210 to 218.

[108] M.S.H. Khan and O. Kayali, “Effect of NaOH Activation on Ettringite in Concrete Containing Ground Granulated Blast Furnace Slag”, Third International Conference on Sustainable Construction Materials and Technologies, 2013.

[109] Attal A, Brigodiot M, Camacho P, Manem J. “Biological Mechanisms of H2S Formation in Sewer Pipes”. Water Sci Technolgy, 26:907–14. 1992

[110] Santhanam M, Cohen MD, Olek J., “Effects of Gypsum Formation on the Performance of Cement Mortars During External Sulfate Attack. Cem Concr Res, 33:325–32. 2003

[111] Glasser FP, Marchand J, Samson E., “Durability of Concrete Degradation Phenomena Involving Detrimental Chemical Reactions”. Cem Concr Res,38:226–46. 2008

[112] Vogel, A. I. (1985). A Textbook of Quantitative Inorganic Analysis, 5th Edition, revised by J. Basset, Longman, London, p. 754.

[113] American Public Health Association (1985). Standard method for the examination of water and wastewater, 16th edition. Washington, D.C., USA

Vitae

Name : Hassan A. Alkhalifah

Nationality : Saudi

Date of Birth : Jan 30th, 1983

Email : Hasan.khalifa@Aramco.com

Address : 19402, Midra Building, Saudi Aramco, Dhahran 31311

Academic Background :

Doctor of Philosophy in Civil Engineering	KFUPM	2018
Master of Engineering in Civil Engineering	Penn State University	2013
Master of Business Administration	KFUPM	2011
Bachelor Degree in Civil Engineering	KFUPM	2005